FORT NELSON TEST SITE – SIMULATION REPORT

Plains CO_2 Reduction (PCOR) Partnership Phase III
Task 9 – Deliverable D67

Prepared for:

Andrea M. Dunn

U.S. Department of Energy
National Energy Technology Laboratory
626 Cochrans Mill Road
PO Box 10940
Pittsburgh, PA 15236-0940

DOE Cooperative Agreement No. DE-FC26-05NT42592

Prepared by:

Guoxiang Liu
Charles D. Gorecki
Terry P. Bailey
Jason R. Braunberger
James A. Sorensen
Edward N. Steadman

Energy & Environmental Research Center
University of North Dakota
15 North 23rd Street, Stop 9018
Grand Forks, ND 58202-9018

August 2011
Revised February 2014
Approved

2014-EERC-03-06

EERC DISCLAIMER

LEGAL NOTICE This research report was prepared by the Energy & Environmental Research Center (EERC), an agency of the University of North Dakota, as an account of work sponsored by the U.S. Department of Energy (DOE) National Energy Technology Laboratory (NETL). Because of the research nature of the work performed, neither the EERC nor any of its employees makes any warranty, express or implied, or assumes any legal liability or responsibility for the accuracy, completeness, or usefulness of any information, apparatus, product, or process disclosed or represents that its use would not infringe privately owned rights. Reference herein to any specific commercial product, process, or service by trade name, trademark, manufacturer, or otherwise does not necessarily constitute or imply its endorsement or recommendation by the EERC.

ACKNOWLEDGMENT

This material is based upon work supported by DOE NETL under Award No. DE-FC26-05NT42592.

DOE DISCLAIMER

This report was prepared as an account of work sponsored by an agency of the United States Government. Neither the United States Government, nor any agency thereof, nor any of their employees, makes any warranty, express or implied, or assumes any legal liability or responsibility for the accuracy, completeness, or usefulness of any information, apparatus, product, or process disclosed, or represents that its use would not infringe privately owned rights. Reference herein to any specific commercial product, process, or service by trade name, trademark, manufacturer, or otherwise does not necessarily constitute or imply its endorsement, recommendation, or favoring by the United States Government or any agency thereof. The views and opinions of authors expressed herein do not necessarily state or reflect those of the United States Government or any agency thereof.

NDIC DISCLAIMER

This report was prepared by the EERC pursuant to an agreement partially funded by the Industrial Commission of North Dakota, and neither the EERC nor any of its subcontractors nor the North Dakota Industrial Commission (NDIC) nor any person acting on behalf of either:

(A) Makes any warranty or representation, express or implied, with respect to the accuracy, completeness, or usefulness of the information contained in this report or that the use of any information, apparatus, method, or process disclosed in this report may not infringe privately owned rights; or

(B) Assumes any liabilities with respect to the use of, or for damages resulting from the use of, any information, apparatus, method, or process disclosed in this report.

Reference herein to any specific commercial product, process, or service by trade name, trademark, manufacturer, or otherwise does not necessarily constitute or imply its endorsement, recommendation, or favoring by the North Dakota Industrial Commission. The views and opinions of authors expressed herein do not necessarily state or reflect those of the North Dakota Industrial Commission.

TABLE OF CONTENTS

LIST OF FIGURES

Continued . . .

LIST OF FIGURES (continued)

LIST OF TABLES

FORT NELSON TEST SITE – SIMULATION REPORT

EXECUTIVE SUMMARY

Spectra Energy Transmission (SET) is working with the Energy & Environmental Research Center and the Plains CO_2 Reduction (PCOR) Partnership to determine the feasibility of long-term storage of sour carbon dioxide (CO_2) in a saline carbonate formation near Fort Nelson, British Columbia, Canada. This document reports the results of a simulation-based feasibility study conducted for the Fort Nelson site. The investigation scenarios include the injection of 50 and 100 million tonnes of CO_2 over a period of 25 and 50 years, respectively. These injection scenarios were followed by 75 (for the 25-year injection scenario) and 50 years (for the 50-year injection scenario) of postinjection monitoring of the CO_2 plume for a total of 100 years in each of the injection cases. The potential for CO_2 plume migration to the adjacent gas pools (Clarke Lake Slave Points A and B) and pressure dissipation during and after injection was also evaluated. The key conclusions include:

- The static geologic model was updated based on commercially available well data, acquisition of existing 2-D and 3-D seismic surveys, well log analysis, review and testing of available core, pressure transient analyses from well testing, and interpretation of the facies for the barrier reef complex that is the target for the Fort Nelson CCS Project. It has resulted in a more realistic static geologic model (Version 3) of the test site.

- A dynamic model based on the completed Version 3 geologic model was constructed for the purpose of matching the historical gas and water production, water disposal data, and scattered bottomhole pressures (BHPs) in the gas pools. This, in turn, re-creates the pressure sink in the model that exists in the project area as a result of significant gas production from nearby gas pools since the 1960's. Through the history-matching process, the geologic model was validated and improved by decreasing the realistic range of several key geological properties, including permeability, fault transmissibility, vertical to horizontal permeability ratio (k_v/k_h), and others. In addition, with the pressure sink from gas production now included in the model, via the history match process, the injection simulation cases will now be more realistic by including the effects of the offset production on CO_2 plume development and pressure effects from the injection.

- Both injection locations (c-47-E and c-61-E) appear to have sufficient storage capacities to accommodate target injection volumes.

- In both injection scenarios, the injected sour CO_2 showed migration structurally upward (buoyancy effects) and plumes developed at the contact between the reservoir (reef) and the cap rock (shale) in structural highs. The plume was contained within the reservoir (reef) in all scenarios over the 100 years.

- Both injection site scenarios showed the required injectivity for the life of the injection periods while ensuring that the maximum injection sandface pressures at each of the injection wells did not exceed 80% of the fracture gradient – an anticipated regulatory restriction. The BHPs of each of the injection wells in the c-47-E location were predicted to be 1000 to 3000 kPa lower than the BHPs at the c-61-E location.

- The c-61-E showed higher reservoir pressures at the end of the injection life than the c-47-E site as the pressure in the c-61-E area was not able to dissipate as easily as the c-47-E site because of the presence of a nearby low-permeability barrier that was identified during the history match process.

- The injection site around c-47-E is a better option compared to the c-61-E area because the injected sour CO_2 plume did not contact the adjacent gas pools during the 100-year simulation period and the resulting reservoir pressures were lower which is a better situation as regards the cap rock integrity.

- The low-permeability cases applied to the c-47-E injection area before the history match process suggests that the CO_2 plume area will be larger and may result in migration of the CO_2 plume into the c-61-E area and a small gas-producing pool; this risk can be managed through application of the first recommendation noted below to further understand the likelihood of this scenario. The impact is likely past the operational life of this small gas pool and potential acquisition of the small gas pool in the c-61-E area.

- The history match process and simulations show that the c-47-E injection area has had some pressure reduction since the 1960s because of the pressure sink in the model area from the gas production and also because the reef is subhydrostatic naturally. The simulation scenarios indicate that, while there are pressure increases in the reservoir from the injection around c-47-E, the maximum reservoir pressure increase basically returns to its 1960 reservoir pressure.

To further confirm the evaluations presented in the study, the following recommendations are suggested to be included in any future modeling and simulation studies:

- Collection of more geological information in the c-47-E area by means of drilling, testing, coring, and logging of a new well and acquisition of a new 3-D seismic survey over the predicted CO_2 plume footprint.

- Integration of various physical phenomena such as geochemical reactions, geomechanical behaviors, and thermal effects into the dynamic model to comprehensively understand the sink–seal system for more reliable predictions.

FORT NELSON TEST SITE – SIMULATION REPORT

INTRODUCTION

The Plains CO_2 Reduction (PCOR) Partnership, led by the Energy & Environmental Research Center (EERC), is working with Spectra Energy Transmission (SET) to investigate the feasibility of a carbon capture and storage (CCS) project to mitigate carbon dioxide (CO_2) emissions from SET's Fort Nelson Gas Plant (FNGP). The FNGP and the proposed CO_2 storage area are located near the town of Fort Nelson in northwestern British Columbia, Canada. The CO_2 source from the FNGP's natural gas processing is expected to be on the order of 2 Mt/year and includes contaminants of up to 5% hydrogen sulfide (H_2S) and a small amount of methane (CH_4). As such, it is referred to as a "sour" CO_2 stream. The sour CO_2 gas stream would be injected into a deep saline carbonate formation for the purpose of long-term storage. A technical team that includes SET, the EERC, and others conducted a variety of activities to 1) determine the geologic, geochemical, and geomechanical properties of the target injection formation and key sealing formations in the vicinity of the injection site; 2) model the effects that large-scale injection of sour CO_2 may have on those properties as well as the performance of the reservoir and containing formations under CCS operations; 3) evaluate the geological risks of this injection process on local and regional scales based on results of the modeling effort combined with other technical analyses; and 4) implement site-specific, risk-based monitoring, verification, and accounting (MVA) technologies to ensure safe and efficient long-term CO_2 storage. The Fort Nelson demonstration project presents a unique opportunity to develop a set of cost-effective risk-based MVA protocols for large-scale (>1 million metric tons a year) CO_2 storage in a saline formation. The activities rely on the development of a thorough site characterization, modeling, and risk assessment effort.

The results of the Fort Nelson activities will provide insight regarding 1) the behavior of dense-phase sour CO_2 in a deep brine-saturated carbonate reservoir environment; 2) the impact of dense-phase sour CO_2 on the integrity of sink and seal rocks in a deep brine-saturated reservoir environment; 3) the effects of large-scale sour CO_2 injection and storage on wellbore integrity, particularly with respect to cements; 4) the effectiveness of selected MVA techniques; and 5) the use of an approach that combines iterative risk assessment, characterization, modeling, and MVA planning to safely and cost-effectively inject and store large volumes of sour CO_2 in geologic formations. The sour CO_2 produced from the FNGP is proposed to be injected into a deep, saline-filled, Devonian-age carbonate formation at a depth of approximately 6900 to 7200 feet (2100 to 2300 meters).

This report describes and discusses the modeling and simulation activities conducted in 2010 and 2011 for this CCS feasibility project (Figure 1). The regional reservoir model covers a

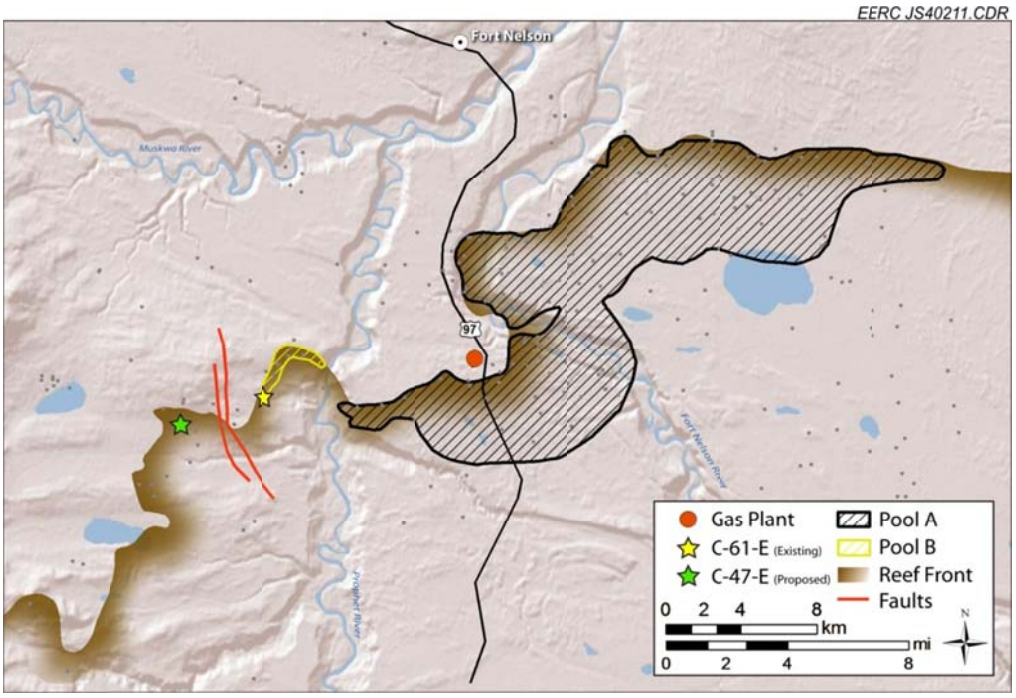

Figure 1. Site map.

volume defined by 39 km × 67 km × 800 m, containing the injection formation and adjacent gas pools (Clarke Lake Slave Points A and B) based on model Versions 1 and 2 (Appendix A). These activities include static geologic model development as well as dynamic modeling and simulations that were conducted for the model validation, predictive simulation, and risk assessment. The current static geologic model (Version 3) has been updated from two previous versions (Version 1 and Version 2) after incorporating new geological information and more detailed data analysis. The dynamic modeling and simulations include base case and initial scenario explorations, modeling optimizations and validations (history matching), and predictive simulations with sour CO_2 injection before and after history matching. It is important to note that the reef front depicted in Figure 1, and all other subsequent map figures in this report, is the reef front as it existed during the time of Slave Point Formation deposition. The reef front during the deposition of the Keg River and Sulphur Point Formations, which underlie the Slave Point, extended a fair distance farther north and west. Thus while some of the maps appear to show the predicted plume extending beyond the reef front, that is never actually the case. The plume remains within the Keg River and/or Sulphur Point Formations and their respective reef fronts.

STATIC GEOLOGIC MODELING DEVELOPMENT

The Version 3 static reservoir model has evolved from a scoping-level model to a more detailed model that was completed in June 2010. The Version 3 model updated the previous two versions with the addition of detailed data such as 2-D and 3-D seismic data and core and well log analyses; refined 13 domains and ten zones; and included surface elevations from the topographic map and a temperature gradient to closely resemble a real sink–seal system for CO_2

storage evaluation and risk assessment after model validation (history matching). An overview of each model version is provided in Appendix A: Static Geologic Modeling Development.

DYNAMIC MODELING AND SIMULATIONS

The dynamic model was built using the static geologic model Version 3. The initial simulations include a base case and initial scenario explorations for investigating the impact of reservoir properties/parameters such as permeability, the ratio of vertical permeability to horizontal permeability (k_v/k_h), and fault transmissibility on CO_2 plume and pressure buildup. The model was then optimized by introducing three techniques: grid-size sensitivity analysis, numerical tuning, and properties/parameters sensitivity analysis, to reduce simulation run time. The optimized model was validated by history matching to obtain a reasonable match between simulated results and historical data. The top two "best" matched numerical models were selected for predictive simulations for both injection locations: c-47-E and c-61-E.

Base Case and Initial Scenario Explorations

Five scenarios were designed for the base case and initial property explorations. It includes base case with and without CO_2 injection for comparing the effect of pressure changes, cap rock and seal capacity by reducing permeability, permeability ratio k_v/k_h, fault transmissibility changes, and regional permeability variations on CO_2 movement. All of these cases are with 25 and 50 years of sour CO_2 injection at a rate of 120 MMscf/d and run up to 100 years from the beginning of the injection to investigate the effects from various properties (Table 1). The results indicate that these key reservoir properties need to be tracked during history matching for model validation. The details on these simulations are provided in Appendix B: Base Case and Initial Scenario Explorations.

Table 1. Five Test Case Scenarios Used in the Base Case and Initial Scenario Explorations

Test Case Scenario	CO_2 Injection	k_v/k_h	Fault Transmissibility	Reservoir Permeability
Base Case (with/without CO_2 injection)	Yes/no	0.2	1	Base case
Cap Rock Reduced Permeability Case*	Yes	0.2	1	Base case
k_v/k_h Case	Yes	0.2, 0.3	1	Base case
Fault Transmissibility Case	Yes	0.2	0, 0.25, 0.75, 1	Base case
Reservoir Permeability Case	Yes	0.2	1	2× and 5× base case

* Cap rock reduced permeability:
The permeability of the Muskwa zone was 0.01 × base case.
The permeability of the Otter Park zone was 0.1 × base case.
Except for breaches in the Watt Mountain zone, the permeability of this zone was 0.1 × base case.

Predictive Simulations Before History Matching

Ten test cases were simulated to compare injection scenarios for overall performance and risk assessment in and around c-47-E and c-61-E locations (Table 2). In view of base case and initial scenario explorations (Table 1), a k_v/k_h ratio of 0.2, a fault transmissibility of 1.0, and an injection rate of 120 MMscf/d were fixed for these cases. Cases 1–4 modeled three injection wells at 25- and 50-year injections, assuming base case reservoir permeability. Cases 5 and 6 assumed lower permeability near c-47-E and required a facies adjustment (i.e., decreasing permeability within model domains for a particular facies, see Appendix C: Predictive Simulations Before History Matching) and a wellbore adjustment (i.e., increasing the number and location of injection wells from three to six). Cases 7 and 8 evaluated injection at two wells near c-61-E. To enhance the sour CO_2 injection, Cases 9 and 10 were designed to examine the cumulative gas improvement with more perforations than Cases 5 and 6. Results of all simulations are given in Appendix C: Predictive Simulations Before History Matching. These results infer that the risk of sour CO_2 injection from c-47-E is lower than the risk from c-61-E. However, that needs to be confirmed after model validation.

Model Optimization and Validation

The dynamic model was optimized and validated by using a dynamic modeling workflow process proposed by the EERC. This workflow process includes three optimization techniques (grid-size sensitivity analysis, numerical tuning, and properties/parameters sensitivity analysis), model validation (history matching), and predictive simulations (Figure 2).

The model validation process was used to improve modeled outputs for obtaining a good match with historical data, which demonstrates the ability of the model to accurately predict reservoir conditions. As a commonly used technique, history matching is a method of adjusting, or tuning, reservoir characteristics (properties) to match historical field data through an iterative trial-and-error process. This trial-and-error process varies parameters and properties within accepted and realistic engineering and geologic ranges, while still reasonably matching the simulated results with the historical data.

History-Matching Validation Data

Gas and water production and water disposal data within the Fort Nelson CCS Project study area were used for the history matching. Available from GeoVista (www.divestco.com/Solutions/Engineering/Software/GeoVista-%281%29.aspx) in the Fort Nelson CCS Project study area are monthly (being averaged as quarterly data set for history matching) gas and water production data, injected water volumes, and scatter points of bottomhole pressure (BHP) for 85 production wells and seven water disposal wells. The data for all of the production wells were collected from 1961 to 2010 (Table D-2 and Figure D-3).

History matching was primarily based on achieving a satisfactory mass balance on the cumulative gas and water production data and water disposal data within the time period from 1961 to 2010. Once primary matching of the mass balances yielded a satisfactory global objective function tolerance, simulated and historical data values for gas and water production and BHPs for all of the individual wells were evaluated.

Table 2. Ten Test Case Scenarios Used in the Predictive Simulations (before history matching) Comparing Injection Locations c-47-E and c-61-E

Test Case Scenario	Location	No. of Injection Wells	Injection Well Names	Injection Time, years	Injection Rate, MMscf/d	k_v/k_h	Fault Transmissibility	Reservoir Permeability
1	c-47-E	3	c-18-E, c-47-E, and c-36-E	25	120	0.2	1.0	Base case
2	c-47-E	3	c-18-E, c-47-E, and c-36-E	50	120	0.2	1.0	Base case
3	c-61-E	3	a-91-E, c-61-E, and c-88-F	25	120	0.2	1.0	Base case
4	c-61-E	3	a-91-E, c-61-E, and c-88-F	50	120	0.2	1.0	Base case
5	c-47-E	6	a-67-E, c-18-E, c-47-E, d-09-E, d-36-E, and d-61-A	25	120	0.2	1.0	Low permeability*
6	c-47-E	6	a-67-E, c-18-E, c-47-E, d-09-E, d-36-E, and d-61-A	50	120	0.2	1.0	Low permeability*
7	c-61-E	2	a-69-F and b-31-E	25	120	0.2	1.0	Base case
8	c-61-E	2	d-49-F and d-11-E	50	120	0.2	1.0	Base case
9	c-47-E	6	a-67-E, c-18-E, c-47-E, d-09-E, d-36-E, and d-61-A (more perforation)	25	120	0.2	1.0	Low permeability*
10	c-47-E	6	a-67-E, c-18-E, c-47-E, d-09-E, d-36-E, and d-61-A (more perforation)	50	120	0.2	1.0	Low permeability*

* Facies adjustments for the low-permeability cases are described in detail in Appendix C.

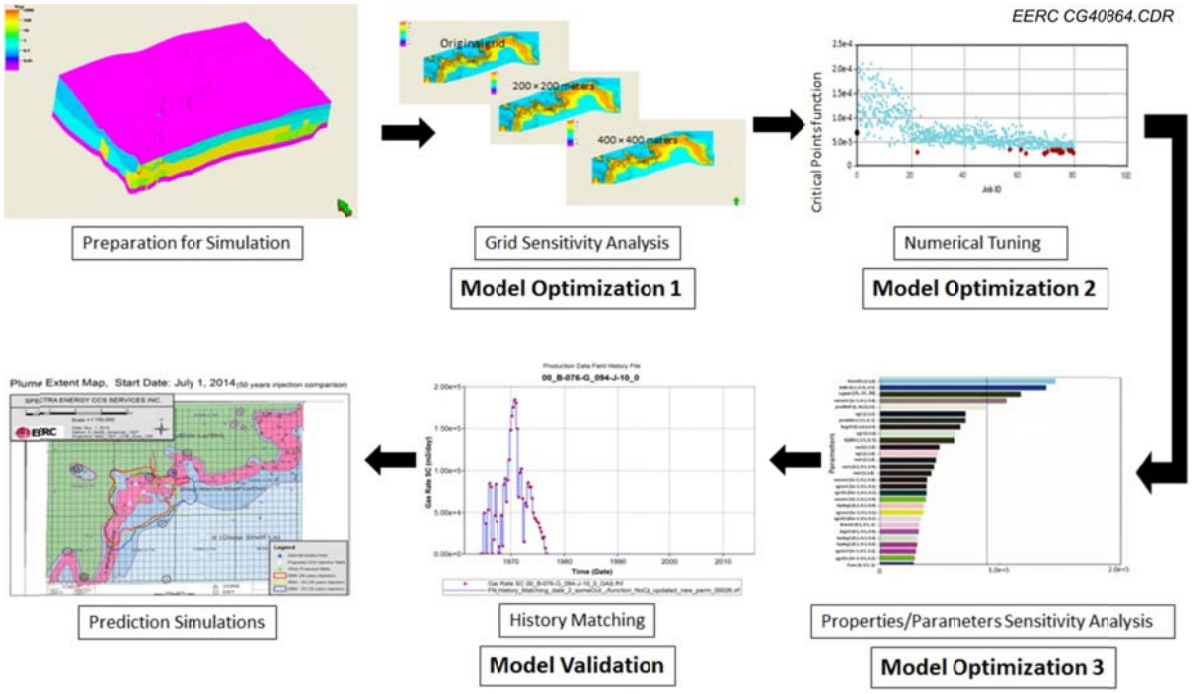

Figure 2. Dynamic modeling workflow process.

A global objective function was used in history-matching processes to measure the relative difference between the historical data and simulation results. Well variables were taken into account in the function via a root mean squared error (RMSE) method. With respect to history matching, smaller error values indicate a smaller difference between historical data and simulated values. As this error value decreases, the matching procedure tends to converge. After multiple iterations, the global objective function can be used to obtain an overall minimum error value. The equation for global objective function, as described by Yang and others (2007), follows:

$$E_g = \frac{1}{\sum_{p=1}^{N(w)} W_{w,p}} \sum_{p=1}^{N(w)} \frac{\sqrt{\dfrac{\sum_{t=1}^{T(w,p)} (R^s_{w,p,t} - R^m_{w,p,t})^2}{T(w,p)}}}{\Delta R^m_{w,p} + 4E^m_{w,p}} \times W_{w,p} \times 100\% \qquad \text{[Eq. 1]}$$

Where subscripts w, p, and t are well, production data, and time, respectively.

$N_{(w)}$ is the total production data from well 1 to w.

$W_{w,p}$ is weight.

$T(w, p)$ is the total of time step.

$R^{s}_{w,p,t}$ represents simulation results while $R^{m}_{w,p,t}$ is measured historical data.

$\Delta R^{m}_{w,p}$ is the measured maximum change for well w and production data p.

$E^{m}_{w,p}$ is measurement error.

In this study, the above-mentioned global objective function (Eq. 1) was used for history matching of gas and water production, water disposal, and BHPs.

History-Matching Process

The history-matching process is iterative, whereby each simulation run produces a new candidate value (or values), which can then be used for the next iteration. As this process is repeated, the difference between historical data and simulation results, as measured by the global objective function error (Eq. 1), decreases to an asymptotical convergence (Figure 3). A flow diagram for this procedure is shown in Figure 4.

History-Matching Results

The final history-matching iteration was obtained after 494 jobs. The matching period covered the injection and production history of the nearby gas pools between January 1, 1961, to October 1, 2010. Based on the convergence of the global objection function (Figure 3), the lowest obtainable errors for gas production, water disposal, and water production are 0.49% (Figure 5), 0.43% (Figure 6), and 7.03% (Figure 7), respectively. When water production results are taken into account, the lowest obtainable global error was 3.91% (Figure 3). The role of gas production rates as a primary dominant parameter for well control may be attributed to the high global error value of water production. The scatter BHP data, which do not cover all simulation period intervals, also appear to affect the value. However, the history-matching results from these efforts are good enough to have confidence in model behaviors and predictions. The matching results of cumulative gas, water, and BHP for the top ten wells are shown in Appendix D: Model Optimization and Validations (history matching).

Predictive Simulations after History Matching

Based on history matching, the top two “best” matching cases were selected for the predictive simulations. According to historical data, a total of 38 active production wells (Appendix E) need to be kept on operation status (open or shut in) from July 2010 to the date when the gas production rate is less than 2500 m^3/day under the minimum BHP limits of the wells. The produced water during this period was then reinjected into one of three nearby water disposal wells (Appendix E). An example of gas rate control and water recycle is shown in Figures E-3–E-12 in Appendix E: Predictive Simulations after History Matching.

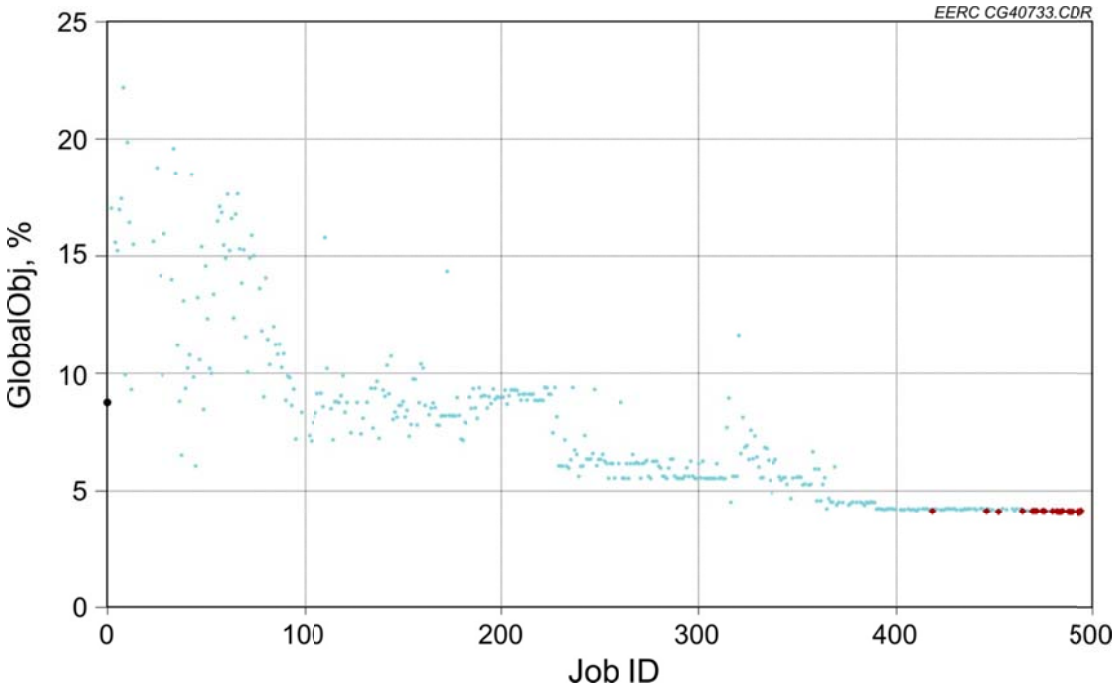

Figure 3. Final history-matching iteration of 494 jobs showing the convergence of the global objective function (red dots represent the lowest error values). The small variation in these values indicates the model can accurately reproduce known subsurface processes.

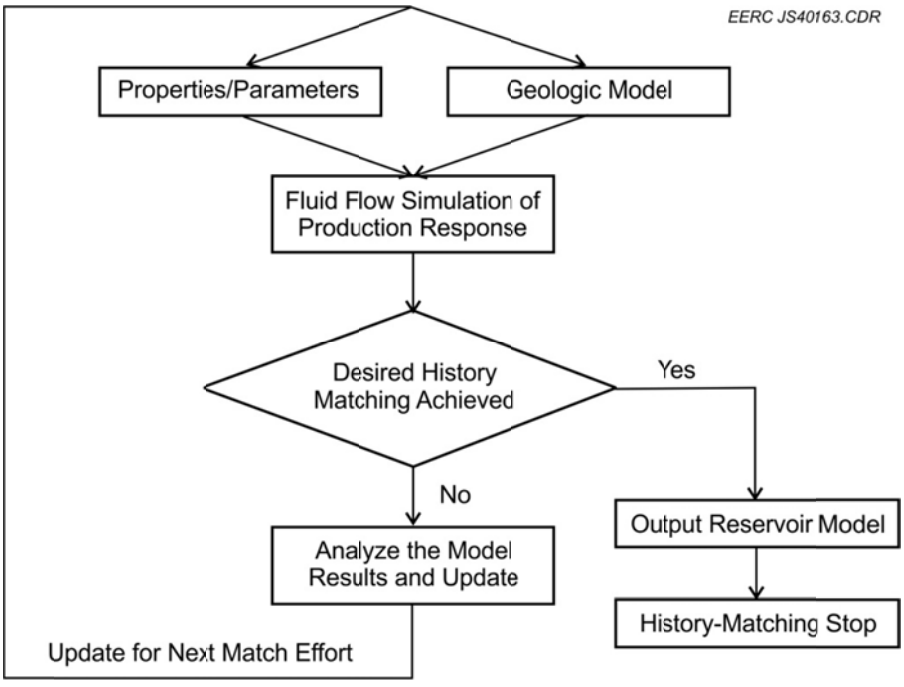

Figure 4. History-matching process.

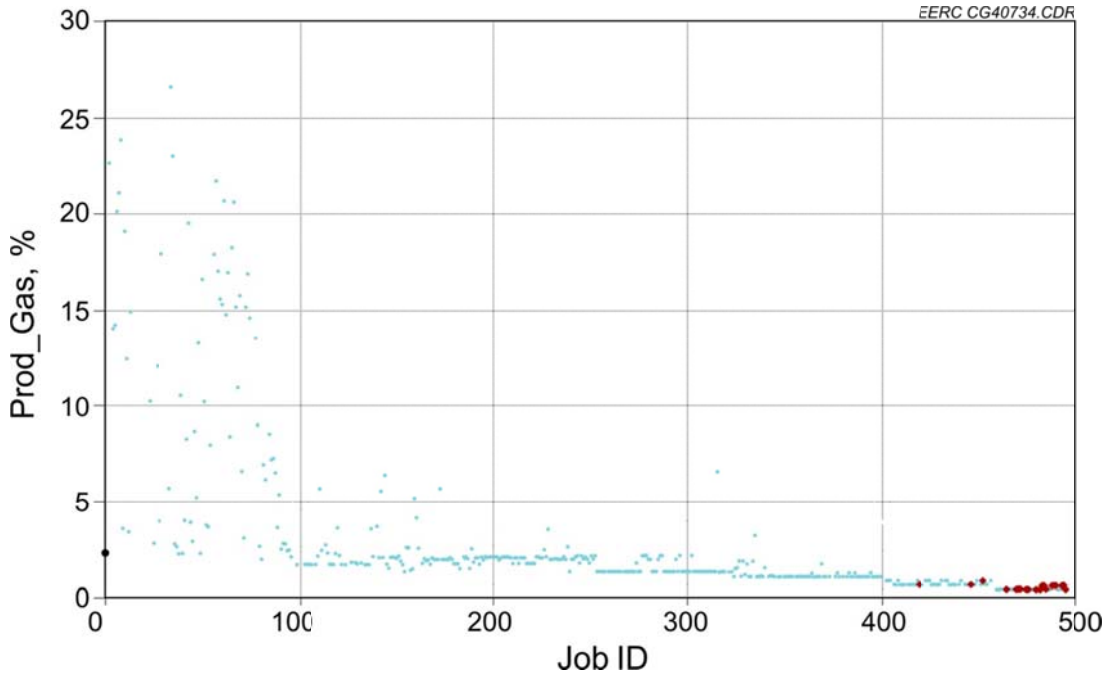

Figure 5. Final history-matching iteration of 494 jobs showing the convergence of the gas production function (red dots represent the lowest error values).

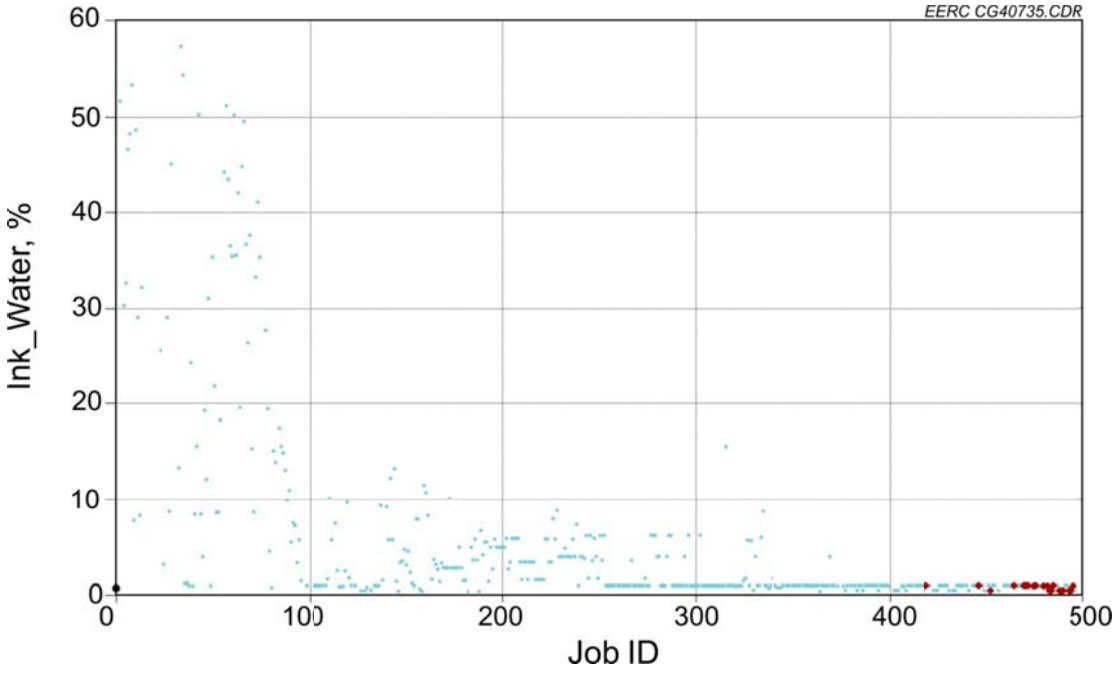

Figure 6. Final history-matching iteration of 494 jobs showing the convergence of the water disposal function (red dots represent the lowest error values).

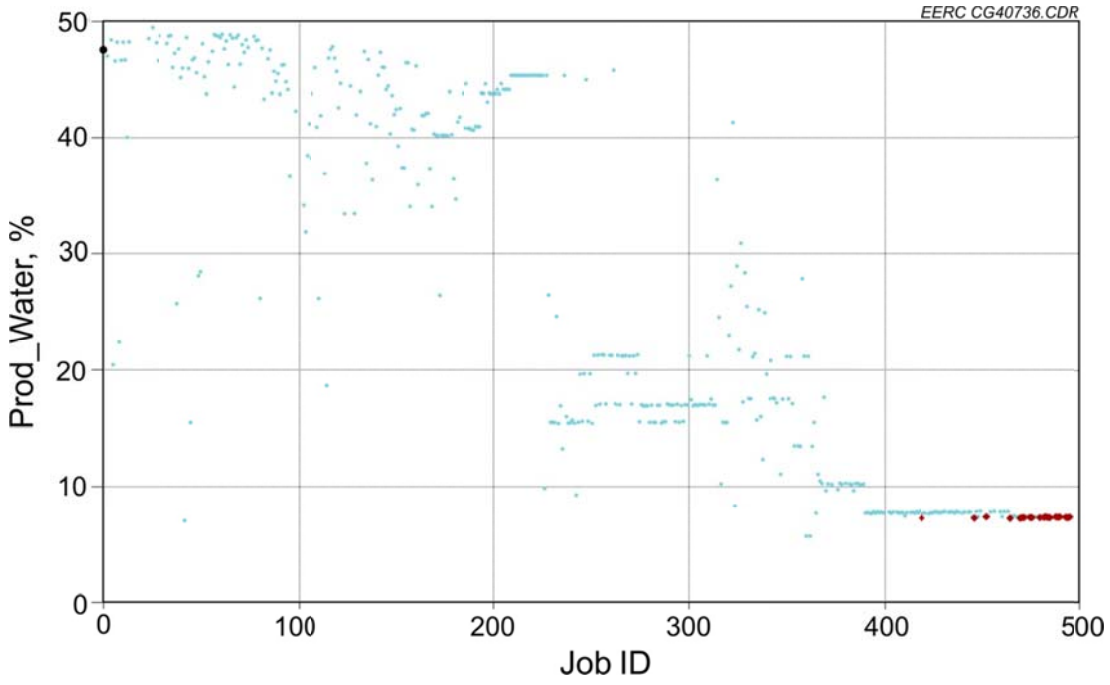

Figure 7. Final history-matching iteration of 494 jobs showing the convergence of the water production function (red dots represent the lowest error values).

During simulations, the sour CO_2 injection was initiated beginning in July 2014. The injection rate for all of the simulation cases was the same as previous cases, i.e., 120 MMscf/d of sour CO_2. Production gas rate control and water recycle were used in all of the predictive simulations.

History-Matching Nos. 1 and 2 are the top two "best" matching cases. Cases 1, 2, 5, and 6 were the 25- (Cases 2 and 6) and 50-year (Cases 1 and 5) injection scenarios in and around c-47-E; Cases 3, 4, 7, and 8 were also the 25- (Cases 4 and 8) and 50-year (Cases 3 and 7) injection scenarios but were in and around the c-61-E region (Table 3). The summaries of the gas-plume outlines for all of the cases are presented in Figures 8–15. The areal and cross-sectional views of the gas plumes and BHPs plots are provided in Figures E-13–E-91 in Appendix E: Predictive Simulations after History Matching.

Gas production was enhanced with water recycle in the CO_2 injection procedure (Figures 16–19). A push to gas flow by the water recycle from three grouped water disposal wells a-065-G, c-089-F, and d-048-L to the production wells may be attributed for this enhancement. The higher gas production was enhanced by 11.76%, while the lower one was enhanced by 6.73% (Figures 16–19). Furthermore, the other properties such as permeability ratio (k_v/k_h), saturation and relative permeability curves, etc., also contributed to gas production enhancement. For water disposal, besides water recycle, injected CO_2 is also an alternate way to increase production, especially with the grouped well c-089-F because of its proximity to the CO_2 injection wells.

Table 3. Eight Test Case Scenarios Used in the Predictive Simulations (after history matching) Comparing Injection Locations c-47-E and c-61-E

History-Matching No.	Test Case Scenario	Location	Injection Wells	Injection Well Names	Injection Time, years	Injection Rate, MMscf/d
1	1	c-47-E	3	c-18-E, c-47-E, and d-36-E	50	120
	2	c-47-E	3	c-18-E, c-47-E, and d-36-E	25	120
	3	c-61-E	3	a-91-E, c-61-E, and c-88-F	50	120
	4	c-61-E	3	a-91-E, c-61-E, and c-88-F	25	120
2	5	c-47-E	3	c-18-E, c-47-E, and d-36-E	50	120
	6	c-47-E	3	c-18-E, c-47-E, and d-36-E	25	120
	7	c-61-E	3	a-91-E, c-61-E, and c-88-F	50	120
	8	c-61-E	3	a-91-E, c-61-E, and c-88-F	25	120

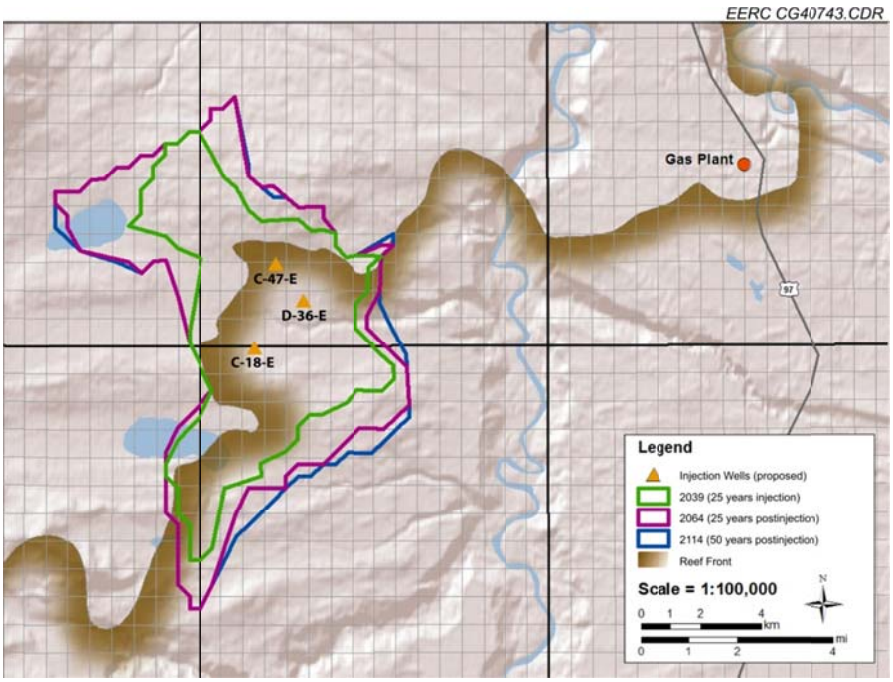

Figure 8. Case 1: CO_2 plume over time for the case with 50 years injection plus 50 years postinjection in and around c-47-E.

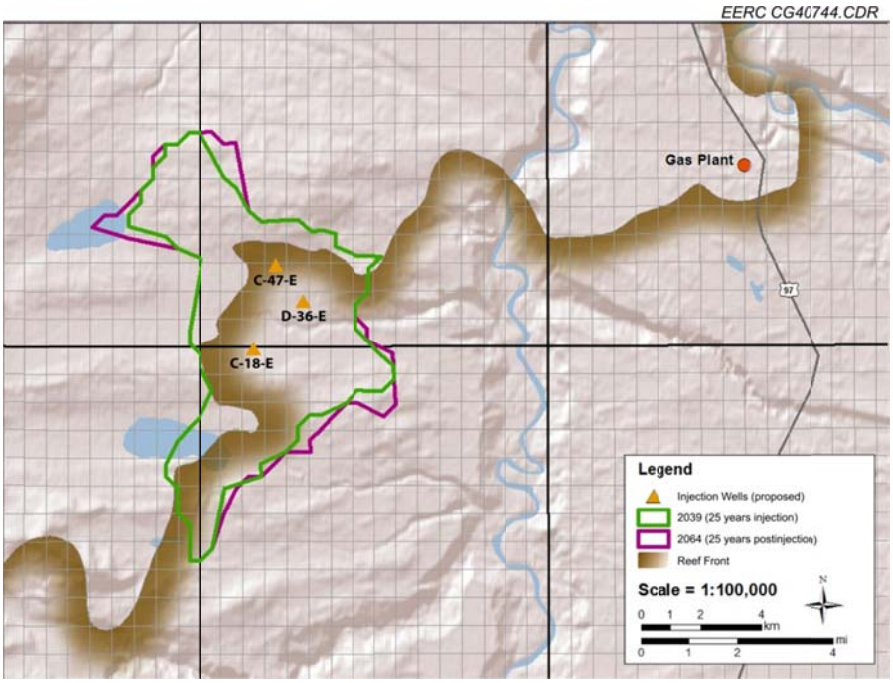

Figure 9. Case 2: CO_2 plume over time for the case with 25 years injection plus 25 years postinjection in and around c-47-E.

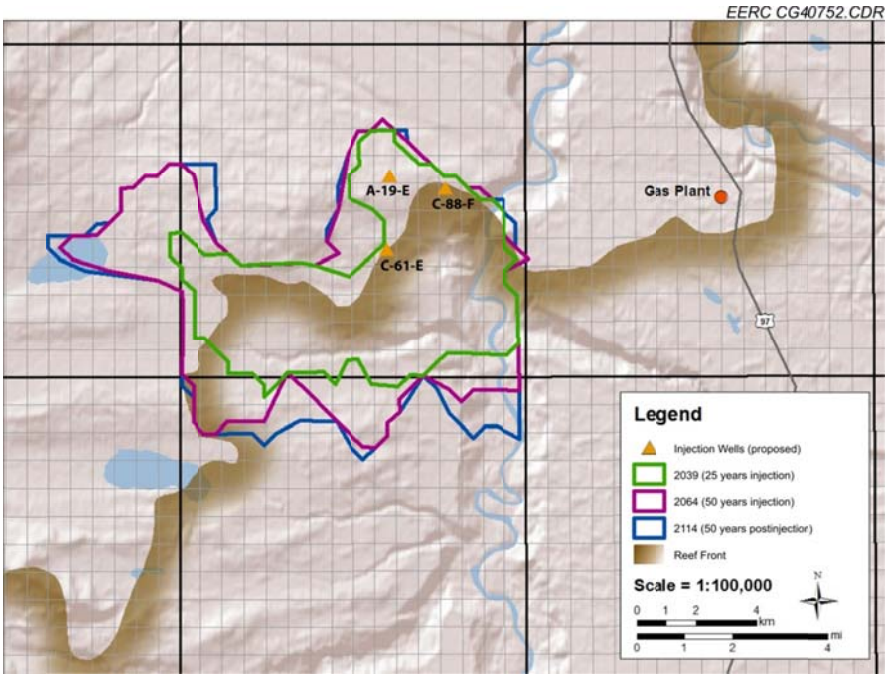

Figure 10. Case 3: CO_2 plume over time for the case with 50 years injection plus 50 years postinjection in and around c-61-E.

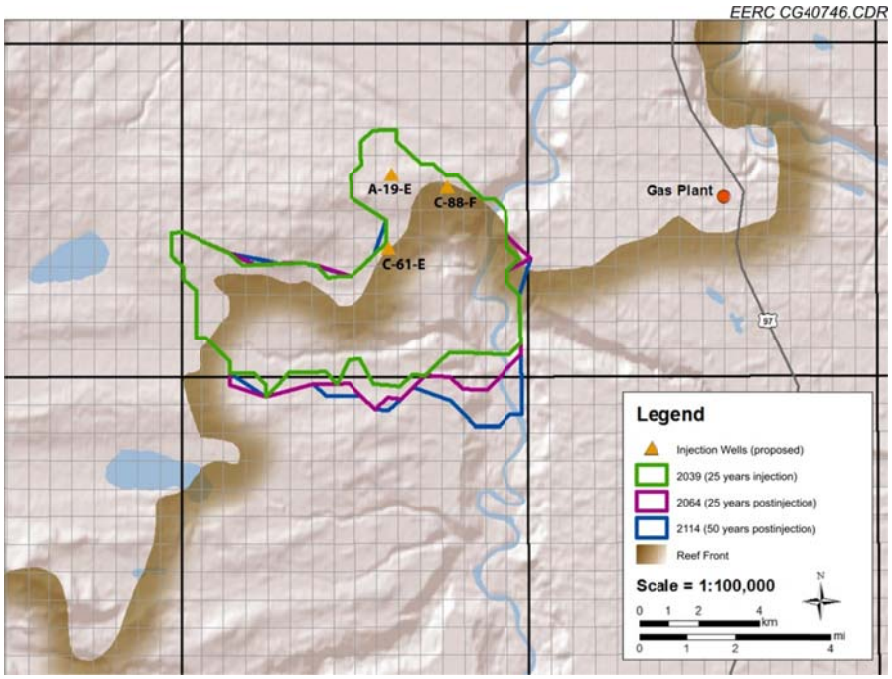

Figure 11. Case 4: CO_2 plume over time for the case with 25 years injection plus 75 years postinjection in and around c-61-E.

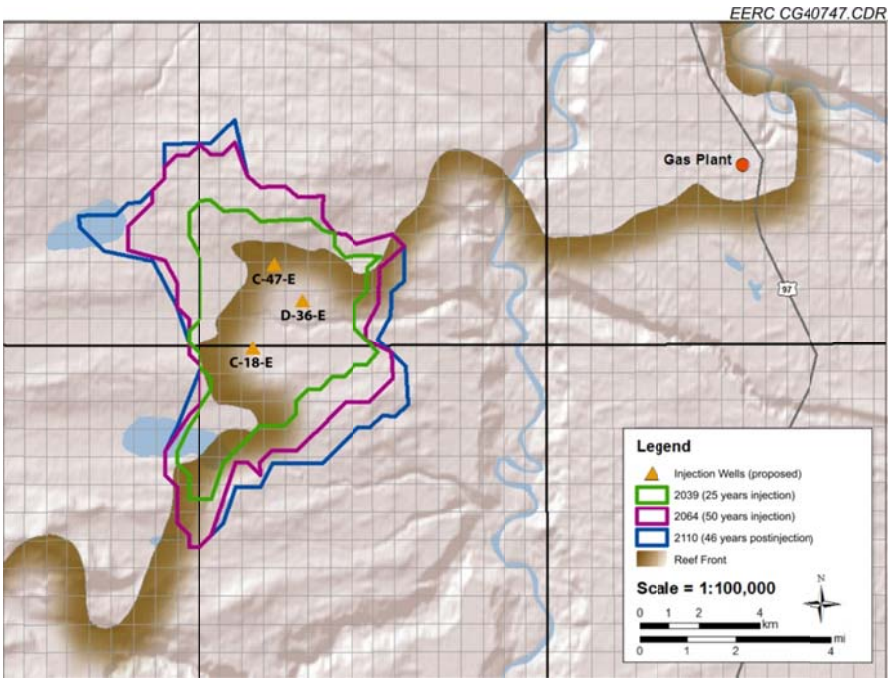

Figure 12. Case 5: CO_2 plume over time for the case with 50 years injection plus 46 years postinjection in and around c-47-E.

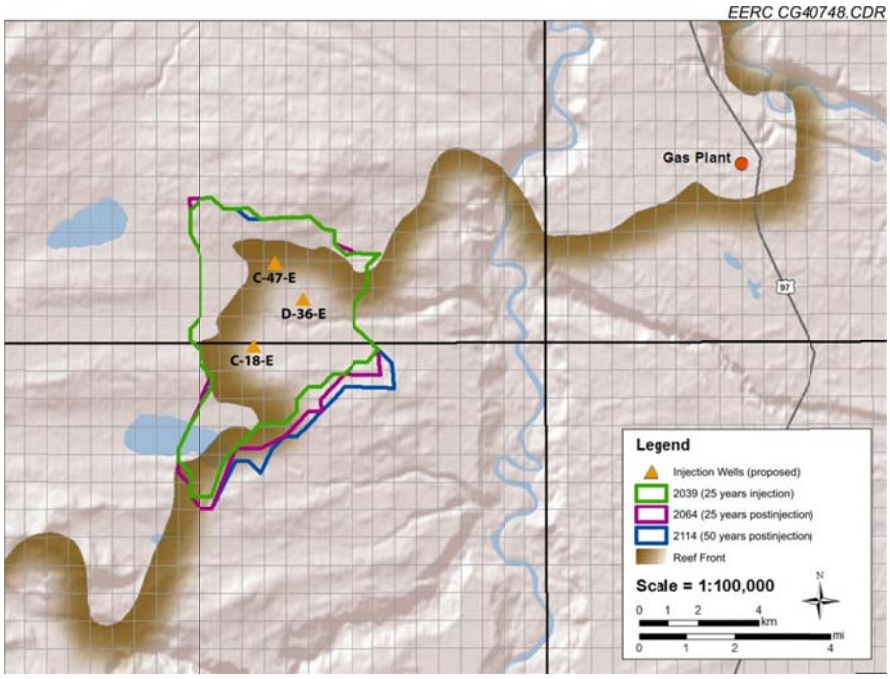

Figure 13. Case 6: CO_2 plume over time for the case with 25 years injection plus 75 years postinjection in and around c-47-E.

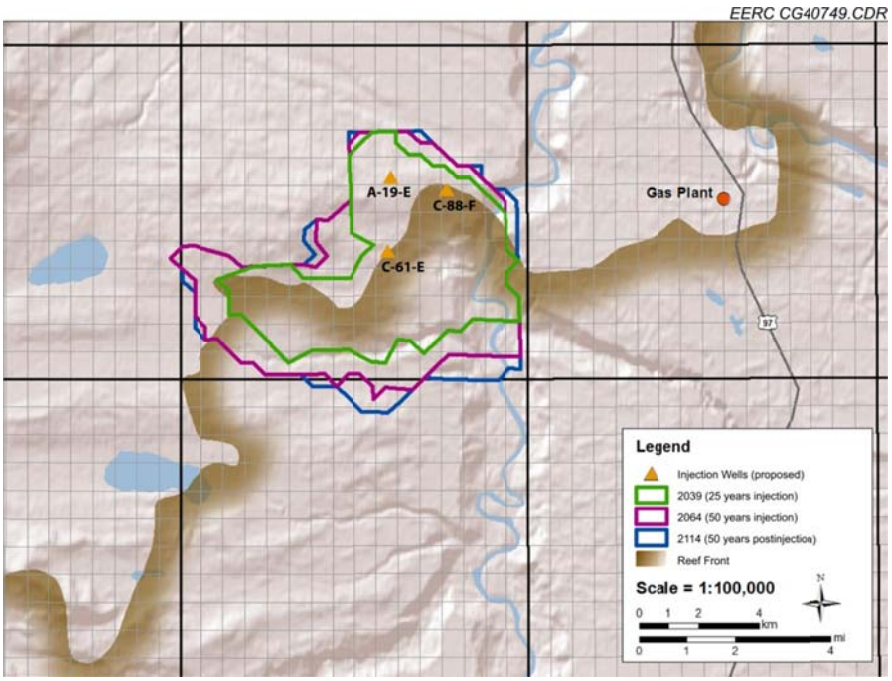

Figure 14. Case 7: CO_2 plume over time for the case with 50 years injection plus 50 years postinjection in and around c-61-E.

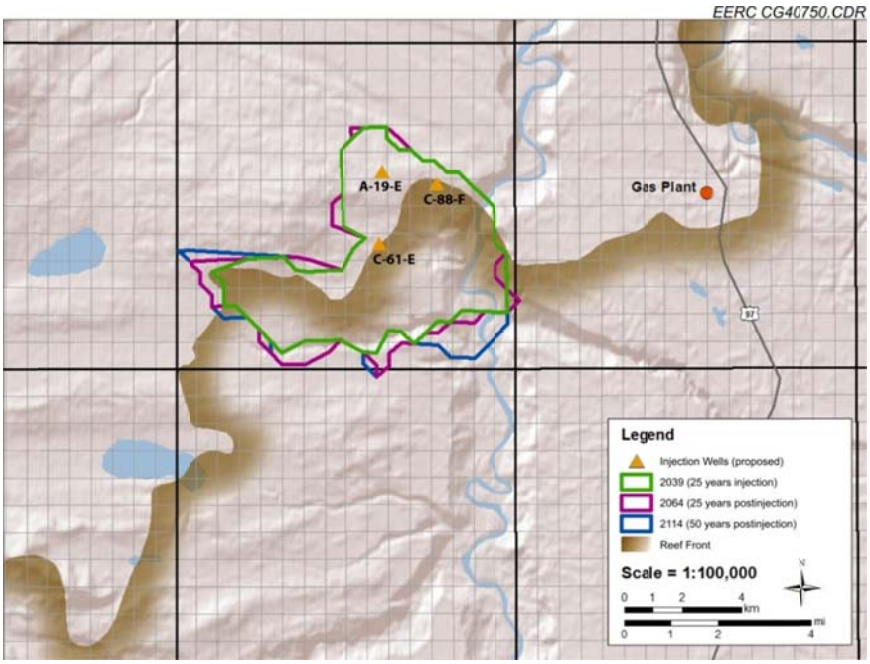

Figure 15. Case 8: CO_2 plume over time for the case with 25 years injection plus 75 years postinjection in and around c-61-E.

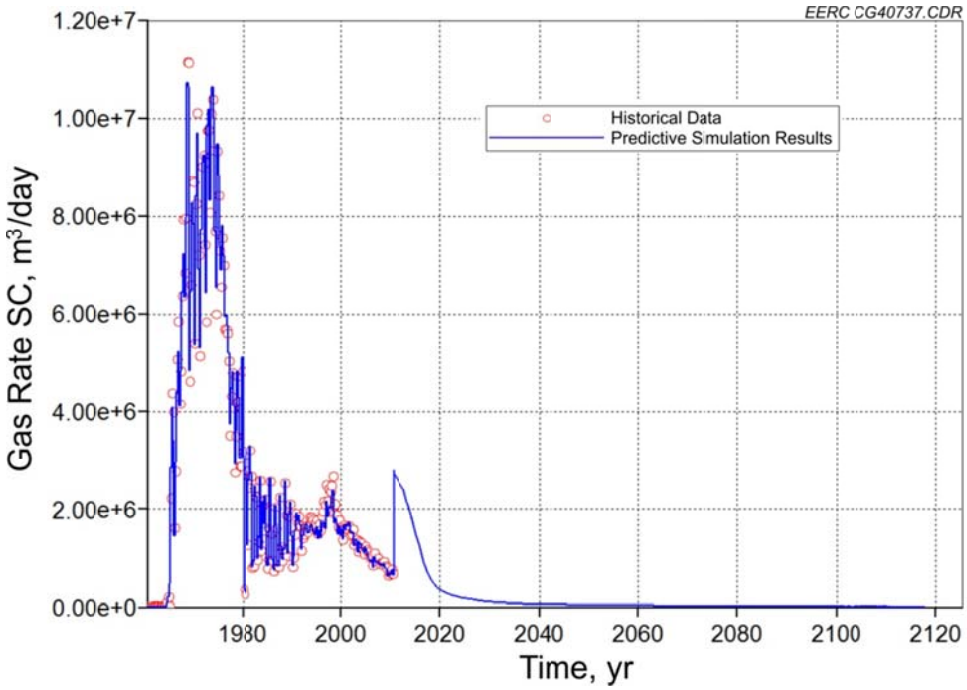

Figure 16. History-Matching No. 1: Production gas rate with production rate control and water recycle at standard conditions (SC). The dot curve represents the historical data that ended in July 2010, while the blue curve is the predictive simulation results with enhanced production by water recycle.

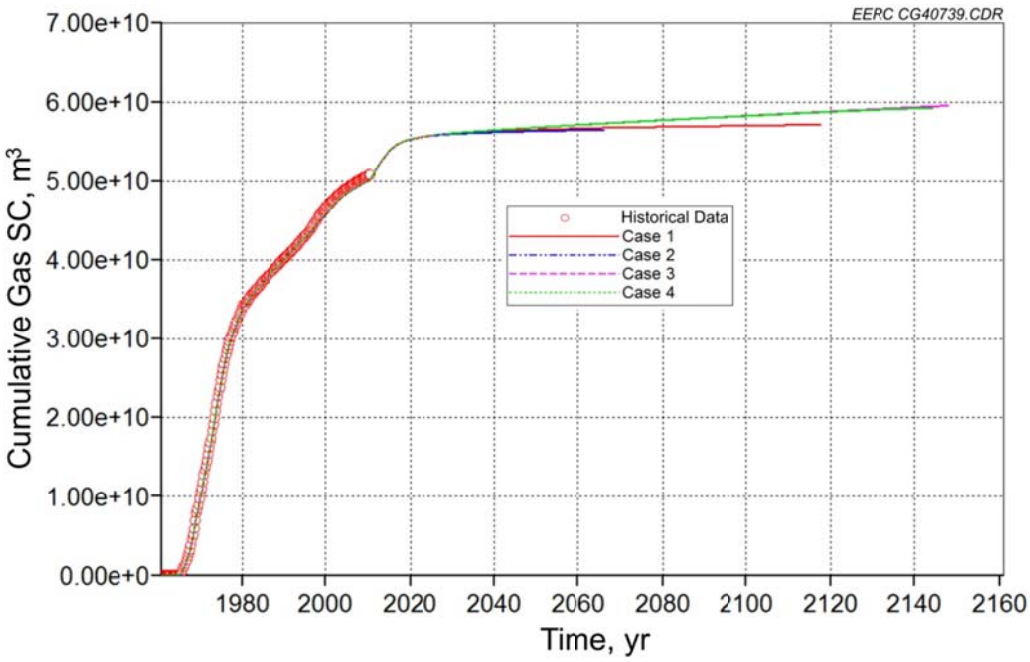

Figure 17. History-Matching No. 1: Cumulative gas production with production rate control and water recycle. The dot curve represents the historical data that ended in July 2010, while the blue curve shows the predictive simulation results with enhanced production by water recycle.

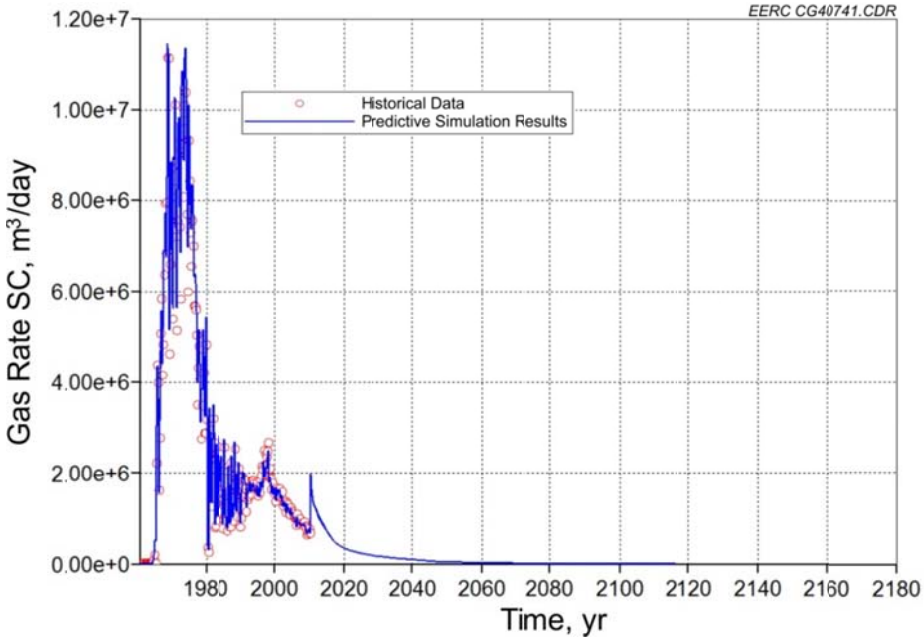

Figure 18. History-Matching No. 2: Production gas rate with production rate control and water recycle. The dot curve represents the historical data that ended in July 2010, while the blue curve shows the predictive simulation results with enhanced production by water recycle.

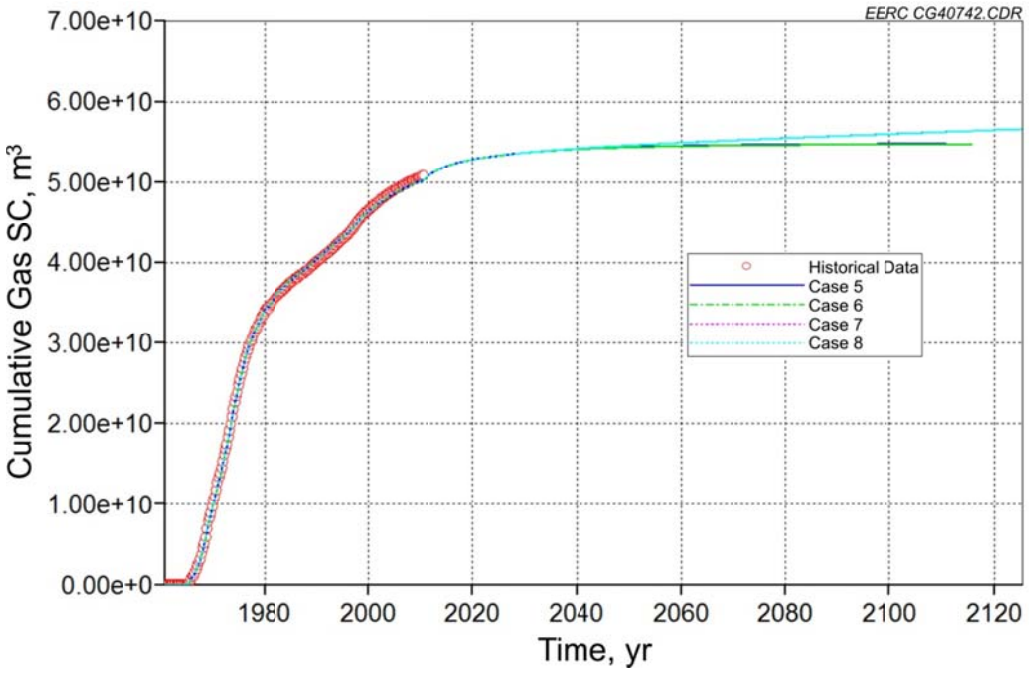

Figure 19. History-Matching No. 2: Cumulative gas production with production rate control and water recycle. The dot curve represents the historical data that ended in July 2010, while the blue curve shows the predictive simulation results with enhanced production by water recycle.

A comparison of pre- and post-history-matching results (Figures 20 and 21) indicates that the gas plumes for the injection site in and around c-47-E after history matching do not contact the gas pool with a 100-year simulation period, even though the plumes are larger than the ones obtained in pre-history matching. Instead of contacting Gas Pool B in the pre-history-matching case, the plumes mostly spread in the injection region for the cases after history matching. The BHPs (Figure E-93) indicate that the cases after history matching are below 23,000 kPa, which are lower than the ones (<25,000 kPa) obtained in pre-history matching. However, for the injection site in and around c-61-E, the plumes after history matching spread larger than the ones before history matching and contact the gas pools (Figures 22 and 23), although the maximum BHPs in all of the cases are within 26,000 kPa (Figure E-113). The details are presented in Figures E-92–E-131 in Appendix E.

As evident from Figures 16–19, simulated production and disposal data obtained in History Matching Cases Nos. 1 and 2 are fairly matched with historical data (from year 1961 to 2010). The simulated BHPs for both cases (Nos. 1 and 2) in the same injection location are also similar (Figures E-93 and E-113). However, both cases exhibited different enhanced gas production (rate and accumulation) and gas plumes over time (Figure 16–23) in predictive simulations. In view of observed variation in these predictive responses, more predictive simulations using "best" matching cases need to be run for further conditioning of dynamic models.

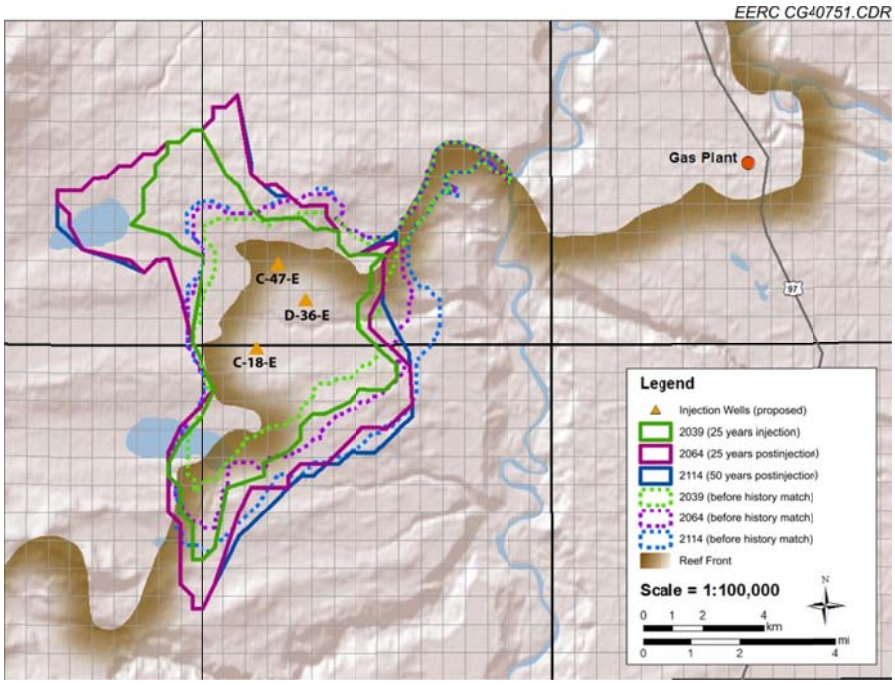

Figure 20. CO_2 plume comparisons over time for Case 1 and the case before history matching with 50 years injection plus 50 years postinjection in and around c-47-E.

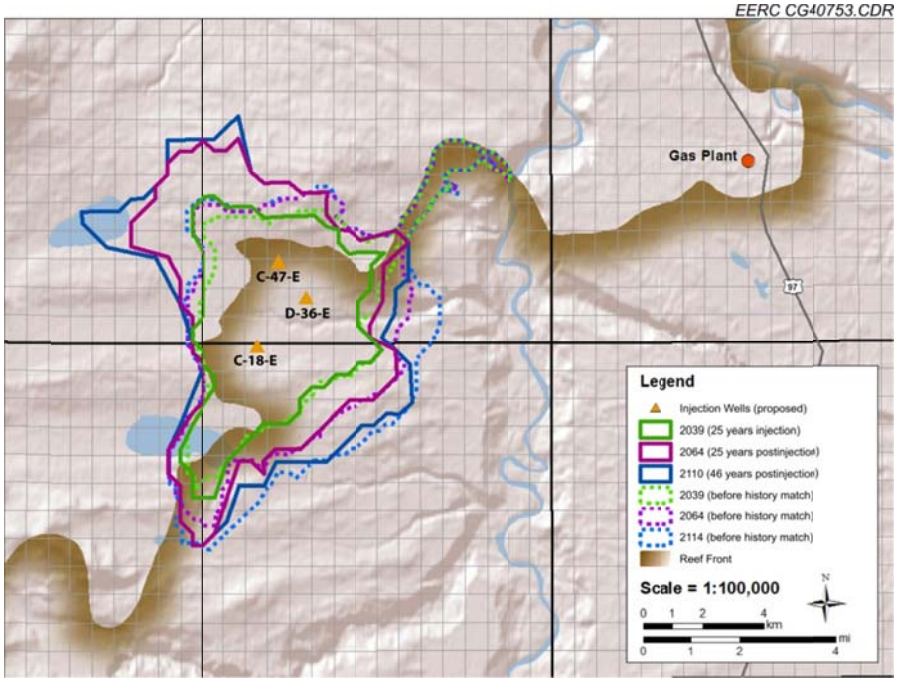

Figure 21. CO_2 plume comparisons over time for Case 5 and the case before history matching with 50 years injection plus 50 years postinjection in and around c-47-E.

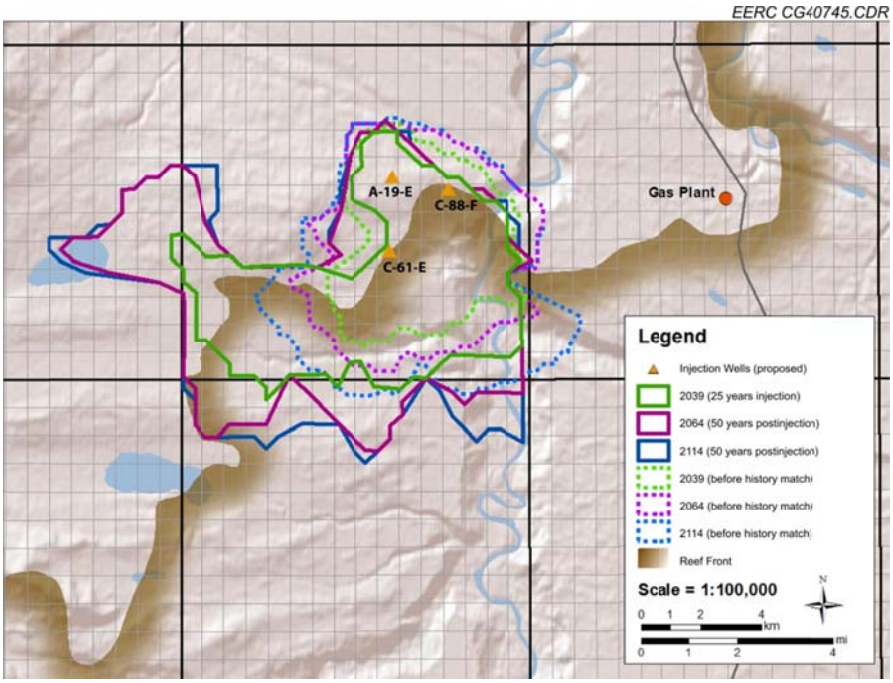

Figure 22. CO_2 plume comparisons over time for Case 3 and the case before history matching with 50 years injection plus 50 years postinjection in and around c-61-E.

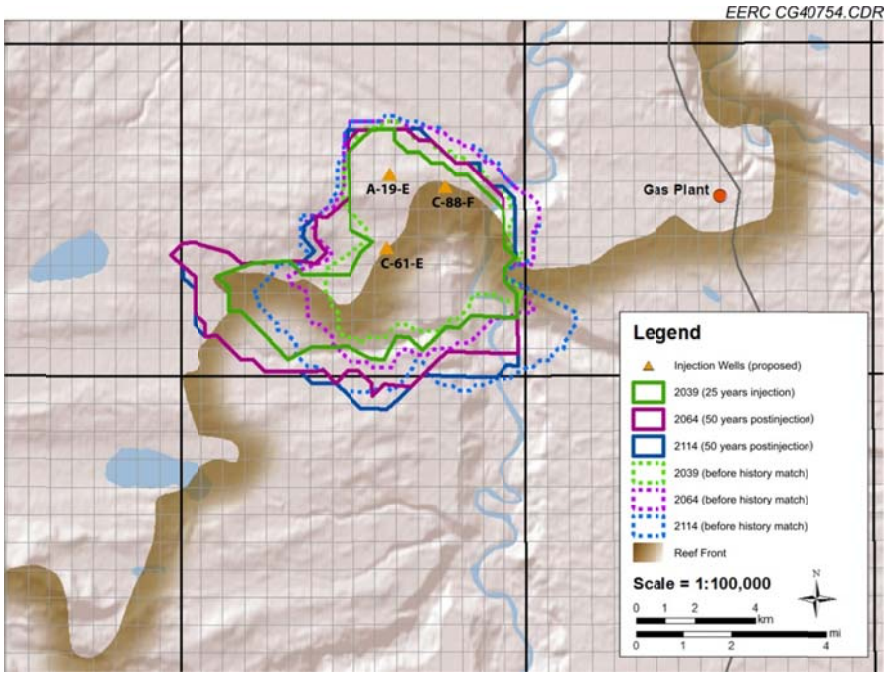

Figure 23. CO_2 plume comparisons over time for Case 7 and the case before history matching with 50 years injection plus 50 years postinjection in and around c-61-E.

MODEL LIMITATIONS AND APPLICABILITY

The historical data used for history matching in this project include the volume of production gas and water, water disposal, and scatter BHPs of wells from 1961 to 2010. For the history-matching period, no well data were available outside of Gas Pools A and B. Therefore, regions beyond the gas pools may introduce uncertainty to the modeling. Despite this potential uncertainty, a good match was obtained for gas and water volumes and BHPs. In view of history-matching results, the pressure distribution in the regions beyond the gas pools may require further examinations and comparison with hydrogeological analyses. The aquifer boundary conditions and low permeability barrier between Gas Pools A and B were introduced to match the pressure that was interpolated from measurements of the Exploratory Well c-061-E in the injection region. Although the pressure prediction was improved, because the data beyond the gas pools were scarce (especially the transient region between injection and gas pools), simulated pressures are quite uncertain.

The amount of CO_2 dissolved into water within the reservoir, and subsequent geochemical reactions, could affect the potential CO_2 storage evaluations, especially with long-term injection and postinjection periods at the reservoir conditions. As the CO_2 dissolves into the formation brine, a change in pH values may increase the chances of various geochemical reactions, including mineral dissolution and/or mineral precipitation. Thus, for predictive purposes, particularly in the longer simulations (> 50 years), the contributions of these geochemical reactions and associated CO_2 mineralization toward the CO_2 plume evolution need to be further studied by means of geochemical modeling. These studies require collection of formation fluid and new mineralogical samples and laboratory testing, both of which are not available at this time.

CO_2 dissolution, coefficients of geochemical reactions, and CO_2 mineralization rates are temperature-dependent. The scale of thermal effects on the simulations mainly depends on the temperature difference between the reservoir and the injected CO_2. If the difference between the injected CO_2 and the formation is large, then the fluid properties such as density and viscosity would be more variable and could have some effect on both the geochemical and potential geomechanical reactions. The thermal effects on long-term storage could also be addressed in geochemical modeling studies, which may not be possible until more accurate temperature, fluid, and mineral samples are collected from the exploratory wells.

SUMMARY

With the optimization and model validation, the Version 3 static geologic model shows a good match with the historical data, especially gas and water production, water disposal, and regional pressure distribution in the gas pools. A good history match for these data has provided improved confidence in the modeling of the geological characteristics in the project area and better appreciation of the performance of a CCS project at this site.

Dynamic predictive model results indicate that the geology in the study area is very conducive for the long-term storage of CO_2. The simulation results also validate prior

assumptions of excellent reservoir injectivity, lateral plume spreading, and the potential effectiveness and risk increases of alternative injection techniques for both injection locations in and around c-47-E and c-61-E. All of the tested injection sites show sufficient storage capacity for injection of the desired amount of CO_2 in the model area. However, the area in and around c-47-E demonstrated the greater capability for storing the desired amount of CO_2 within the model area because there is no contact to the gas pools within the 100-year simulation period and the maximum BHPs are below 23,000 kPa for all cases after history matching.

To further confirm the evaluations presented in the study, two main recommendations are suggested to be included in the future modeling and simulation study: 1) more geological information for the injection region, especially in the c-47-E region and the transient region between gas pools and injection area, to confirm the existence of adequate reservoir rock and the presence or lack of any low-permeability barrier (or fault) that was artificially introduced in the dynamic model and 2) integrating various physical phenomena such as geochemical reactions, geomechanical behaviors, and geothermal effects into the dynamic model. Such integration will improve the understanding of the sink–seal system comprehensively for more accurate predictions.

REFERENCE

Yang, C., Nghiem, L., Card, C., and Bremeier, M., 2007, Reservoir model uncertainty quantification through computer-assisted history matching: 2007 SPE Annual Technical Conference and Exhibition, Anaheim, California, November 11–14, 2007, 109825-MS.

APPENDIX A

STATIC GEOLOGIC MODELING DEVELOPMENT

STATIC GEOLOGIC MODELING DEVELOPMENT

GEOLOGIC BACKGROUND

The Fort Nelson area in northeastern British Columbia lies within the northwestern corner of the Alberta Basin (Figure A-1). The sedimentary succession in the Fort Nelson area consists, in ascending order from the Precambrian crystalline basement to the surface, of Middle and Upper Devonian carbonates, and shales; Mississippian carbonates; and Lower Cretaceous shales overlain by Quaternary glacial drift unconsolidated sediments (Figures A-2 and A-3).

Figure A-1. Location of the Fort Nelson demonstration site and sedimentary basins within the PCOR Partnership region.

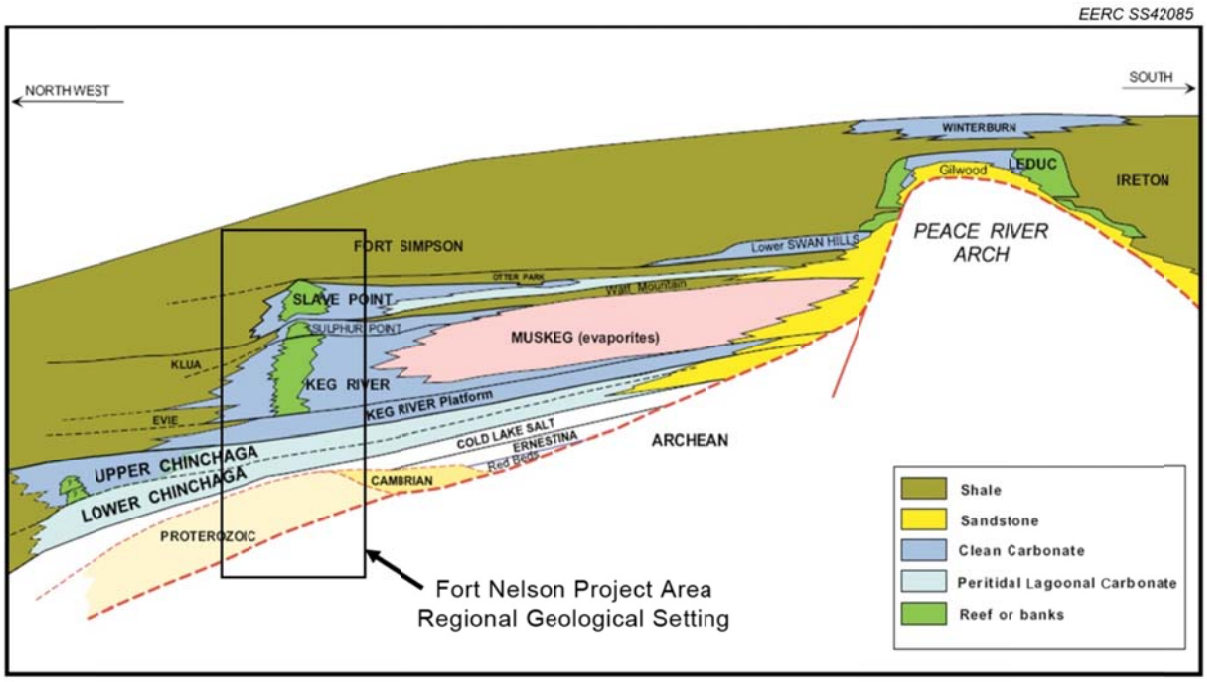

Figure A-2. Stratigraphic architecture of the Middle Devonian Formations in the Fort Nelson area, northeastern British Columbia (British Columbia Ministry of Energy, Mines, and Petroleum Resources, 2007).

Exploration activities for mineral and energy resources in the area over the last 50 years have yielded a significant amount of information about the geology of northeastern British Columbia and northwestern Alberta. The carbonate platforms and reefs of the Middle Devonian Formations in the northern Alberta Basin are known to contain large quantities of hydrocarbons, which suggests that the formations have adequate porosity, permeability, and trapping mechanisms to support the long-term storage of large volumes of CO_2 (Sorensen and others, 2005; Stewart and Bachu, 2000). Hydrocarbon production in the Fort Nelson area, in the form of natural gas, is primarily from reservoirs in reefs of the Middle Devonian Slave Point Formation. It is anticipated that saline-filled formations within the underlying Middle Devonian Elk Point Group, specifically the Sulphur Point and Keg River formations, will be the primary injection zones for the Fort Nelson carbon capture and storage (CCS) project. Between the Slave Point Formation and the underlying Sulphur Point and Keg River Formations is the Watt Mountain Formation, a primarily silty mudstone unit with low permeability. However, because it is relatively thin (approximately 5 meters thick or less in some parts of the Fort Nelson area), it is discontinuous and lacks consistent porosity and permeability. The Watt Mountain is, therefore, considered to be a local low permeability barrier within the reef, retarding upward movement of injected CO_2 into the Slave Point Formation, which is part of the overall storage capacity.

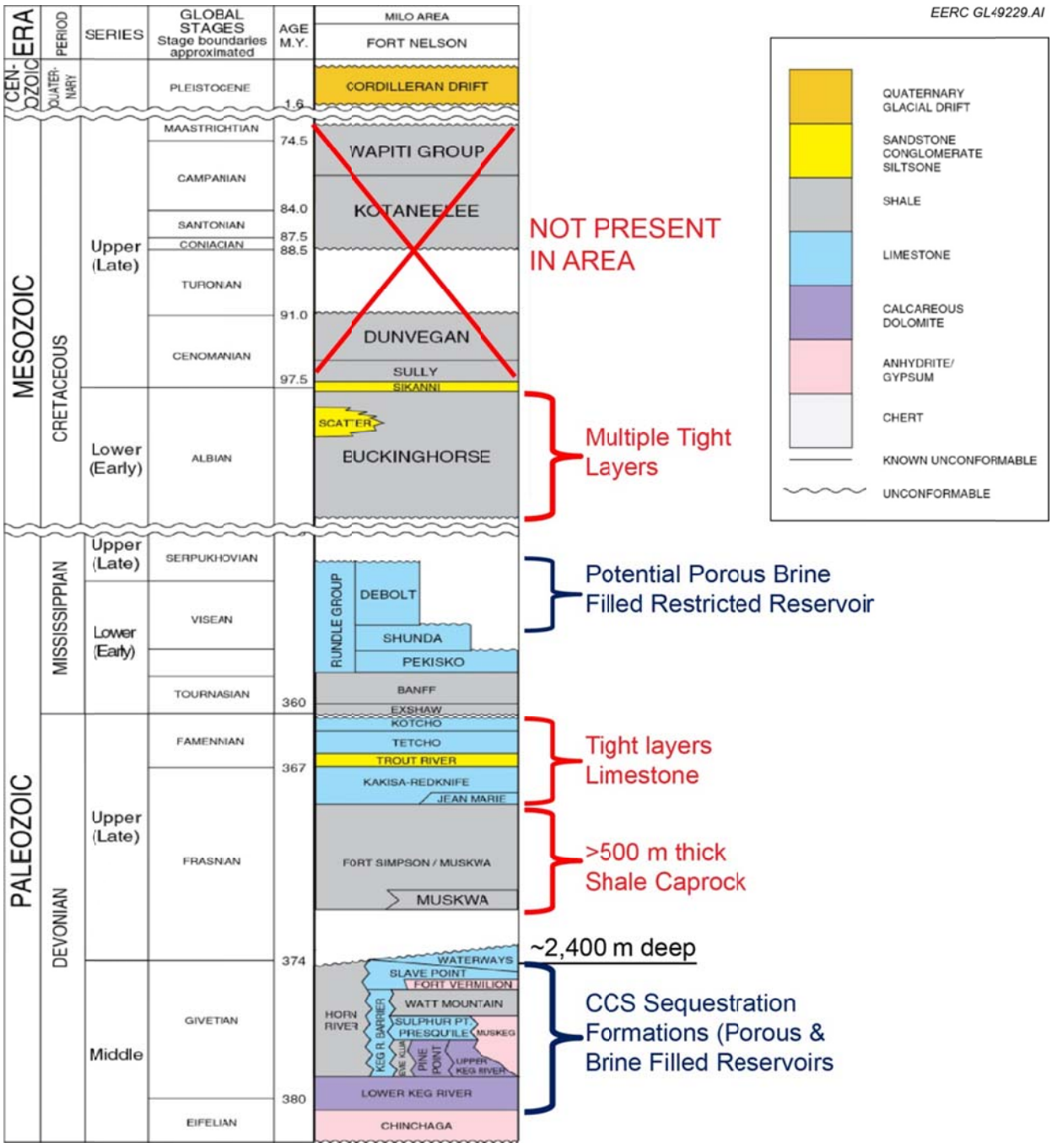

Figure A-3. Stratigraphic column for the Fort Nelson CCS project area.

In the Fort Nelson area, potential injection strata, the Sulphur Point and Upper Keg River formations, are dominated by carbonate rocks (limestones and dolomites) with prominent reef and/or bank structures that have porosity and permeability characteristics adequate for large-scale CO_2 injection. Only a few wells have been drilled into the these formations in the vicinity of the proposed injection area because of a lack of hydrocarbon resources in this lower part of the reef. Therefore, data on the porosity and permeability of those rock formations in the area are

sparse. However, although rock property data for the area are limited, the data that do exist suggest that porosity and permeability are likely adequate to support large-scale injection of CO_2. The lack of existing data below the upper portion of the Slave Point Formation (i.e., for the Watt Mountain, Sulphur Point and Keg River formations) in the Fort Nelson area means that exploration-level geological characterization activities (e.g., well drilling and testing, seismic data acquisition and processing, etc.) must be conducted to evaluate storage capacity, injectivity, and other containment parameters of the sink–seal system.

With respect to seals that will prevent upward migration of the injected sour CO_2, the Watt Mountain is expected to be an internal reef baffle slowing down the upward migration of injected CO_2 from the Sulphur Point/Keg River Formations into the Slave Point Formation. Above the Slave Point Formation, the shale formations of the overlying Middle Devonian Muskwa and Fort Simpson shales will provide the primary seal with respect to preventing leakage to the surface. Above the Fort Simpson shale are several additional regional aquitard layers providing additional containment between the target injection formations and the surface, specifically tight limestone formations Redknife, Tetcho, and Kotcho and the Mississippian-age Banff Formation. It is to be noted that the Mississippian age Rundle Group may be potentially porous in the project area, but the porosity lacks continuity and is brine-filled where it is porous. Above the Rundle Group is the shale of the Cretaceous-age Buckinghorse formation, which provides yet another layer of protection from leakage to the surface. In the project area, the Scatter Formation exists which is believed, at the date of this report, to be providing some of the groundwater in the project area.

VERSIONS OF THE STATIC MODEL

Static reservoir modeling based on the geological characterizations included Versions 1–3, evolving from a scoping-level model to a more detailed model. An overview for each model version is provided below.

Version 1 Scoping Model

The Version 1 scoping model was developed by Computer Modelling Group Ltd. (CMG) and Spectra Energy's Geologic Characterization Team. It was developed after Exploratory Well c-61-E was drilled in March 2009. The Version 1 scoping model was an initial "flow units" model designed to do a quick check on the risk of impact to offset Slave Point gas cap resources and included the following:

- Preliminary data from the logging, testing, and coring of Well c-61-E.
- A stratigraphic and structural model that was developed using a preliminary geological understanding of the flowing units (aquifers) and the aquitard layers that included only the formation brine and injected CO_2 and no in situ gas pools present.
- Generic reservoir properties, such as permeability and porosity, distributed homogeneously by model flowing zone and aquitard layer.

A 200-year simulation was run, with carbon dioxide (CO_2) injection conducted over the first 100 years and the second 100 years representing the postinjection period during which the CO_2 was allowed to migrate by buoyancy. Predictive injection simulations were run using Well c-61-E and a second generic well located about 5 km to the west as injection wells. Each well was simulated to inject 1.1×10^6 tonnes per year of CO_2. Outlines of two nearby gas pools (Clark Lake Slave Point A and B) were included in the model to determine when and if the injected CO_2 from Well c-61-E would potentially contact either gas pool over a 100-year time frame. The results of these simulations were favorable, as they predicted that:

- Formation pressures would not exceed 80% of the estimated fracture pressure gradient (17 kPa/m), indicating that the mechanical strength of the reservoirs and seals is adequate to hold the injected volumes of CO_2 without fracturing.

These predictions were considered to represent the worst-case scenarios for CO_2 migration, since the injection "flowing unit" was direct aquifer to offset gas pools, only had homogeneous properties, and only structural CO_2 trapping was considered. Other CO_2-trapping mechanisms that would further restrict migration, such as capillarity and aqueous dissolution and mineral formation, were not included.

Version 2 Model

The Version 2 model was developed by Spectra Energy's Geologic Characterization Team and the Energy & Environmental Research Center (EERC) immediately after the Version 1 scoping model (summer 2009). The Version 1 scoping model and the preliminary results of the Version 2 model were used as the basis for the first-round risk assessment. Details of the Version 2 model included the following:

- A more rigorous understanding of the structure, reef edge, facies, or zones and a more detailed understanding of the reservoir and cap rock properties.

- Reasonable variations on many of the reservoir parameters, including the level of communication between different formations or horizons and the influence of the production and injection activities in the nearby gas pools (Figure A-4).

- A geologic model using Schlumberger's Petrel seismic-to-simulation software, which was imported into CMG's generalized equation-of-state model (GEM) simulator for predictive simulations.

- Models for the formation brine, in situ natural gas (methane, CO_2, and H_2S), and injected sour CO_2 (composition ranging from 85% CO_2 and 15% H_2S to 95% CO_2 and 5% H_2S), which were imported into the CMG GEM simulators for all simulation in this report.

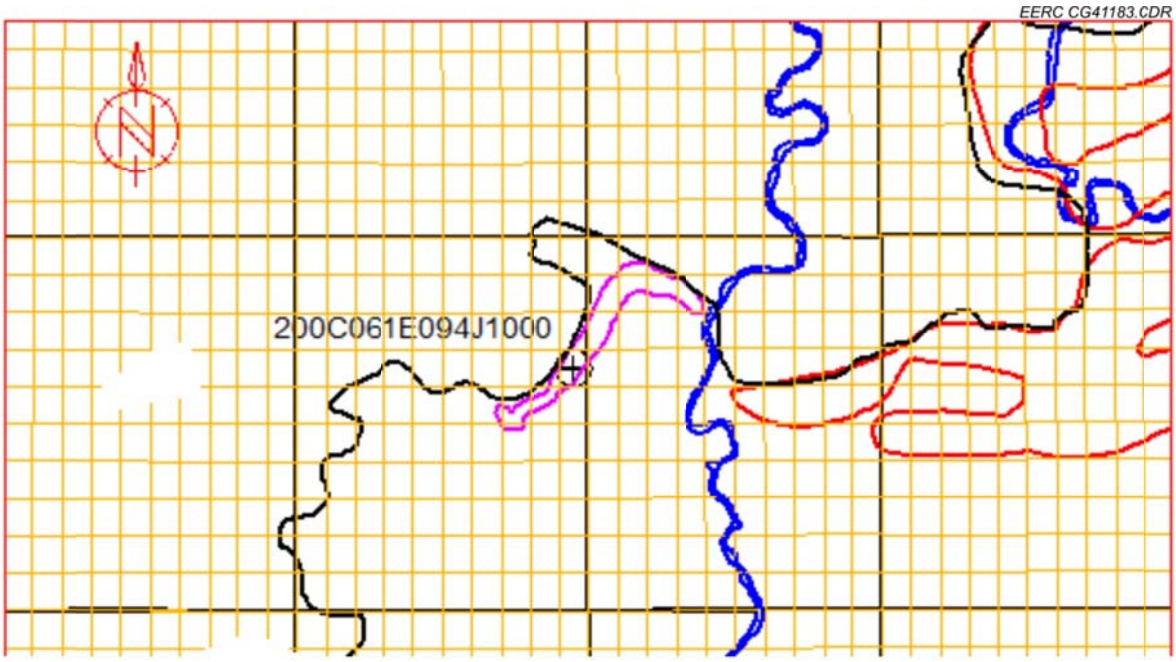

Figure A-4. Plan view of Clark Lake Slave Point A gas pool (red outline), B gas pool (violet outline), reef front (black outline), and Injection Well c-61-E.

- Processes for 1) modeling multiphase flow of water (brine) and gas (methane, CO_2, and H_2S), 2) modeling mass transfer between water and gas phases (special focus on CO_2 and H_2S dissolution into formation brine), and 3) uncoupled geochemical modeling (i.e., the geochemical modeling was a stand-alone model and not "coupled" with the reservoir model).

Multiple injection scenarios, both in terms of location of the injection points and in the number of injectors, were tested using Version 2 of the model. Typically, three to six injectors were modeled, including Well c-61-E. For all model runs, 2 million tonnes a year of CO_2 were injected for a duration of 50 years (100 million tonnes over the life of the project), without exceeding 80% of the fracture gradient (17 kPa/m). Some of the injection scenarios showed that the injected sour CO_2 may contact the neighboring Clark Lake Slave Point A gas pool before the end of the expected productive life of the field (another 30 years). This was identified as a potential risk, and additional data collection and a reevaluation of the potential injection scenarios resulted in the movement of possible injection sites to areas farther to the west to avoid contacting the Clark Lake Slave Point A gas pool during its productive life.

During the winter of 2009–2010, additional two- and three-dimensional (2-D and 3-D) seismic data were purchased and reprocessed. In addition, Well c-61-E was reentered and subjected to leakoff and a water injection test in the commingled Slave Point and Sulphur Point Formations. Results of the water injection test indicated that the permeability of the primary target injection zone is high enough to support large-scale injection of CO_2 and connectivity to a large volume of the permeable reservoir. These data were integrated into the next version of the model, i.e., the Version 3 model.

Version 3 Model

The Version 3 model was jointly developed by the EERC and Spectra Energy's Geologic Characterization Team. Based on available geophysical and seismic data, 13 domains and ten zones were identified. Domains were based on zones of consistent rock properties that may relate to a depositional setting or structural feature. In some cases, a domain may cross formation boundaries (e.g., Upper Chinchaga and Lower Keg River). The formation intervals that were included in the 13 domains include Fort Simpson Formation, Muskwa Formation, Otter Park Formation, Upper and Lower Slave Point Formation, Watt Mountain Formation, Sulphur Point Formation, Upper and Lower Keg River Formation, and Upper and Lower Chinchaga Formation (Table A-1 and Table A-2).

Table A-1. June 2010 Petrophysical Reservoir Model Domains

Spectra Domain Number	Domain Name	Formation
1	Shelf margin dolomite	Sulphur Point
2A	Shelf margin dolomite	Upper and Lower Slave Point
2B	Shelf dolomite	Upper and Lower Slave Point
3	Upper foreslope to shelf/reef margin dolomite	Lower Keg River/Upper Chinchaga
4	Restricted intertidal shelf dolomite	Upper and Lower Slave Point
5	Deep marine shelf dolomite/limestone	Upper Slave Point/Sulphur Point Upper and Lower Keg River
6	Unstable slope limestone/dolomite	Lower Keg River/Upper Chinchaga
7	Restricted shelf platform dolomite/anhydrite	Chinchaga
8	Deep shelf limestone	Upper and Lower Slave Point Sulphur Point
9	Otter Park basinal calcareous shale	Otter Park
10	Sulphur Point/Evie shelf limestone	Muskwa/Sulphur Point Upper and Lower Keg River/Chichanga
11	Sags	Vertical hydrothermal conduits
12	Shallow marine	Watt Mountain

Table A-2. Model Domains and Parameters

				Porosity			Permeability, mD		
					Sensitivity Range		Sensitivity Range		
	Rock Type	Formation	Dolomitization	Base Case	Low	High	Base Case	Low	High
1	Dolomite	Basal Slave Point/Sulphur Point/Top Keg River	Pervasive HTD, vugs, fractures	8%	5%	11%	600	200	1000
2A	Dolomite	Upper Slave Point	Extensive HTD, vugs, fractures	9%	6%	10%	200	50	300
2B	Dolomite	Upper Slave Point/Lower Slave Point	Extensive HTD, vugs, small fractures	6%	5%	9%	10	1	40
3	Dolomite	Keg River/Upper Chinchaga	Regional matrix HTD, pores, vugs, fractures	5%	4%	6%	10	5	20
4	Dolomite	Upper Slave Point and Sulphur Point	Variable, strata-selective HTD, small vugs, fractures	Interlayer 9%/6%	5%/9%	6%/9%	100/10	200/0.1	200/1
5	Dolomite/limestone	Lower Slave Point/Sulphur Point/Keg River	Variable, strata-selective HTD	Interlayer 9%/2%	2%/3%	6%/9%	100/0.1	200/.01	200/0.1
6	Limestone/dolomite	Keg River	Regional matrix	Interlayer 2%/6%	2%/3%	5%/9%	0.1/10	.01/40	.01/41
7	Dolomite/anhydrite	Chinchaga	Regional matrix	0%	0%	0%	0	0	0
8	Limestone	Slave Point/Sulphur Point	None/minor local HTD overprint	2%	1%	3%	0.1	0.01	1
9	Calcareous shale	Otter Park	None	3%	2%	4%	100	50	100
10	Shale/limestone	Upper Keg River/Klua/Evie	None/minor local HTD	6%	4%	9%	250	175	335
11	Dolomite	Vertical Hydrothermal Conduits	Pervasive HTD	5%	1%	10%	30	1	100
12	Silty dolomite/limestone	Watt Mountain	Matrix to none	3%	2%	4%	0.01	0.01	1

Note: Suphur Point and Keg River Aquifer domains projected from Slave Point model; domains arranged from most to least permeable/porous.

From available petrophysical and seismic data, the potential injection unit was modeled as primarily dolostone rock (~95%), representing depositional environments of middle and upper foreslope to reef margin shoal. The lithofacies were determined as grainstones, rudstones, and floatstones. Dominant biota is represented mainly by dendroid to tabular stromatoporoids and thamnoporid corals. The matrix includes secondary pervasive hydrothermal dolomitization (HTD), vugs, and fractures. Average porosity, determined from core analysis, was estimated as 9%, and permeability, based on drillstem testing analysis, was estimated in the range of 50–800 mD.

Based on the available geophysical data, testing analyses, petrophysical analyses, review of available core, and interpretation of the facies for the barrier reef complex within the Fort Nelson CCS project area, several iterative static models were constructed. After a meeting in June of 2010 and after the additional information became available, a revised static geologic model was constructed. Porosity and permeability by domain and zone were populated with a data set provided by Spectra Energy. Surface elevation from the topographic map was added, and the temperature gradient, salinity, and pressure information was updated with data from Canadian Discovery Ltd. (CDL) (Canadian Discovery Ltd., 2009). Seismic data in conjunction with analyses of drillstem tests, core analyses, and facies interpretation were used as an aid in assessing the variogram ranges. Refined interpretation of structure contour and small synthetic and antithetic faults from seismic data were populated (Figures A-5 and A-6).

The main updates in the Version 3 model are summarized as follows:

- More detailed log analyses and the newly reprocessed 2-D and 3-D seismic data.

- An updated structural model developed by Spectra Energy's Geologic Characterization Team to include a better definition of the reef edge, formation tops and isopachs, faults, and features which create a structural trap.

- Heterogeneous reservoir properties, such as permeability and porosity, based on a more detailed understanding of their distribution throughout the model, not only vertically, but also laterally.

Three to six injection wells were utilized in the Version 3 model simulations. Most were focused on an area located more than 5 km west from the original Well C-61-E, although there were a few cases run around the original c-61-E for more comparison. Injection and CO_2 plume migration simulations were conducted under a variety of different injection locations and operational scenarios (Appendixes C and E of the main report).

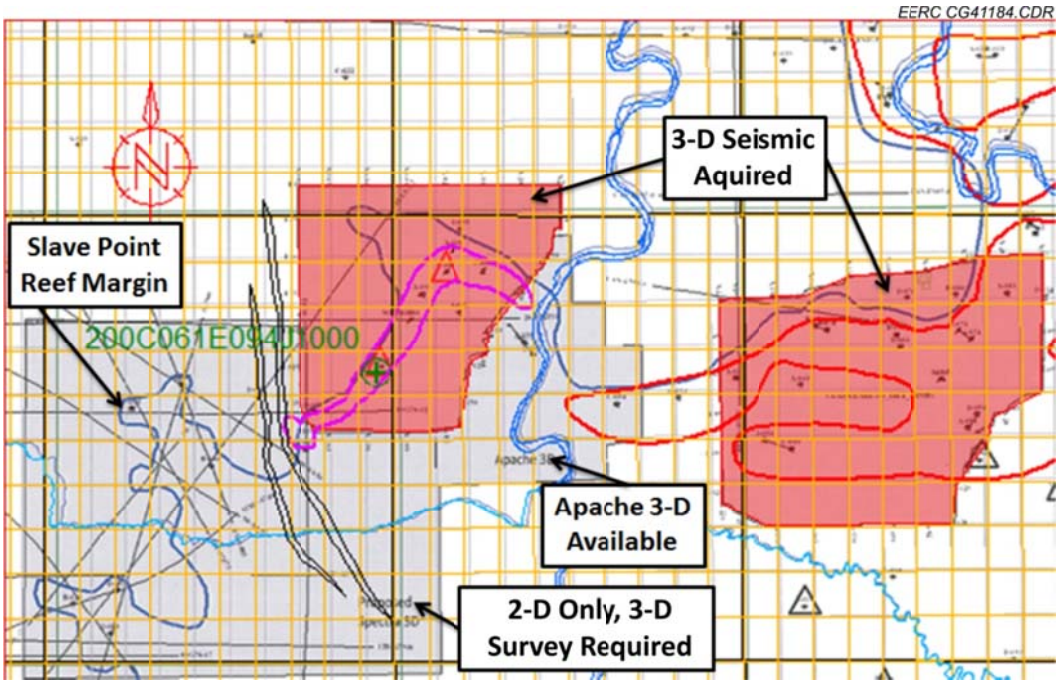

Figure A-5. Plan view showing relationship of seismic survey data locations (acquired, available, and proposed) to Clark Lake Slave Point A gas pool (red outline), B gas pool (violet outline), former Injection Well c-61-E, and faulting (black outline).

REFERENCES

British Columbia Ministry of Energy, Mines, and Petroleum Resources, 2007, www.em.gov.bc.ca/subwebs/oilandgas/petroleum_geology/cog/nebc.htm (accessed November 2007).

Canadian Discovery Ltd., 2009, Hydrogeology of the Mid-Devonian carbonate bank complex, Milo-Clarke Lake area, northeastern British Columbia: Confidential report to Spectra Energy, July.

Sorensen, J.A., Jensen, M.D., Smith, S.A., Fischer, D.W., Steadman, E.N., and Harju, J.A., 2005, Geologic sequestration potential of the PCOR Partnership region: Plains CO_2 Reduction (PCOR) Partnership topical report, www.netl.doe.gov/technologies/carbon_seq/partnerships/phase1/pdfs/MDJ-Geologic%20Sequestration%20Potential.pdf (accessed October 15, 2007).

Stewart, S., and Bachu, S., 2000, Suitability of the western Canada sedimentary basin for carbon dioxide sequestration in geological media: Presented at the 2000 Canadian Society of Exploration Geophysicists Conference, August 6–11, 2000.

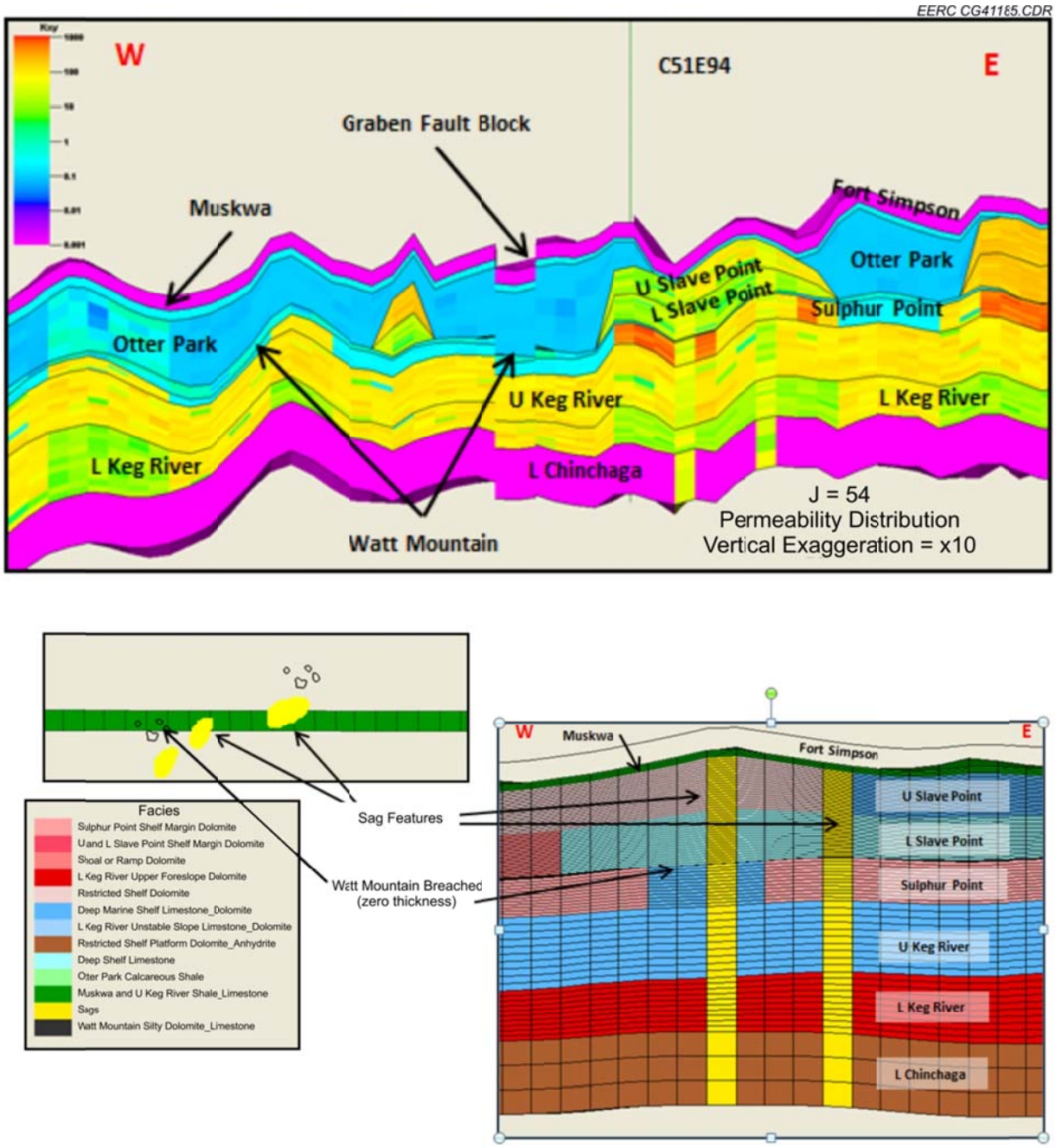

Figure A-6. Fort Nelson CCS project Version 3 Model (June 2010).

APPENDIX B

BASE CASE AND INITIAL SCENARIO EXPLORATIONS

BASE CASE AND INITIAL SCENARIO EXPLORATIONS

INTRODUCTION

Based on the latest geologic model Version 3, a base case was constructed and scaled up for scenarios of initial exploration which includes variations of permeability on cap rock and reservoir, fault transmissibility, and vertical to horizontal permeability ratio (Table 1 of the main report). The purpose of such tests is to explore the effects on CO_2 plume and pressure buildup because of the various properties listed above and provide insight on potential risks and what further areas of reservoir investigation should be undertaken to more accurately determine the permeabilities and fault transmissibility for future modeling and risk assessments.

The geologic model of the Version 3 Model was clipped from an original area of 2030 to 967 km^2 (Figure B-1). Three proposed CO_2 injection wells (c-18-E, c-47-E, and d-36-E) were used in each of the five simulations (Table 1 of the main report). Each test case scenario is described in detail below.

TEST CASE SCENARIO 1: BASE CASE, WITH AND WITHOUT CO_2 INJECTION

The purpose of the Scenario 1 base case was to monitor the contact between the injected CO_2 plume and the Clarke Lake Slave Point A and B gas pools with 50 years injection and 50 years postinjection. As illustrated in Figures B-1 and B-2, the results showed that injected CO_2:

- Reaches the B pool after approximately 25 years of injection and then keeps on contaminating the B pool.

- Has not reached the A pool 100 years after injection is initiated.

For example, a comparison of simulated gas per unit area (i.e., the CO_2 plume) between models with and without CO_2 injection shows that gas per unit area increases near the injection locations but does not propagate to the Clarke Lake Slave Point A gas pool during the 5-, 25-, 50-, or 100-year time intervals (Figure B-2).

The results also indicate that there is a potential risk for the CO_2 plume to contact the Clarke Lake Slave Point B gas pool after approximately 25 years of injecting and contact the Slave Point A gas pool over a longer time interval, e.g., 500 years after injection (Figure B-3); however, these time frames far exceed the estimated productive life of these pools.

The injection well bottomhole pressure (BHP) profiles over time are shown in Figure B-4. As evident from this figure, there was an increase of approximately 4500 kPa in BHP (i.e., still below the maximum sandface injection pressure estimated at 80% of the estimated fracture gradient) near the injection wells at the end of CO_2 injection in year 2061 (after 50 years of

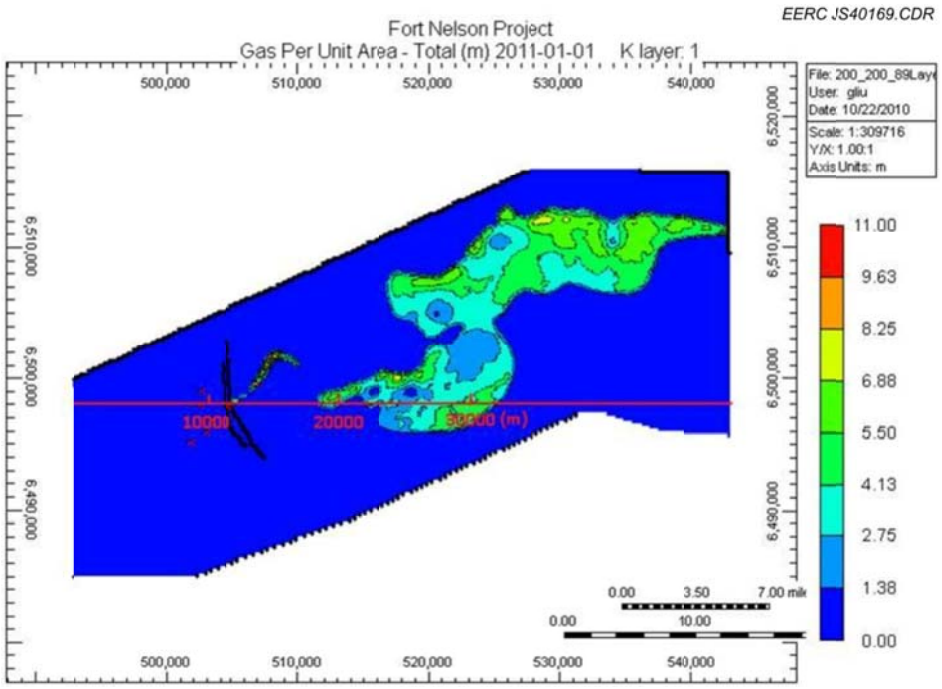

Figure B-1. Comparisons of the modeled CO_2 plume to the Clarke Lake Slave Point A gas pool. Three proposed CO_2 injection wells (c-18-E, c-47-E, and d-36-E) were used in each of the test scenarios (red dots in the figure).

injection). BHP in these wells returned to close to 10% above the initial reservoir pressure within 50 years postinjection in year 2111 (Figure B-4).This may be considered to be almost back to 2010 pre-injection pressures within the accuracy of this model.

Other injection effects on the formation because of CO_2 injection such as fluid interactions, geochemical effects, cooler temperature of the injected CO_2, and geomechanical stresses with injection were not incorporated in the tested scenarios present here but will need to be addressed in later modeling cases.

TEST CASE SCENARIO 2: CAP ROCK REDUCED PERMEABILITY CASE

The Fort Nelson carbon capture and storage (CCS) project area stratigraphy comprises multiple geologic layers, listed from top to bottom (Figure B-5):

- Fort Simpson/Muskwa shale (cap rock)
- Upper Slave Point (carbonate reservoir)
- Lower Slave Point (carbonate reservoir)
- Watt Mountain shale (aquitard)
- Sulphur Point (carbonate reservoir – CO_2 injection target)
- Upper Keg River (carbonate reservoir)

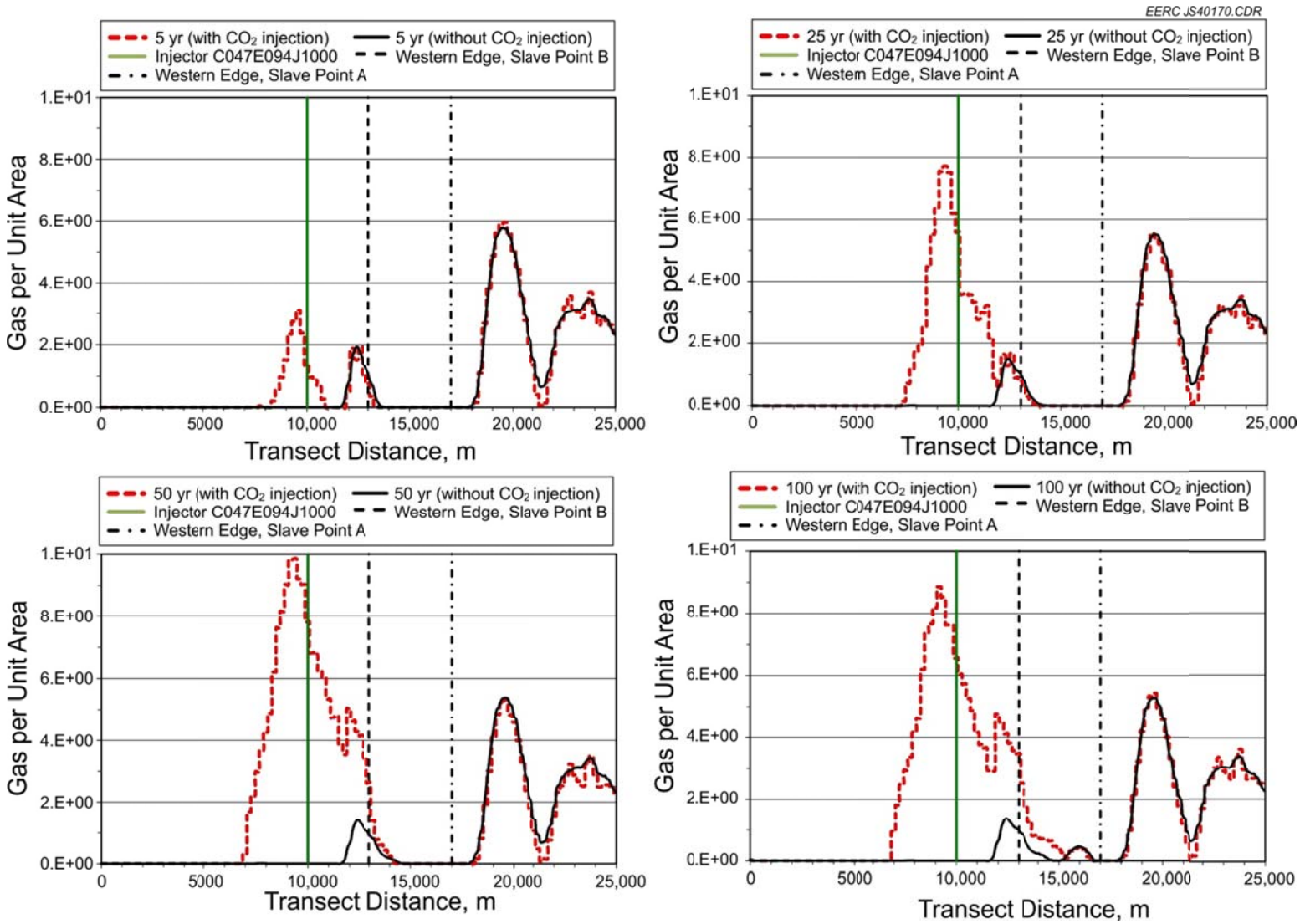

Figure B-2. Simulated gas per unit area with CO_2 injection (red dotted line) and without CO_2 injection (black solid line) taken along transect (red line) that is shown in Figure B-1. Simulated injection scenarios of 5-, 25-, 50-, and 100-year time intervals are shown.

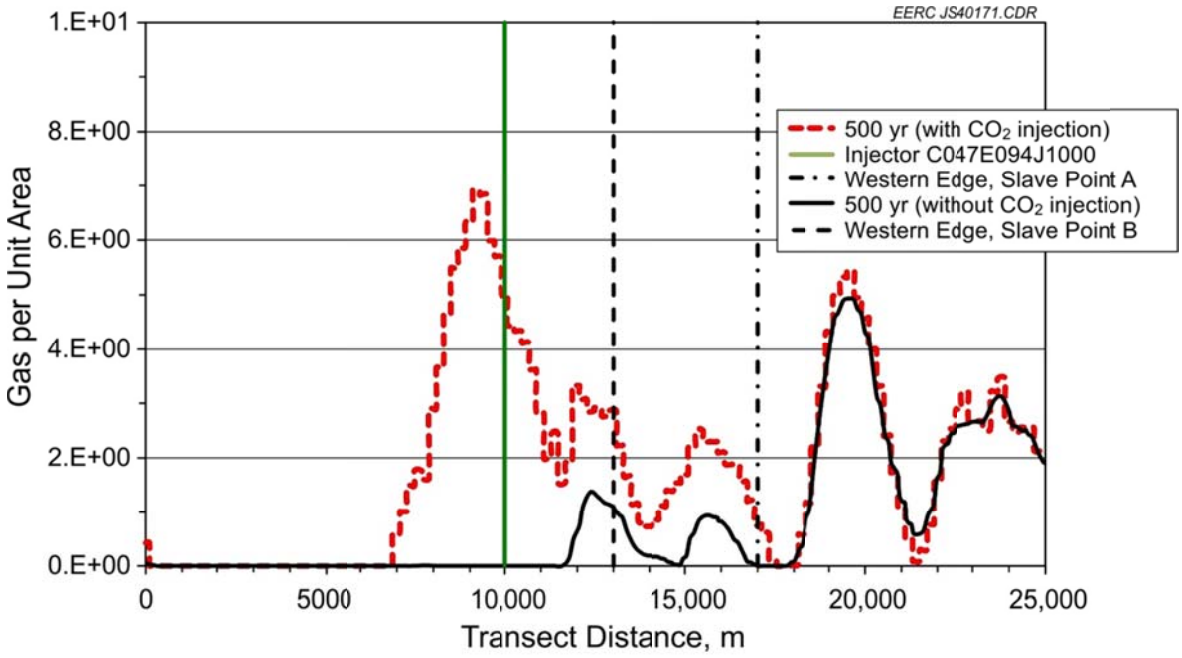

Figure B-3. Simulated gas per unit area with CO_2 injection (red dotted line) and without CO_2 injection (black solid line) for the 500-year time interval taken along transect (red line) that is shown in Figure B-1.

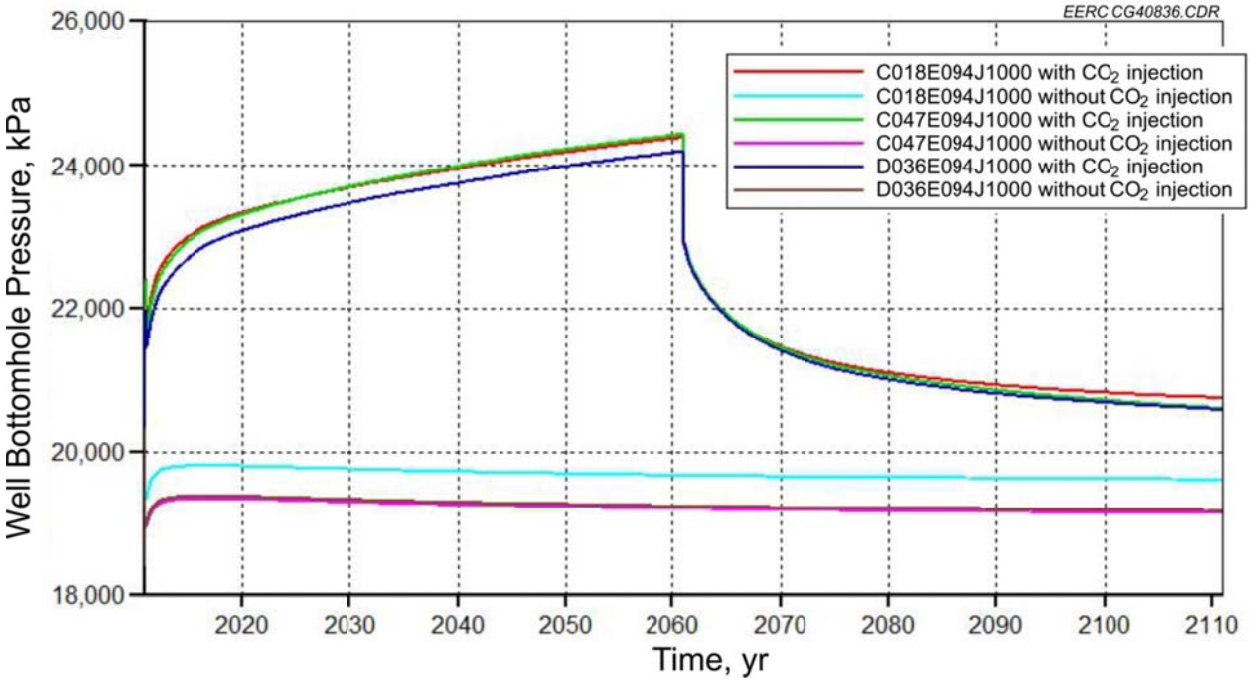

Figure B-4. Simulated injection well BHPs with and without CO_2 injection over a 100-year time interval assuming a 50-year injection (injection from 2011 through 2061, postinjection monitoring from 2061 to 2111).

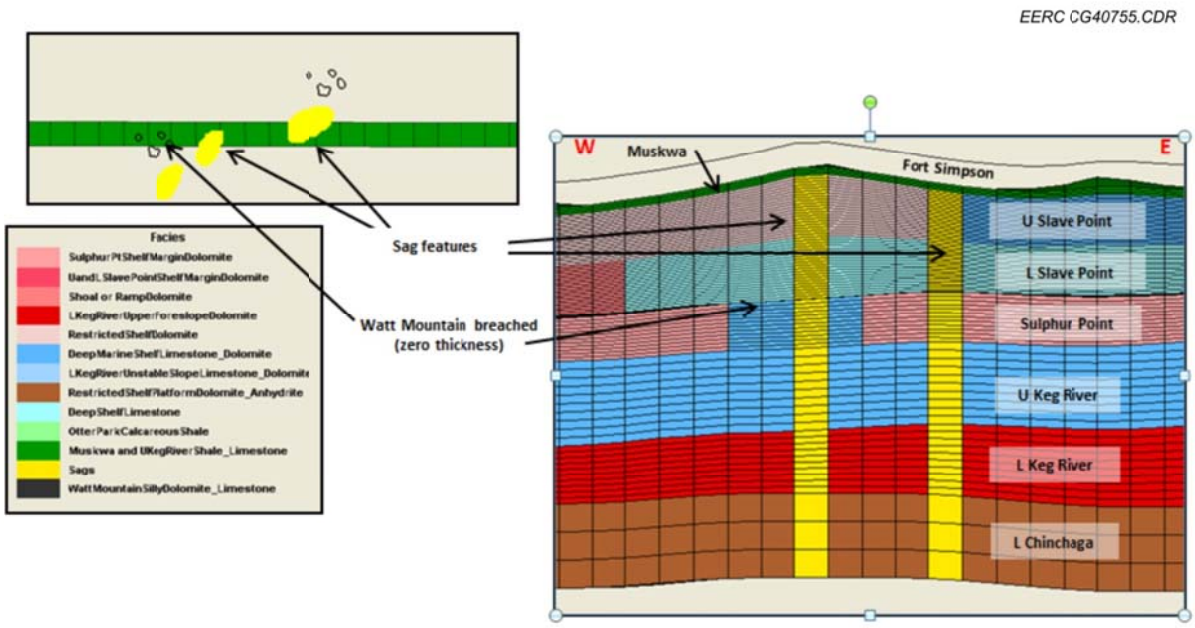

Figure B-5. Fort Nelson CCS project area stratigraphy used in the simulations.

- Lower Keg River (carbonate reservoir)
- Chinchaga (carbonate reservoir)

Kilometer-sized hydrothermal vents or "sags" have been identified, which extend from the Keg River up through the Slave Point reservoirs. Pressure data indicate that there is good vertical connectivity among the Keg River, Sulphur Point (CO_2 injection target), and Slave Point reservoirs, which could allow injected CO_2 to move vertically as well as laterally within the system. The Watt Mountain is an internal baffle within the reef that will slow the upward migration of injected sour CO_2. Therefore, the Fort Simpson/Muskwa shale cap rock represents an important boundary condition for the predictive simulations.

This scenario was designed to investigate the sealing ability of the Muskwa Formation against the gas plume of the A and B pools and provide comparison to Scenario 1. The base case values collected from core analysis indicate that permeability ranging from 0.1 to 0.9 mD was regarded as too high for a sealing formation, as simulations revealed that the unit was even transmissible to the A and B pool gas. Available test data do not incorporate permeability data at reservoir conditions including fluid saturation, which leads to the uncharacteristically high values. As there is no historical or analytical evidence for gas leakage, a reduction by two orders of magnitude is considered reasonable until permeability data can be confirmed by laboratory testing on core samples which are expected to more accurately reflect the seal's permeability.

Based on the discussions above, the permeability of the Muskwa Formation was decreased by a factor of 100 from the base case (i.e., 0.01 × the Scenario 1 base case) to assess the impact of cap rock permeability on the model simulations of CO_2. In addition, permeability of the Otter

Park and Watt Mountain zones was both decreased by 0.1 × the Scenario 1 base case (Table 1 of the main report). The plume results are shown in Figure B-6.

TEST CASE SCENARIO 3: k_V/k_H RATIO COMPARISONS

The Scenario 3 simulations were designed to test the sensitivity of CO_2 plume vertical migration to different vertical hydraulic conductivity/horizontal hydraulic conductivity ratios (k_v/k_h). Two k_v/k_h ratios were used: 0.2 and 0.3. The results show that the vertical migration of the CO_2 plume increased with higher k_v/k_h ratio (Figure B-7).

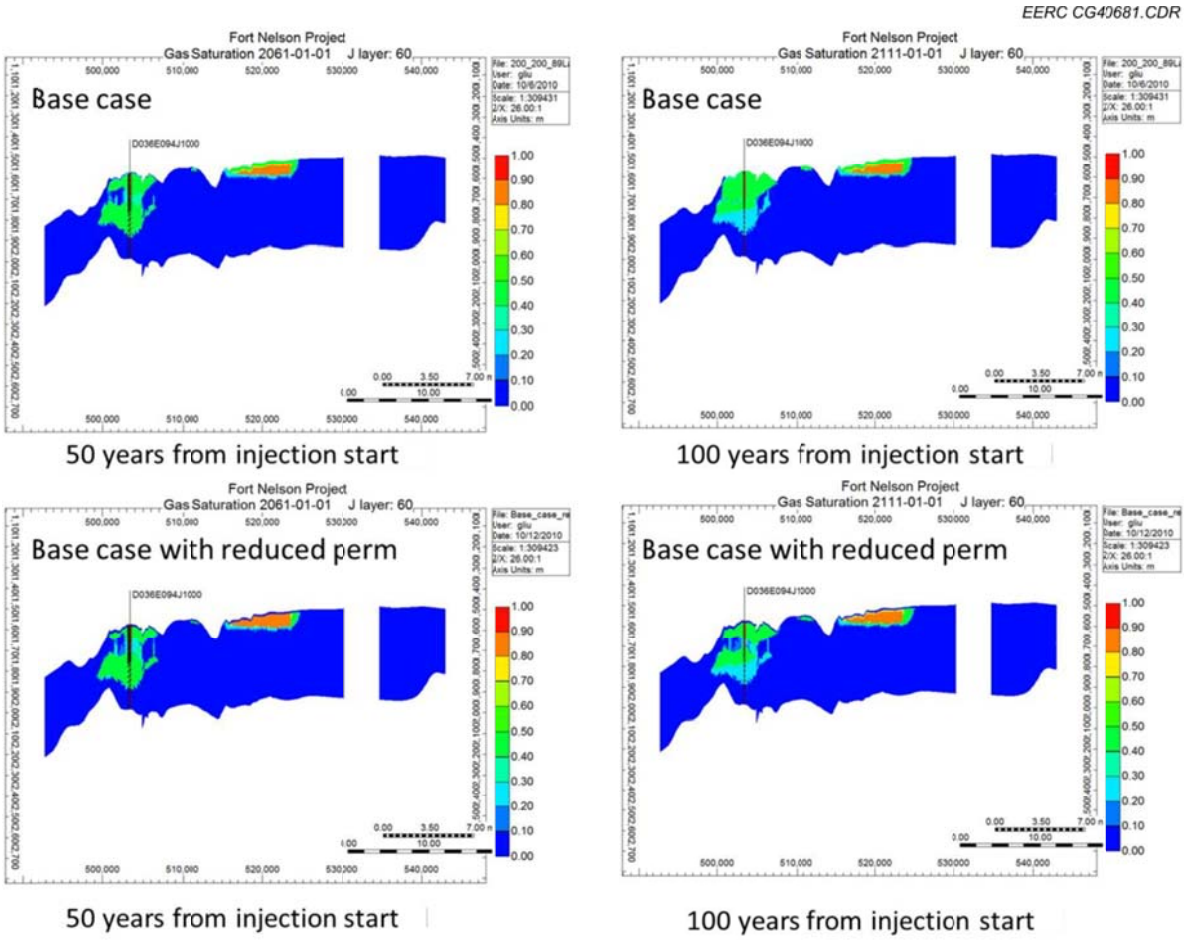

Figure B-6. Comparisons of CO_2 plume migration for the Scenario 1 base case (top) to the Scenario 2 case where the Muskwa shale cap rock permeability was decreased by a factor of 100 (i.e., 0.01 × base case) (bottom).

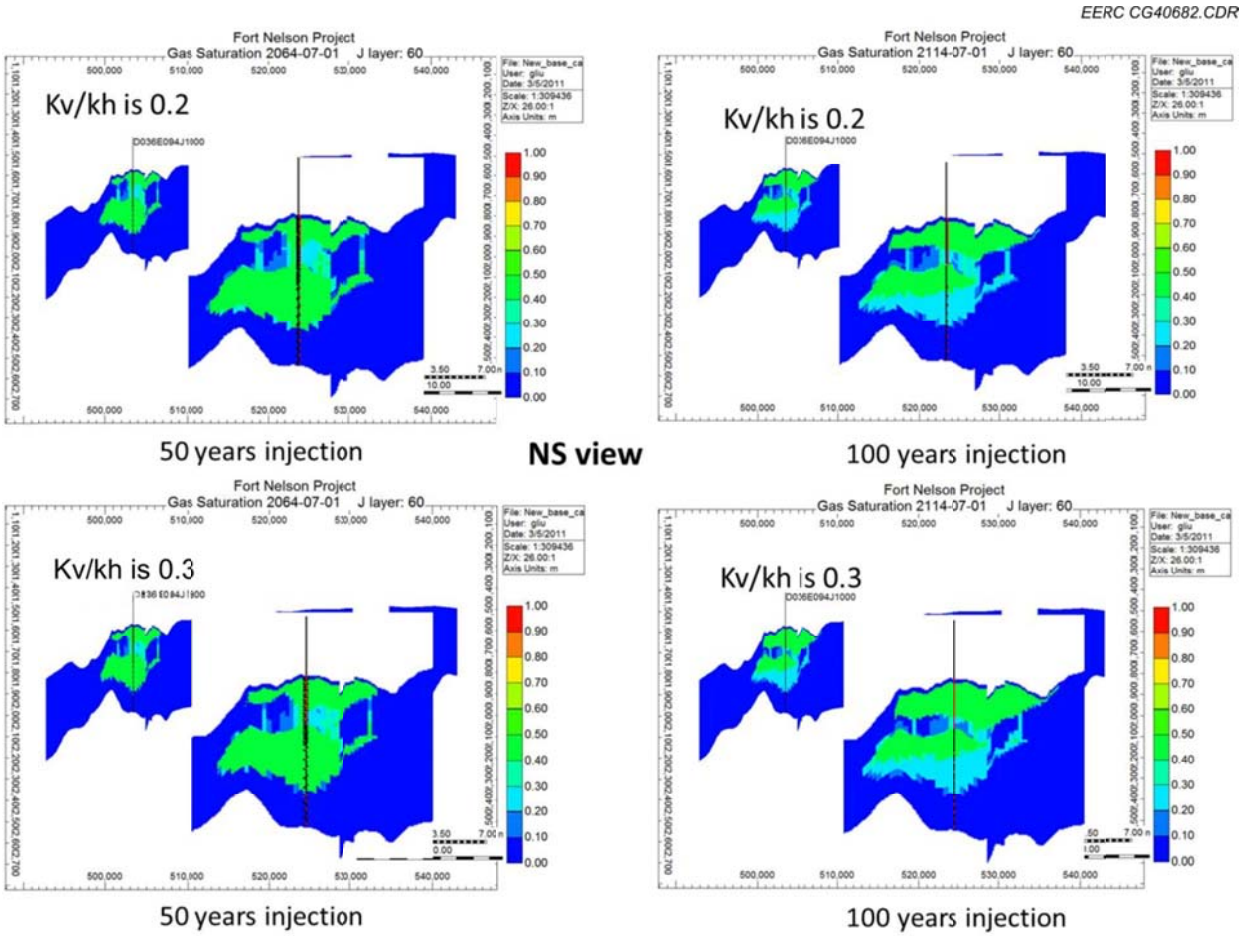

Figure B-7. Model simulation results comparing k_v/k_h ratios of 0.2 (top) and 0.3 (bottom). In each representation of this figure, the right image is an enlargement of the left image.

TEST CASE SCENARIO 4: FAULT TRANSMISSIBILITY COMPARISONS

In the Scenario 4, four different fault transmissibility values (0.00, 0.25, 0.75, and 1.00) were tested to compare the effects on CO_2 plume migration (Figures B-8 and B-9). The results indicate that the CO_2 plume migration increased with the higher transmissibility value of faults.

TEST CASE SCENARIO 5: RESERVOIR PERMEABILITY COMPARISONS

In Scenario 5, three different reservoir permeability scenarios (base case, 2 × base case, and 5 × base case) were tested to compare their effects on CO_2 plume migration. The purpose of the testing was to monitor the CO_2 plume under very high permeability conditions (even unrealistically high) to provide a conservative estimate of CO_2 plume migration.

The results indicate that in the case of highest permeability value (5 × base case), the CO_2 plume spreads much more rapidly than ones with lower values (base case and 2 × base case).

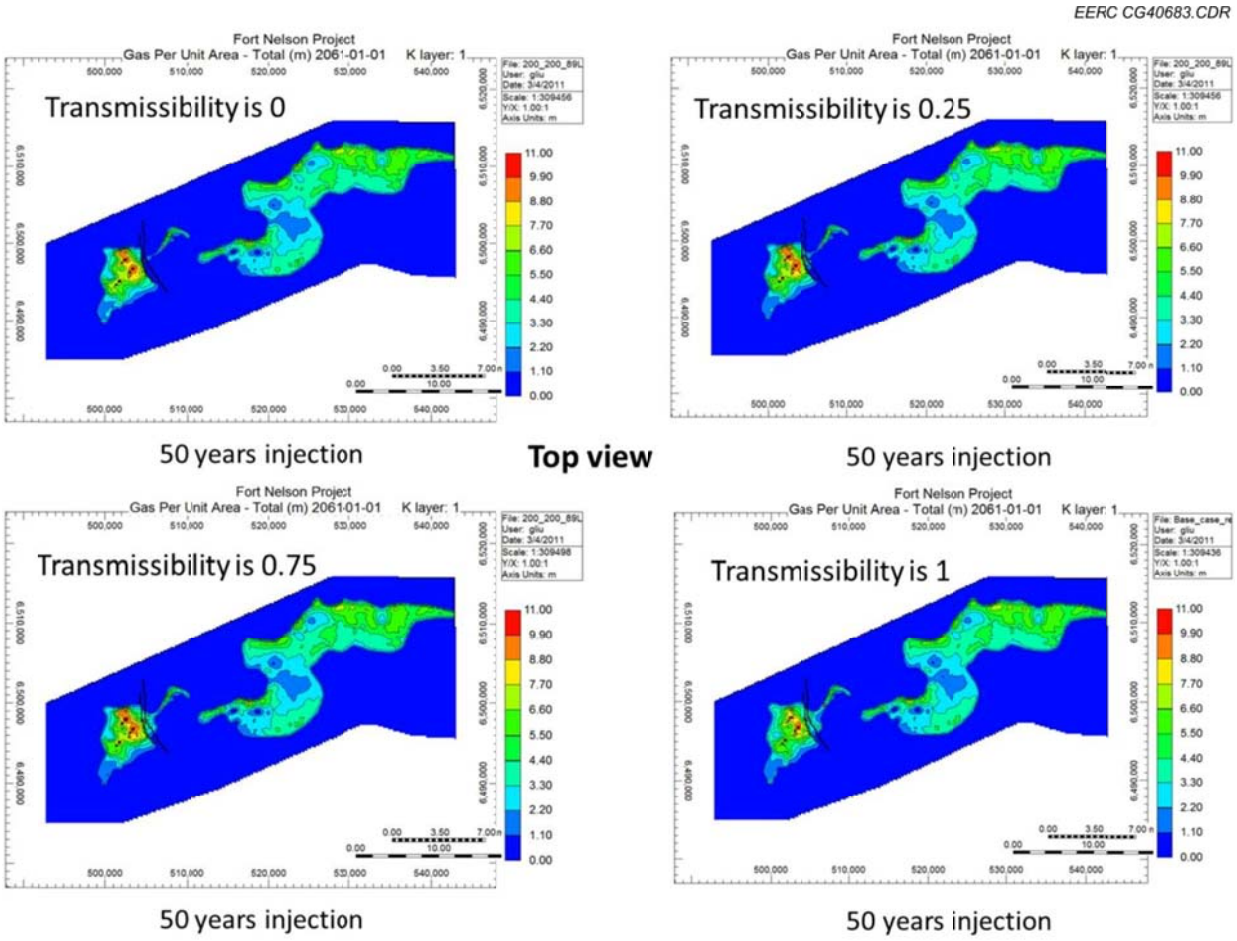

Figure B-8. Effects of fault transmissibility on simulated CO_2 plume migration (50 years).

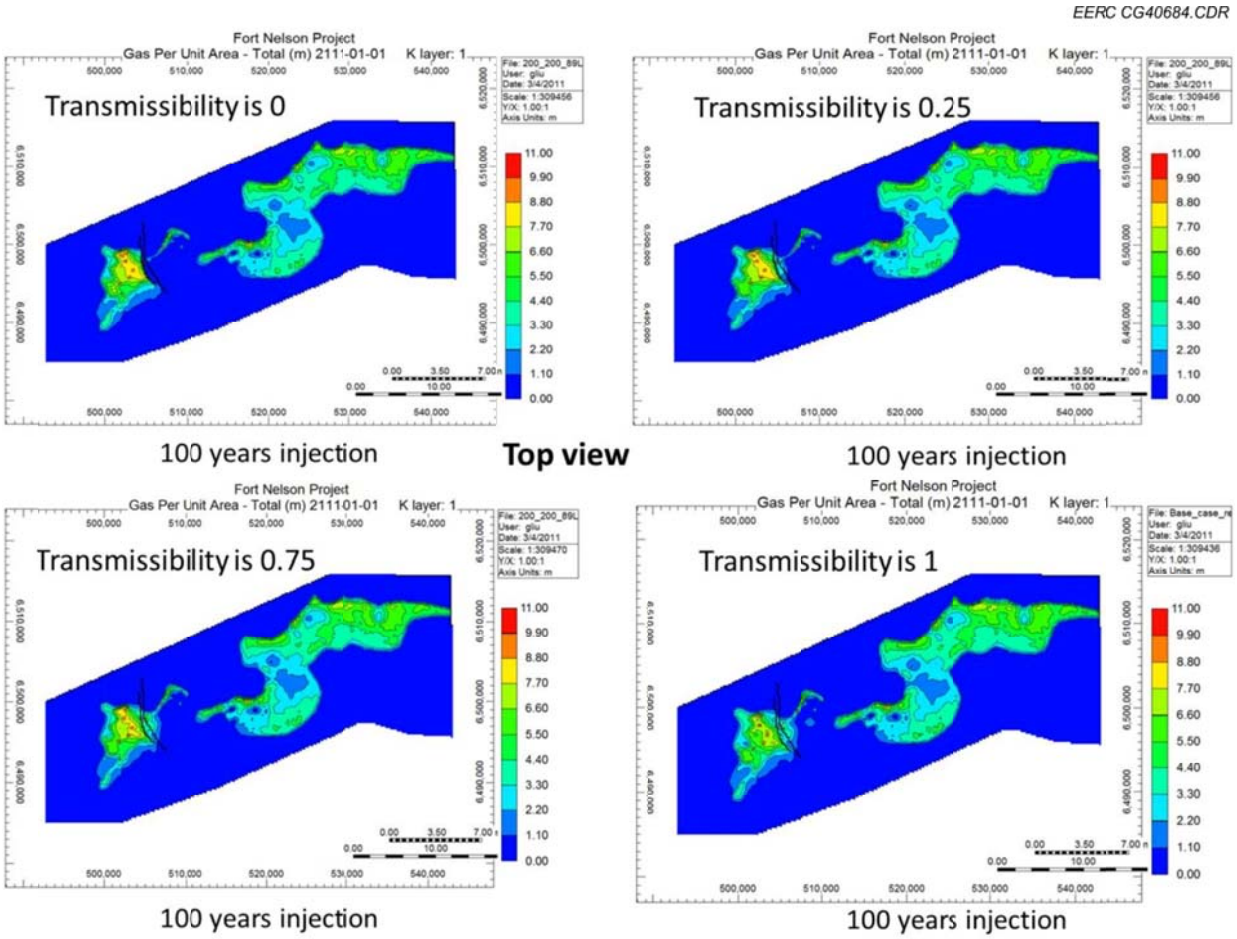

Figure B-9. Effects of fault transmissibility on simulated CO_2 plume migration (100 years).

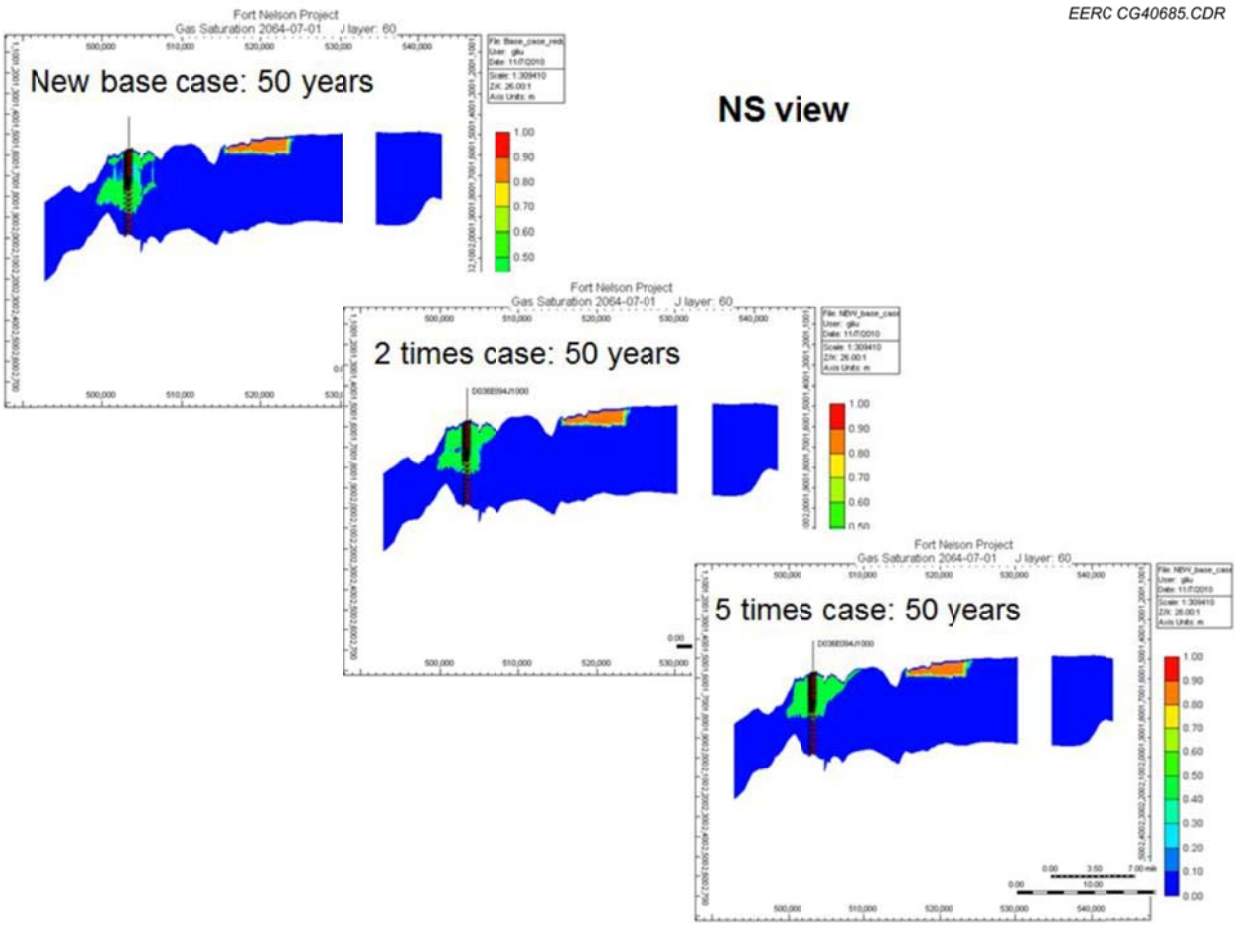

Figure B-10. Cross sections showing simulated CO_2 plume migration 50 years from the beginning of injection for three different permeability scenarios: base case (left), permeability = 2 × base case (middle), and permeability = 5 × base case (right).

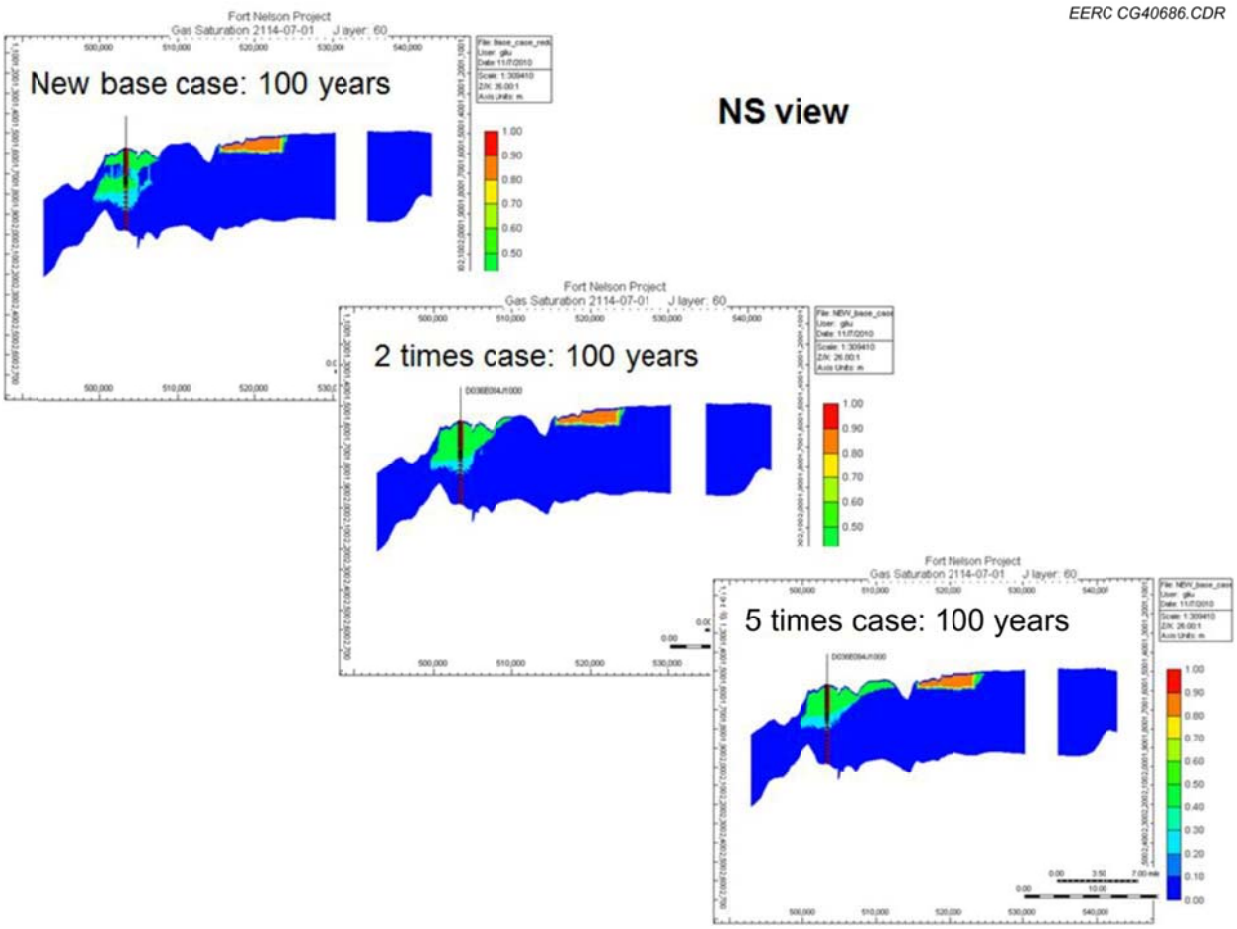

Figure B-11. Cross sections showing simulated CO_2 plume migration 100 years from the beginning of injection for three different permeability scenarios: base case (left), permeability = 2 × base case (middle), and permeability = 5 × base case (right).

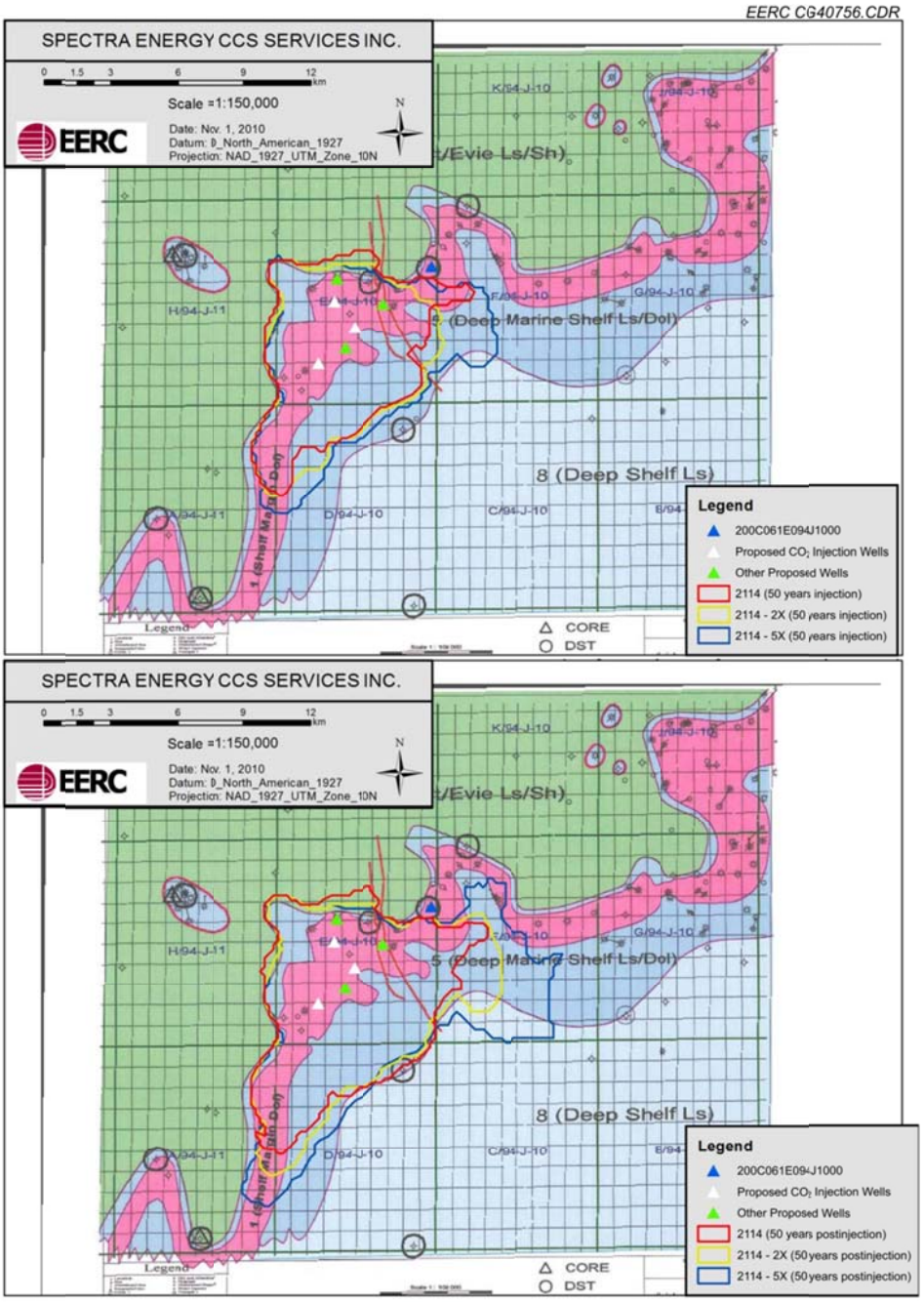

Figure B-12. Plan view showing simulated CO_2 plume migration 50 years (top) and 100 years (bottom) from the beginning of injection for three different permeability scenarios: base case (red), 2 × base case (yellow), and 5 × base case (blue).

APPENDIX C

PREDICTIVE SIMULATIONS BEFORE HISTORY MATCHING

PREDICTIVE SIMULATIONS BEFORE HISTORY MATCHING

INTRODUCTION

To address the differences between injecting in and around well c-61-E as compared to the location in and around c-47-E, ten test cases were designed and implemented (Table 2 of the main report). For all simulation runs, the k_v/k_h ratio was 0.2, fault transmissibility was 1.0, and injection rates were 120 MMscf/d.

Cases 1–4 modeled three injection wells at 25- and 50-year injections, assuming base case reservoir permeability (the same base case as was used above).

Cases 5 and 6 assumed low permeability near c-47-E and required a facies adjustment (i.e., decreasing permeability within model domains for a particular facies) and a wellbore adjustment (i.e., increasing the number and location of injection wells from three to six). These cases are geared toward seeing the impacts of a lesser quality reservoir overall and far less permeable section in the Slave Point so upward movement of the CO_2 is limited. The facies adjustments based on the domains are described below. One example of facies adjustments based on domains is shown in Figure C-1.

- Facies adjustments only applied to the facies/domains within the graben and on the west side of the graben where c-47-E is planned (i.e., the rest of the facies remains base case).

- Upper Slave Point domains:
  - Domain 2A was reduced to 50 mD.
  - Domain 2B was reduced to 1 mD.
  - Domain 5 was reduced to 25 mD for the higher-permeability streaks and 0.1 mD for the lower-permeability streaks (Domain 5 is interfingering).
  - Domains 8 (back reef) and 9 (shale basin) were not changed from the base case.

- Lower Slave Point domains:
  - Domain 2A was reduced to 50 mD.
  - Domain 2B was reduced to 1 mD.
  - Domains 8 (back reef) and 9 (shale basin) were not changed from the base case.

- Sulphur Point domains:
  - Domain 1 was reduced to 100 mD.
  - Domain 5 was reduced to 25 mD for the higher-permeability streaks and 0.1 mD for the lower-permeability streaks (Domain 5 is interfingering).

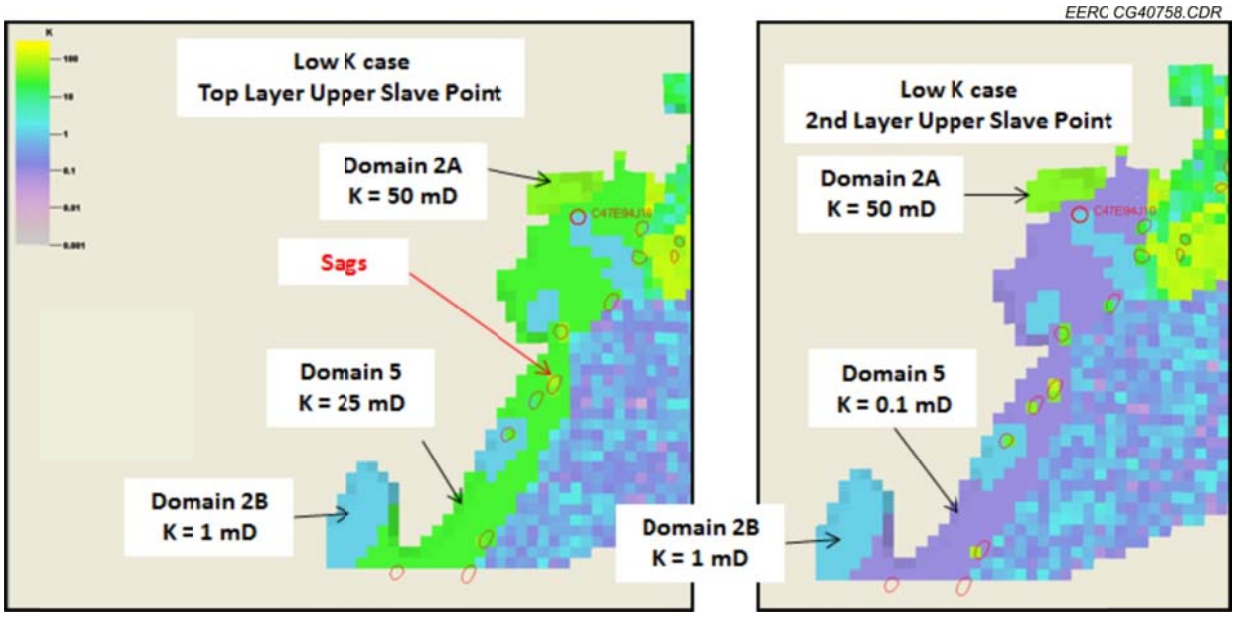

Figure C-1. Example of facies adjustments based on the domains for Cases 5 and 6. The permeability of domain 5 is 25 mD in the top layer of Upper Slave Point (left), and it changes to 0.1 mD in the second layer of Upper Slave Point (right).

  - Domains 8 (back reef) and 10 (Evie shale equivalent) were not changed from the base case.

- Upper and Lower Keg River domains:
  - Domains were all set to low permeability except for Domains 6 and 8 (back reef) and shale areas, which were not changed from the base case.

Cases 7 and 8 evaluated injecting at two wells near c-61-E. Results of the test case simulations are summarized below.

Cases 9 and 10 were designed to examine the cumulative gas improvement with more perforations than Cases 5 and 6.

SIMULATION CASES 1 AND 2

Simulation Cases 1 and 2 were the 25- and 50-year injection scenarios, respectively, in and around c-47-E, assuming the base case reservoir properties (Table 2 of the main report). Both models were run for 100 years to evaluate 75 and 50 years postinjection migration of injected CO_2, respectively. The results show that the CO_2 plume with either 25 years of injection (Figures C-2 and C-3) or 50 years of injection (Figures C-4 and C-5) would not come into contact with Clarke Lake Slave Point A or B gas pools within 100 years from the beginning of injection. However, it is to be noted that the structure on the west side of the double-fault graben, where there is only sparse 2-D seismic lines available, allows for the collection of buoyant CO_2 next to

the graben feature in the simulation runs. It will be important to get a much improved understanding of the structure via planned 3-D seismic survey. In addition, the double-fault graben may have a transmissibility of less than 1.0 as per the cases in which situation the graben would restrict/slow down CO_2 plume migration to the east. It is to be noted that, in the 50-year injection scenario, the CO_2 plume is starting to migrate across the graben but not reaching the Slave Point B pool, so understanding the structure and the fault transmissibility is important.

The highest bottomhole pressure (BHP) for both cases is less than 25,000 kPa (Figure C-6).

SIMULATION CASES 3 AND 4

Simulation Cases 3 and 4 were the 25- and 50-year injection scenarios, respectively, in and around c-61-E, assuming the base case reservoir properties (Table 2 of the main report). Both models were run for 100 years to evaluate 75 and 50 years postinjection migration of injected CO_2, respectively. The results show that the CO_2 plume with either 25 years of injection (Figures C-7 and C-8) or 50 years of injection (Figures C-9 and C-10) did come in contact with Clarke Lake Slave Point A or B gas pools within 100 years from the beginning of injection. This would be a higher risk area to inject the large volume of 120 MMcf/d than the c-47-E area.

The highest BHP for Case 3 was less than 25,000 kPa. The highest BHP for Case 4 was between 25,000 and 26,000 kPa (Figure C-11). Both of these cases suggest that injecting into the c-61-E area would create a higher pressure situation than Cases 1 and 2 injecting at the c-47-E area.

SIMULATION CASES 5 AND 6

Simulation Cases 5 and 6 were the 25- and 50-year injection scenarios, respectively, in and around c-47-E, assuming the lower-permeability facies as described before (Figure C-1 and Table 2 of the main report). Both models were run for 100 years to capture 75 and 50 years postinjection migration of injected CO_2, respectively. Because of the low permeability of the Sulphur Point and Slave Point Formations in the c-47-E area in these cases, the CO_2 plume is much larger where it migrates much more laterally in the c-47-E area, and once it gets past the graben into the base case conditions reservoir, then it moves more vertically and laterally. End results is that in the low permeability cases described, the CO_2 plume covers a larger area to a greater extent than in the base cases, which causes the CO_2 plume to come in contact with Clarke Lake Slave Point A or B gas pools within 100 years from the beginning of injection (Figures C-12–C-15). This is a potential risk so it is important to understand the reservoir rock in the area of c-47-E by drilling and testing a well and shooting a 3-D seismic survey in this area.

Because of the low permeability of the injection region, the target CO_2 injection rate cannot be met even if the BHPs reach the maximum constraint of 28,000 kPa (Figure C-16 and Table C-1). Therefore, assuming the lower-permeability facies, the total injected gas for wells in

and around c-47-E is lower than the target injection volume. This means more wells would be required and properly spaced to minimize injection well interference issues.

SIMULATION CASES 7 AND 8

Simulation Cases 7 and 8 were the 25- and 50-year injection scenarios, respectively, in and around c-61-E, assuming the injection at two different well locations (Table 2 of the main report). The results show that the CO_2 plume with either 25 years of injection (Figures C-17 and C-18) or 50 years of injection (Figures C-19 and C-20) may come in contact with Clarke Lake Slave Point A or B gas pools within 100 years from the beginning of injection. To achieve the target injection rate, the BHPs exceed the maximum constraint of 28,000 kPa (Figure C-21). As exceeding the maximum sandface injection pressure would not be permitted by the regulator, the BHP would be curtailed to the permitted maximum, and the entire volume would not be able to be injected.

SIMULATION CASES 9 AND 10

Simulation Cases 9 and 10 were designed to increase vertical well perforations for the target CO_2 injection rate that cannot be met even if the BHPs reach the maximum constraint of 28,000 kPa (Table C-1 and Figure C-16) in Cases 5 and 6 because of the low permeability of the injection region. With more perforations, more sour CO_2 can be injected than the ones in Cases 5 and 6, and the BHPs are less than the ones in Cases 5 and 6. Particularly, for 25 years injection, Cases 5 and 9, the expected sour CO_2 can be fully injected (the reference) while the amount increases from 93.5% to 98.7% for 50 years injection by comparing Cases 6 and 10 (Figure C-22 and Table C-1). The BHPs were never beyond the maximum limitation of 28,000 kPa for Cases 9 and 10 (Figures C-23 and C-24). The areal and cross-sectional views of the gas plume for Cases 9 and 10 are shown in Figures C-25–C-28.

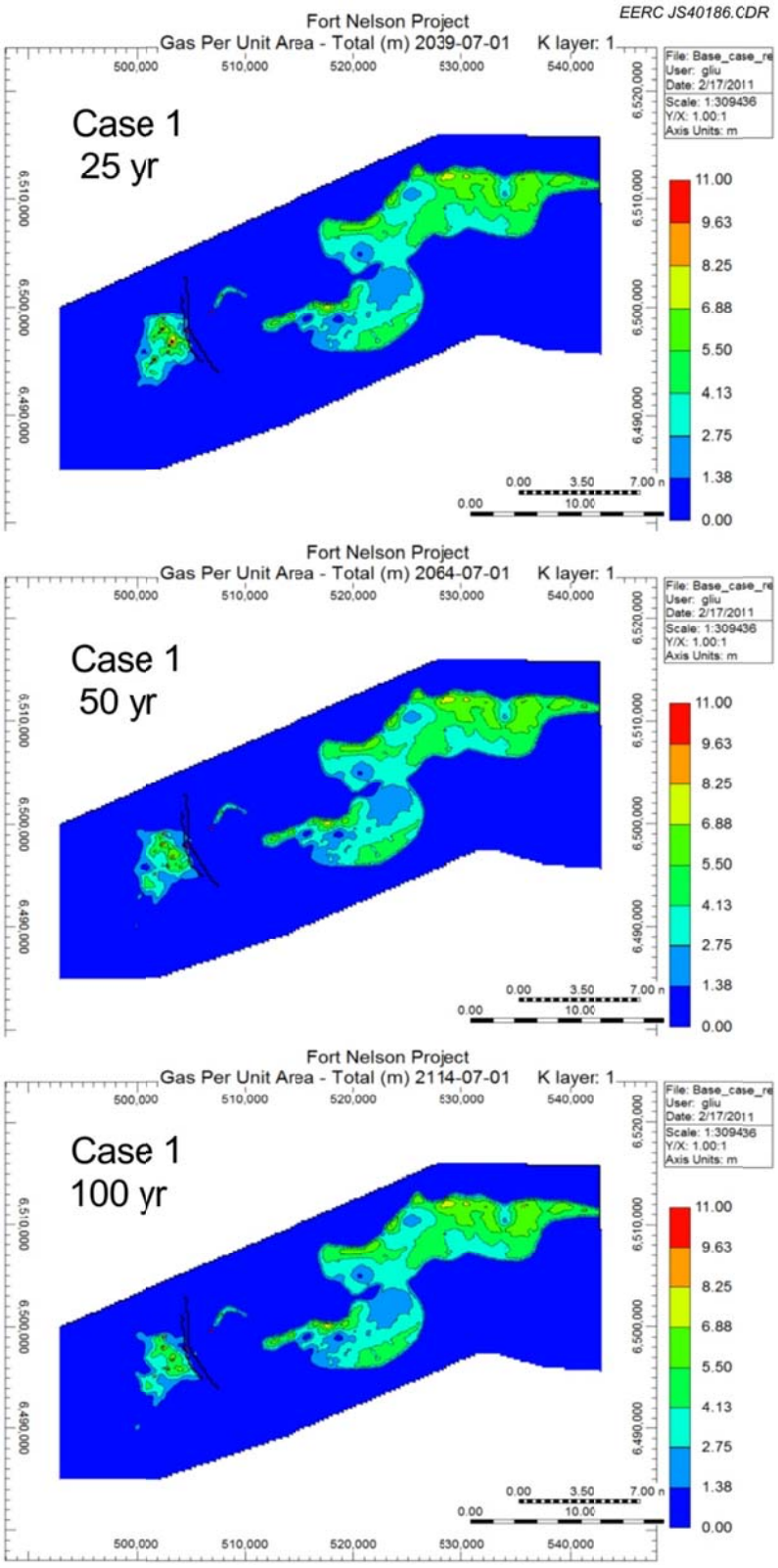

Figure C-2. Areal view of Case 1: 25 years of injection plus 75 years postinjection in and around c-47-E using the base case reservoir properties.

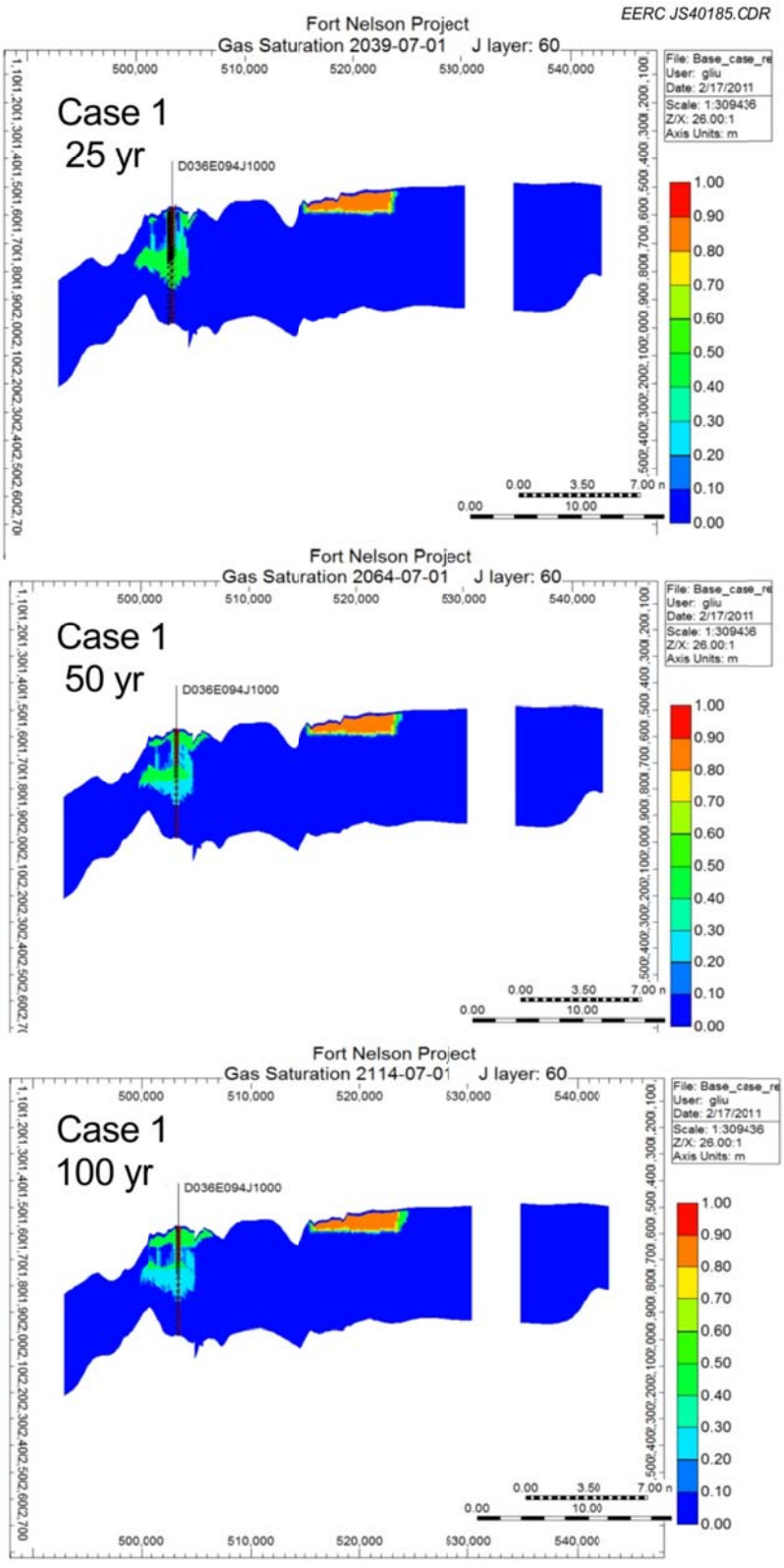

Figure C-3. Cross-sectional view of Case 1: 25 years of injection plus 75 years postinjection in and around c-47-E using the base case reservoir properties.

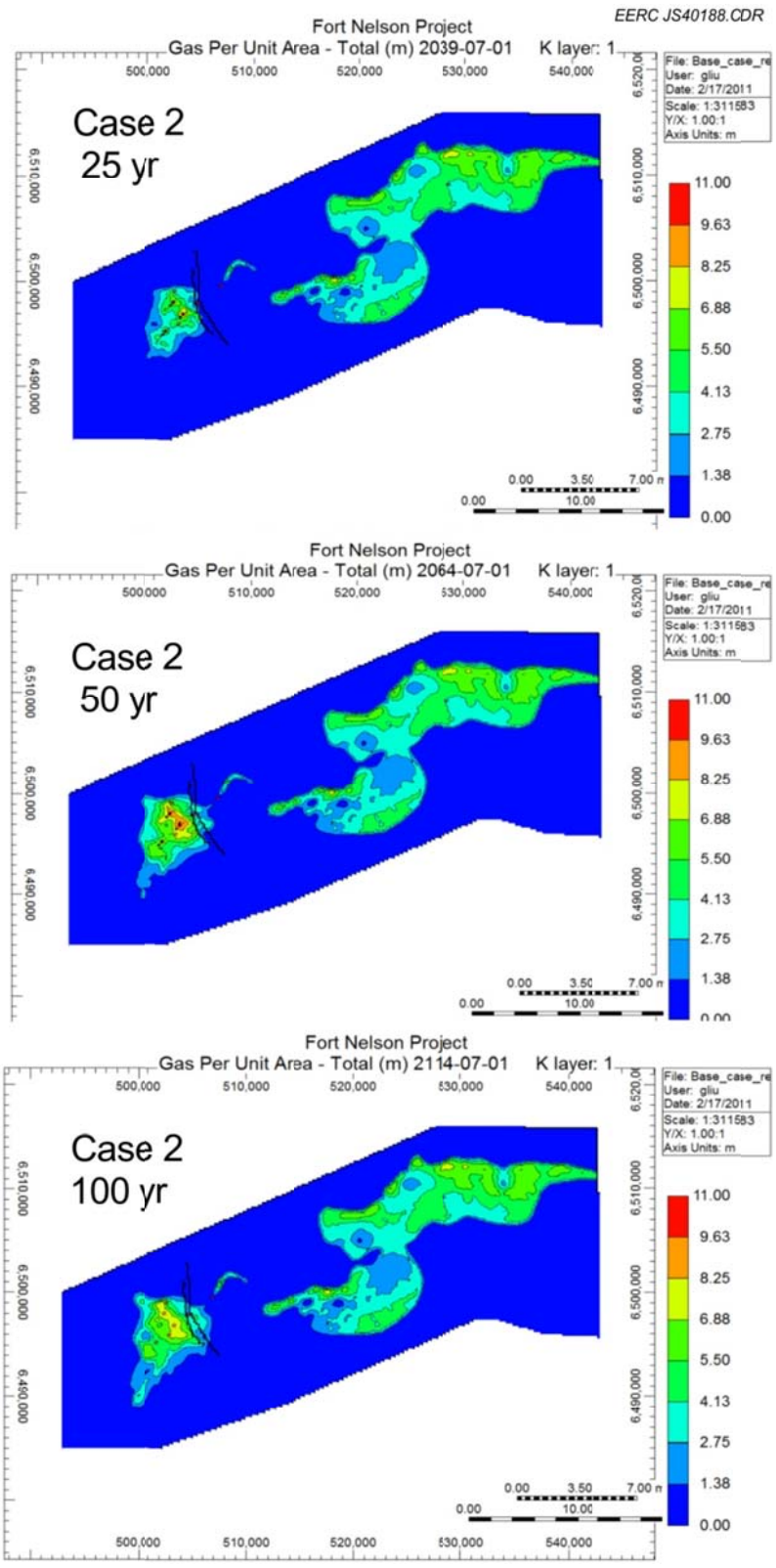

Figure C-4. Areal view of Case 2: 50 years of injection plus 50 years postinjection in and around c-47-E using the base case reservoir properties.

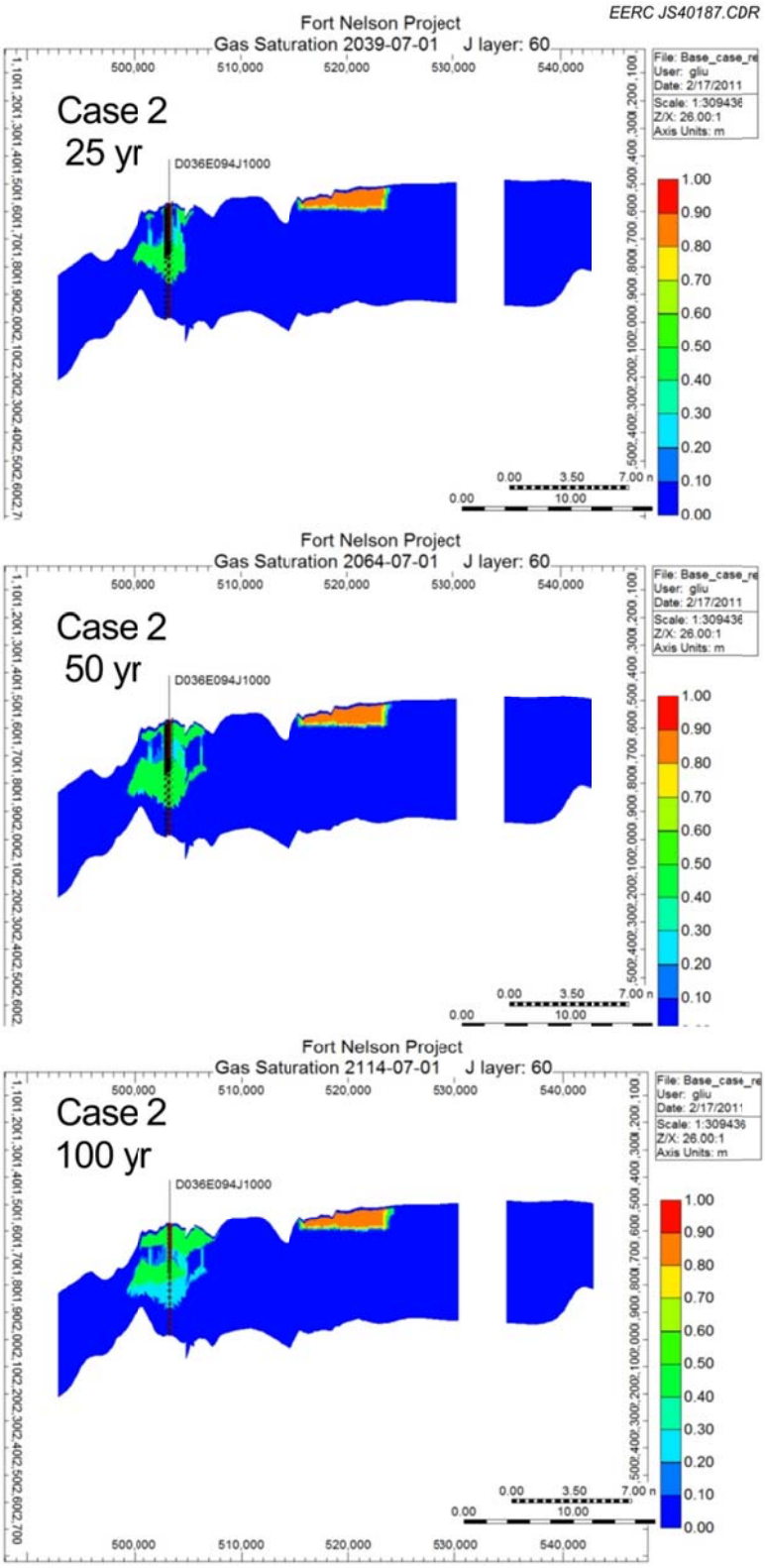

Figure C-5. Cross-sectional view of Case 2: 50 years of injection plus 50 years postinjection in and around c-47-E using the base case reservoir properties.

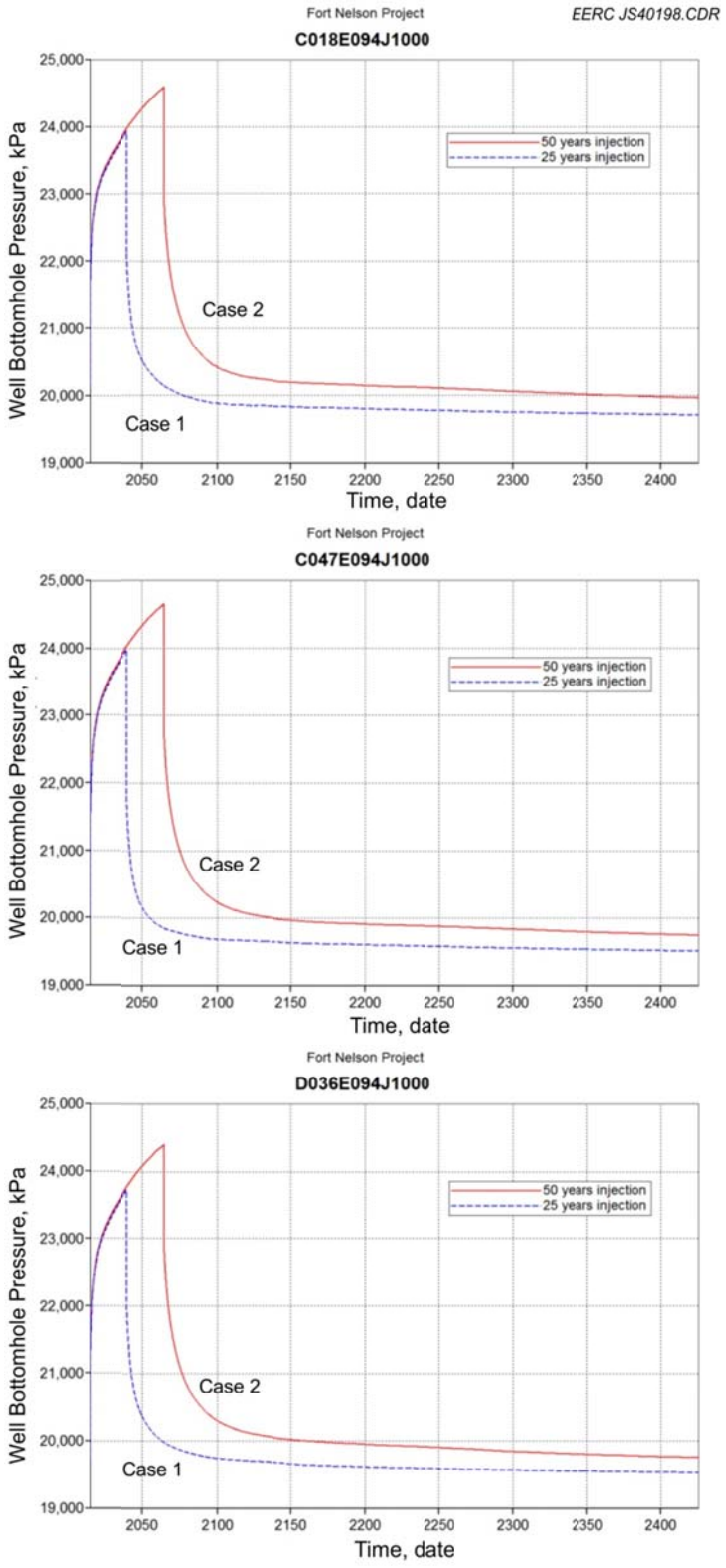

Figure C-6. BHPs at the injection wells for Cases 1 and 2.

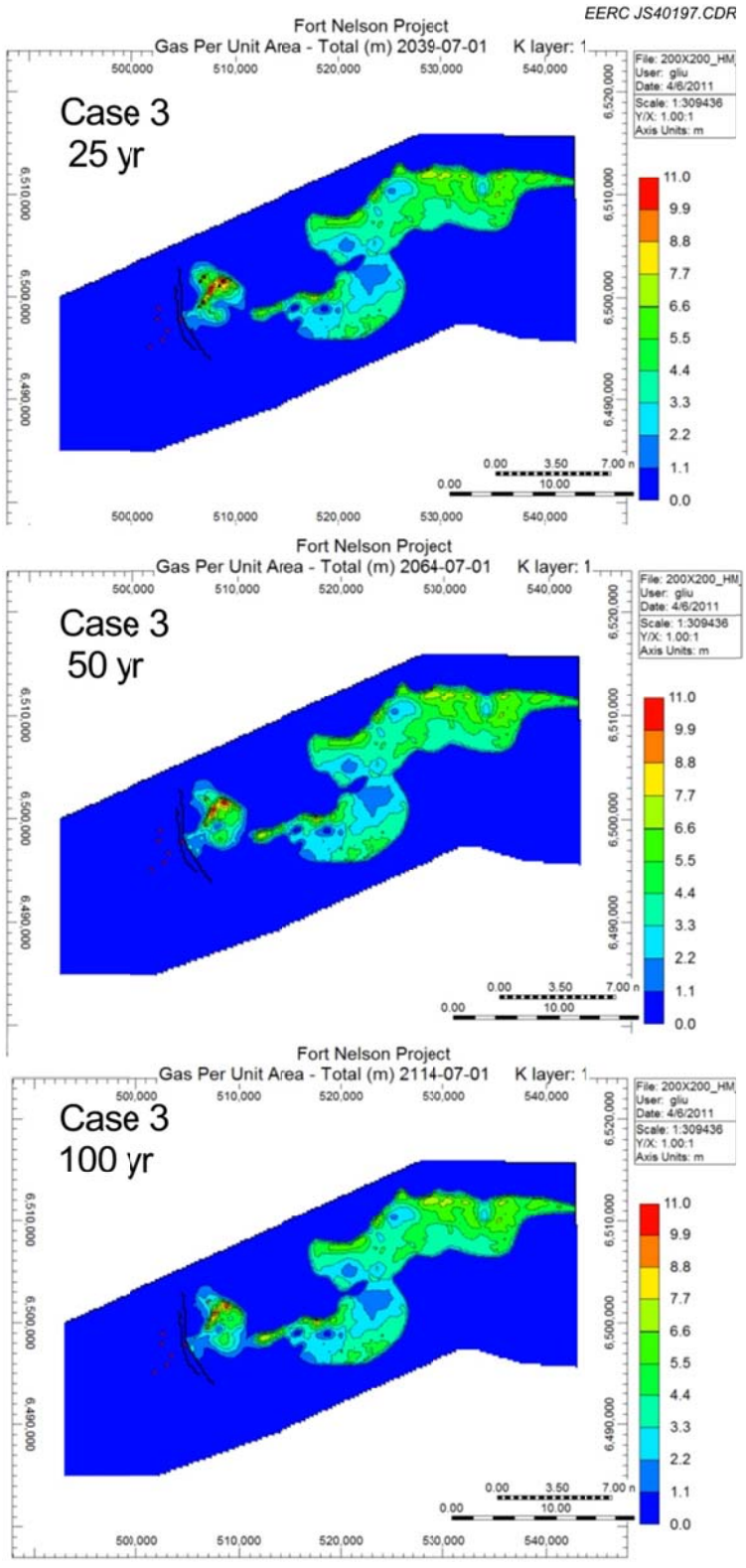

Figure C-7. Areal view of Case 3: 25 years of injection plus 75 years postinjection in and around c-61-E using the base case reservoir properties.

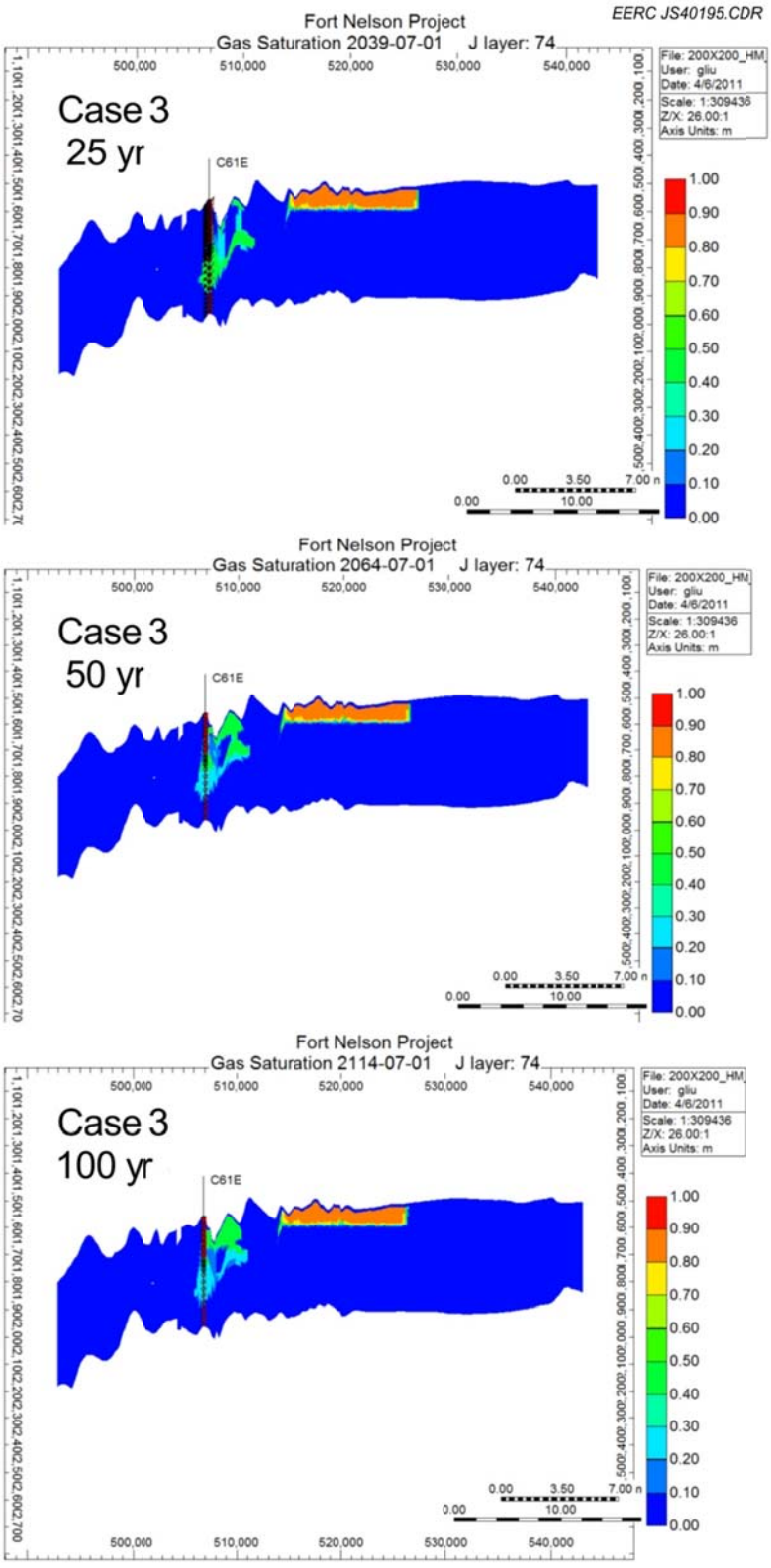

Figure C-8. Cross-sectional view of Case 3: 25 years of injection plus 75 years postinjection in and around c-61-E using the base case reservoir properties.

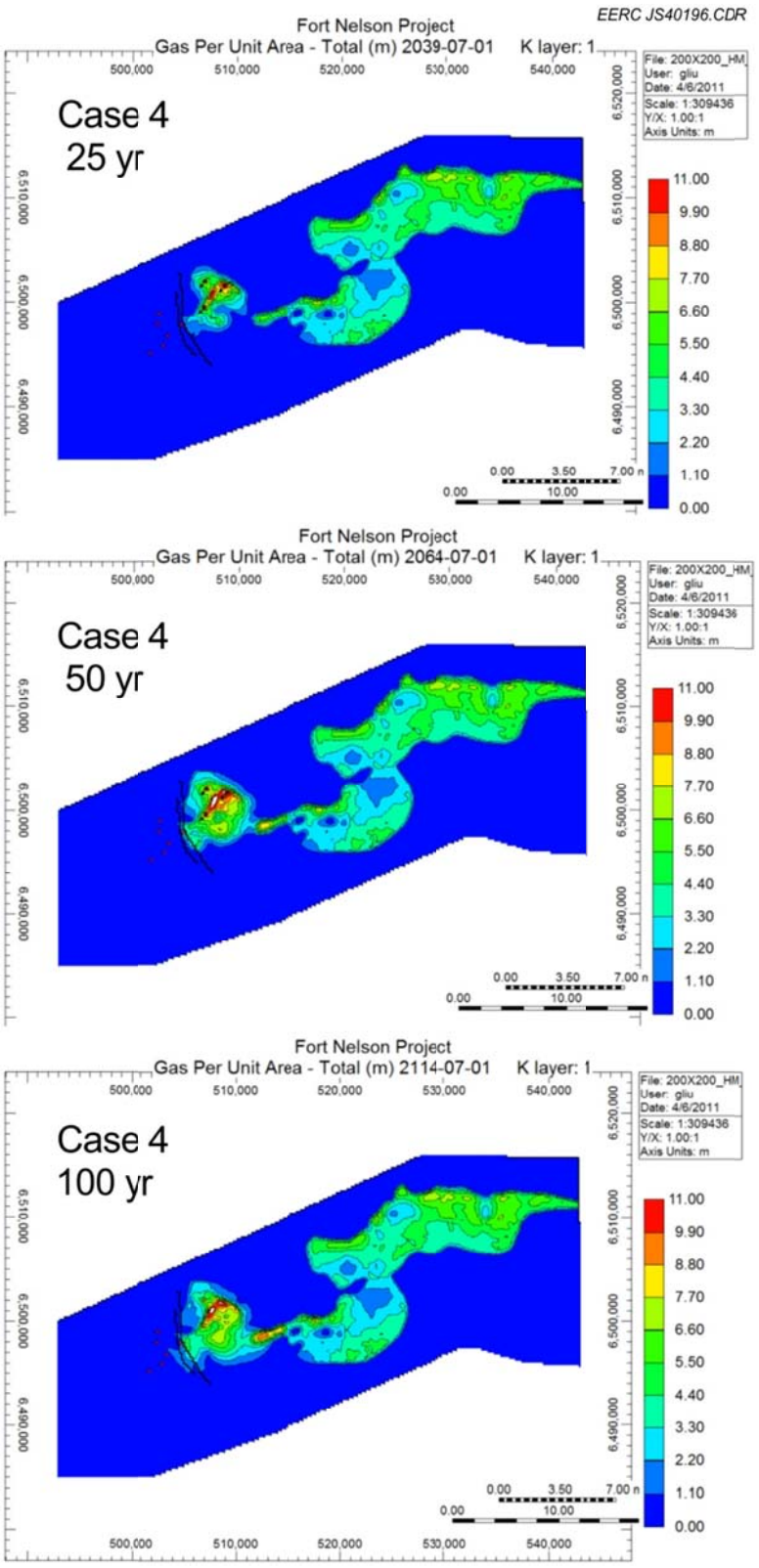

Figure C-9. Areal view of Case 4: 50 years of injection plus 50 years postinjection in and around c-61-E using the base case reservoir properties.

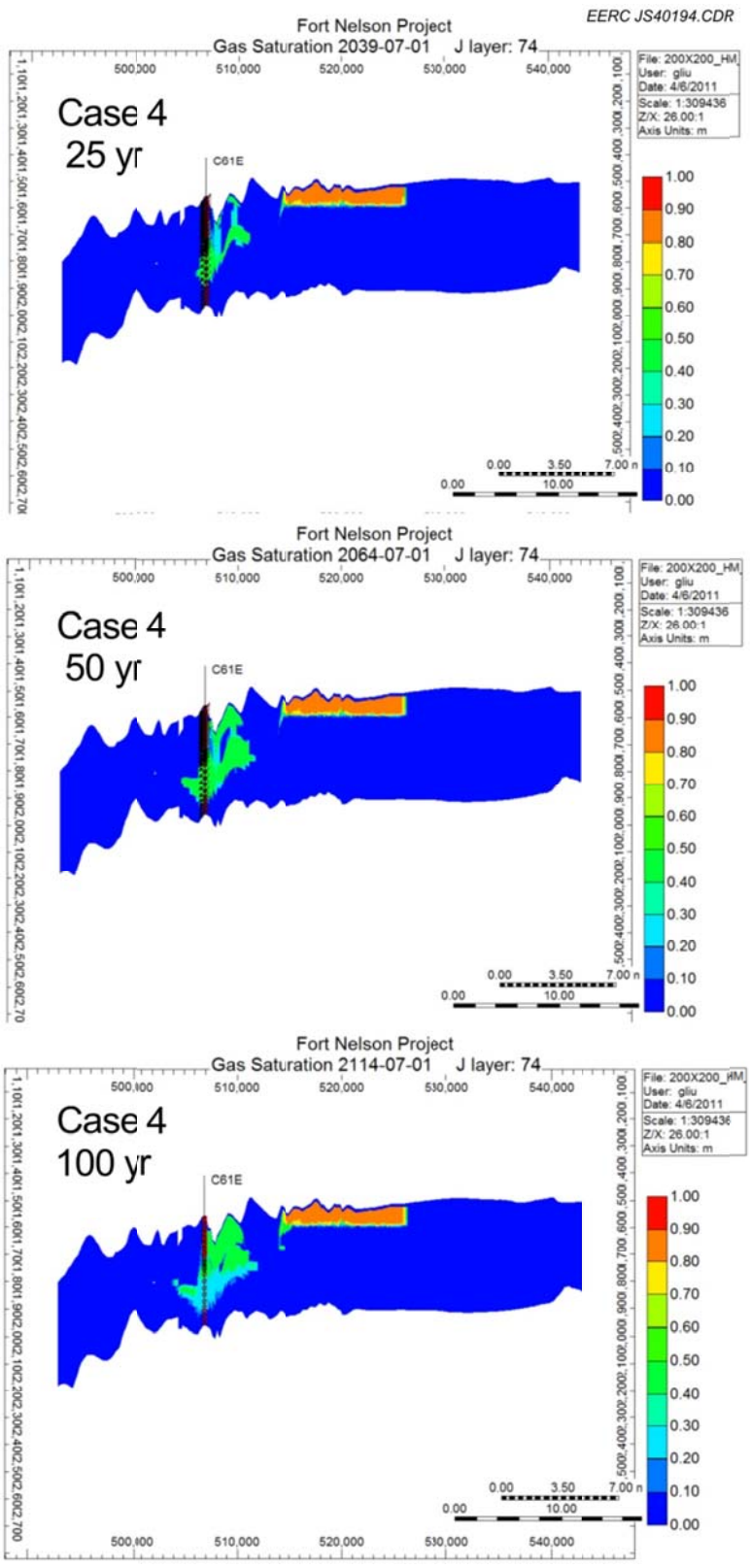

Figure C-10. Cross-sectional view of Case 4: 50 years of injection plus 50 years postinjection in and around c-61-E using the base case reservoir properties.

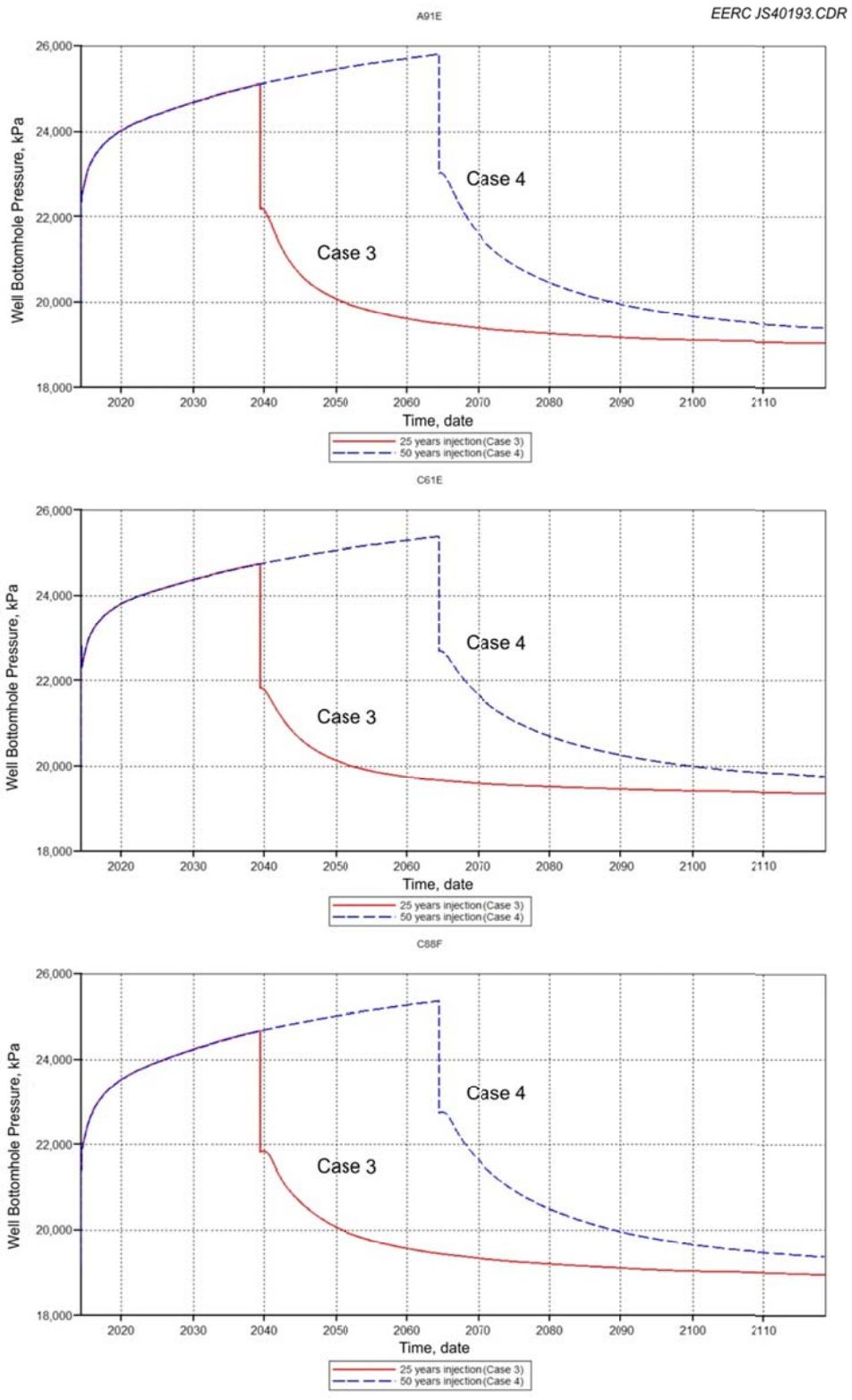

Figure C-11. BHPs at the injection wells for Cases 3 and 4.

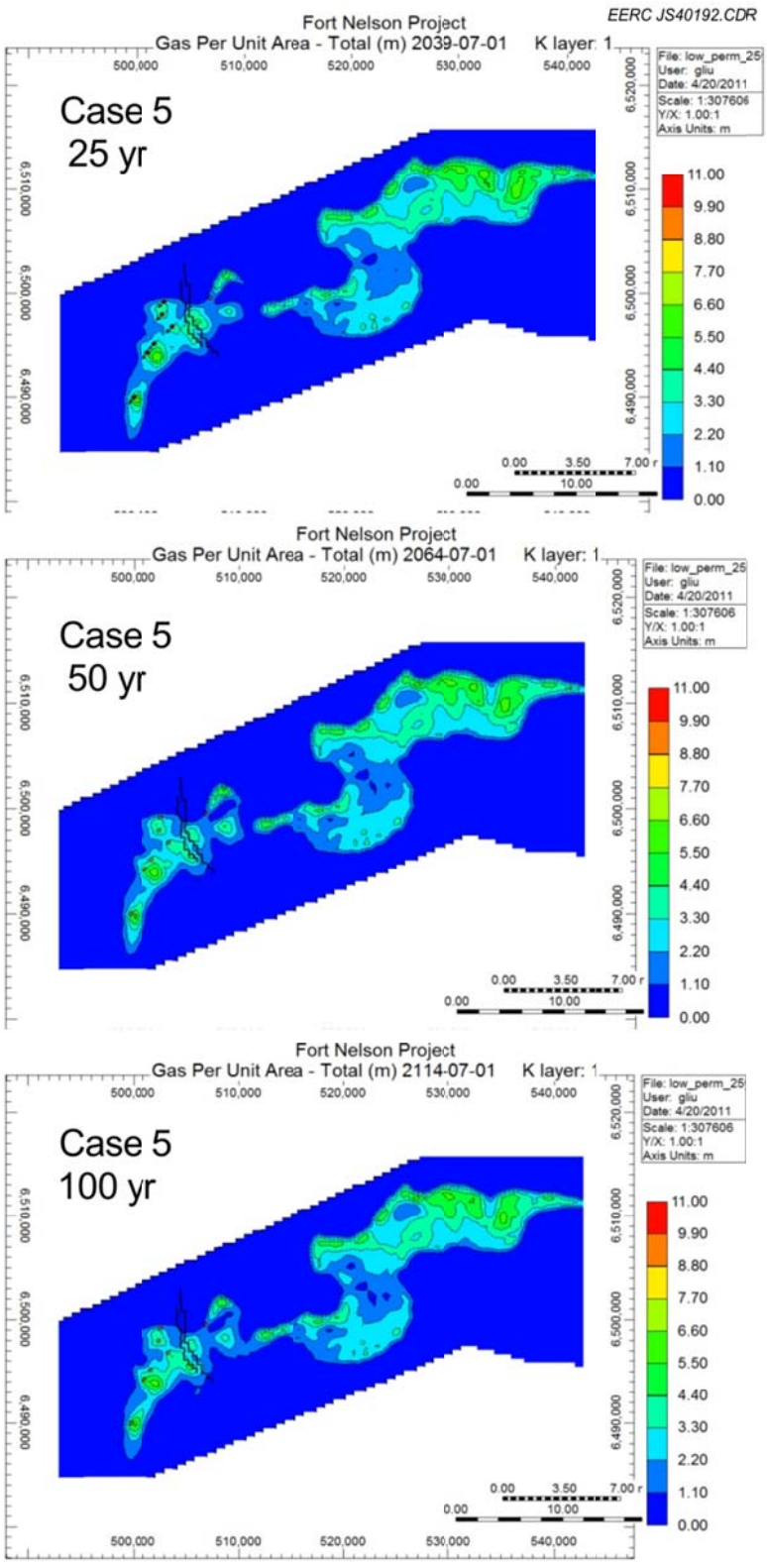

Figure C-12. Areal view of Case 5: 25 years of injection plus 75 years postinjection in and around c-47-E using the reduced permeability reservoir properties.

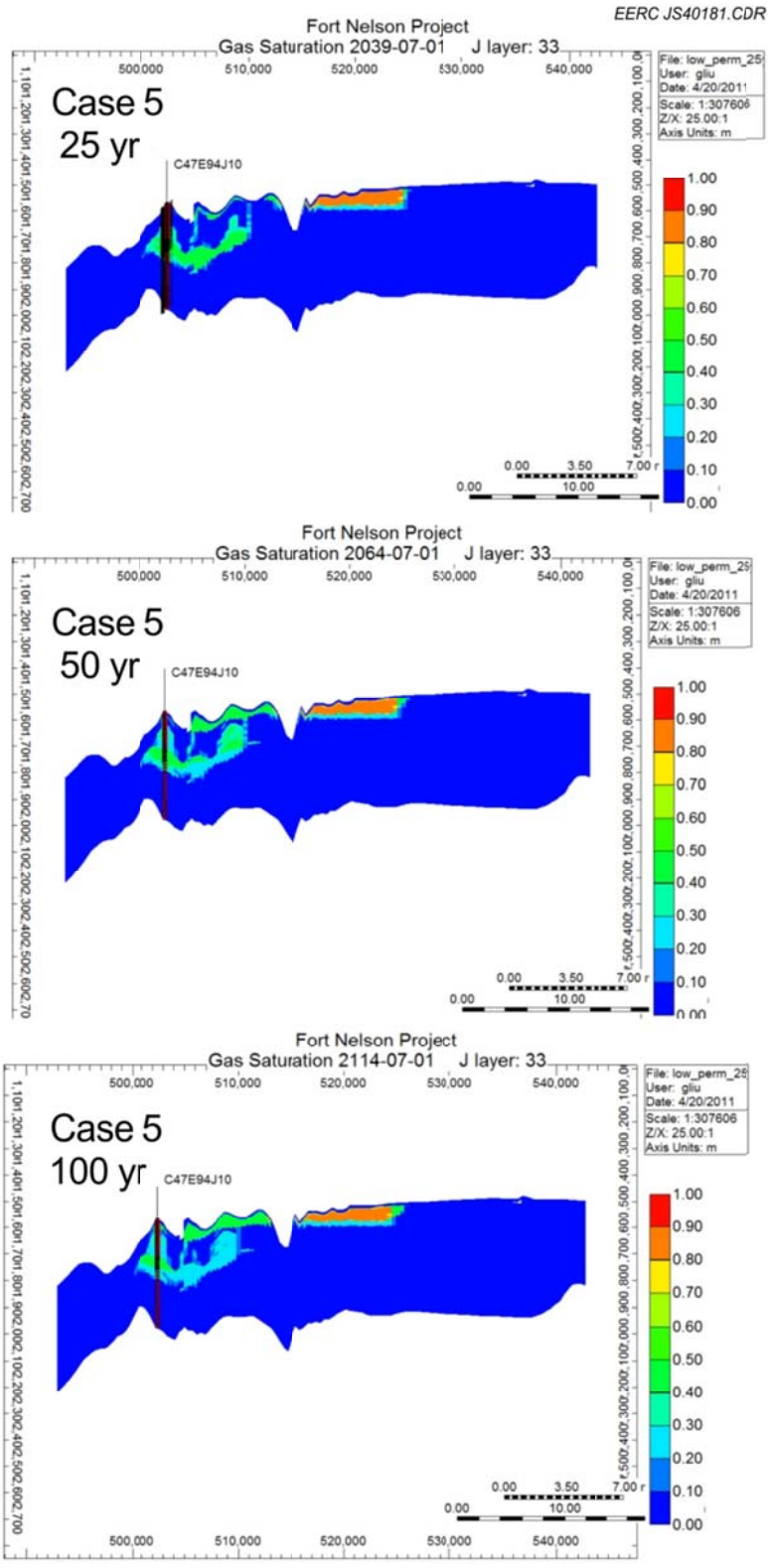

Figure C-13. Cross-sectional view of Case 5: 25 years of injection plus 75 years postinjection in and around c-47-E using the reduced permeability reservoir properties.

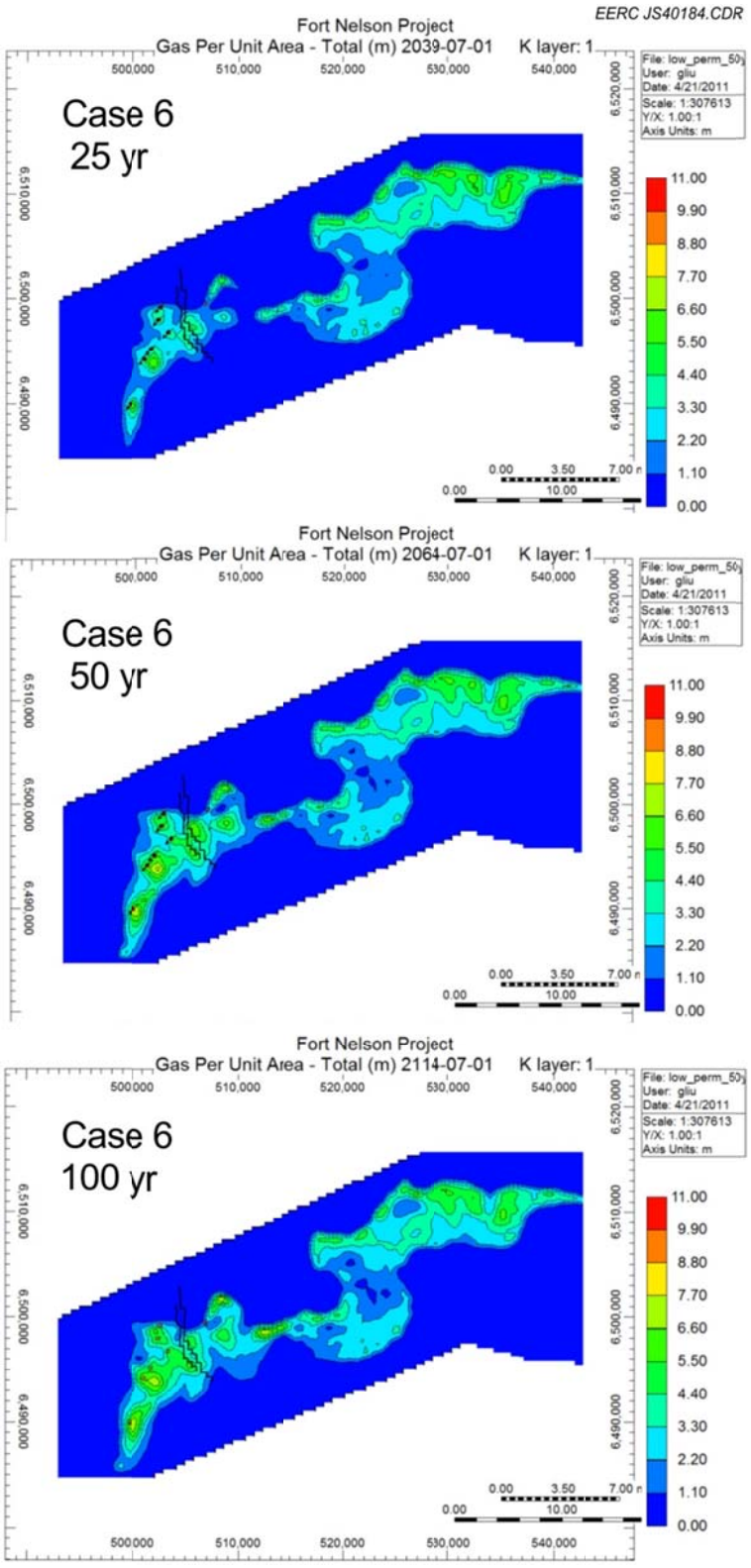

Figure C-14. Areal view of Case 6: 50 years of injection plus 50 years postinjection in and around c-47-E using the reduced permeability reservoir properties.

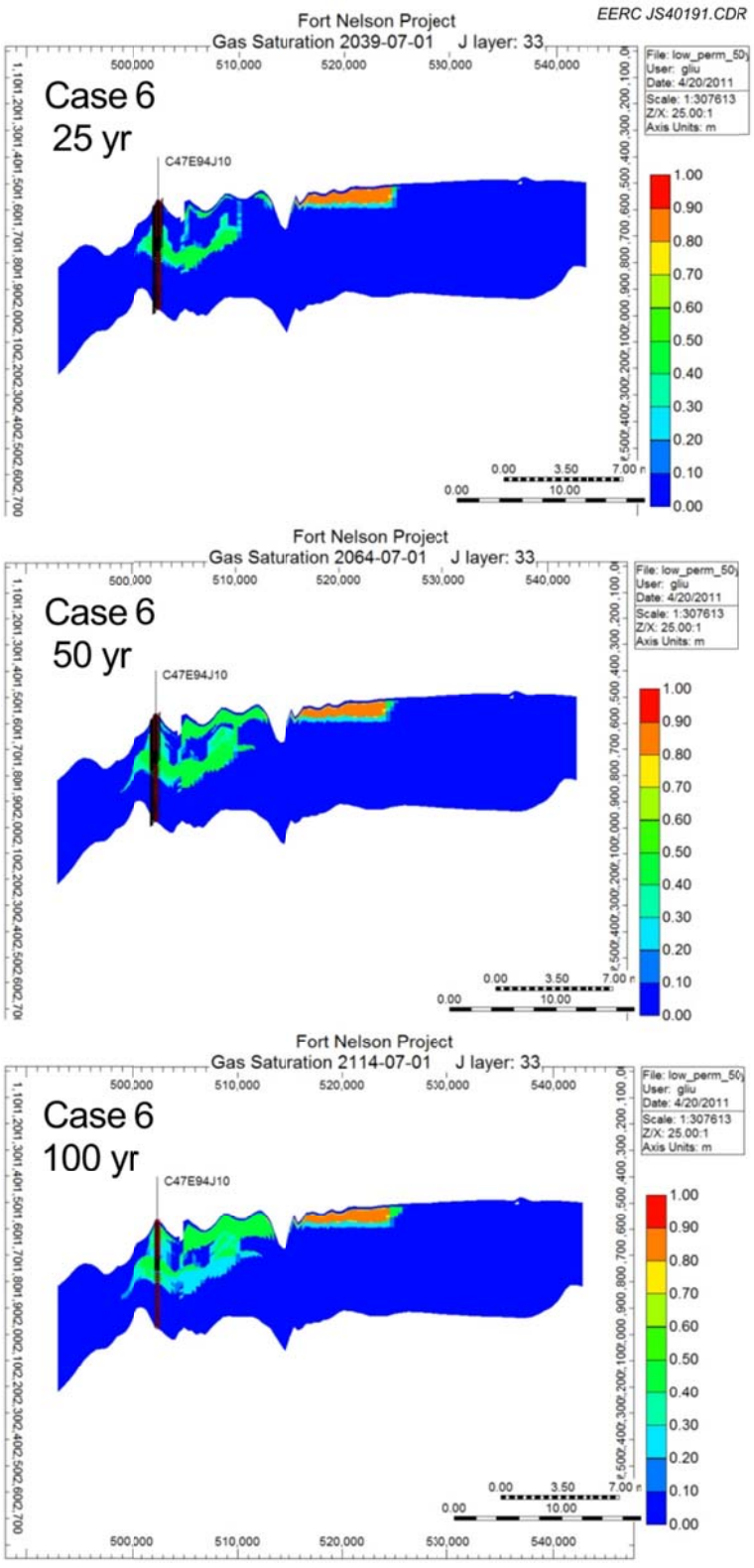

Figure C-15. Cross-sectional view of Case 6: 50 years of injection plus 50 years postinjection in and around c-47-E using the reduced permeability reservoir properties.

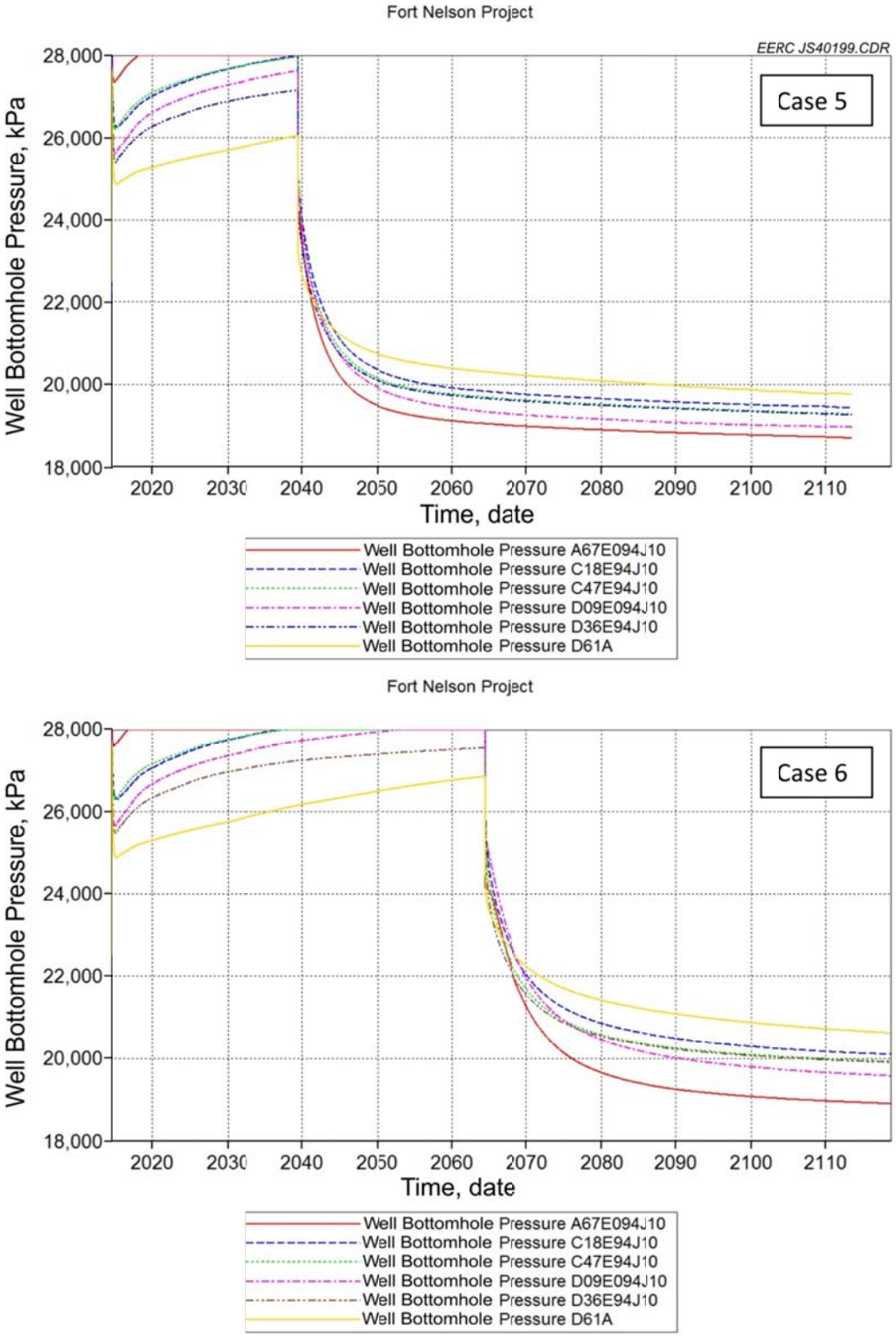

Figure C-16. BHPs at the injection wells for Cases 5 and 6.

Table C-1. Comparisons of Injected Sour Gas Volume of Cases 5, 6, 9, and 10

Cases	Volume Comparisons	
	25 years (m^3)	50 years (m^3)
Fully Injected (reference)	3.08307E + 10	6.24593E + 10
Case 5 (25 years)	2.99646E + 10	
Case 6 (50 years)		5.83754E + 10
Percentage (over fully injected)	97.19	93.46
Case 9 (25 years)	3.08307E + 10	
Case 10 (50 years)		6.16651E + 10
Percentage (over fully injected)	100.00	98.73

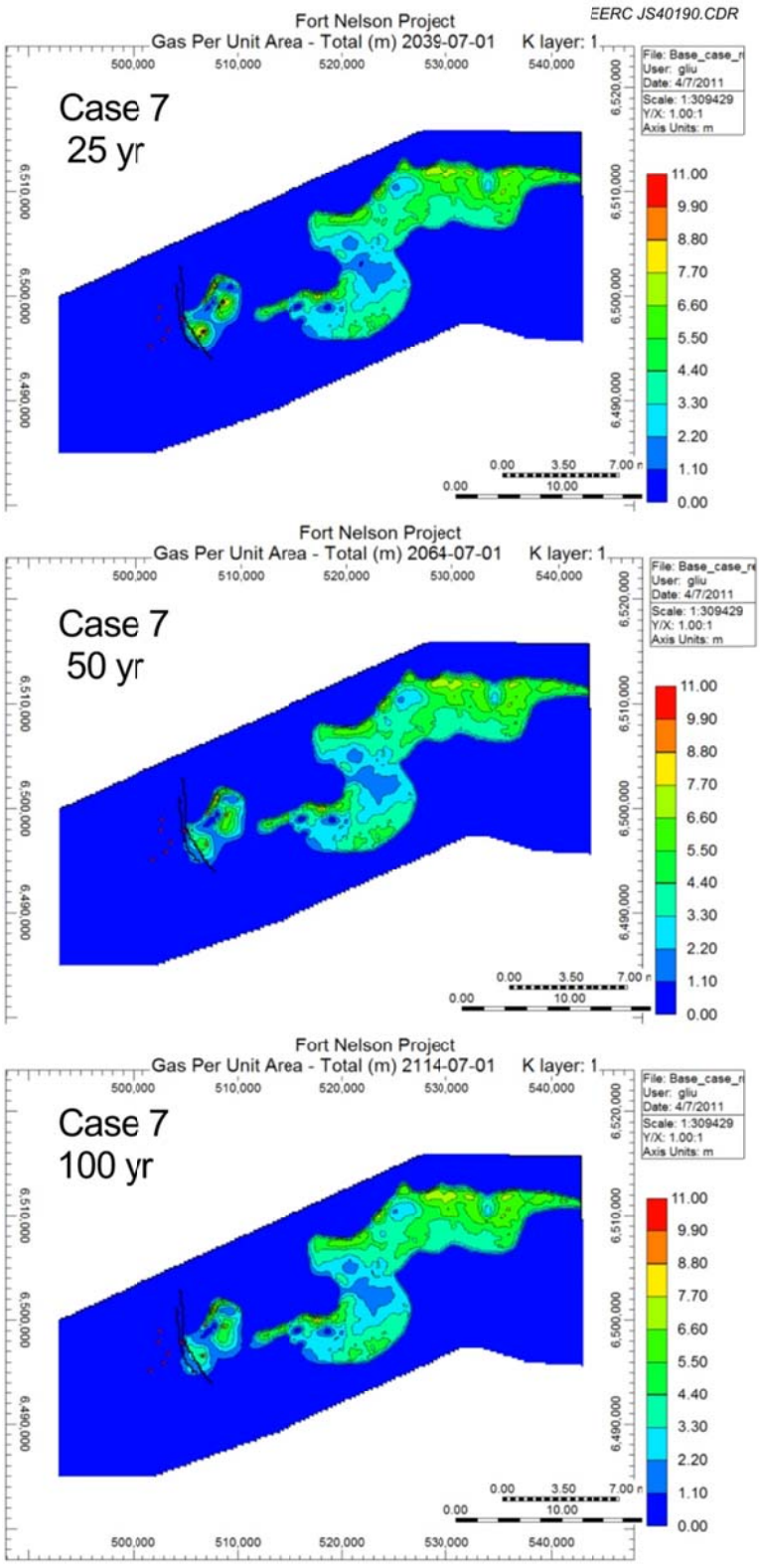

Figure C-17. Areal view of Case 7: 25 years of injection plus 75 years postinjection in and around c-61-E using the base case reservoir properties and two new injection wells.

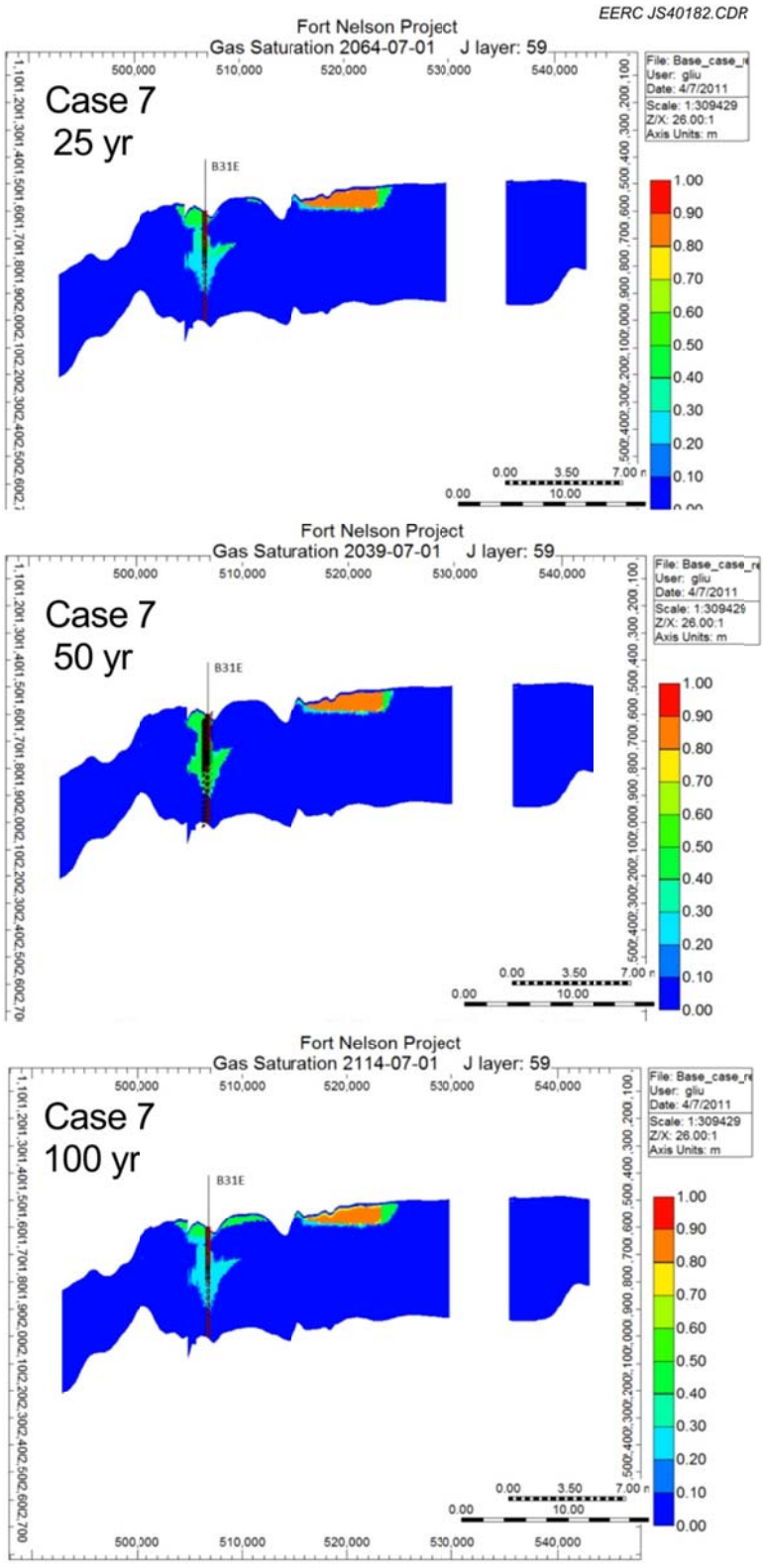

Figure C-18. Cross-sectional view of Case 7: 25 years of injection plus 75 years postinjection in and around c-61-E using the base case reservoir properties and two new injection wells.

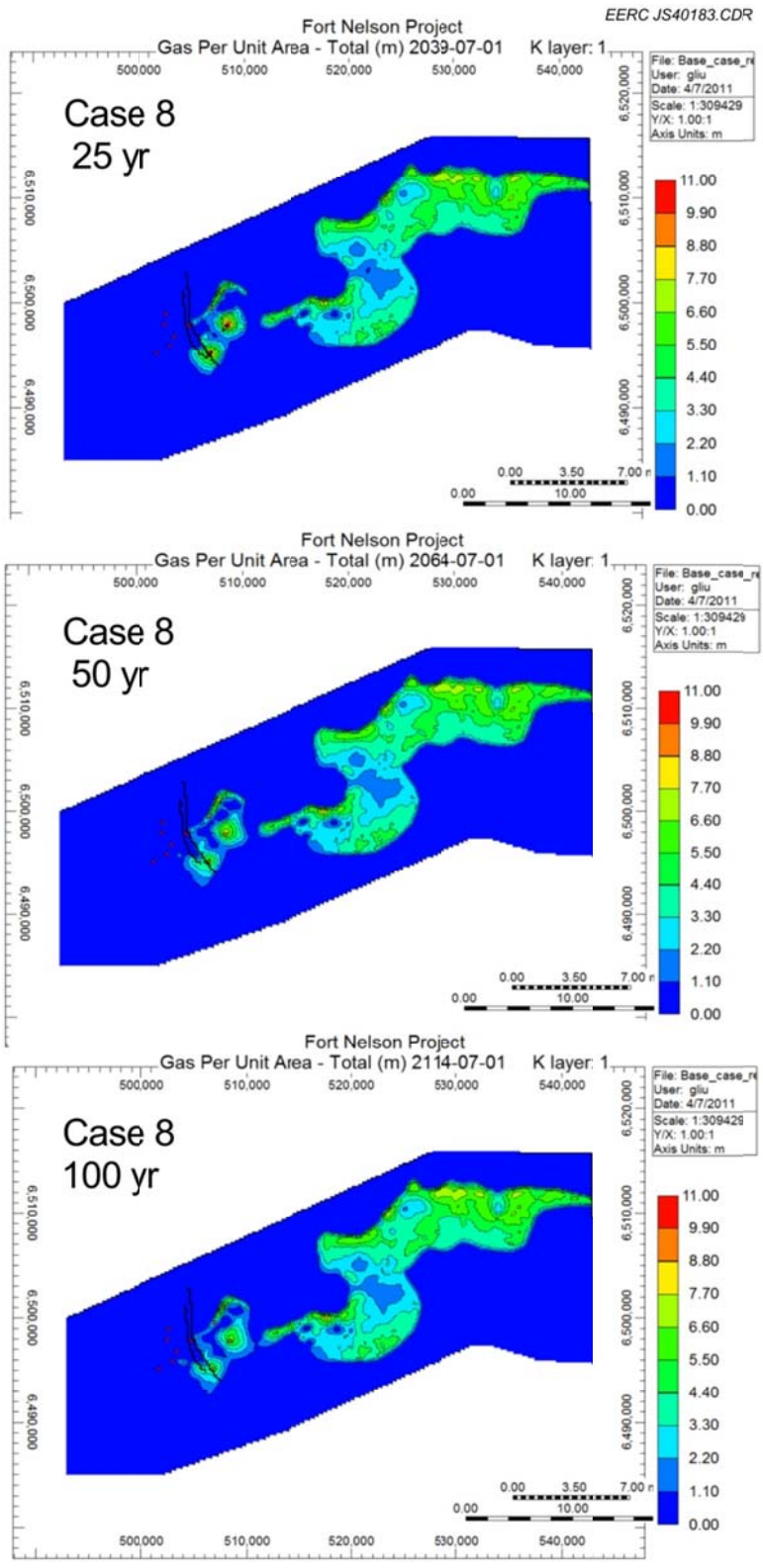

Figure C-19. Areal view of Case 8: 50 years of injection plus 50 years postinjection in and around c-61-E using the base case reservoir properties and two new injection wells.

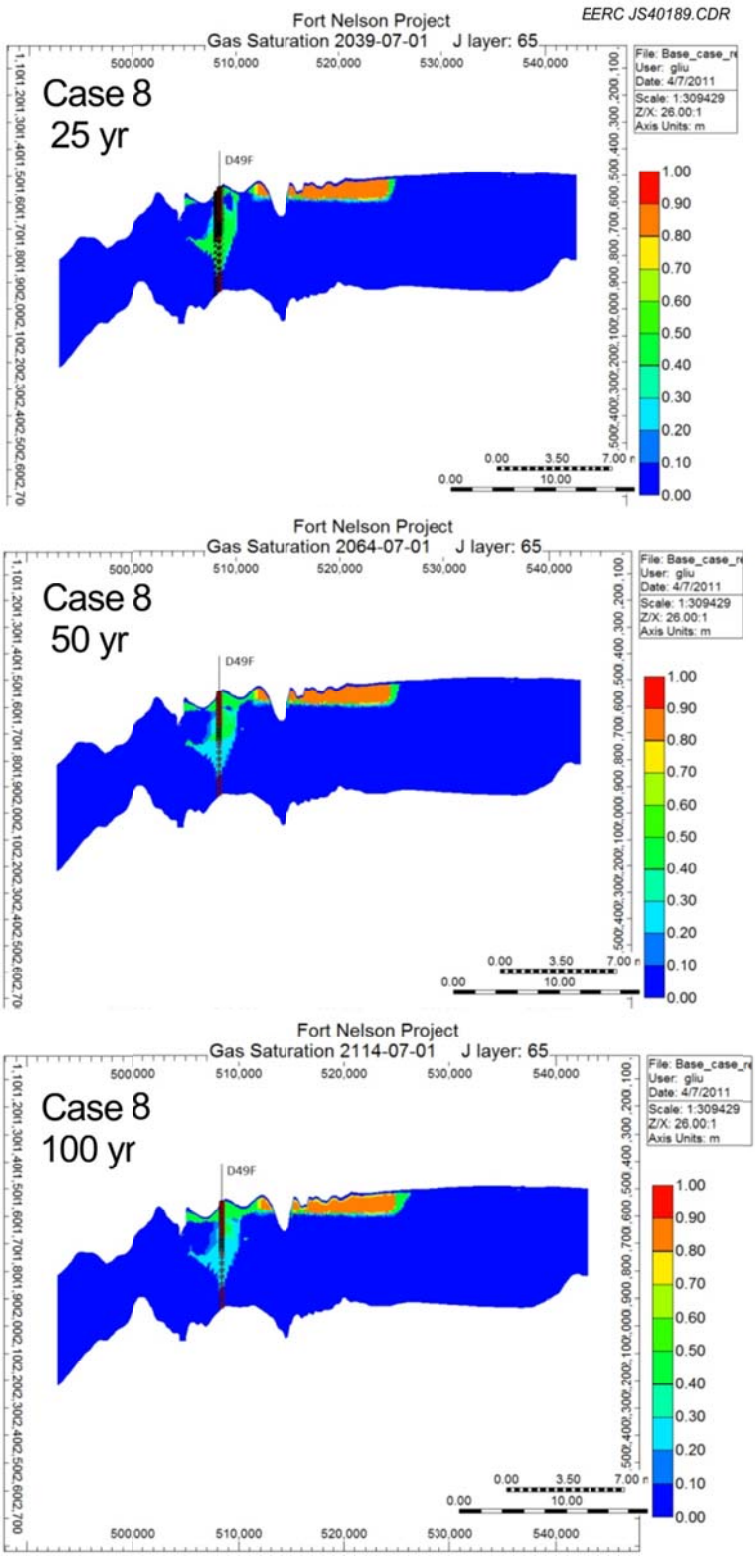

Figure C-20. Cross-sectional view of Case 8: 50 years of injection plus 50 years postinjection in and around c-61-E using the base case reservoir properties and two new injection wells.

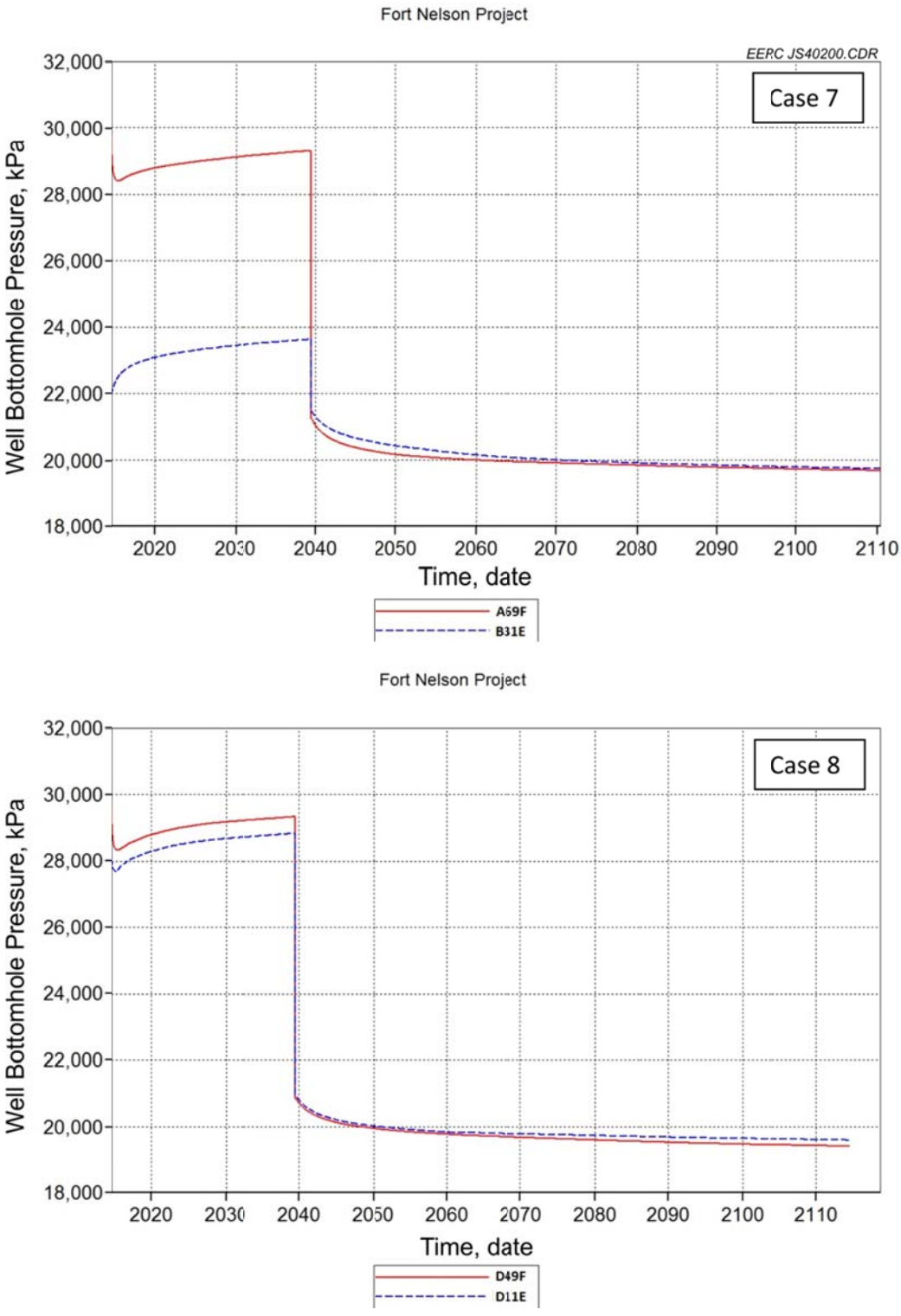

Figure C-21. BHPs at the injection wells for Cases 7 and 8.

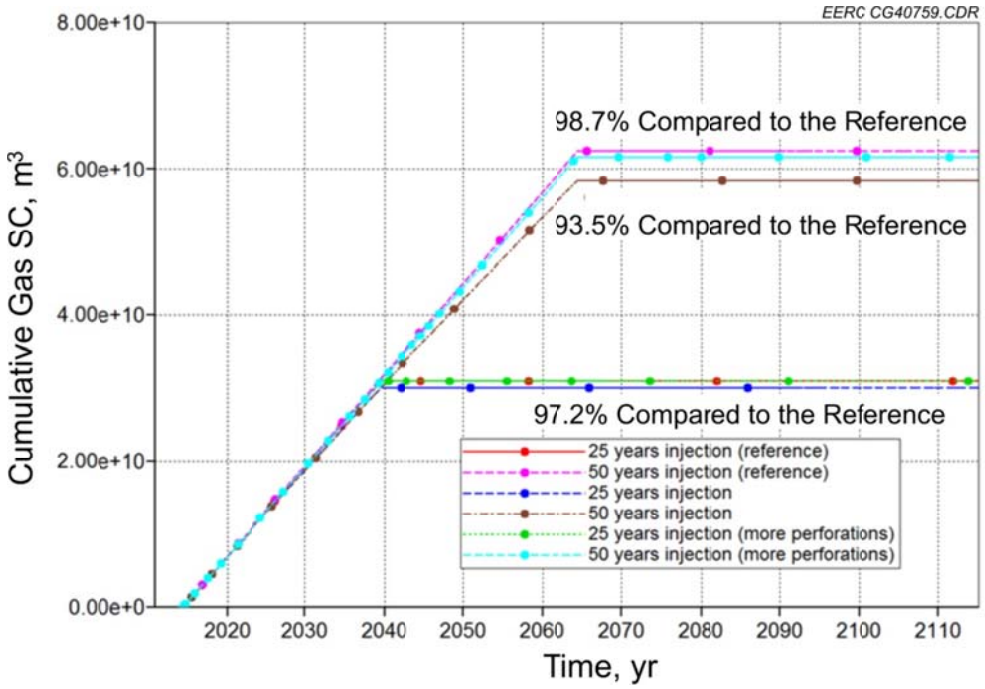

Figure C-22. Cumulative gas volume injection from wells in comparison to Cases 5 and 6 and reference.

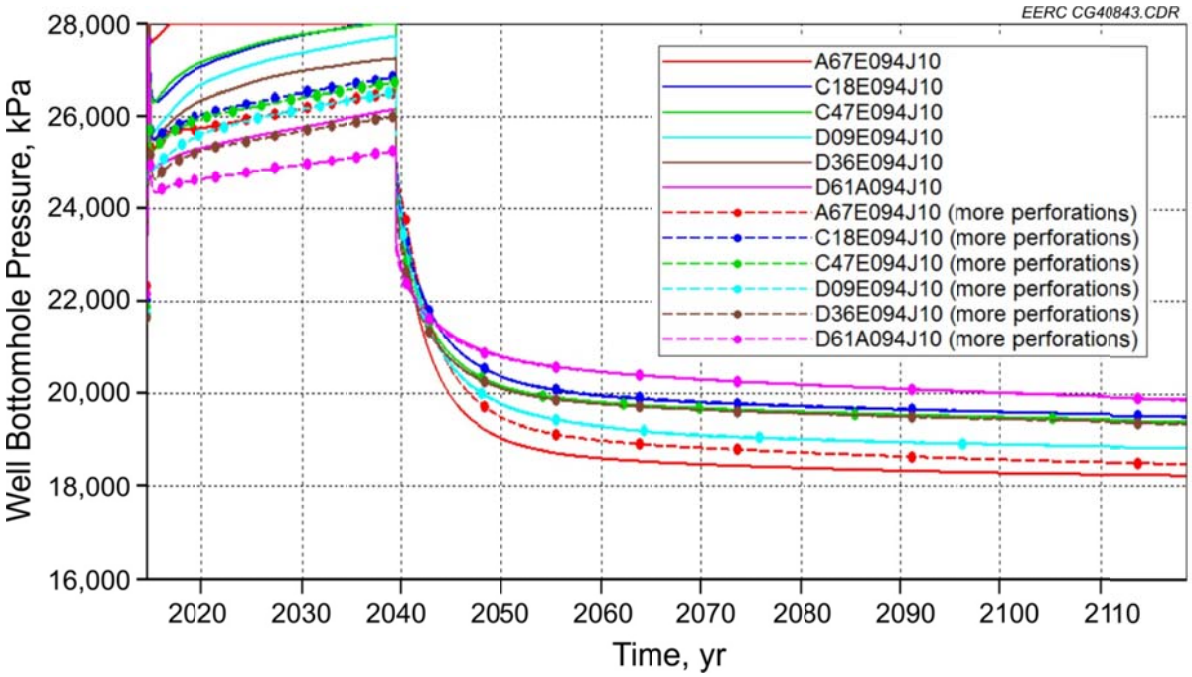

Figure C-23. BHPs at the injection wells for Cases 5 and 9.

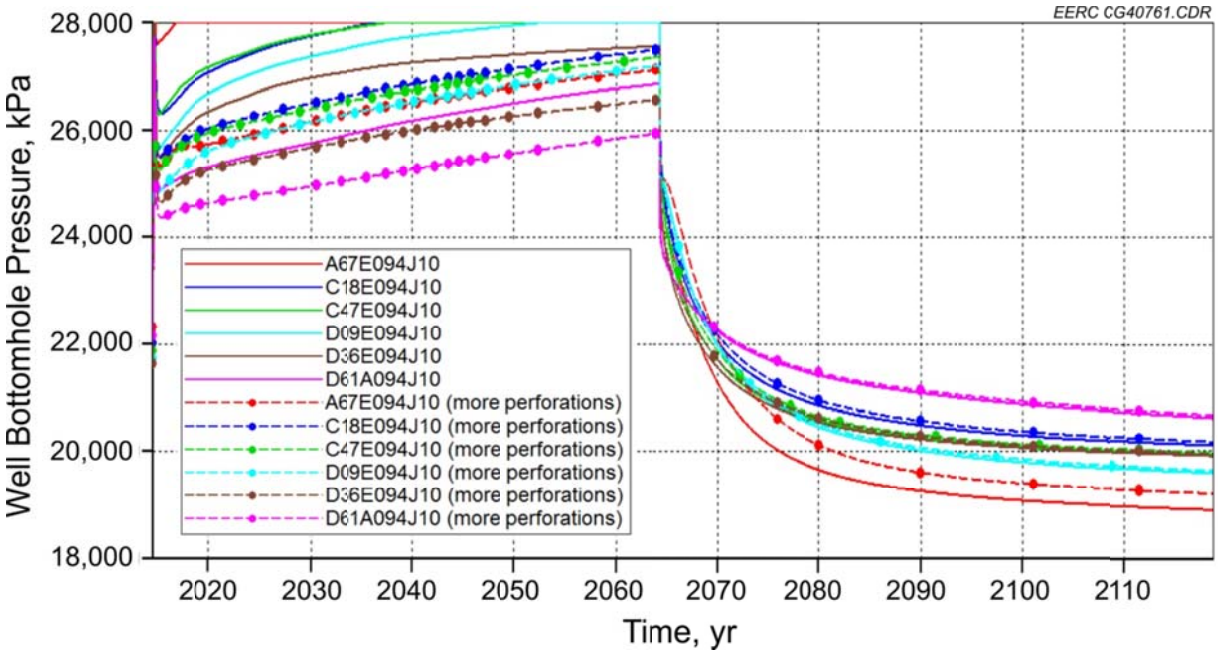

Figure C-24. BHPs at the injection wells for Cases 6 and 10.

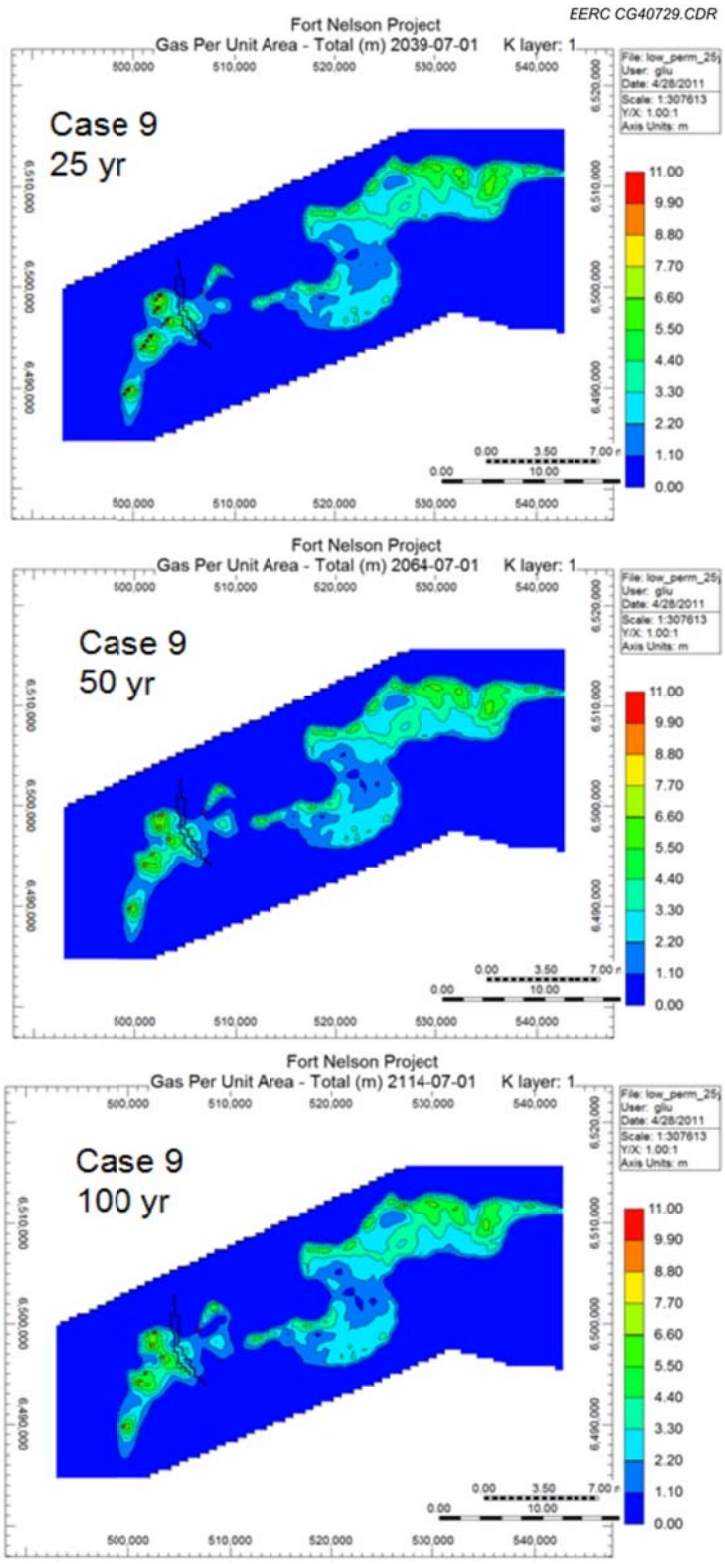

Figure C-25. Areal view of Case 9: 25 years of injection plus 75 years postinjection in and around c-61-E using the base case reservoir properties and three injection wells.

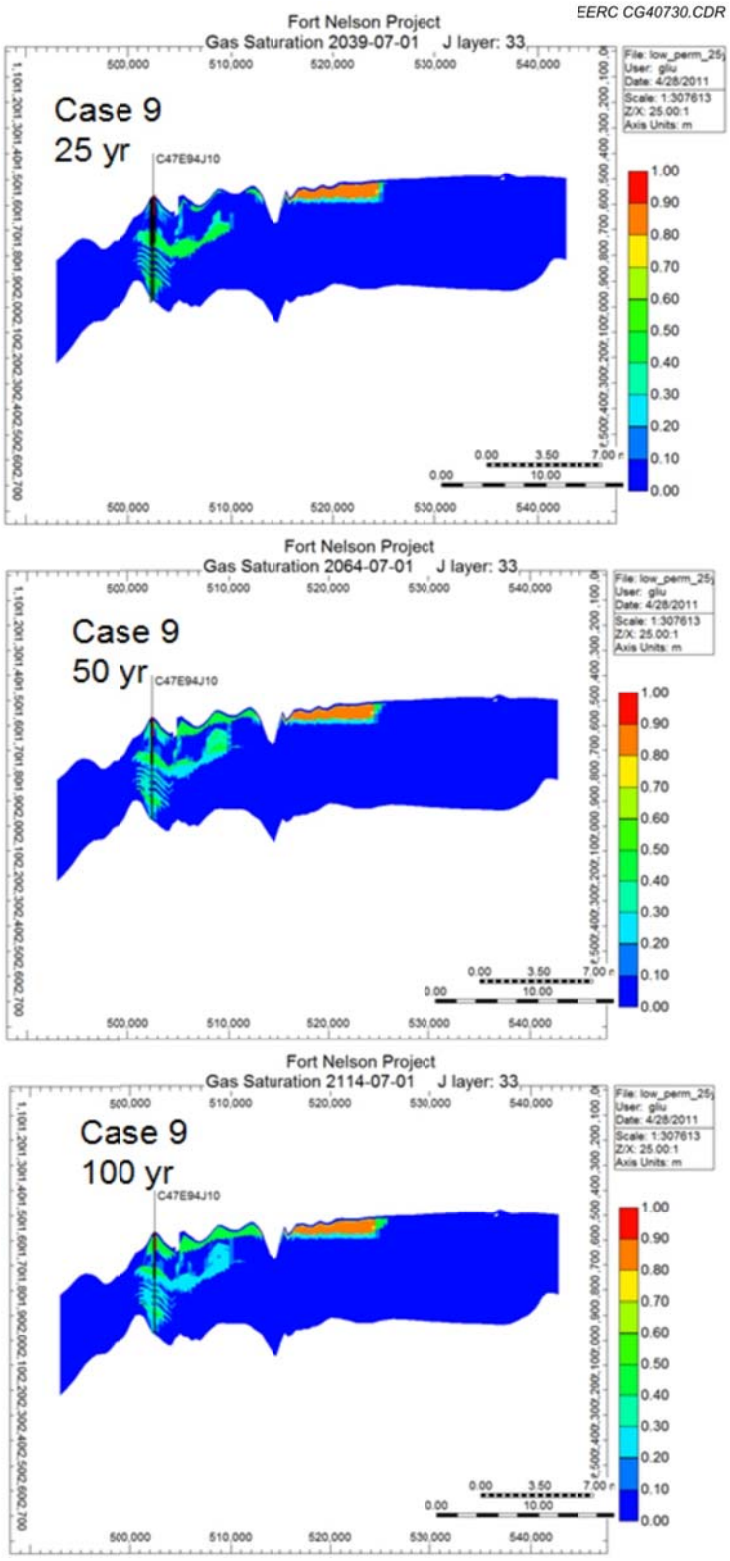

Figure C-26. Cross-sectional view of Case 9: 25 years of injection plus 75 years postinjection in and around c-61-E using the base case reservoir properties and three injection wells.

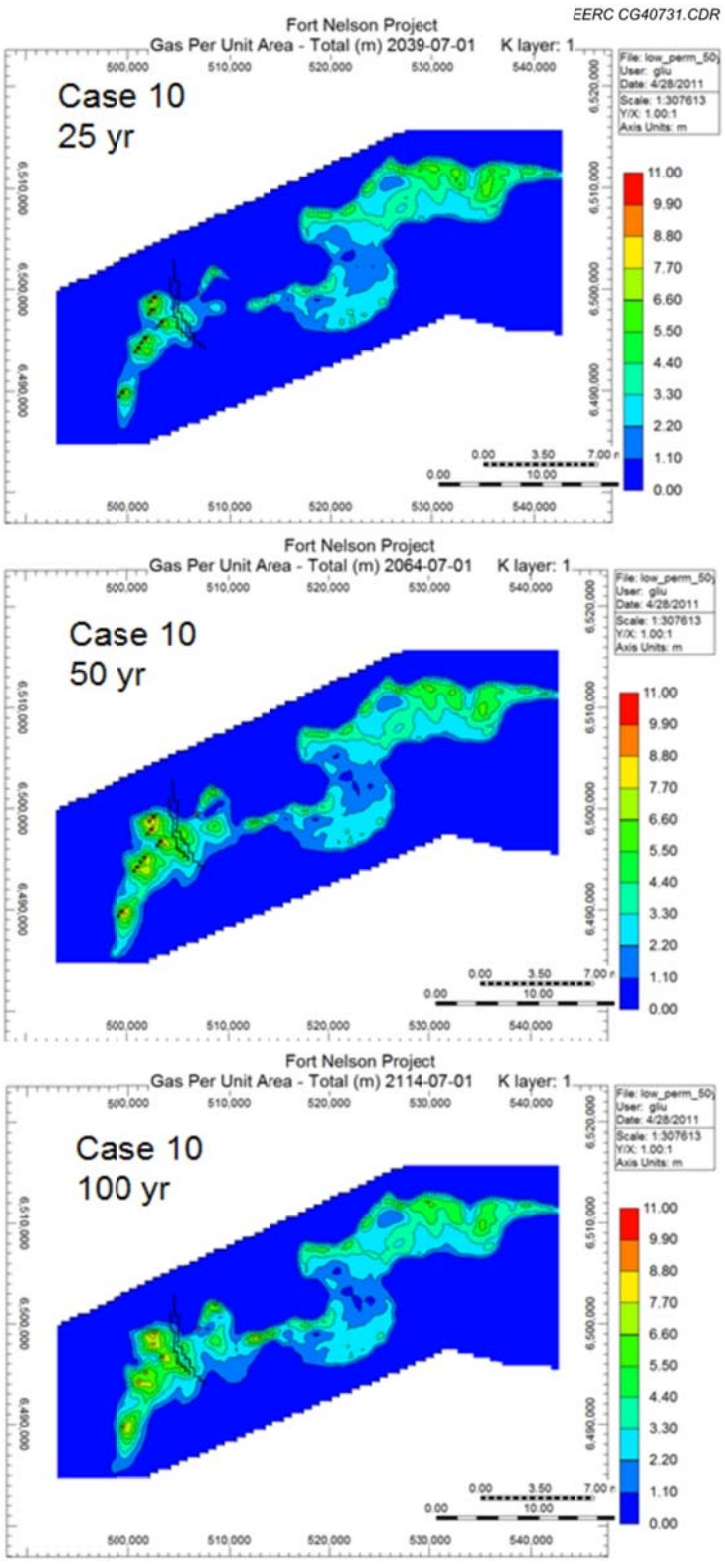

Figure C-27. Areal view of Case 10: 50 years of injection plus 50 years postinjection in and around c-61-E using the base case reservoir properties and three injection wells.

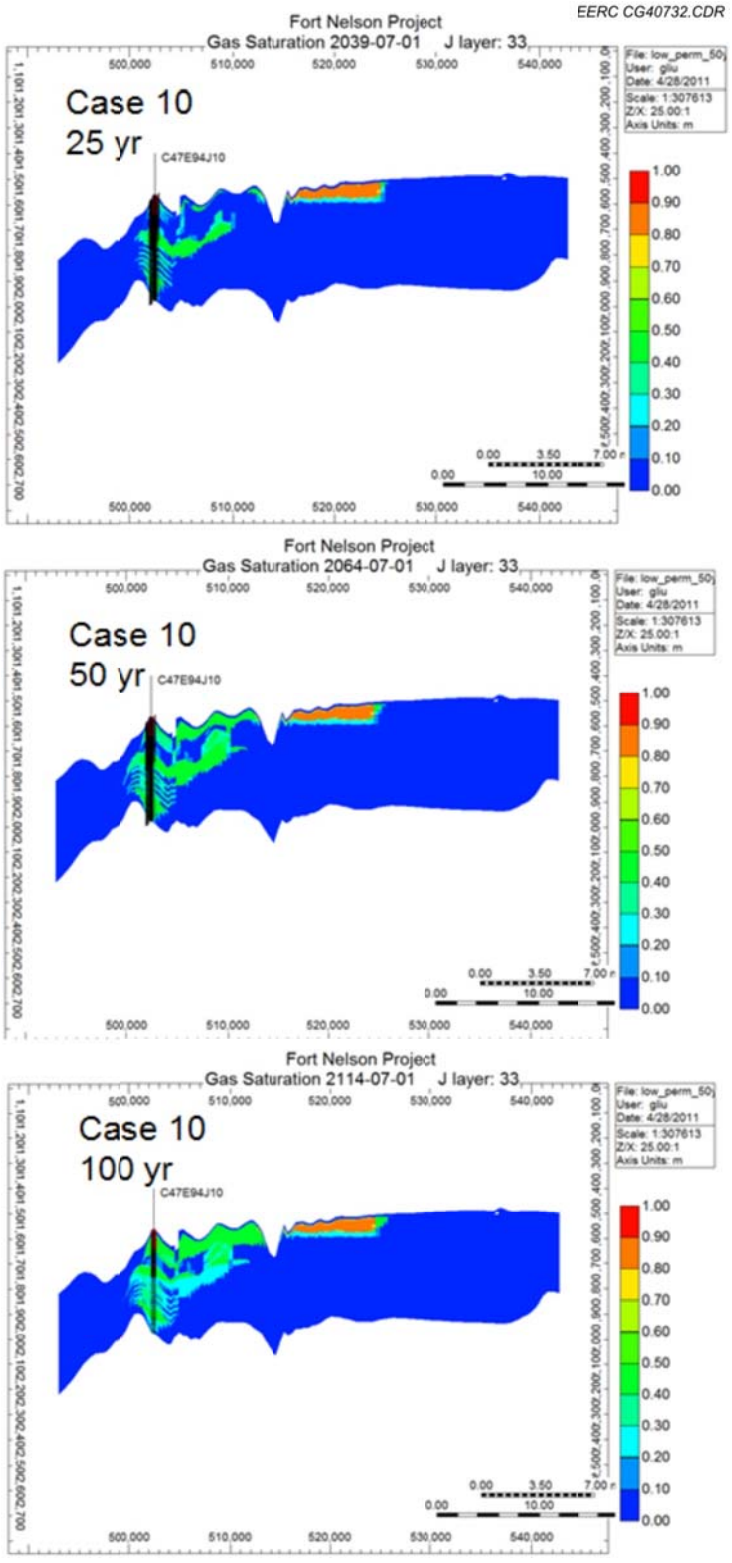

Figure C-28. Cross-sectional view of Case 10: 50 years of injection plus 50 years postinjection in and around c-61-E using the base case reservoir properties and three injection wells.

APPENDIX D

MODEL OPTIMIZATION AND VALIDATIONS (HISTORY MATCHING)

MODEL OPTIMIZATION AND VALIDATIONS (HISTORY MATCHING)

DYNAMIC MODELING WORKFLOW PROCESS

The workflow process that has been proposed by the Energy & Environmental Research Center (EERC) for this dynamic modeling study includes three optimization techniques (grid-size sensitivity analysis, numerical tuning, and properties/parameters sensitivity analysis), which are followed by history matching for model validation and predictive simulations (Figure 2 of the main report). A brief discussion on the optimization techniques and history matching is provided below.

Optimization Techniques

Each of the three optimization techniques improves the overall efficiency of dynamic modeling by reducing the computing power and time required for a particular simulation run. Details of each optimization technique are presented as follows.

Grid-Size Sensitivity Analysis

Grid-size sensitivity analysis compares various model grid sizes so that the coarsest mesh size possible can be utilized while still producing reasonable model outputs. For the Fort Nelson carbon capture and storage (CCS) project, four grid resolutions scaled up from the geologic model Version 3 were examined:

Very fine:	200 × 200 meters; total 2,061,965 cells
Fine:	250 × 250 meters; total 1,420,668 cells (69% of the very fine)
Medium:	300 × 300 meters; total 1,211,280 cells (59% of the very fine)
Coarse:	400 × 400 meters; total 601,524 cells (29% of the very fine)

After testing, the coarse grid resolution was found to be capable of producing reasonable results as compared to the other finer grid resolutions. Thus the 400 × 400-meter grid resolution was chosen for further simulations in this project.

Numerical Tuning

The numerical tuning technique was used to optimize the numerical settings for increasing the speed of the simulation runs. In the case of the Fort Nelson CCS project, various numerical parameters such as pressure change, saturation change, and the tolerance of convergence over each time step were tracked to tune the integrated settings for producing the lowest optimization critical points (Griffith and Nichols, 1996; Hutchinson, 1989; LeDimet et al., 1995). The optimization critical points used in the project included material balance error, central processing unit (CPU) time, and solver failure percent. The original time spent on a single job with 400 × 400-meter grid resolution prior to numerical tuning was more than 60 hours for a 100-year simulation period. After numerical tuning, depending on the simulation scenario, up to 40% reduction in the running time was achieved.

Properties/Parameters Sensitivity Analysis

Sensitivity analysis is a method used to determine the most influential variables for a given simulation by varying one variable over a realistic range while setting all other values to a constant. This is followed by an examination of the net effect of these changes on the results. Once the sensitivity analysis is completed for each variable used in the simulation model, they are compared and analyzed to determine the most influential variables affecting the model output.

A sensitivity analysis was conducted using CMG's Computer-Assisted History Matching, Optimization and Uncertainty Assessment Tool (CMOST). The significant variables were allowed to fluctuate over realistic ranges to produce a valid history match, while variables that were determined to be insignificant were set to a constant value (selected from available data) for the rest of the simulation runs. The values that were altered during the history-matching exercise were then compared to available data sources to ensure that they remained within the expected variability in the existing data.

A preliminary properties sensitivity analysis was performed to determine the "heavy hitter" variables for a given simulation. The ranges were based on the geology of the Fort Nelson CCS feasibility project study area and known gas reservoirs in the region. The preliminary analysis showed that the most sensitive parameters were permeability multiplier (PermR1); relative permeability function for phases that are determined by end points and coefficients (such as kegcl3, ng1, etc.); vertical/horizontal hydraulic conductivity anisotropy (k_v/k_h); injection bottomhole pressure (BHP) (injBHP); capillary entry pressure (determined by end points and coefficients); and gas and water residual saturation (swcon1 and sgcon1) (Figures D-1 and D-2, Table D-1).

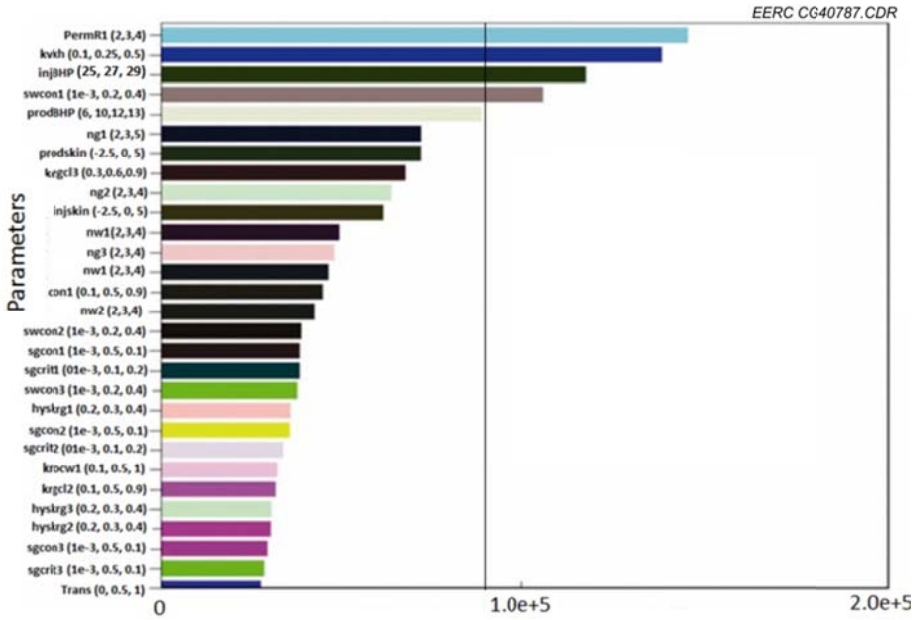

Figure D-1. Version 3 model parameters ranked according to their sensitivity for matching gas production well data.

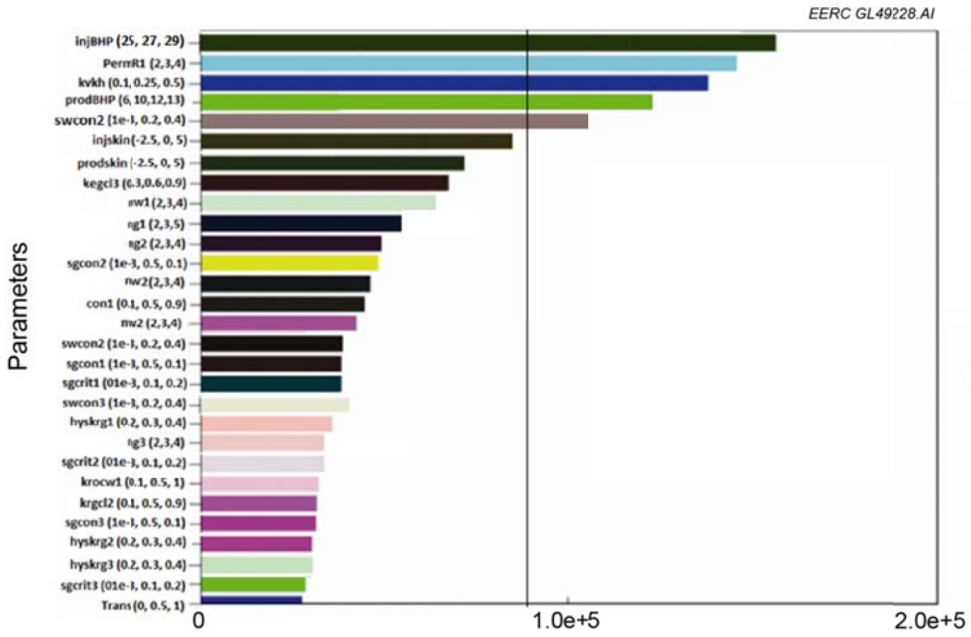

Figure D-2. Version 3 model parameters ranked according to their sensitivity for matching water production well data.

History Matching

The Version 3 static geological model (Appendix A) was used to build the dynamic model for history matching. Once optimized for grid size, numerical tuning, and properties/parameters, the Version 3 model was validated by matching of historical production and pressure data with the simulated results.

History-Matching Validation Data

Historical data were collected from 85 production wells and seven water disposal wells (total 92 wells). The 85 production wells include 42 currently active wells, 21 abandoned wells, 13 suspended wells, and nine undefined wells. In addition to the historical data, information from Well c-61-E was also incorporated; thus a total of 93 wells (Table D-2 and Figure D-3) were used for history matching. All 93 wells penetrate the Slave Point Formation, and 29 out of these 93 wells penetrate the Sulphur Point Formation in the Fort Nelson CCS project study area. Many of the wells did not have complete data records in GeoVista throughout the entire period from 1961 to 2010. GeoVista is a database developed by Divestco which provides current and reliable industry information for Alberta, British Columbia, Saskatchewan, and Manitoba (www.divestco.com/ Solutions/Engineering/Software/GeoVista-%281%29.aspx).

An in-house program was developed and used to sort, filter, and reformat all of the historical data to fit the data format suitable for the simulator. A total of 494 simulations were performed in the final iteration to obtain a reasonable history match. The results are summarized as follows.

Table D-1. Parameters/Properties That Were Tracked During Sensitivity Analysis

Variables		Descriptions
PermR1		Permeability multiplier
k_v/k_h		Vertical and horizontal permeability ratio
ProdBHP		BHP of production wells, kPa
Production Skin		Skin of production wells
Injection BHP, kPa		BHP of injection wells, kPa
Injection Skin		Skin of injection wells
Trans		Fault transmissibility
HYSKRG1		Relative permeability hysteresis of the rock with permeability larger than 1 mD
HYSKRG2		Relative permeability hysteresis of the rock with permeability range 0.01 to 1 mD
HYSKRG3		Relative permeability hysteresis of the rock with permeability less than 0.01 mD
End Points	Swcon1 to Swcon3	Connate water saturation
	Swcrit1 to Swcrit3	Critical water saturation
	Sgcrit1 to Sgcrit3	Critical gas saturation
	Sgcon1 to Sgcon3	Connate gas saturation
	Krgcl1 to Krgcl3	Gas relative permeability at connate water
	Krocw1 to Krocw3	Water relative permeability at connate gas
Exponents and Coefficients	nw1 to nw3	Exponents for water relative permeability curves
	ng1 to ng3	Exponents for gas relative permeability curves
	Excp1 to Excp3	Exponents for capillary pressure curves
	Con1 to Con3	Coefficient for capillary pressure curves

Table D-2. Wells Used for History Matching

Well ID	Well Type	Well ID	Well Type	Well ID	Well Type
00/A-005-A/094-J-15/0	Production well	00/B-053-J/094-J-10/0	Production well	00/C-078-I/094-J-10/0	Production well
00/A-010-D/094-J-16/0	Production well	00/B-061-G/094-J-10/0	Production well	00/C-078-K/094-J-10/0	Production well
00/A-030-A/094-J-15/2	Production well	00/B-069-L/094-J-09/0	Disposal well	00/C-080-F/094-J-10/0	Production/disposal well
00/A-030-A/094-J-15/3	Production well	00/B-070-I/094-J-10/0	Production well	00/C-080-L/094-J-09/0	Production well
00/A-051-J/094-J-10/0	Production well	00/B-072-L/094-J-09/0	Production well	00/C-085-I/094-J-10/0	Production well
00/A-052-J/094-J-10/0	Production well	00/B-073-L/094-J-09/0	Production well	00/C-087-I/094-J-10/0	Production well
00/A-053-J/094-J-10/0	Production well	00/B-074-G/094-J-10/2	Production well	00/C-088-F/094-J-10/0	Production/disposal well
00/A-055-J/094-J-10/0	Production well	00/B-075-H/094-J-10/0	Production well	00/C-089-F/094-J-10/0	Disposal well
00/A-056-J/094-J-10/0	Production well	00/B-076-G/094-J-10/0	Production well	00/C-092-G/094-J-10/3	Production well
00/A-061-F/094-J-10/0	Production well	00/B-078-G/094-J-10/2	Production well	00/C-092-I/094-J-10/0	Production well
00/A-065-G/094-J-10/0	Production/disposal well	00/B-078-I/094-J-10/0	Production well	00/C-092-L/094-J-09/0	Production well
00/A-065-L/094-J-09/0	Production well	00/B-088-L/094-J-09/0	Production well	00/C-094-L/094-J-09/0	Production well
00/A-068-H/094-J-10/0	Production well	00/B-091-G/094-J-10/0	Production well	00/C-096-I/094-J-10/0	Production well
00/A-074-G/094-J-10/0	Disposal well	00/B-092-G/094-J-10/0	Production well	00/C-099-K/094-J-10/2	Production well

Continued . . .

Table D-2. Wells Used for History Matching (continued)

Well ID	Well Type	Well ID	Well Type	Well ID	Well Type
00/A-075-L/094-J-09/0	Production well	00/B-097-L/094-J-09/0	Production well	00/C-100-L/094-J-09/0	Undefined well
00/A-077-L/094-J-09/0	Production well	00/B-098-L/094-J-09/3	Production well	00/C-100-L/094-J-09/2	Production well
00/A-081-G/094-J-10/0	Production well	00/C-008-D/094-J-16/0	Undefined well	00/D-013-J/094-J-10/2	Production well
00/A-083-G/094-J-10/0	Production well	00/C-020-I/094-J-10/0	Production well	00/D-021-J/094-J-10/0	Production well
00/A-089-K/094-J-10/0	Production well	00/C-029-I/094-J-10/0	Production well	00/D-029-K/094-J-09/0	Production well
00/A-090-F/094-J-10/0	Production well	00/C-043-J/094-J-10/0	Production well	00/D-031-K/094-J-10/0	Production well
00/A-092-I/094-J-10/0	Production well	00/C-050-K/094-J-09/0	Production well	00/D-037-J/094-J-10/2	Production well
00/A-094-I/094-J-10/0	Production well	00/C-052-F/094-J-10/0	Production well	00/D-048-L/094-J-09/0	Disposal/undefined well
00/A-099-F/094-J-10/0	Production well	00/C-054-F/094-J-10/0	Production well	00/D-051-G/094-J-10/2	Production well
00/B-006-D/094-J-16/0	Production well	00/C-056-L/094-J-09/0	Production well	00/D-054-G/094-J-10/2	Production well
00/B-008-D/094-J-16/2	Undefined well	00/C-057-I/094-J-10/0	Production well	00/D-066-G/094-J-10/0	Production well
00/B-008-I/094-J-10/0	Production well	00/C-066-H/094-J-10/0	Production well	00/D-072-G/094-J-10/0	Production well
00/B-010-D/094-J-16/0	Production well	00/C-066-L/094-J-09/3	Production well	00/D-072-L/094-J-09/0	Production well
00/B-018-I/094-J-10/0	Production well	00/C-069-H/094-J-10/0	Production well	00/D-091-L/094-J-09/0	Production well

Continued . . .

Table D-2. Wells Used for History Matching (continued)

Well ID	Well Type		Well ID	Well Type		Well ID	Well Type
00/B-026-J/094-J-10/0	Production well		00/C-069-I/094-J-10/2	Production well		00/D-092-L/094-J-09/0	Production well
00/B-029-A/094-J-15/2	Production well		00/C-073-I/094-J-10/0	Production well		00/D-094-I/094-J-10/2	Production well
00/B-046-J/094-J-10/0	Production well		00/C-075-L/094-J-09/0	Production well		00/D-096-L/094-J-09/0	Production well
00/B-048-I/094-J-10/0	Production well		00/C-076-H/094-J-10/0	Undefined well		02/D-088-L/094-J-09/0	Production well

History-Matching Results

After 494 history matching simulation runs, an asymptotical convergence was achieved. Upon convergence, the global objective function error between the simulation runs and the historical data for gas and water production and water disposal are 0.49%, 7.03%, and 0.43% respectively. The matched wells (total 92 wells) were shown in Figure D-3. Correspondingly, Figures D-4–D-6 show a comparison of the historical and simulation data for cumulative gas production, cumulative water disposal, and cumulative water production. The history-matching results indicate a good match for gas production and water disposal. BHP of all wells is close to scatter points of the historical data. However, only results of the top ten highest gas production wells (Table D-3 and Figure D-7) were presented in this report (Figures D-8–D-27).

The purpose of the history match was to help verify site characterization or identify where there are issues with the site characterization. The history match also creates the pressure sinks in the reservoir model due to the effects of gas production and water disposal which, in turn, will allow for more accurate simulation of the effects of a CCS operation.

The fieldwide distributions of the initial pressure (before history matching) and the current measured pressure are shown in Figures D-28 (1960 time frame) and D-30 (2010 time frame). As shown, there is a pressure sink in the reservoir model as a result of the significant gas production and water disposal operations. Further, it can be seen that the largest pressure drop is in the area of the Slave Point A gas pool which has produced some 1.8 Tcf of raw gas. Secondly, the pressure sink effects ripple outward in the reef bank area, but the pressure drop is less with more distance away from the Slave Point A production.

The simulated pressure distributions obtained after history matching (Figure D-29) in the injection side regions were found to be lower than the measured field pressures (Figure D-30). This can be attributed to the nonavailability of production/injection wells out of the gas pools.

To further match the pressure in these regions, especially the front of the reefs and injection regions, two methods were used:

- Boundary conditions: introduction of new boundary conditions, especially the settings of the aquifer on boundaries (Figure D-31).

- Lower-permeability barrier: the barrier was used to mimic the low permeability barrier between Gas Pools A and B for potential geological insight (Figure D-32).

It appears that the results with aquifer boundaries and lower permeability barriers show a reasonable match of the pressure profile (Figure D-33) in the front of reefs and injection region even though the transient area between injection and gas pools does not.

A reasonable history match obtained for production and pressure data, particularly where historical production and disposal data are available, has resulted in improved confidence in the geologic model. Achievement of a satisfactory global objective function to match historical data will yield more reliable behavior of CO_2 injection during predictive simulations. This would also help in obtaining a more accurate assessment of the site for better prediction and risk analysis.

The availability of more information in the rest of the region away from the gas pools (such as the injection region) would definitely increase the confidence of further site assessment for prediction and risk analysis.

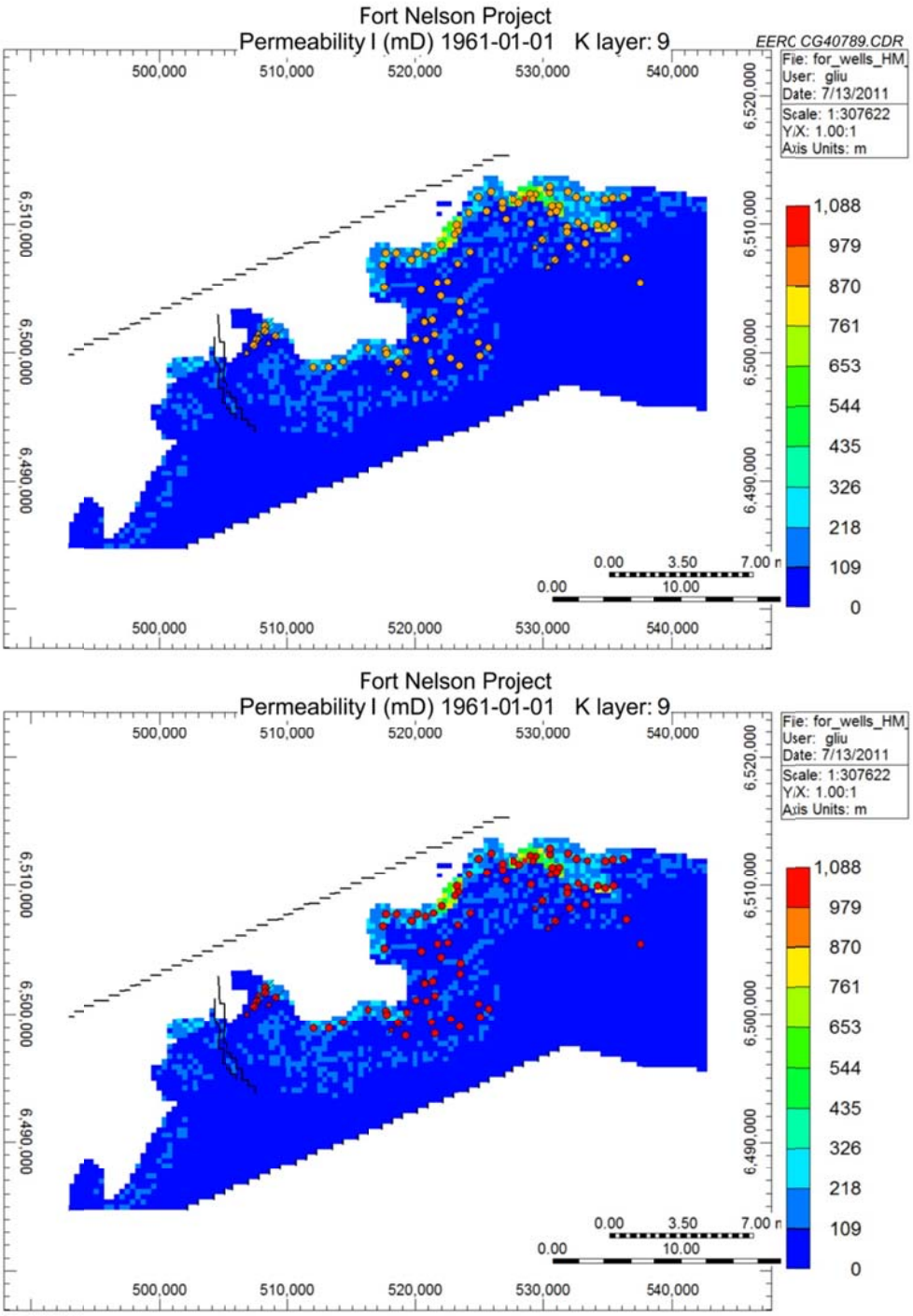

Figure D-3. Plan view showing the gas and water production wells and water disposal wells used for the history matching (top) and the wells that have currently achieved a satisfactory history match (bottom).

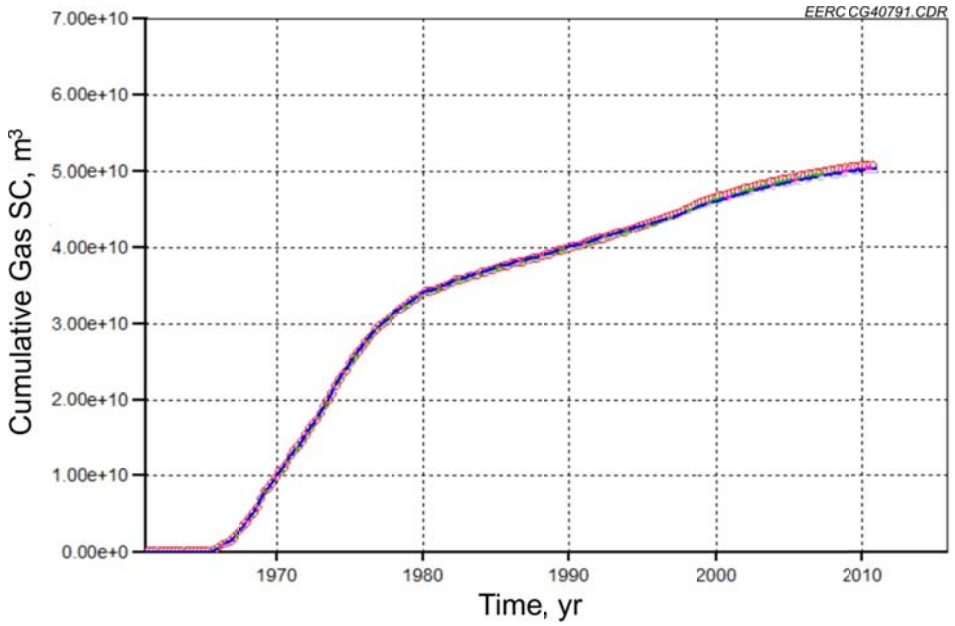

Figure D-4. Cumulative gas production from all production wells. Red circles are the historical data, and the others are the top five simulation results.

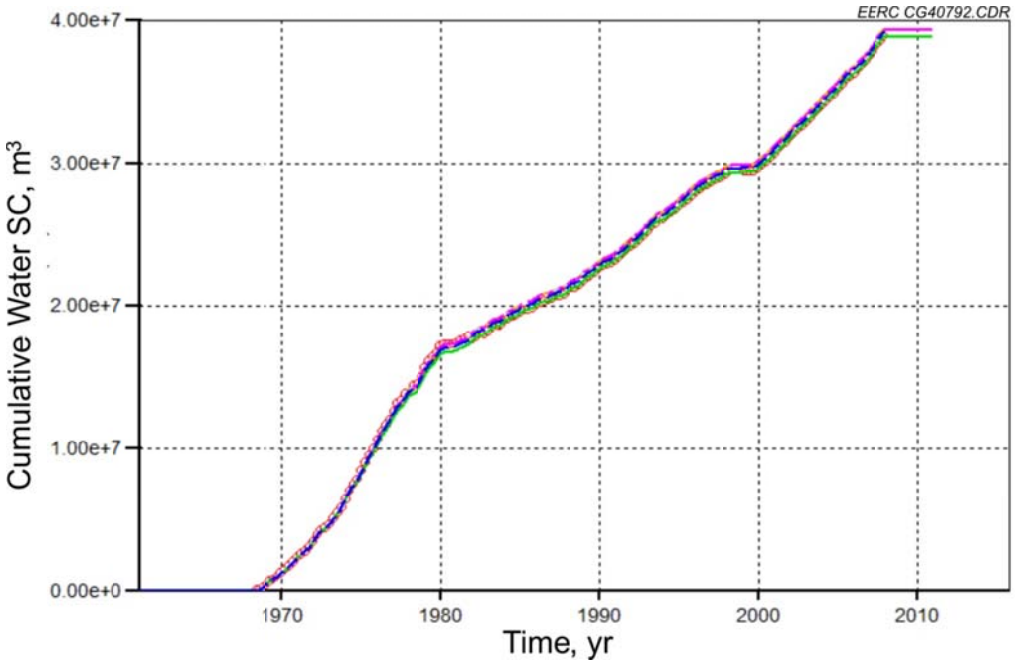

Figure D-5. Cumulative water disposal from all disposal wells. Red circles are the historical data, and the others are the top five simulation results.

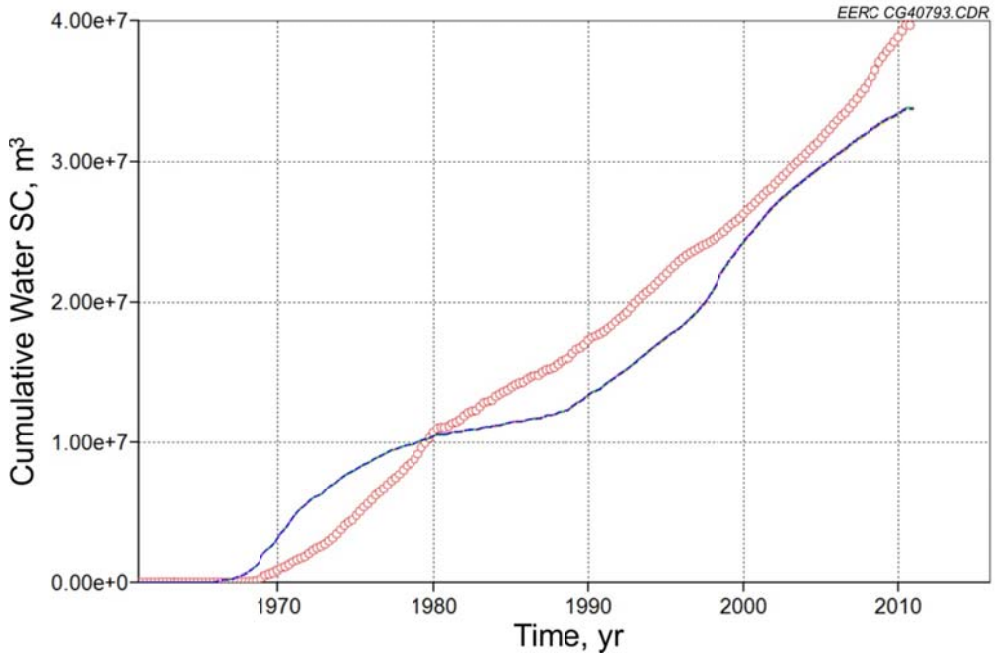

Figure D-6. Cumulative water production from all production wells. Red circles are the historical data, and the others are the top five simulation results.

Table D-3. Top Ten Highest Gas Production Wells

No.	Well Name	Gas Production	Gas Production
1	00_C-078-I_094-J-10_0	4,091,518,800.00	4.09E+09
2	00_C-092-I_094-J-10_0	3,811,927,700.00	3.81E+09
3	02_D-088-L_094-J-09_0	2,513,338,500.00	2.51E+09
4	00_B-072-L_094-J-09_0	2,317,654,900.00	2.32E+09
5	00_B-010-D_094-J-16_0	2,066,321,400.00	2.07E+09
6	00_B-070-I_094-J-10_0	1,773,025,500.00	1.77E+09
7	00_B-018-I_094-J-10_0	1,741,398,500.00	1.74E+09
8	00_A-010-D_094-J-16_0	1,704,810,500.00	1.70E+09
9	00_C-020-I_094-J-10_0	1,676,268,900.00	1.68E+09
10	00_C-069-I_094-J-10_2	1,651,351,200.00	1.65E+09

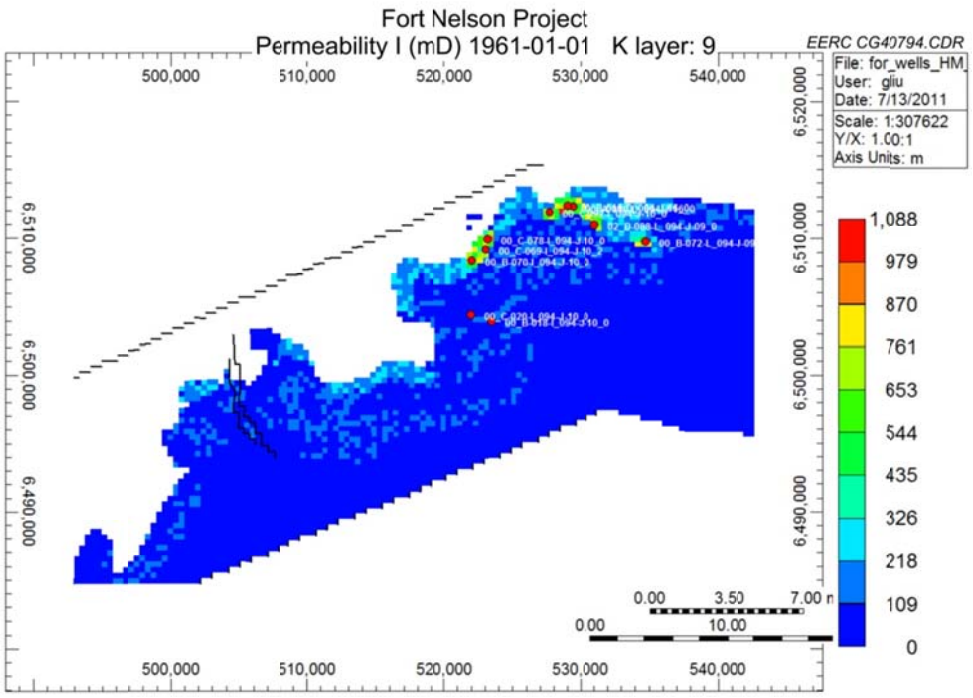

Figure D-7. Locations of the top ten highest wells.

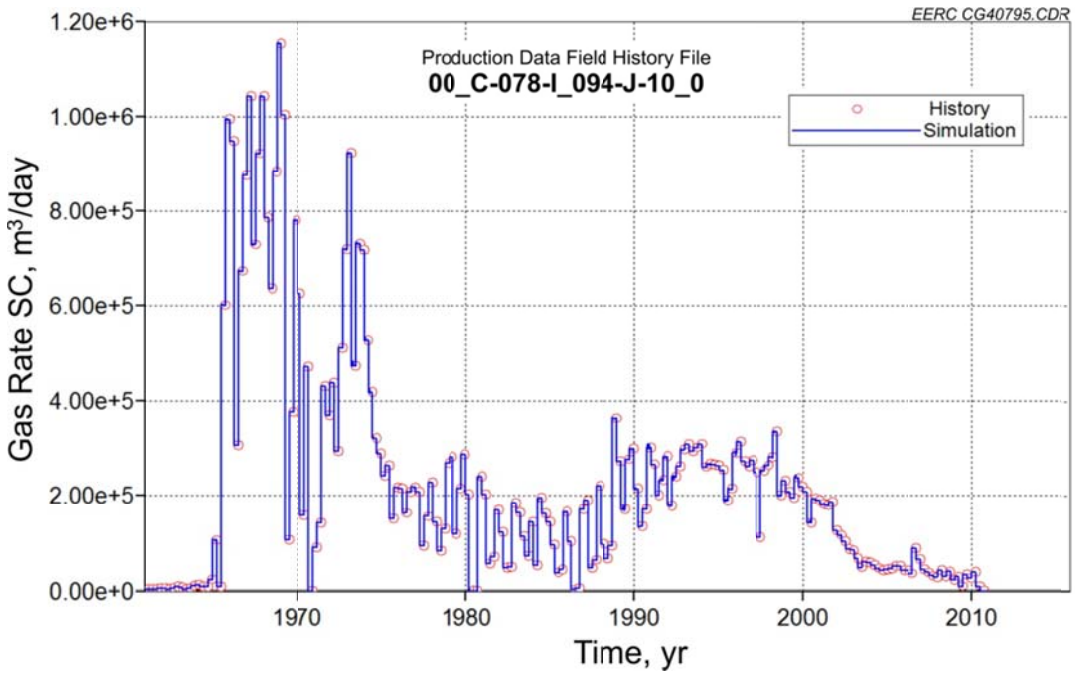

Figure D-8. Gas production rate of the well. Red circles are the historical data, and the other is the top simulation result.

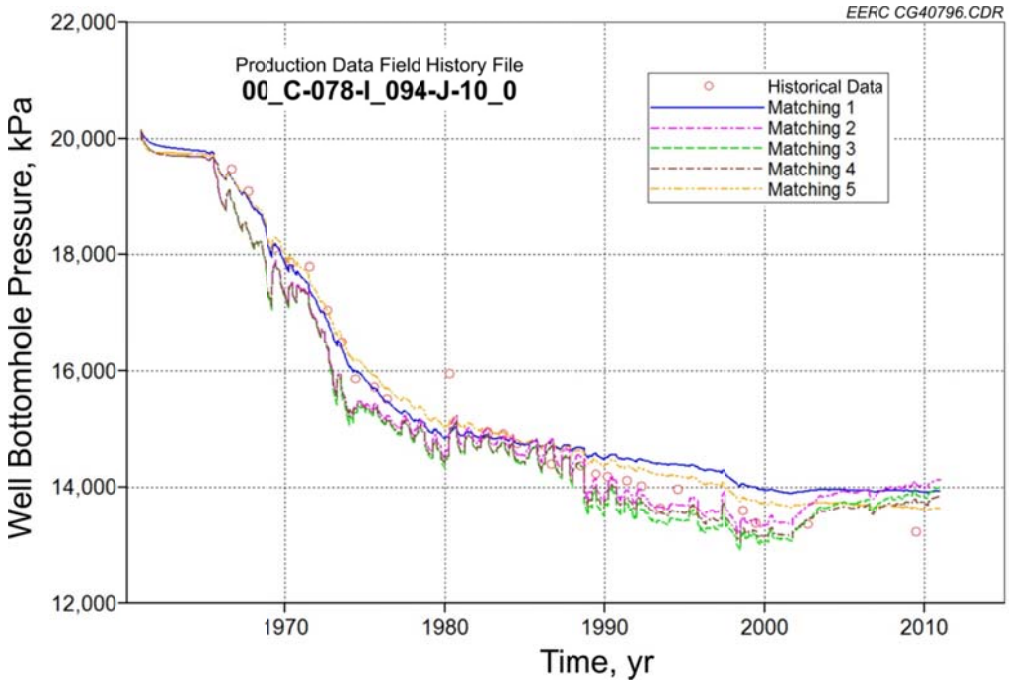

Figure D-9. BHP of the well. Red circles are the historical data, and the others are the top five simulation results.

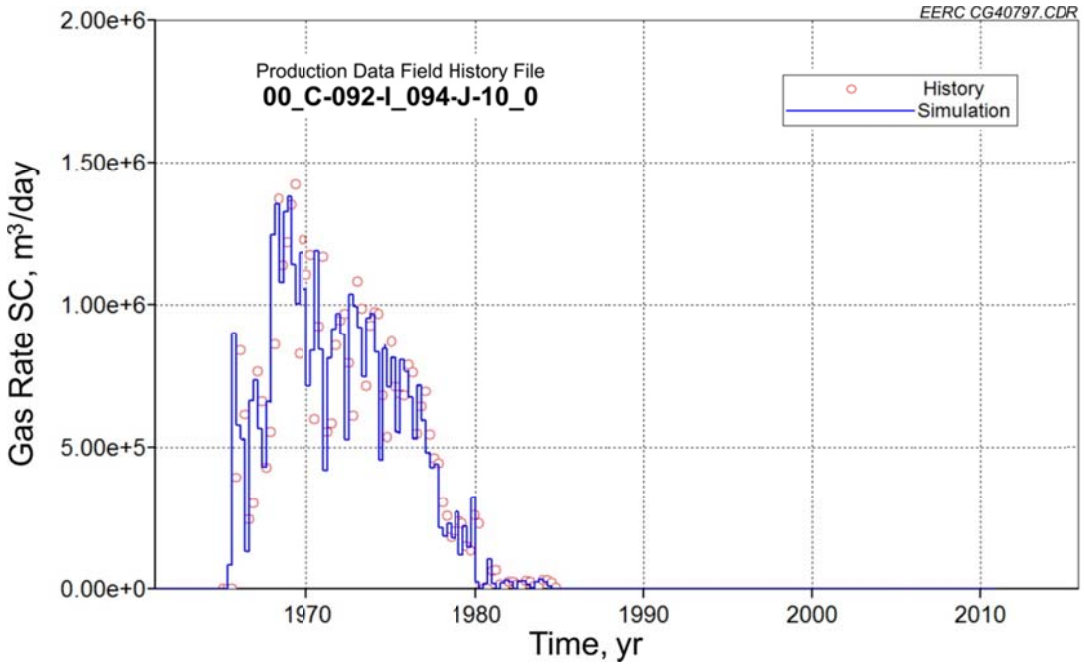

Figure D-10. Gas production rate of the well. Red circles are the historical data, and the other is the top simulation result.

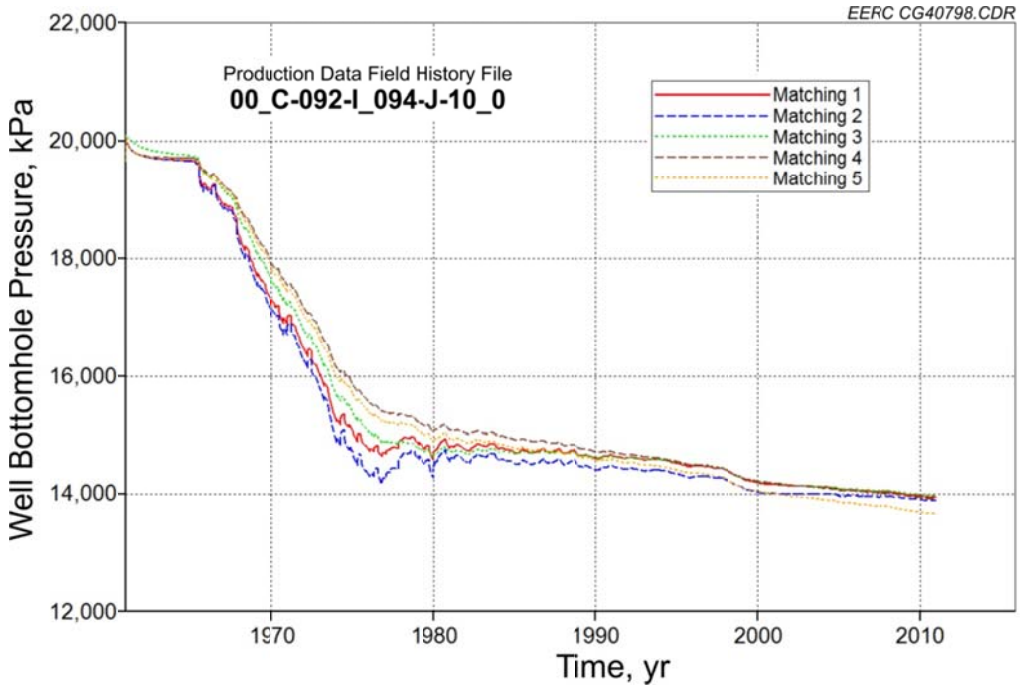

Figure D-11. BHP of the well from the top five simulation results.

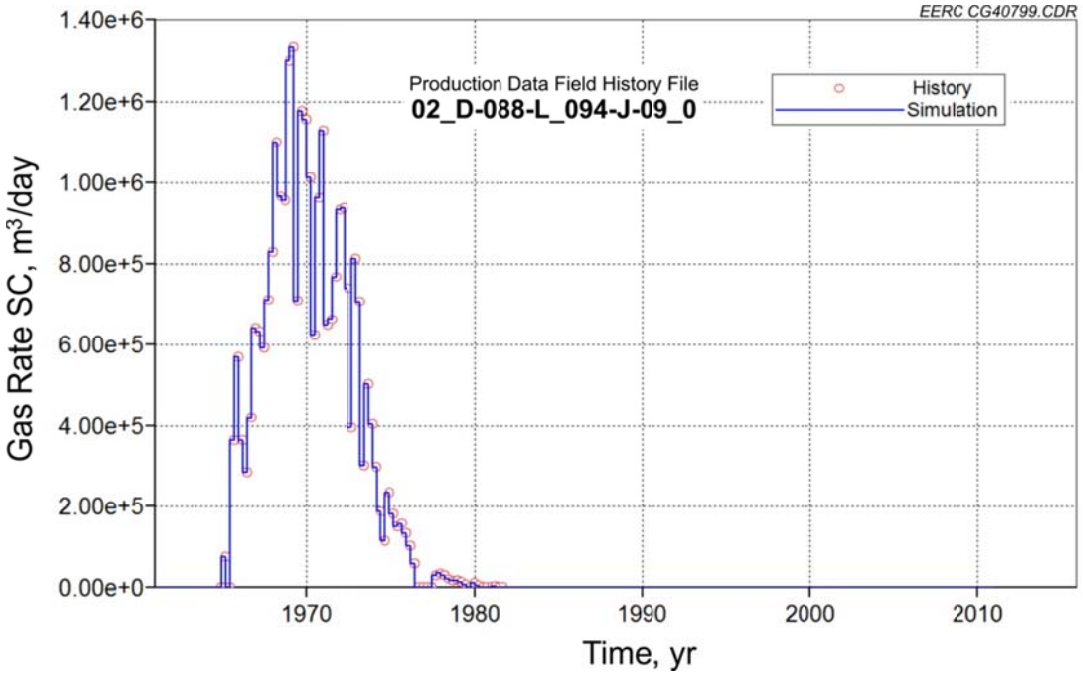

Figure D-12. Gas production rate of the well. Red circles are the historical data, and the other is the top simulation result.

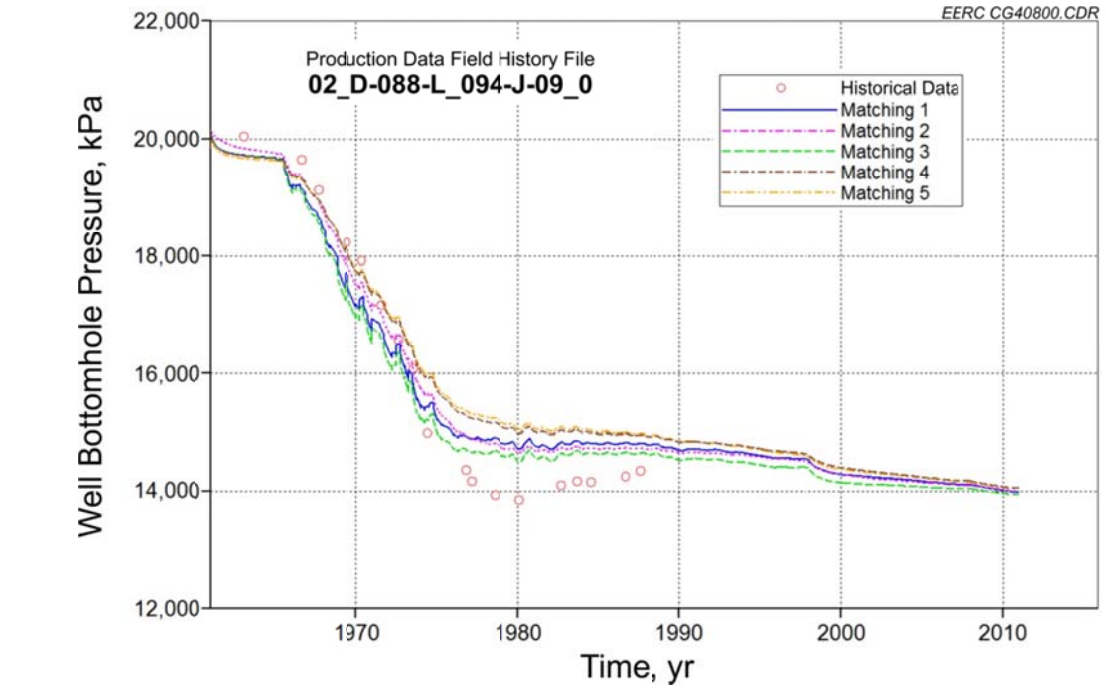

Figure D-13. BHP of the well. Red circles are the historical data, and the others are the top five simulation results.

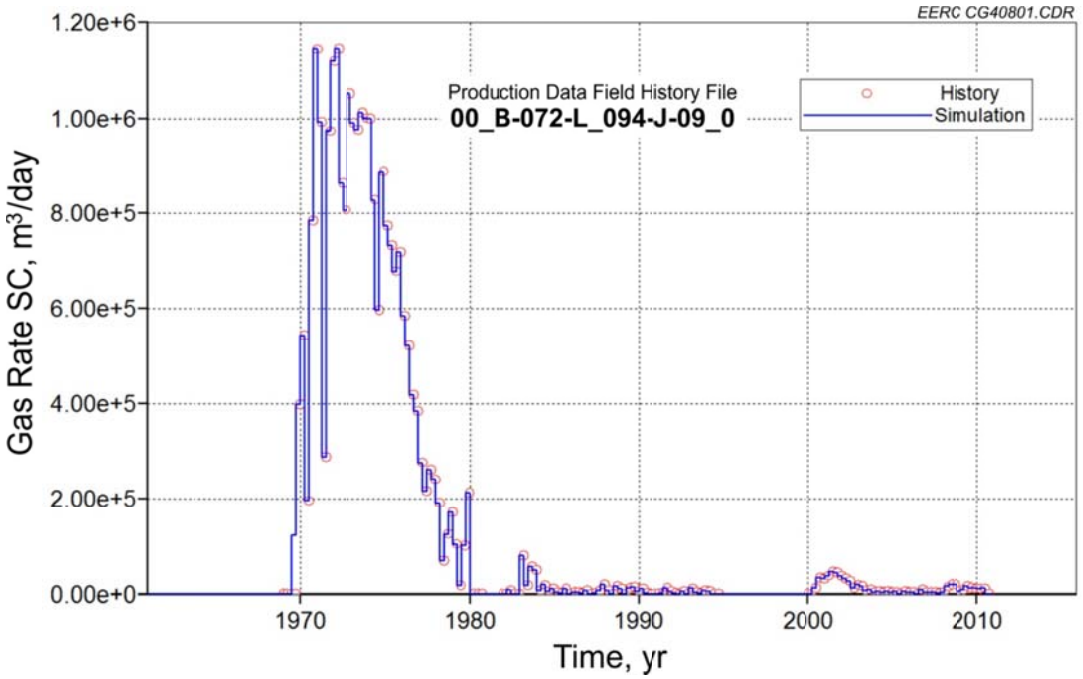

Figure D-14. Gas production rate of the well. Red circles are the historical data, and the other is the top simulation result.

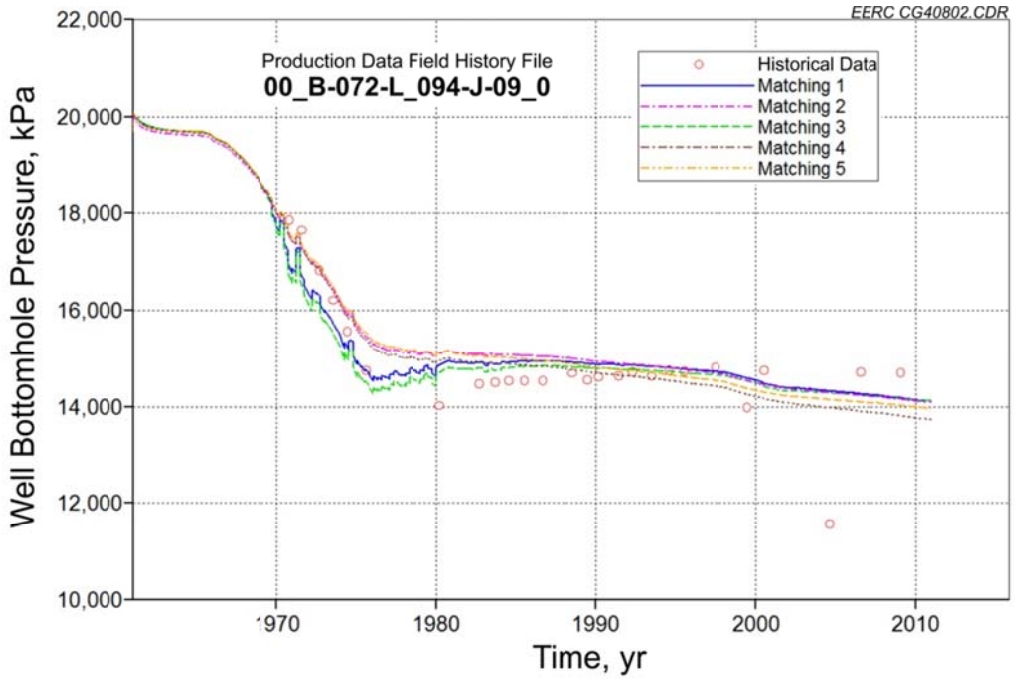

Figure D-15. BHP of the well. Red circles are the historical data, and the others are the top five simulation results.

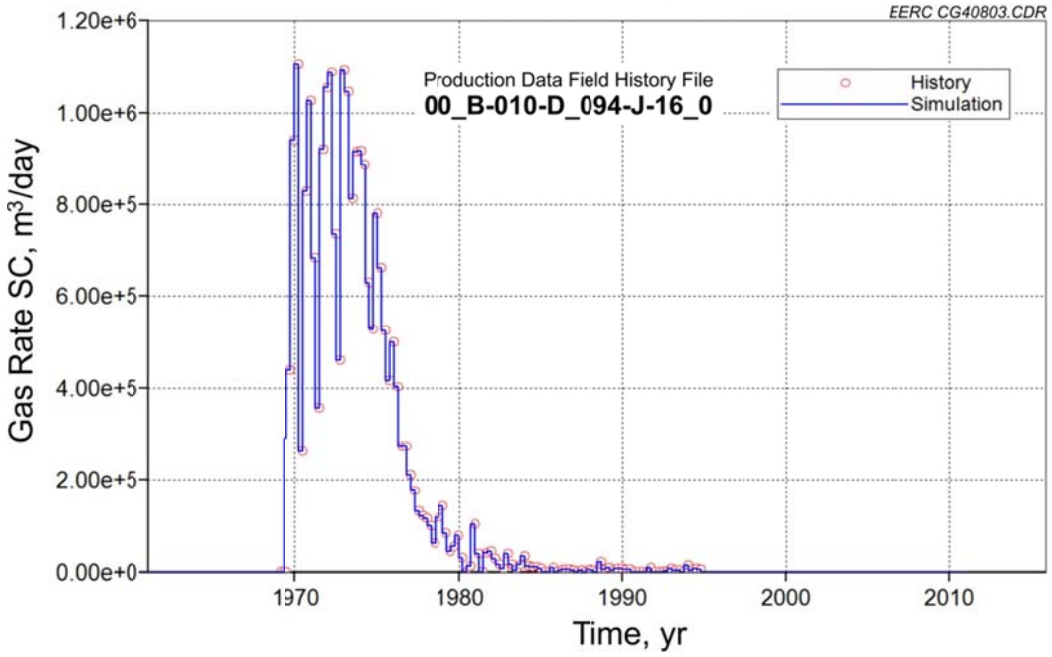

Figure D-16. Gas production rate of the well. Red circles are the historical data, and the other is the top simulation result.

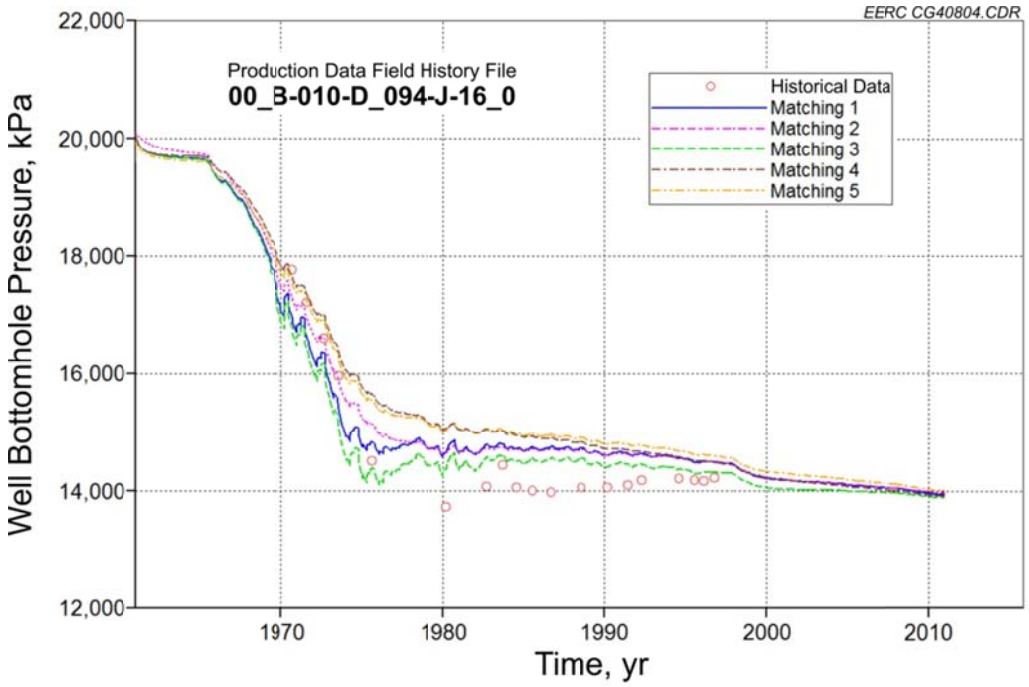

Figure D-17. BHP of the well. Red circles are the historical data, and the others are the top five simulation results.

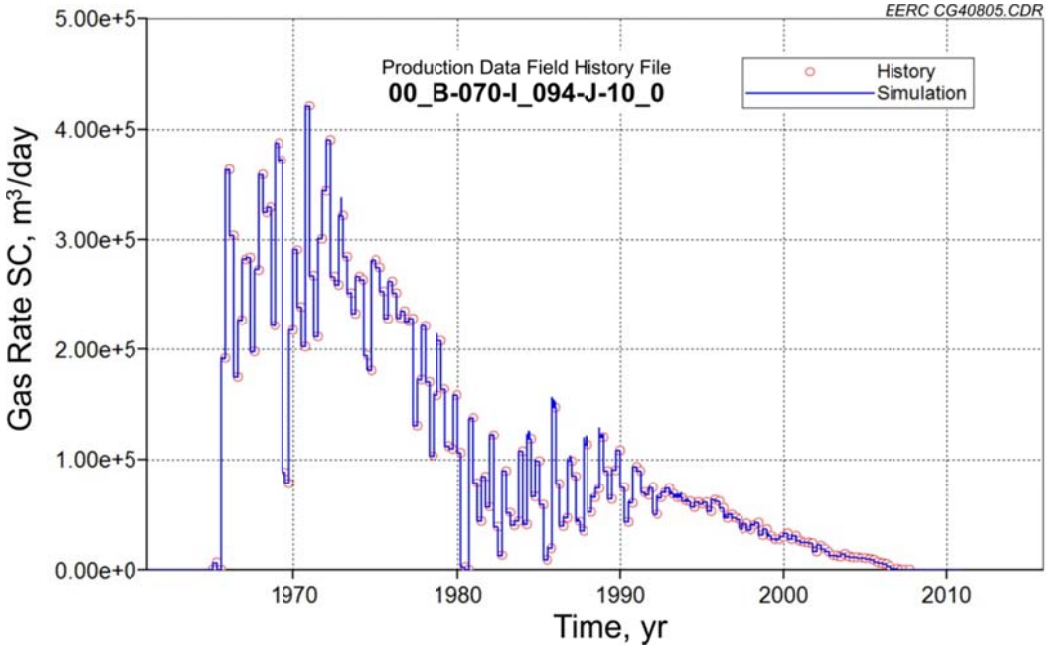

Figure D-18. Gas production rate of the well. Red circles are the historical data, and the other is the top simulation result.

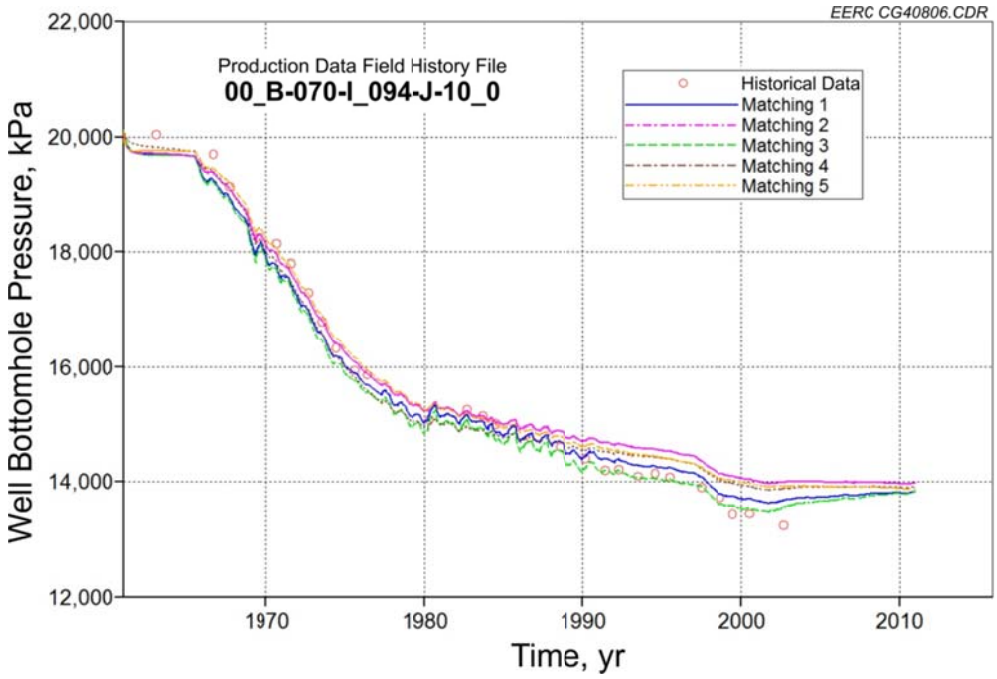

Figure D-19. BHP of the well. Red circles are the historical data, and the others are the top five simulation results.

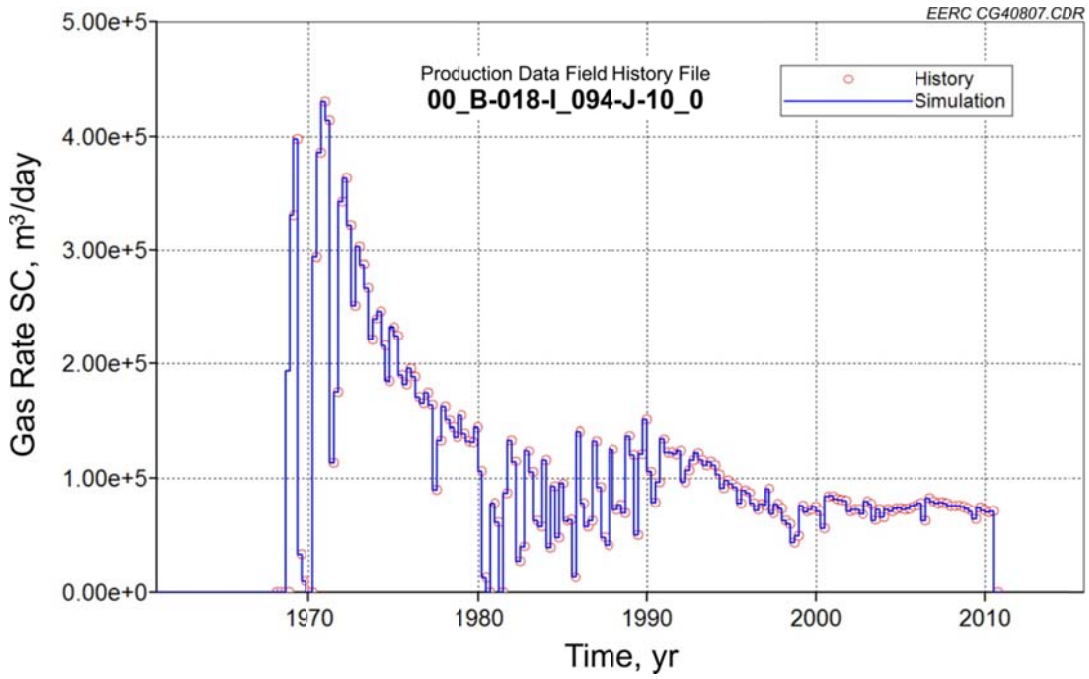

Figure D-20. Gas production rate of the well. Red circles are the historical data, and the other is the top simulation result.

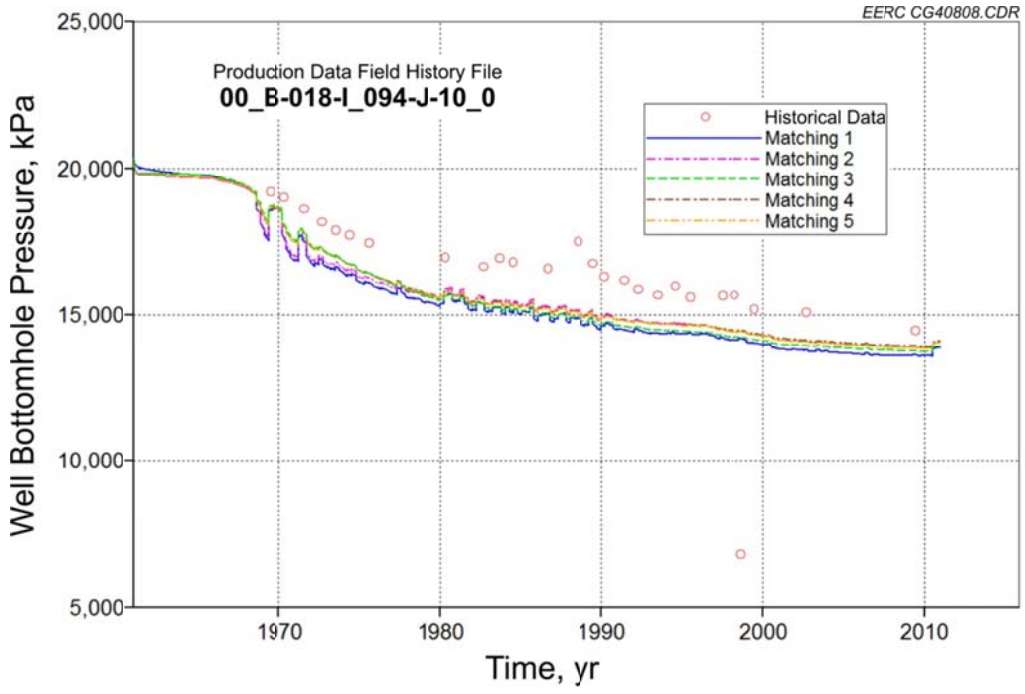

Figure D-21. BHP of the well. Red circles are the historical data, and the others are the top five simulation results.

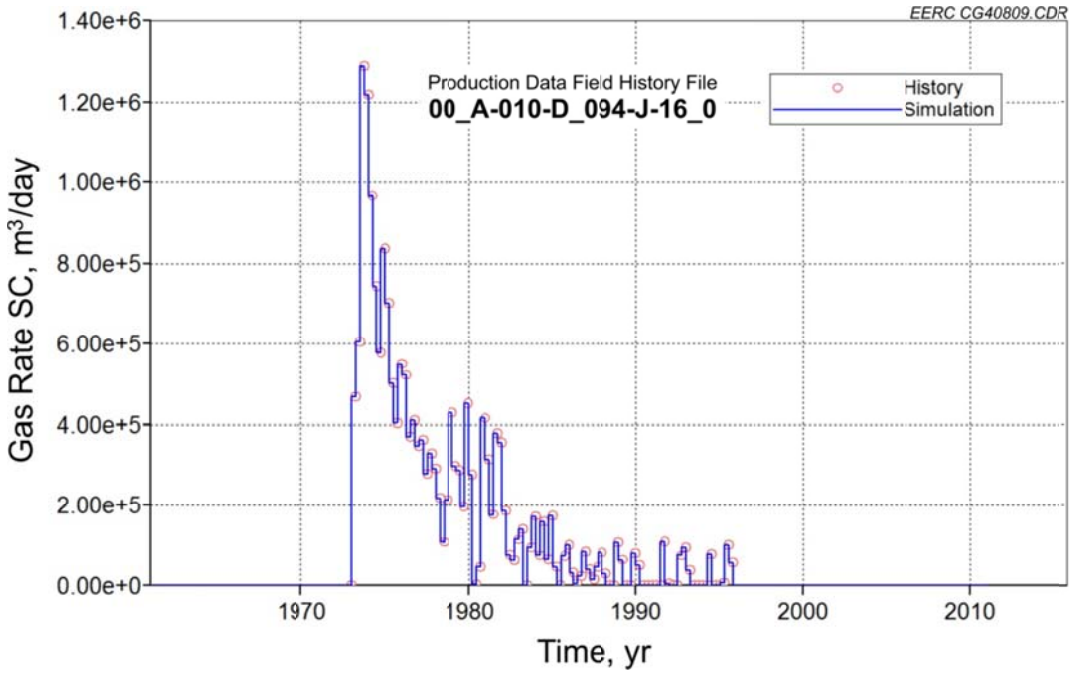

Figure D-22. Gas production rate of the well. Red circles are the historical data, and the other is the top simulation result.

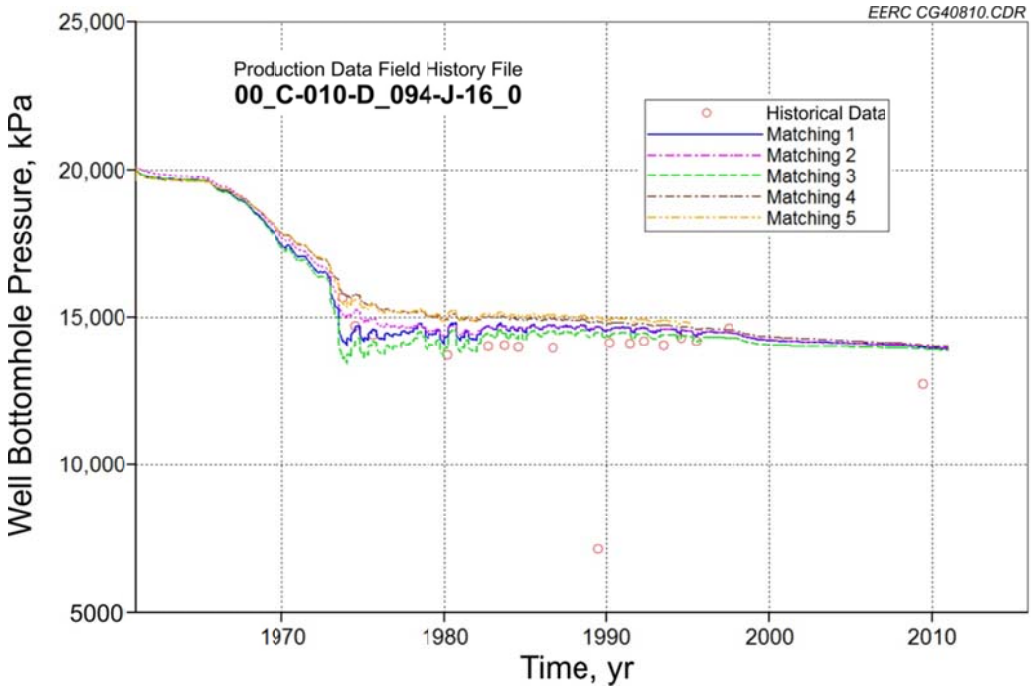

Figure D-23. BHP of the well. Red circles are the historical data, and the others are the top five simulation results.

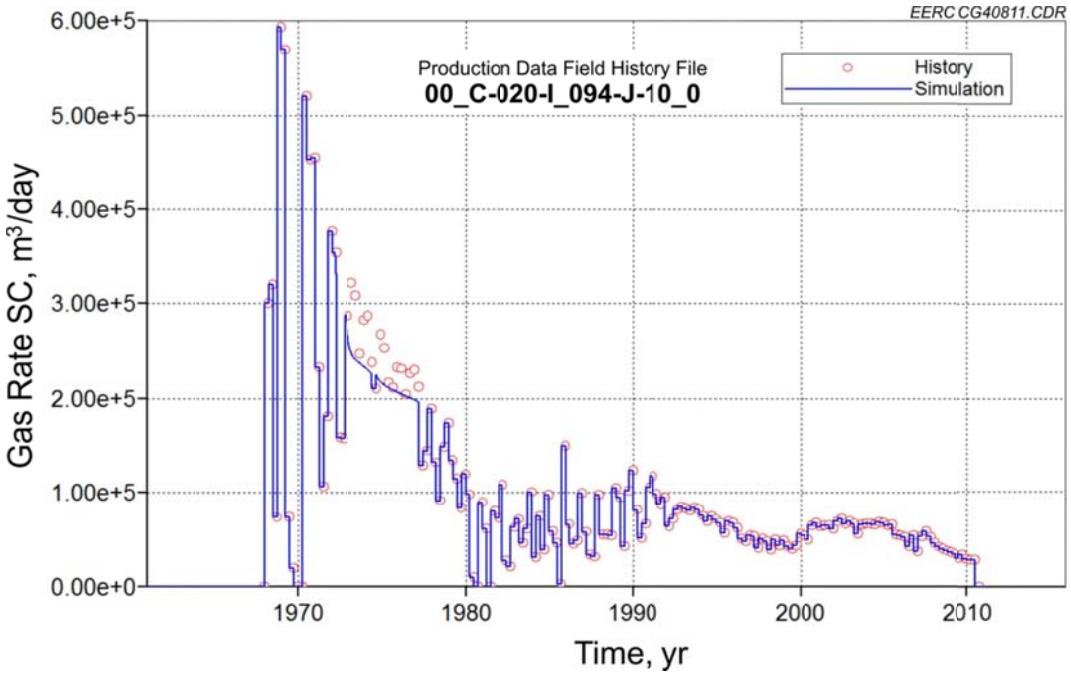

Figure D-24. Gas production rate of the well. Red circles are the historical data, and the other is the top simulation result.

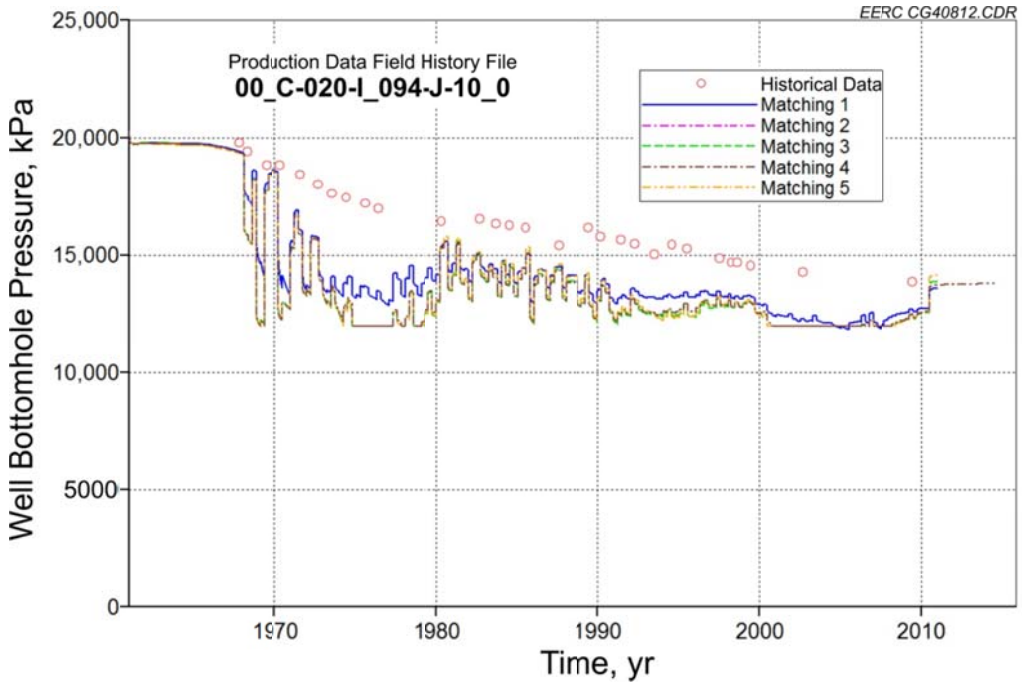

Figure D-25. BHP of the well. Red circles are the historical data, and the others are the top five simulation results.

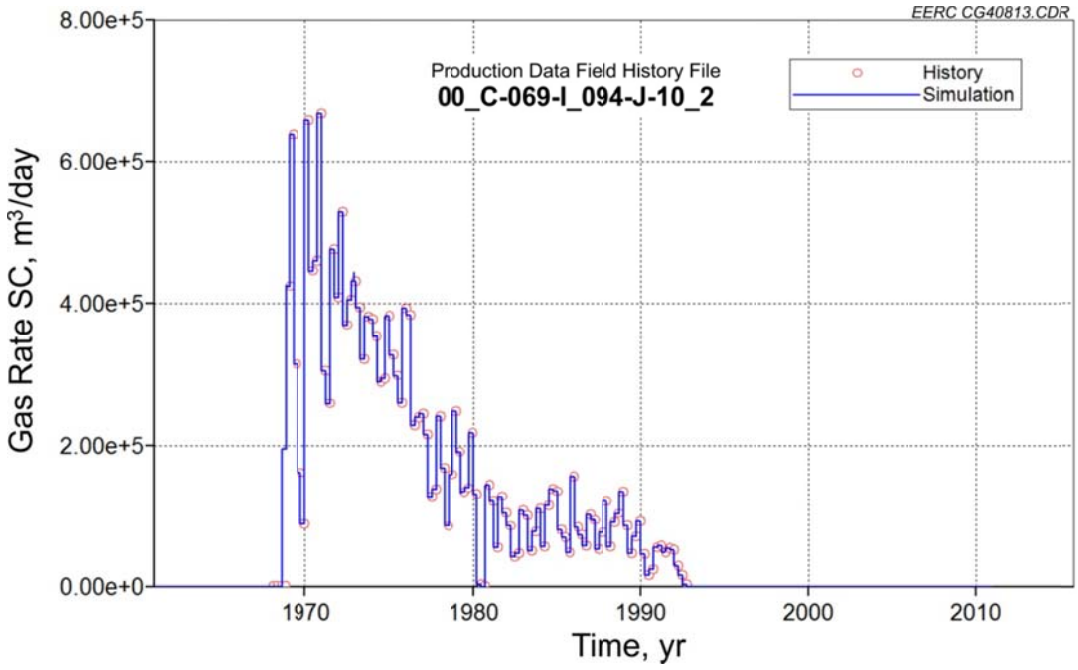

Figure D-26. Gas production rate of the well. Red circles are the historical data, and the other is the top simulation result.

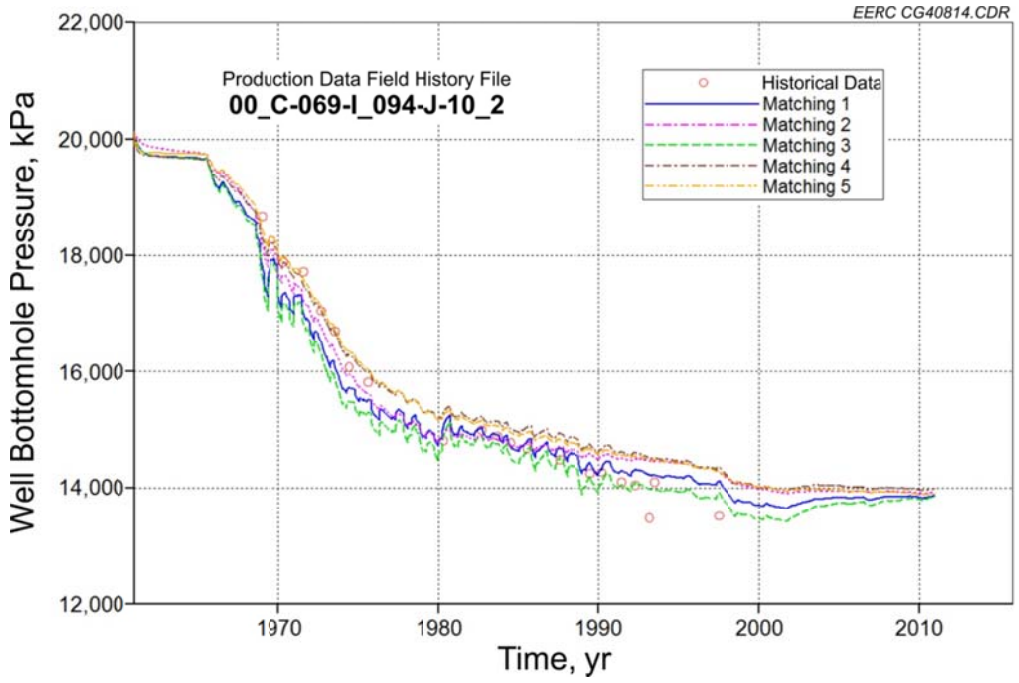

Figure D-27. BHP of the well. Red circles are the historical data, and the others are the top five simulation results.

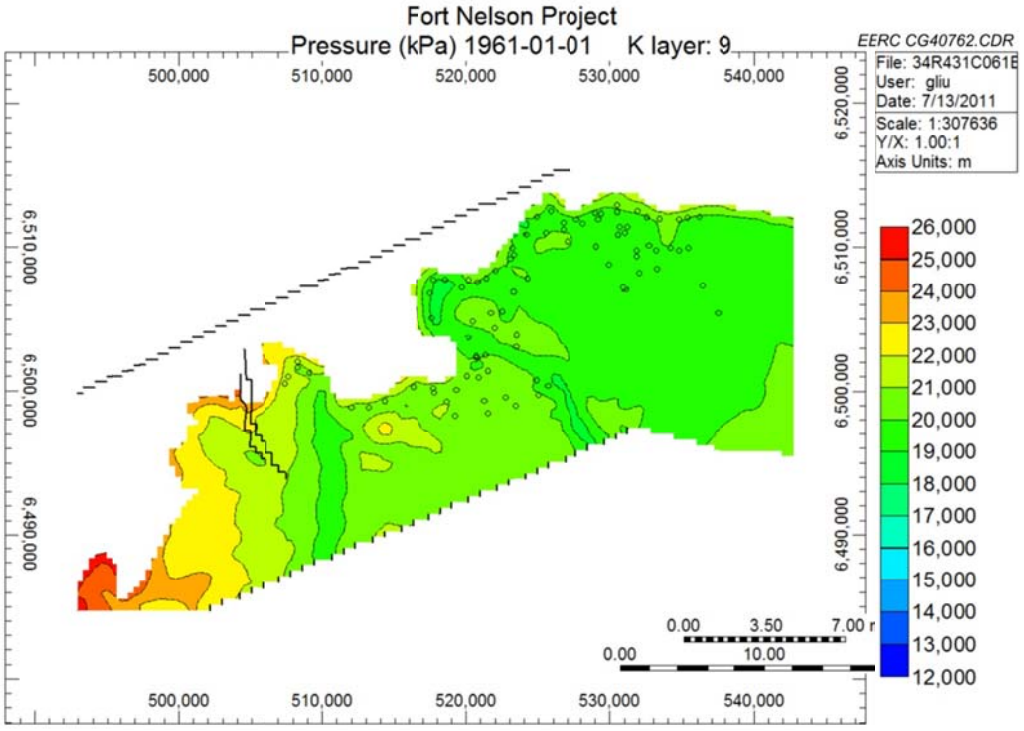

Figure D-28. Pressure profile. Initial pressure before production and injection operations.

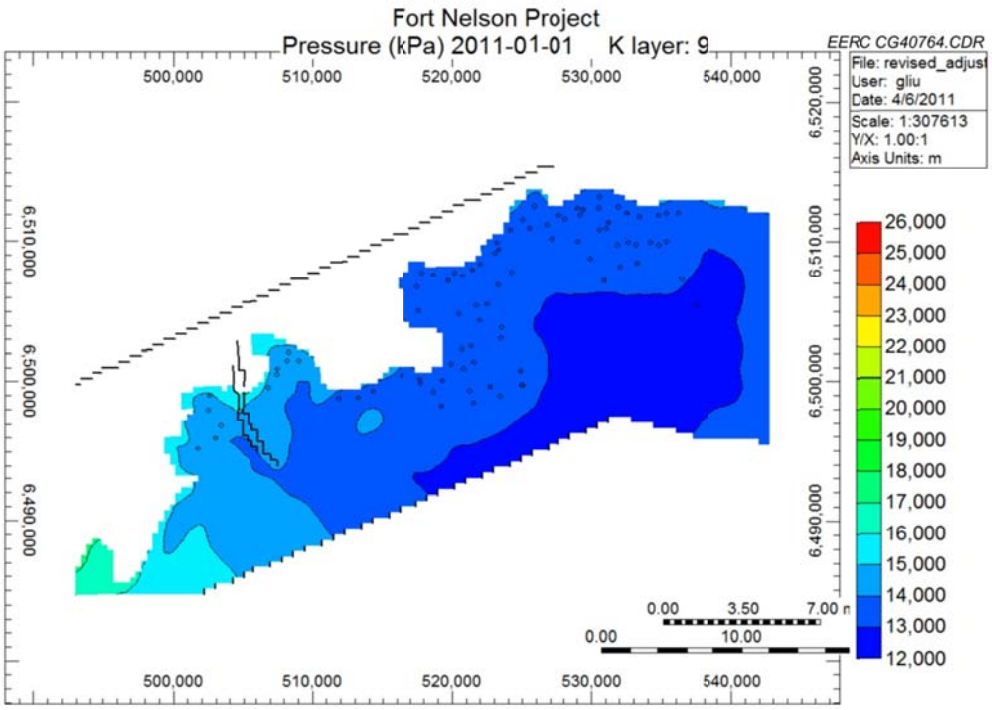

Figure D-29. Pressure profile. Current pressure obtained after history matching.

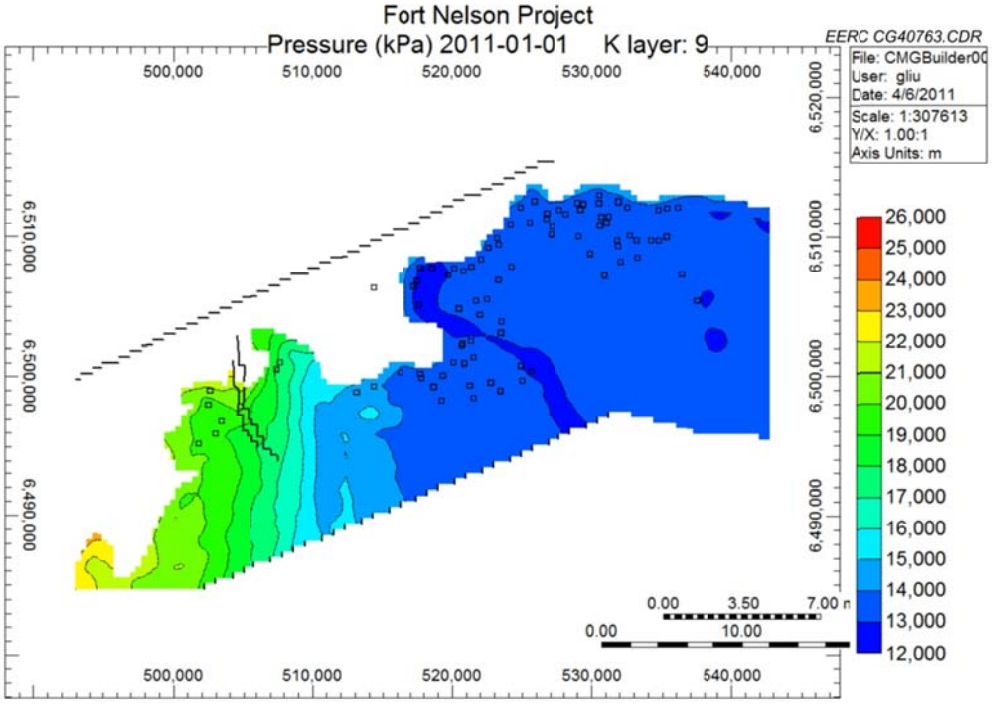

Figure D-30. Pressure profile. Current measurement pressure from field.

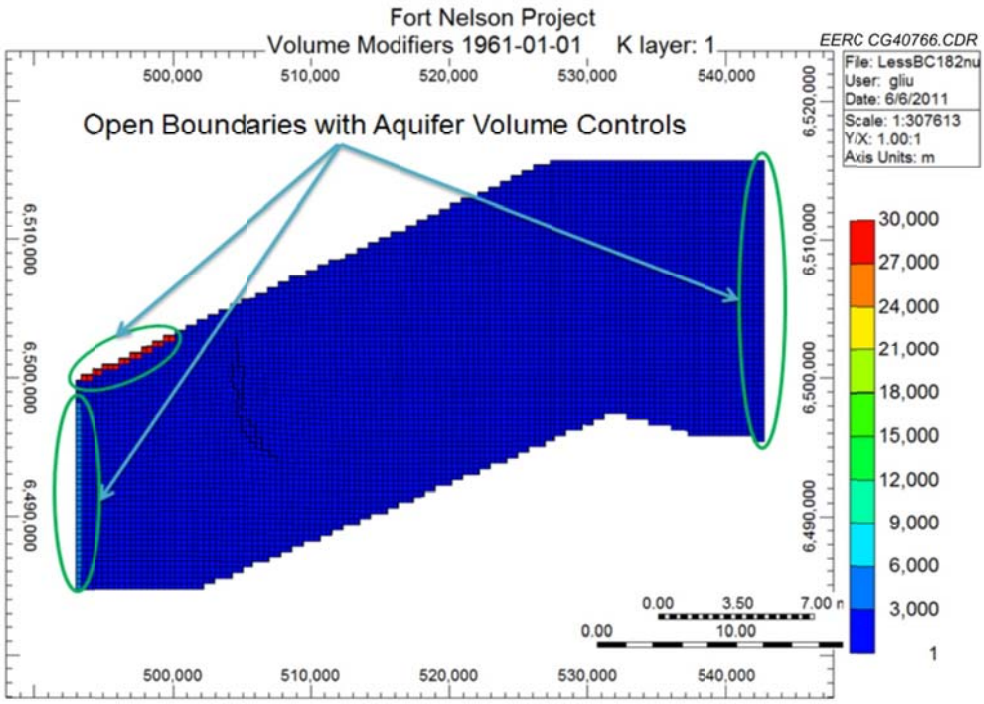

Figure D-31. Boundary settings with aquifer volume control.

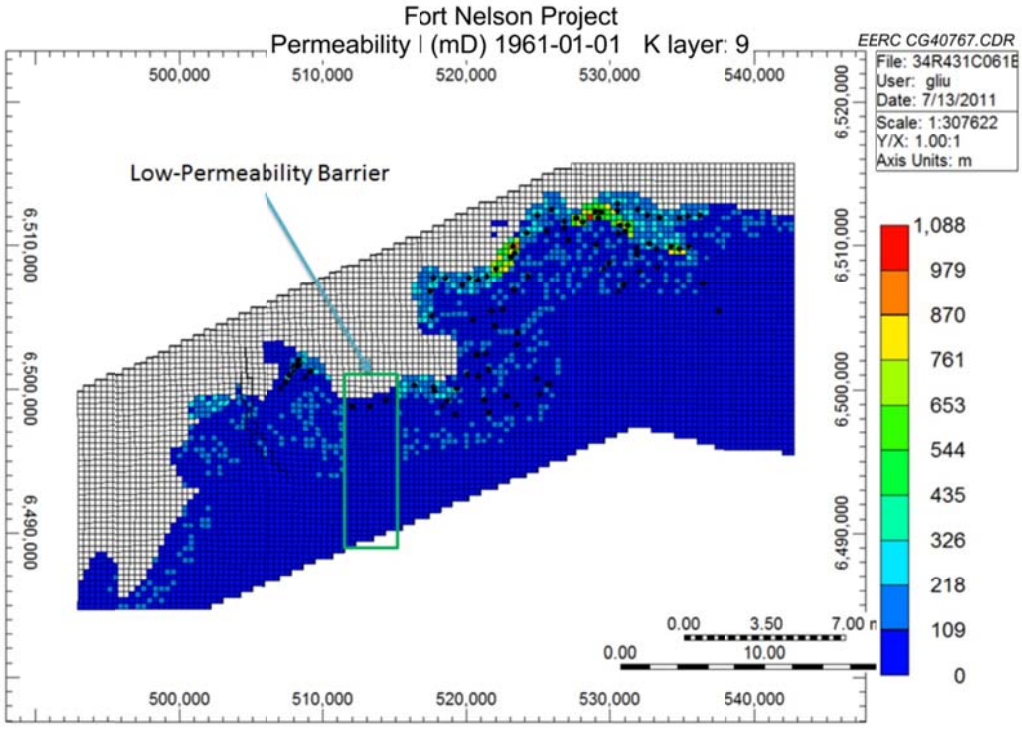

Figure D-32. Low-permeability barrier location between Gas Pools A and B.

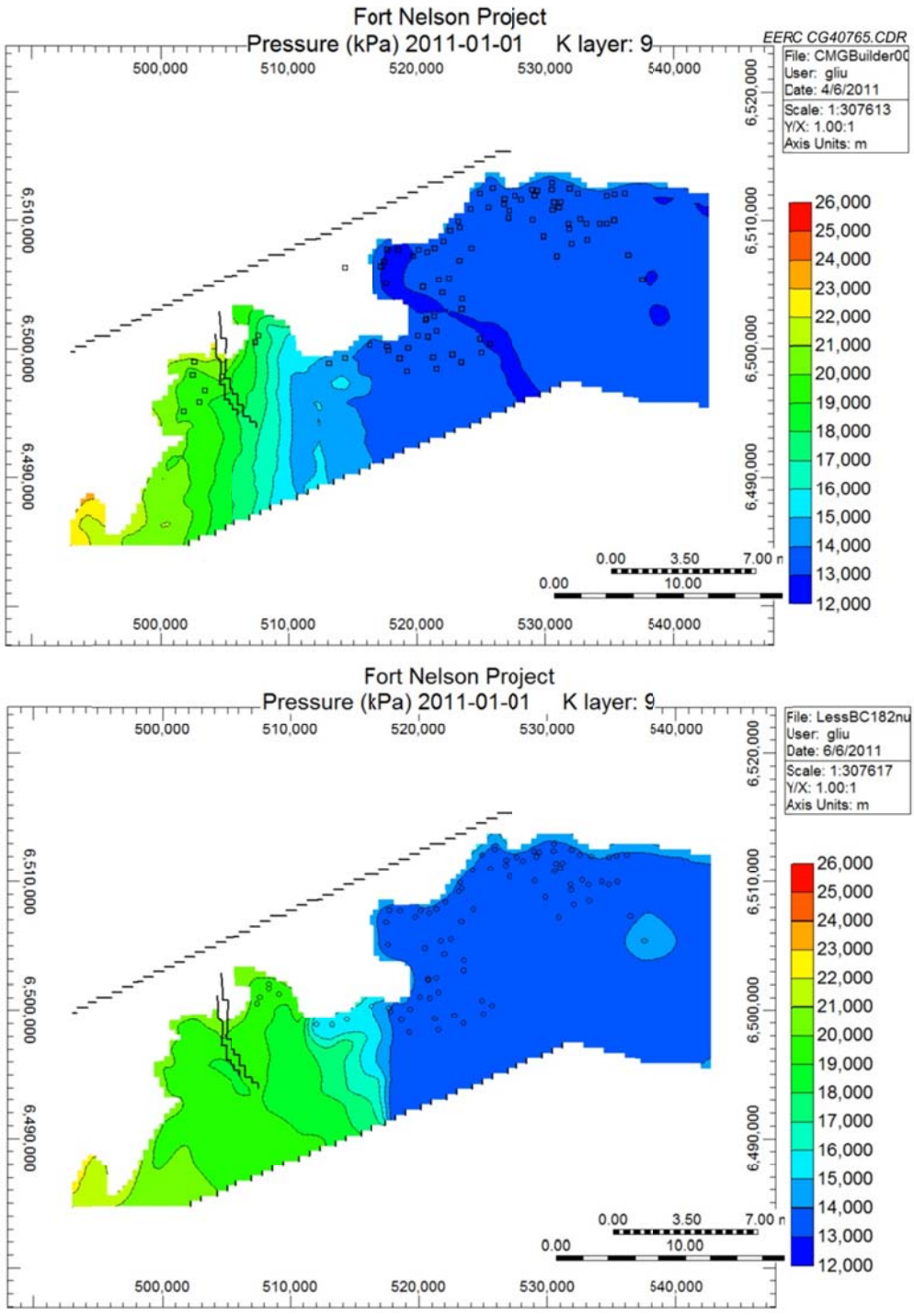

Figure D-33. Pressure profile comparisons between measured distributions (top, current measurement pressure from field after production but before injection operations) and simulation results (bottom, current pressure from simulation after history matching before injection operations).

REFERENCES

Griffith, A., and Nichols, N., 1996, Accounting for model error in data assimilation using adjoint methods, *in* Computational Differentiation: Techniques, Applications and Tools, Proceedings.

Hutchinson, M., 1989, A stochastic estimator of the trace of the influence matrix for Laplacian smoothing splines. Communication in Statistics – Simulation and Computation, v. 19, no. 2, p. 433–450.

LeDimet, F., Ngodock, H., and Navon I., 1995, Sensitivity analysis in variational data assimilation: Supercomputer Computations Research Institute Technical Report, FSU-SCRI-95T-103, The Florida State University, Tallahassee, Florida.

APPENDIX E

PREDICTIVE SIMULATIONS AFTER HISTORY MATCHING

PREDICTIVE SIMULATIONS AFTER HISTORY MATCHING

This appendix provides the results of the predictive simulations based on the dynamic simulation models that exhibited a reasonable history match. The top two "best" matching cases were selected for conducting predictive simulations. Water recycle (collection of produced water from the production well being injected into the reservoir) was considered in all of these predictive runs.

WATER RECYCLE

Based on the analysis of historical data, active production wells were kept on operation status (open or shut in) beginning July 2010 to the date when the gas production rate was less than 2500 m^3/day under the minimum bottomhole pressure (BHP) limits. As of July 2010, there were a total of 38 active wells (Figure E-1 and Table E-1). Based on the relative distance to the water disposal wells a-48-L, c-89-F, and a-65-G (Table E-1 and Figure E-2), these wells were divided into three groups, namely, TWP_D048L, TWP_C089F, and TWP_A065G for gas production control and water recycle. Examples of water recycle using available water disposal wells are shown in Figures E3–E8. The gas production rate control under the minimum BHP limits with water recycle is shown in Figures E9–E12.

PREDICTIVE SIMULATIONS

To compare the effects of injection in and around both injection locations (Well c-47-E and Well c-61-E) on the gas plumes, eight test cases were designed and implemented (Table 3 of the main report). The first four cases are based on History-Matching No. 1 and the last four cases are based on History-Matching No. 2. All cases include two injection periods of 25 and 50 years. The results indicate that the gas plumes in injection location c-47-E did not contact the gas pools. However, in the case of injection location c-61-E, the gas plumes did contact the gas pools. The simulated BHPs for the c-47-E location were found to be 1000 to 3000 kPa lower than the BHPs obtained for the c-61-E location. The detailed results for water recycle, BHPs, areal view of gas plumes (gas per area unit), areal view of saturation at the top of Upper Slave Point, cross-sectional view of gas plumes, and pressure distribution over time are shown in Figures E-13–E-91.

COMPARISONS OF PRE- AND POST-HISTORY MATCHING

The cases of pre- and post-history matching with a 50-year injection period in both injection locations were also compared. Cases 1 and 3 belong to History-Matching No. 1 and Cases 5 and 7 belong to History-Matching No. 2. For Cases 1 and 5, injection was done at the c-47-E location, whereas Cases 3 and 7 deal with injection at location c-61-E. These four cases were compared with the cases before history matching. A comparison of results in the case of location c-47-E shows that the gas plumes obtained post-history matching are bigger than the

ones obtained in pre-history matching but did not contact the gas pools (Figures E-94–E-111) during the 100-year simulation period. Also, for the same sour CO_2 injection volume, the BHPs obtained in post-history matching were found to ~2000 kPa lower than the pre-history-matching values (Figures E-92 and E-93). However, for the injection location c-61-E, all of the gas plumes (Figures E-114–E-131) appear to contact the gas pool within the 100-year simulation period. In the case of location c-61-E, the BHPs were found to be around 26,000 kPa (Figures E-112 and E-113) in both pre- and post-history matching.

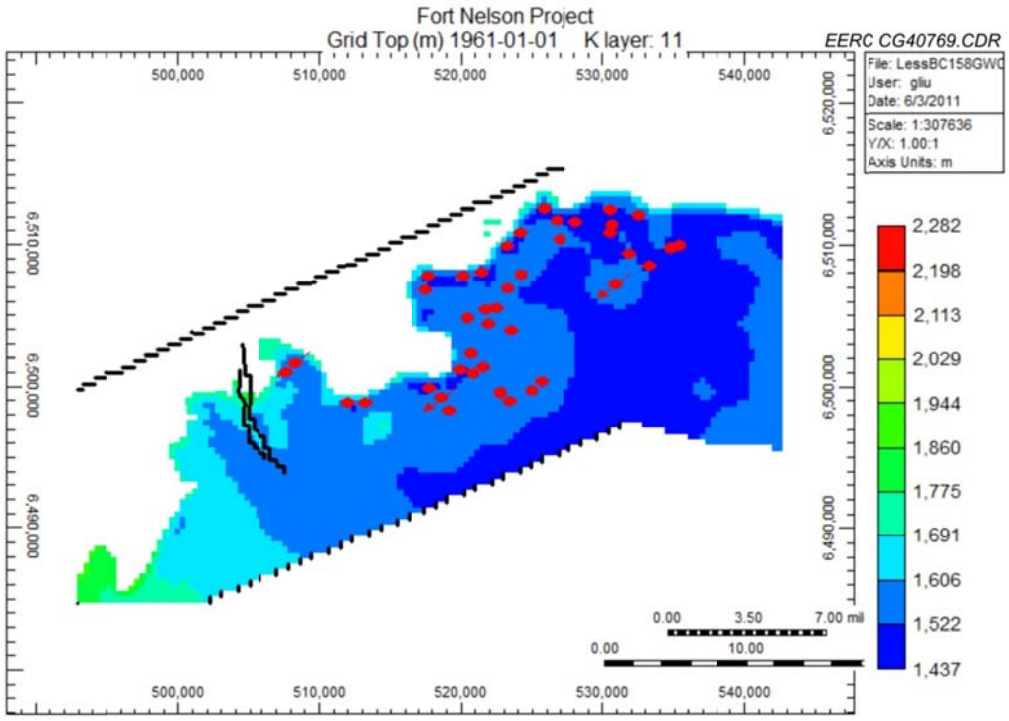

Figure E-1. Location of the active production wells after July 2010.

Table E-1. Grouped Active Production Wells

No.	Wells	Groups		No.	Wells	Groups
1	00_A-005-A_094-J-15_0	TWP_D048L		20	00_D-096-L_094-J-09_0	TWP_D048L
2	00_A-051-J_094-J-10_0	TWP_D048L		21	00_A-090-F_094-J-10_0	TWP_C089F
3	00_A-056-J_094-J-10_0	TWP_D048L		22	00_A-068-H_094-J-10_0	TWP_A065G
4	00_A-065-L_094-J-09_0	TWP_D048L		23	00_A-081-G_094-J-10_0	TWP_A065G
5	00_A-092-I_094-J-10_0	TWP_D048L		24	00_A-083-G_094-J-10_0	TWP_A065G
6	00_B-008-D_094-J-16_2	TWP_D048L		25	00_B-018-I_094-J-10_0	TWP_A065G
7	00_B-048-I_094-J-10_0	TWP_D048L		26	00_B-075-H_094-J-10_0	TWP_A065G
8	00_B-053-J_094-J-10_0	TWP_D048L		27	00_C-020-I_094-J-10_0	TWP_A065G
9	00_B-072-L_094-J-09_0	TWP_D048L		28	00_C-029-I_094-J-10_0	TWP_A065G
10	00_B-088-L_094-J-09_0	TWP_D048L		29	00_C-052-F_094-J-10_0	TWP_A065G
11	00_B-098-L_094-J-09_3	TWP_D048L		30	00_C-054-F_094-J-10_0	TWP_A065G
12	00_C-057-I_094-J-10_0	TWP_D048L		31	00_C-066-H_094-J-10_0	TWP_A065G
13	00_C-066-L_094-J-09_3	TWP_D048L		32	00_C-069-H_094-J-10_0	TWP_A065G
14	00_C-073-I_094-J-10_0	TWP_D048L		33	00_C-092-G_094-J-10_3	TWP_A065G
15	00_C-078-I_094-J-10_0	TWP_D048L		34	00_D-013-J_094-J-10_2	TWP_A065G
16	00_C-087-I_094-J-10_0	TWP_D048L		35	00_D-021-J_094-J-10_0	TWP_A065G
17	00_D-037-J_094-J-10_2	TWP_D048L		36	00_D-054-G_094-J-10_2	TWP_A065G
18	00_D-072-L_094-J-09_0	TWP_D048L		37	00_D-066-G_094-J-10_0	TWP_A065G
19	00_D-094-I_094-J-10_2	TWP_D048L		38	00_D-072-G_094-J-10_0	TWP_A065G

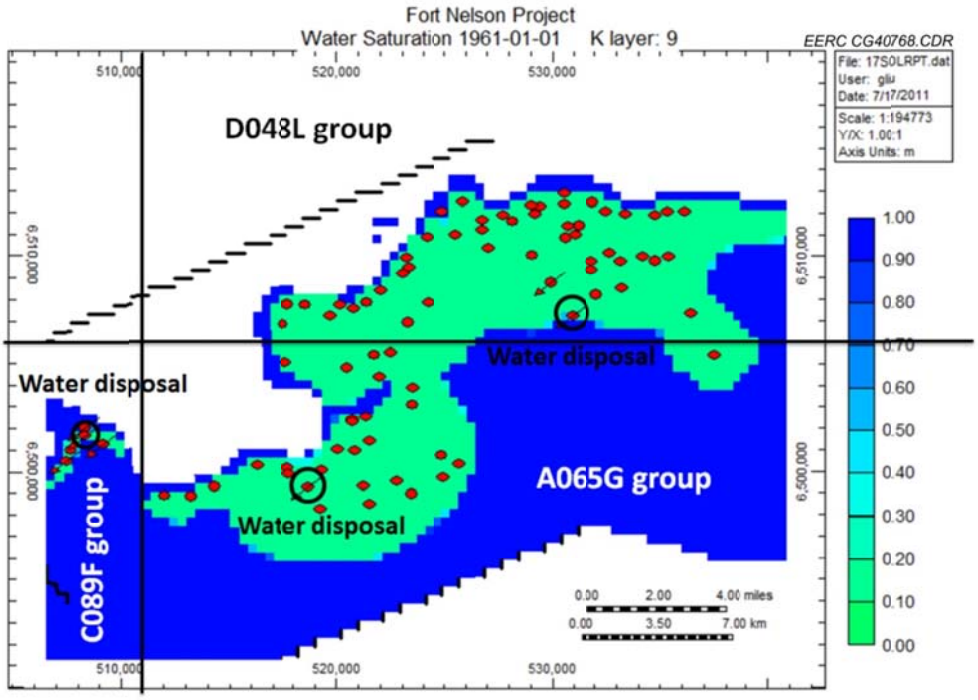

Figure E-2. Location of grouped active production wells and water disposal wells.

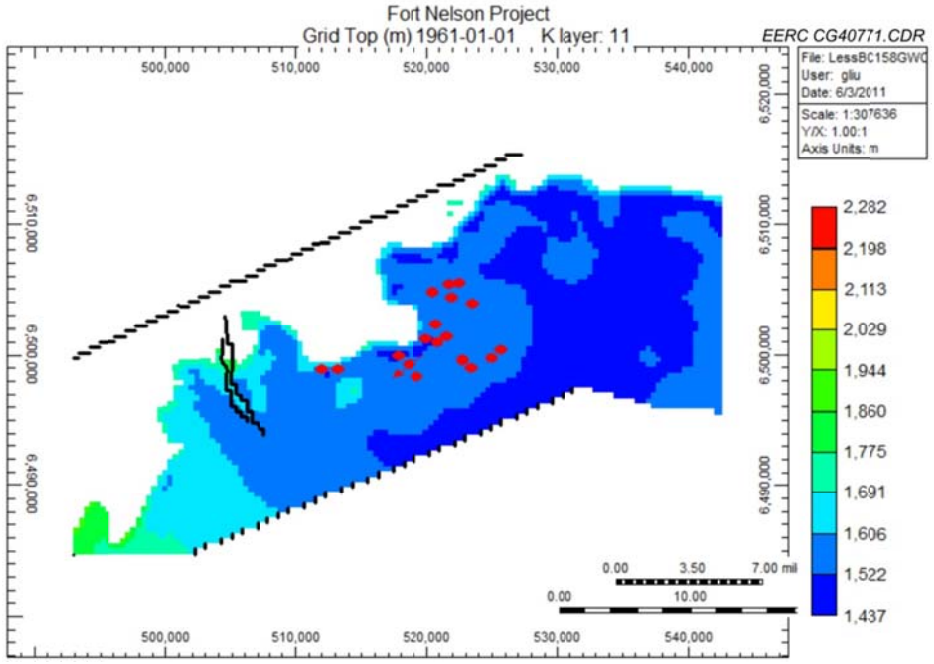

Figure E-3. Location of the water recycle group A065G.

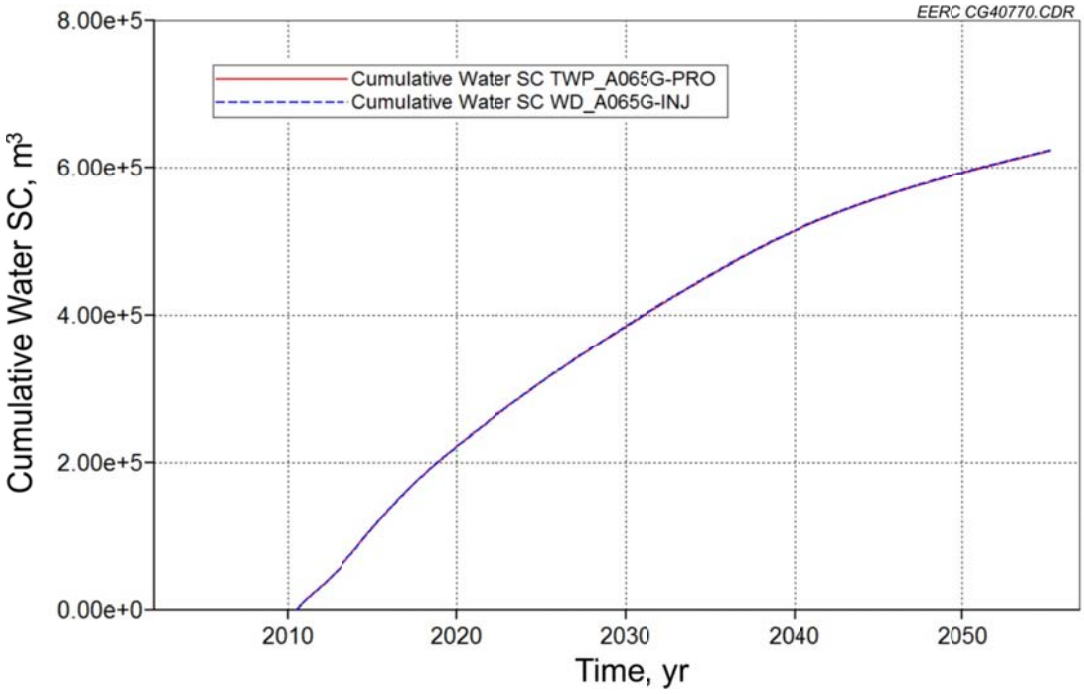

Figure E-4. Example of production and injection from the water recycle group A065G at standard conditions (SC).

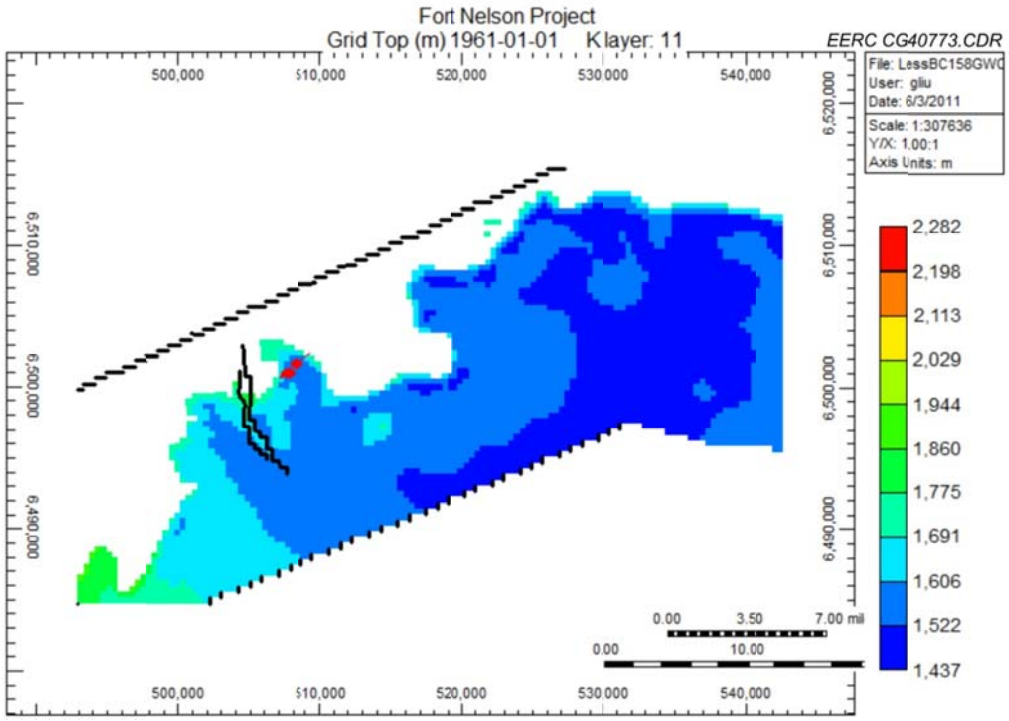

Figure E-5. Location of the water recycle group C089F.

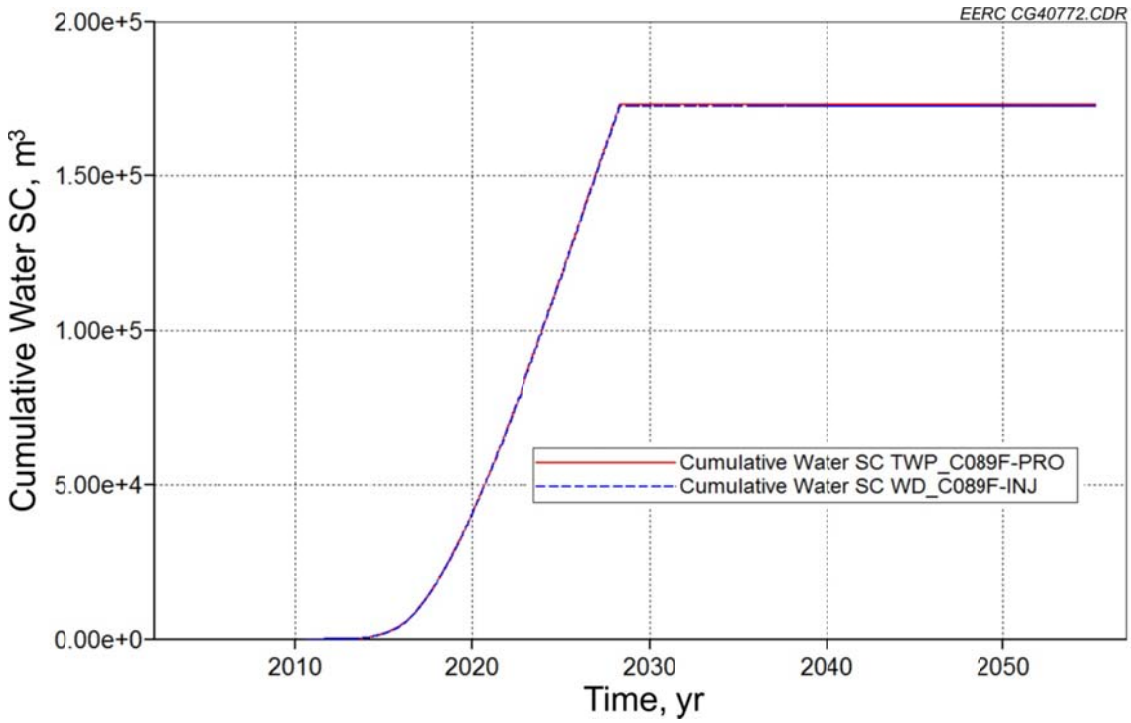

Figure E-6. Example of production and injection from the water recycle group C089F.

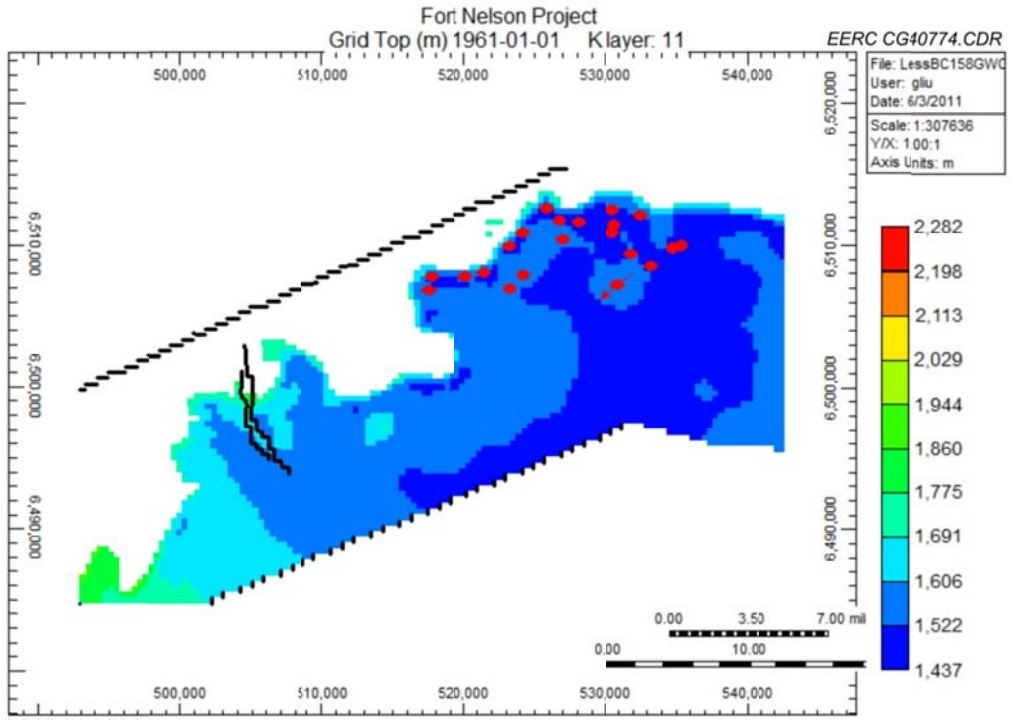

Figure E-7. Location of the water recycle group D048L.

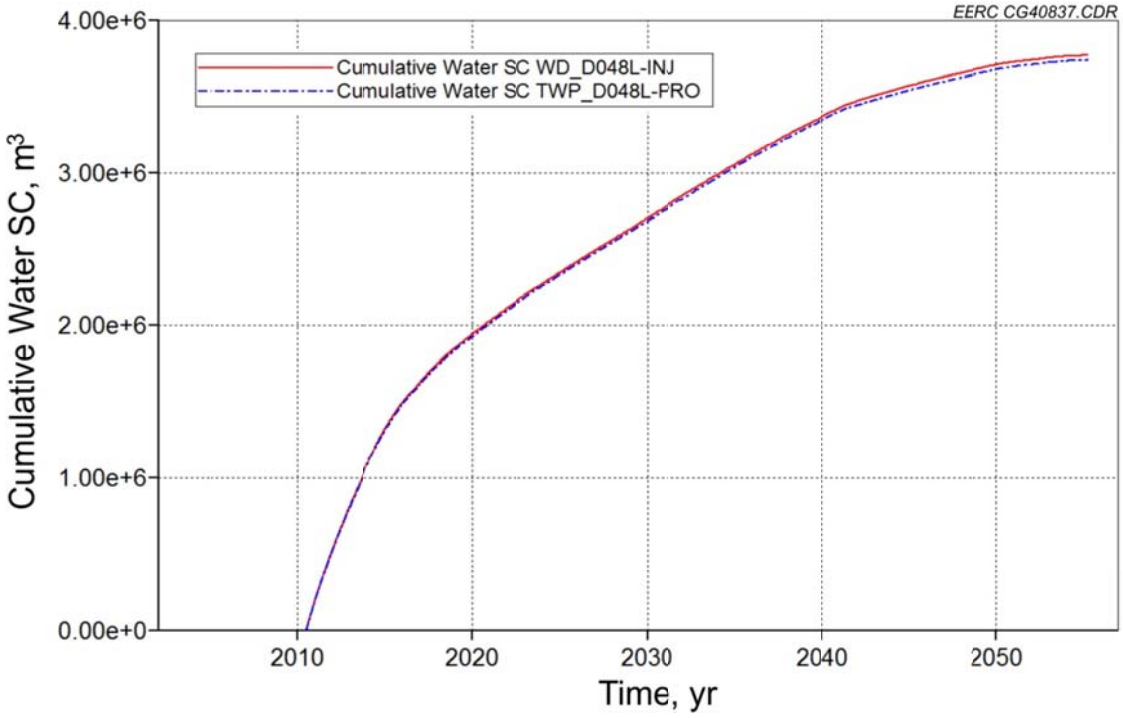

Figure E-8. Example of production and injection from the water recycle group D048L.

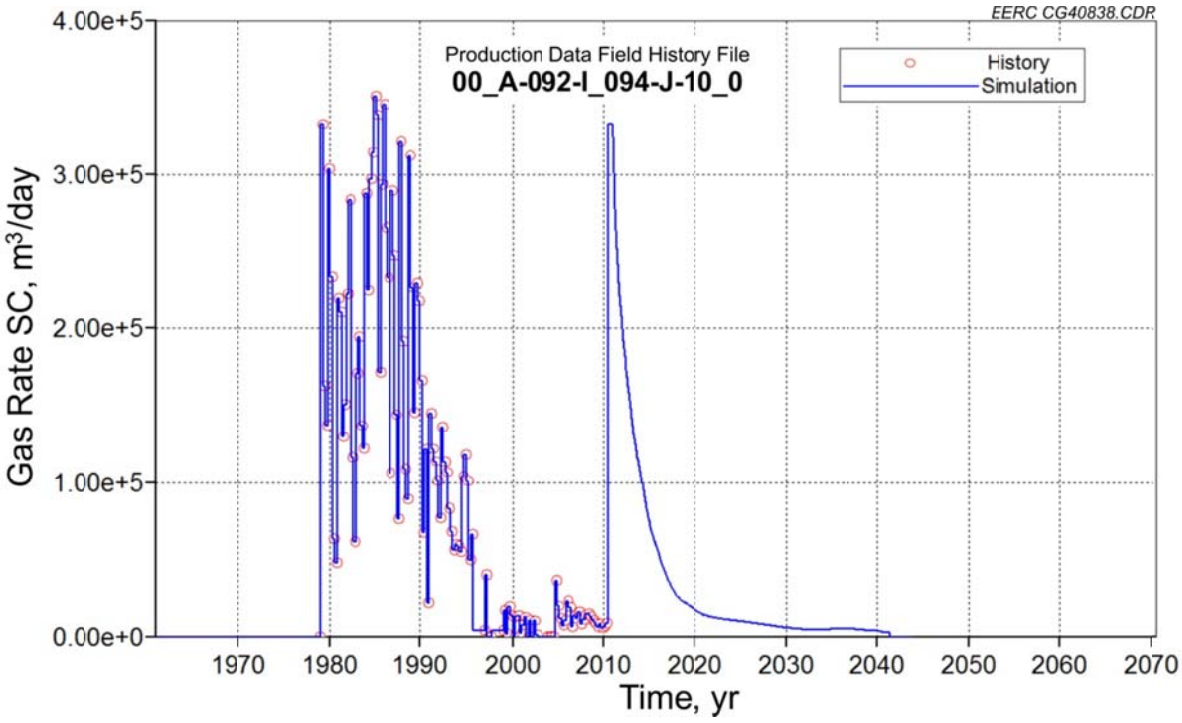

Figure E-9. Example of gas production rate control with water recycle.

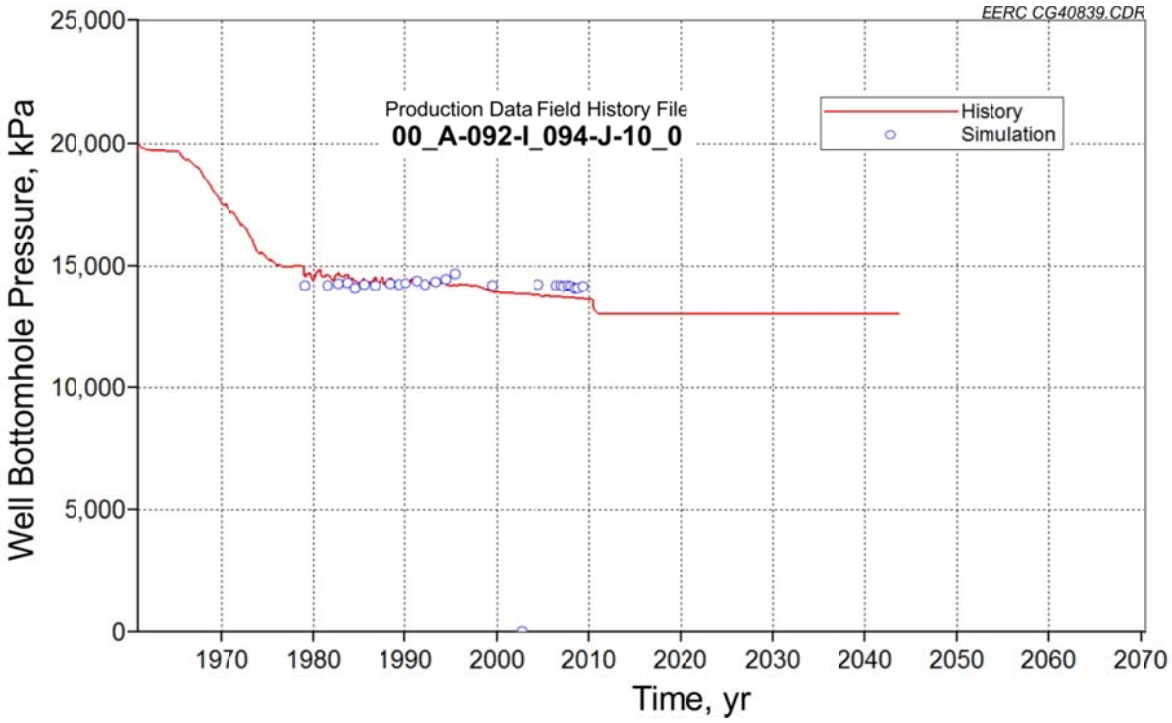

Figure E-10. BHPs of the sample well in Figure E-9.

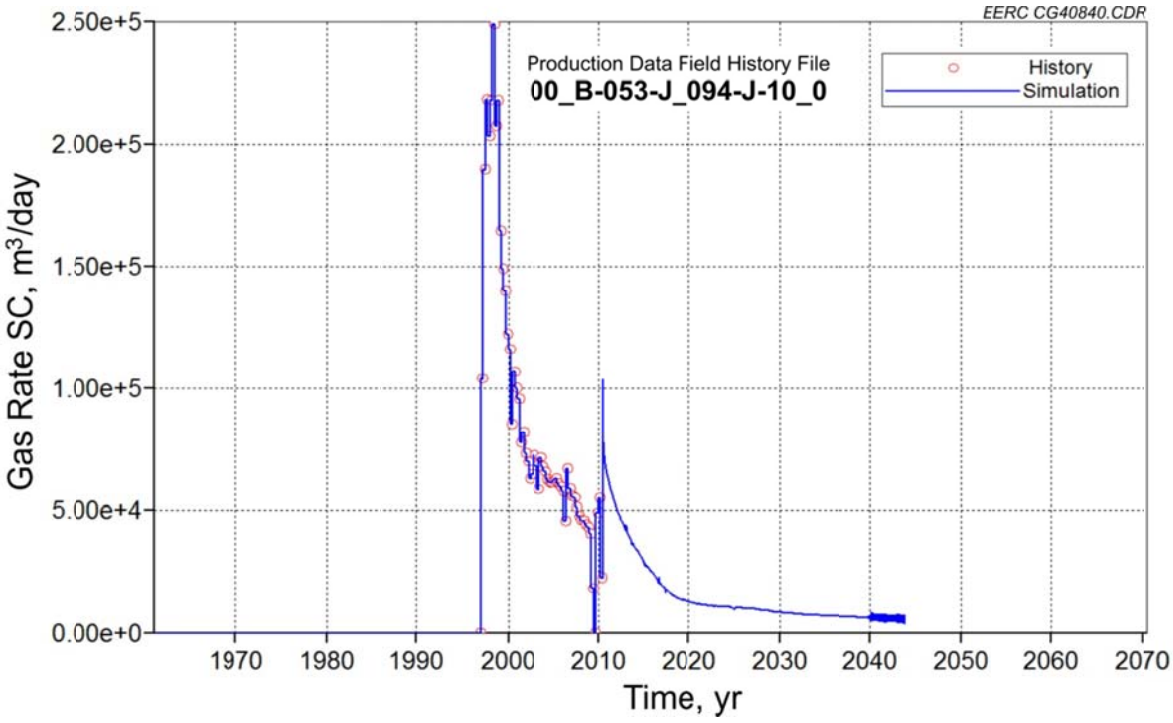

Figure E-11. Example of gas production rate control with water recycle.

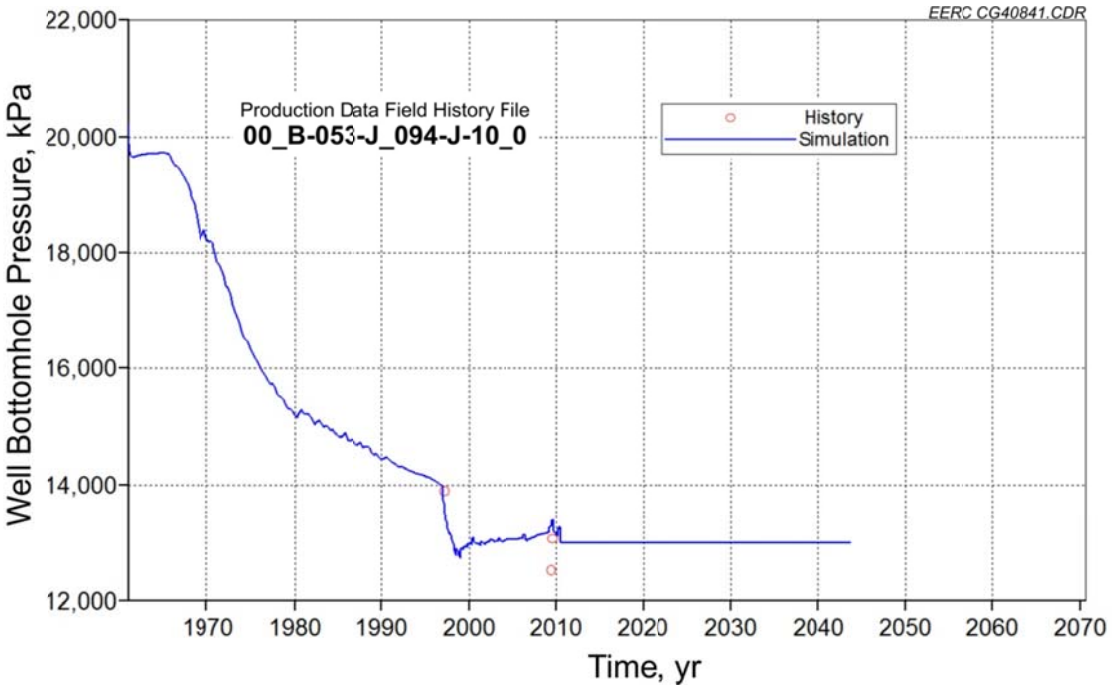

Figure E-12. BHPs of the sample well in Figure E-11.

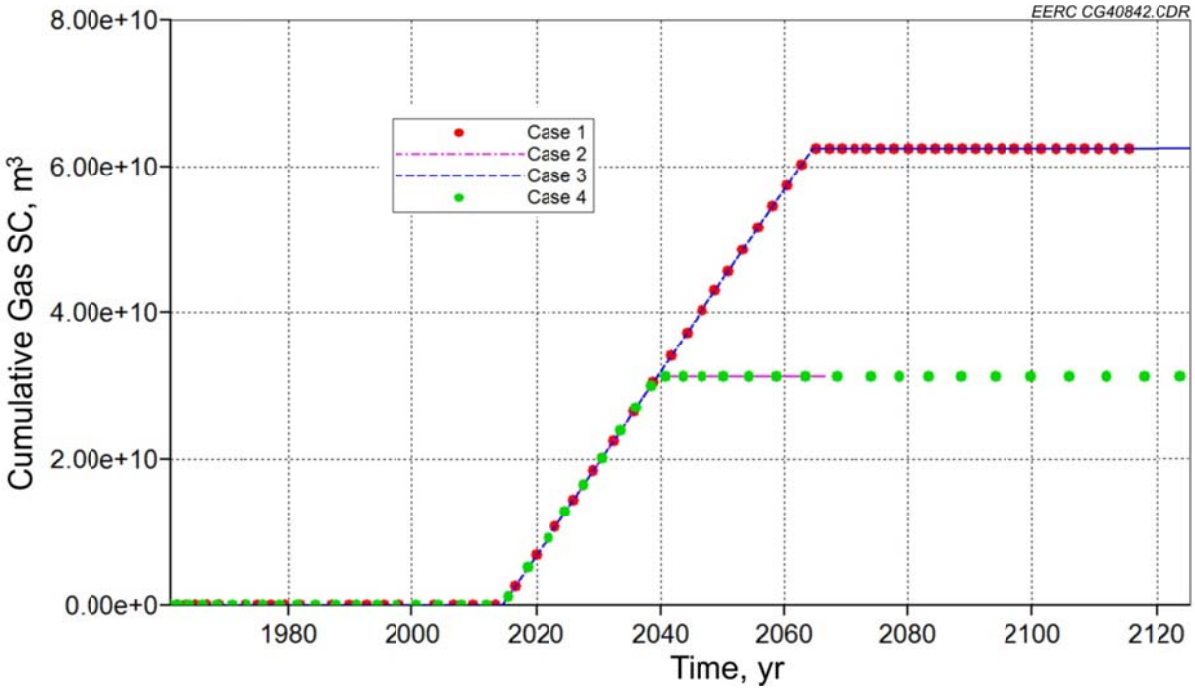

Figure E-13. Cumulative gas injection for four test cases of History-Matching No. 1.

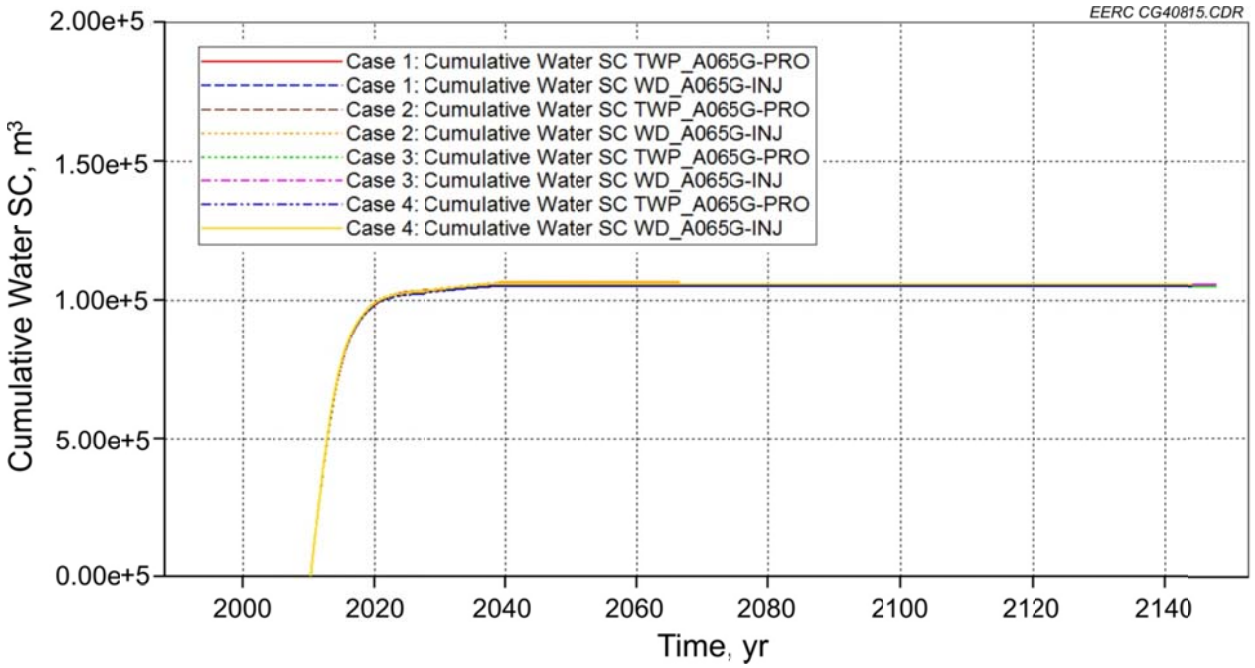

Figure E-14. Production and injection from the Water Recycle Group A065G of History-Matching No. 1.

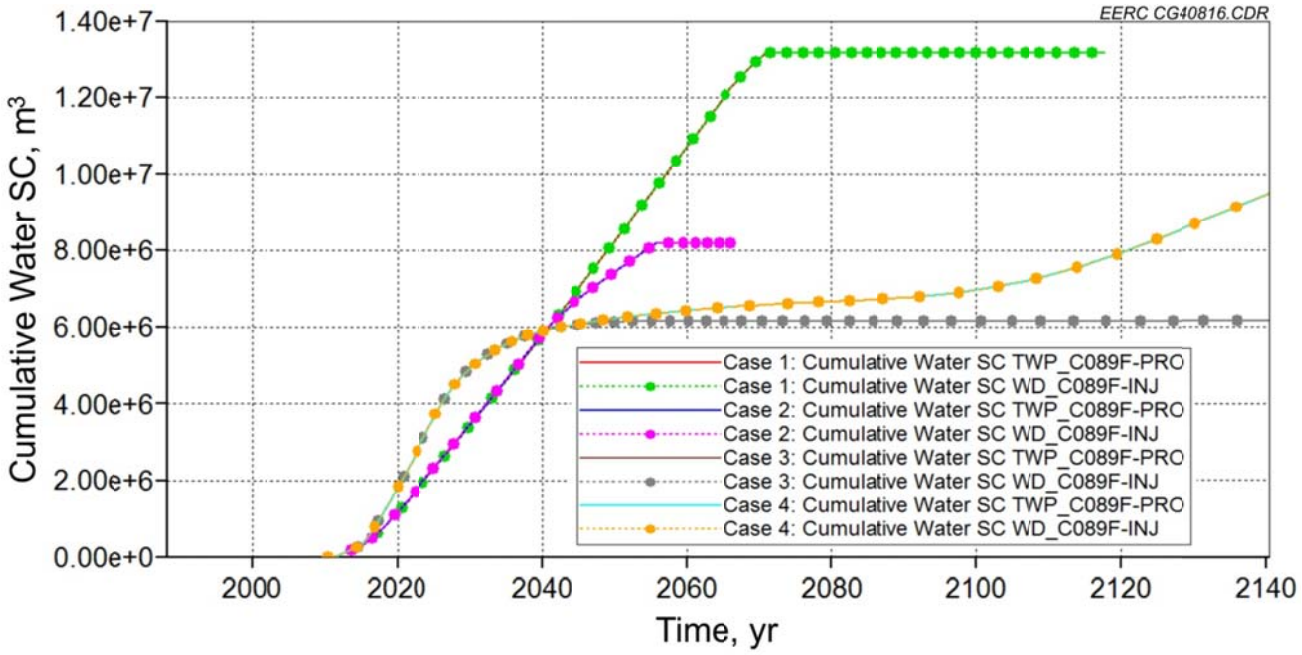

Figure E-15. Production and injection from the Water Recycle Group C089F of History-Matching No. 1.

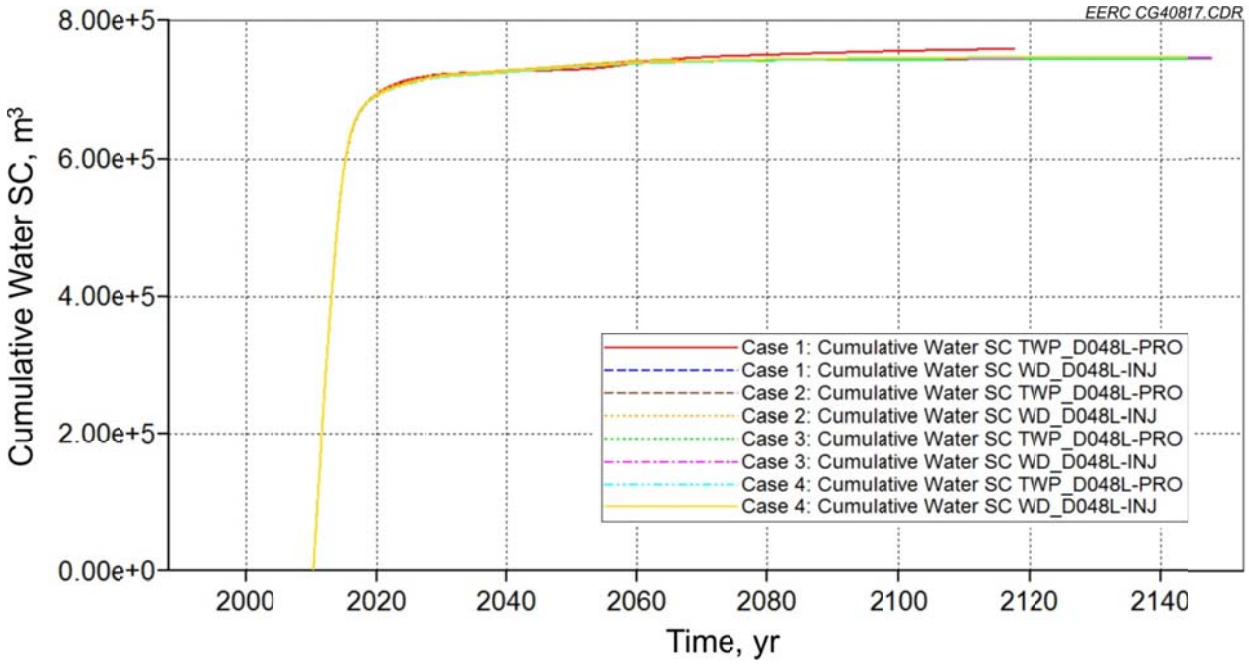

Figure E-16. Production and injection from the Water Recycle Group D048L of History-Matching No. 1.

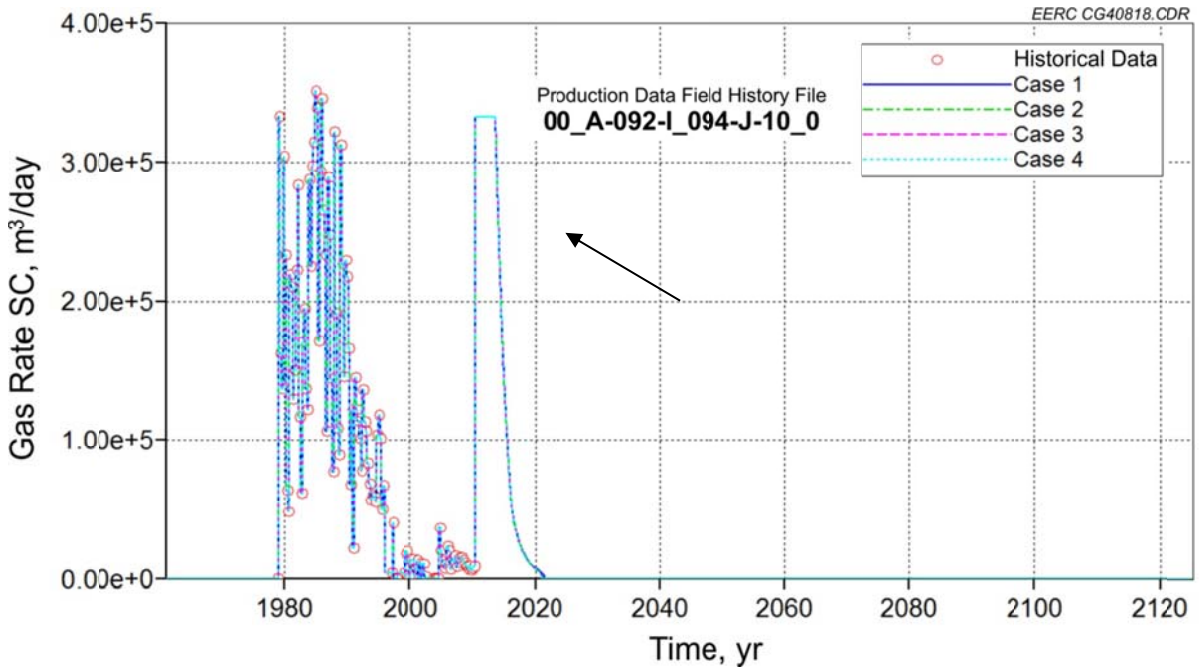

Figure E-17. Example of a well's gas production rate for four test cases of History-Matching No. 1.

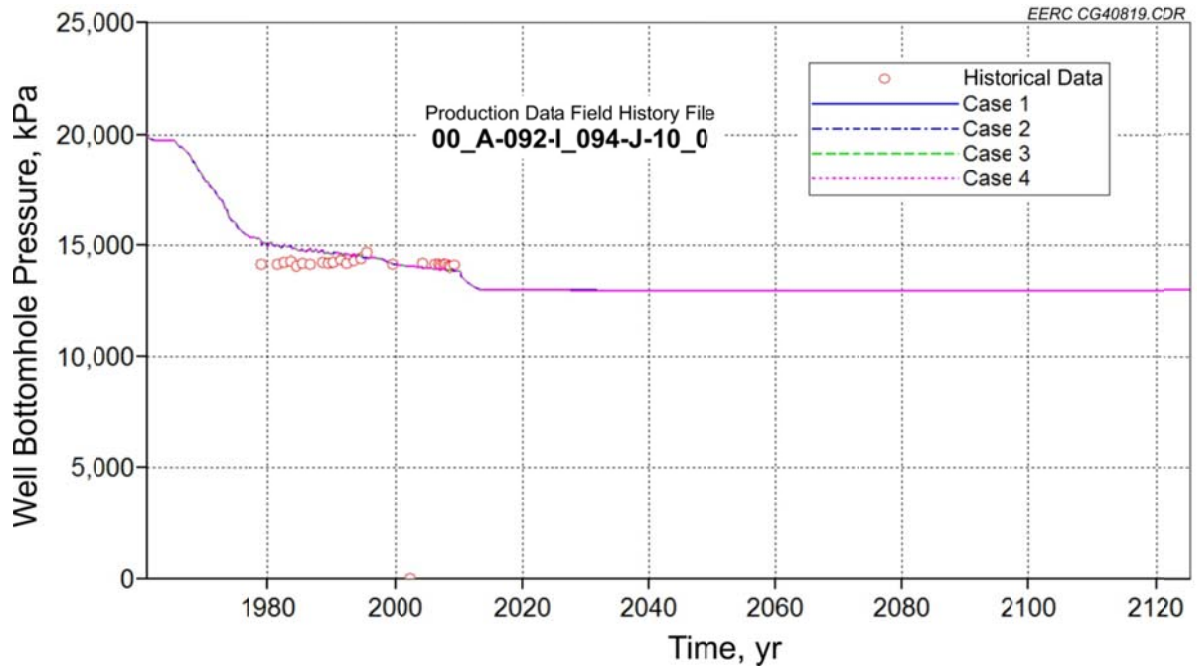

Figure E-18. BHPs of a sample well in Figure E-17.

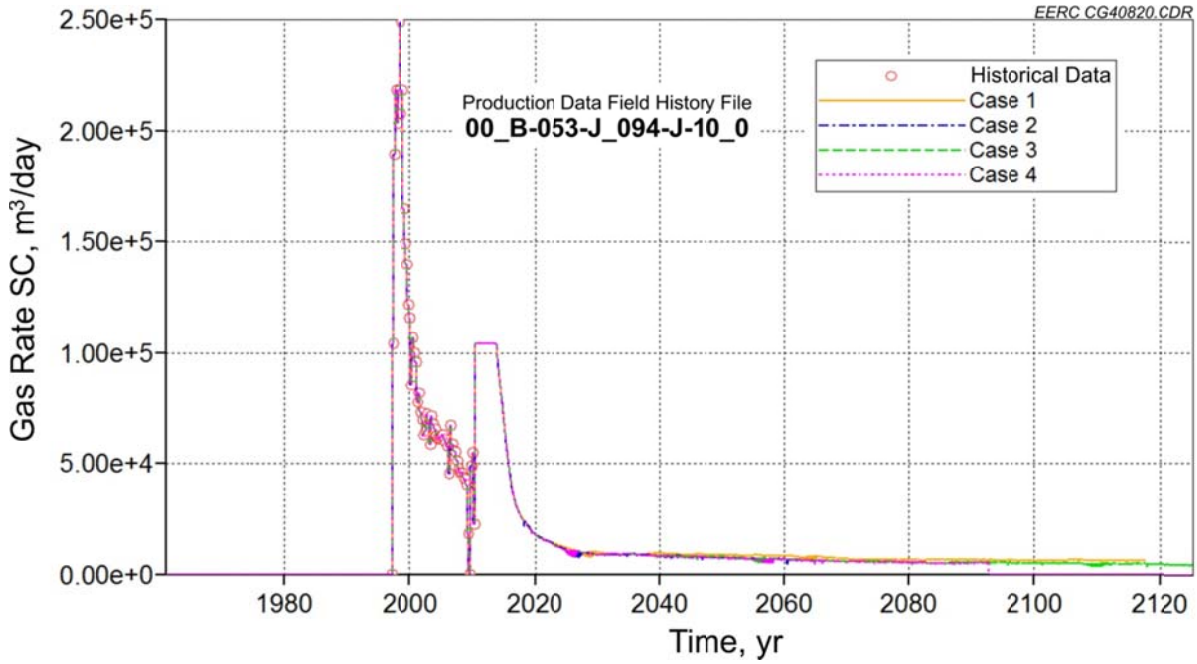

Figure E-19. Example of a well's gas production rate for four test cases of History-Matching No. 1.

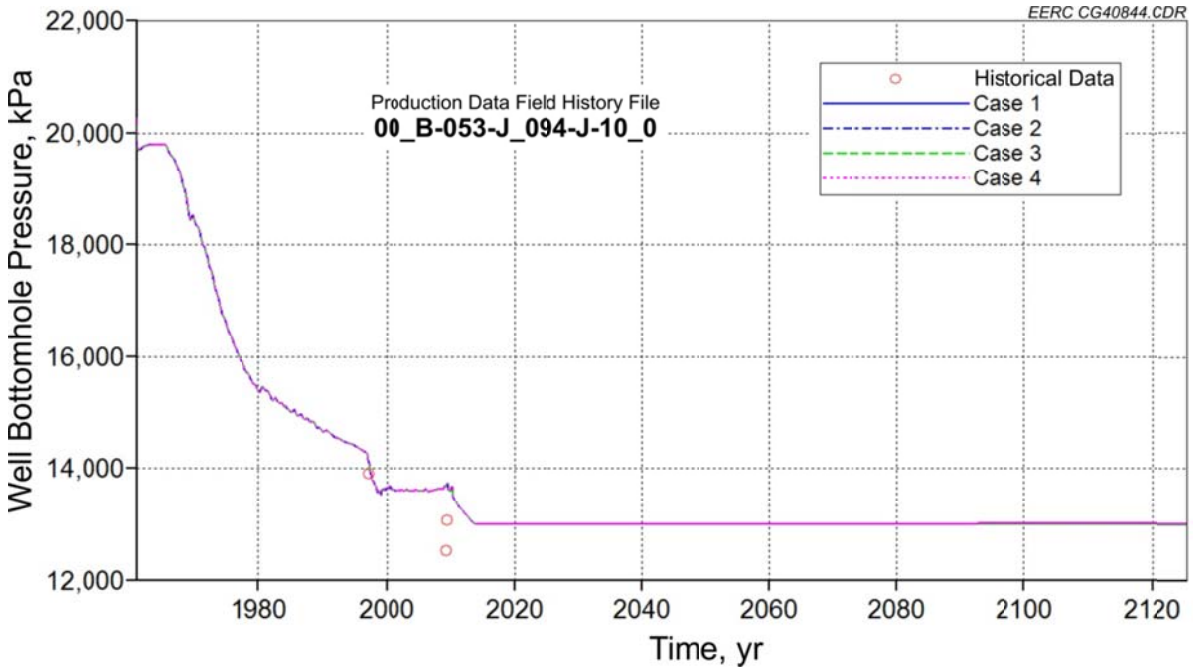

Figure E-20. BHPs of a sample well in Figure E-19.

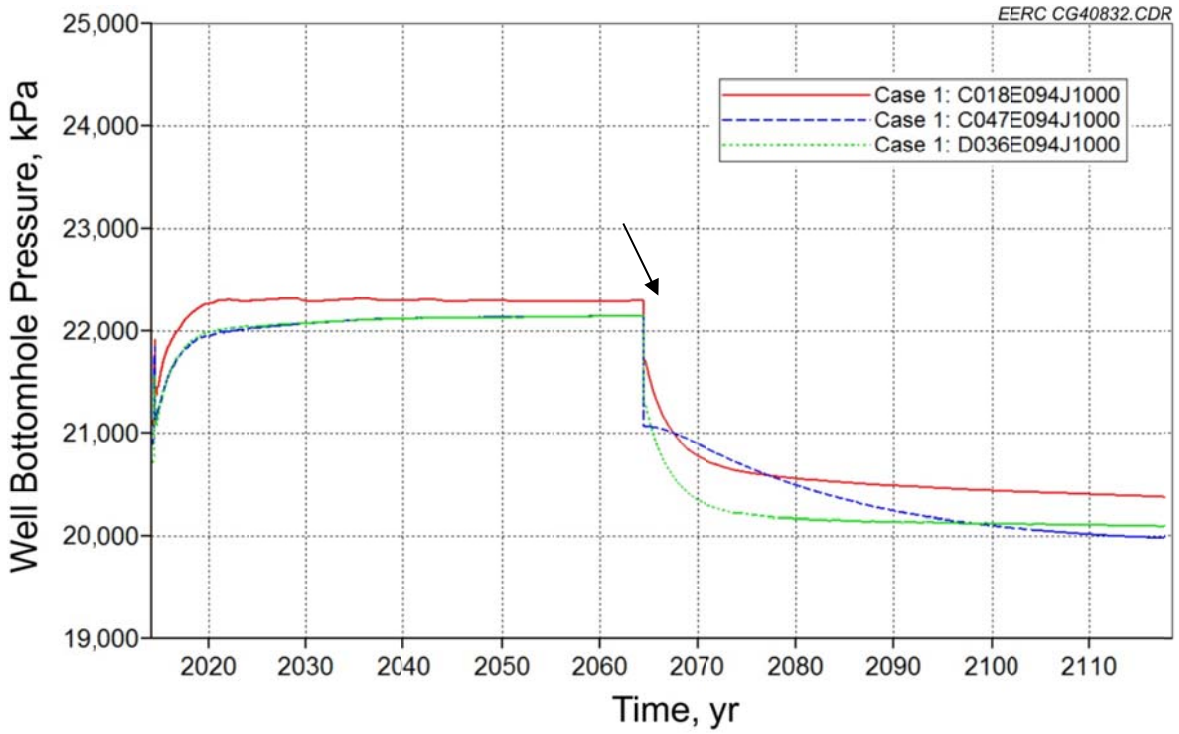

Figure E-21. BHPs of injection wells in Case 1 of History-Matching No. 1.

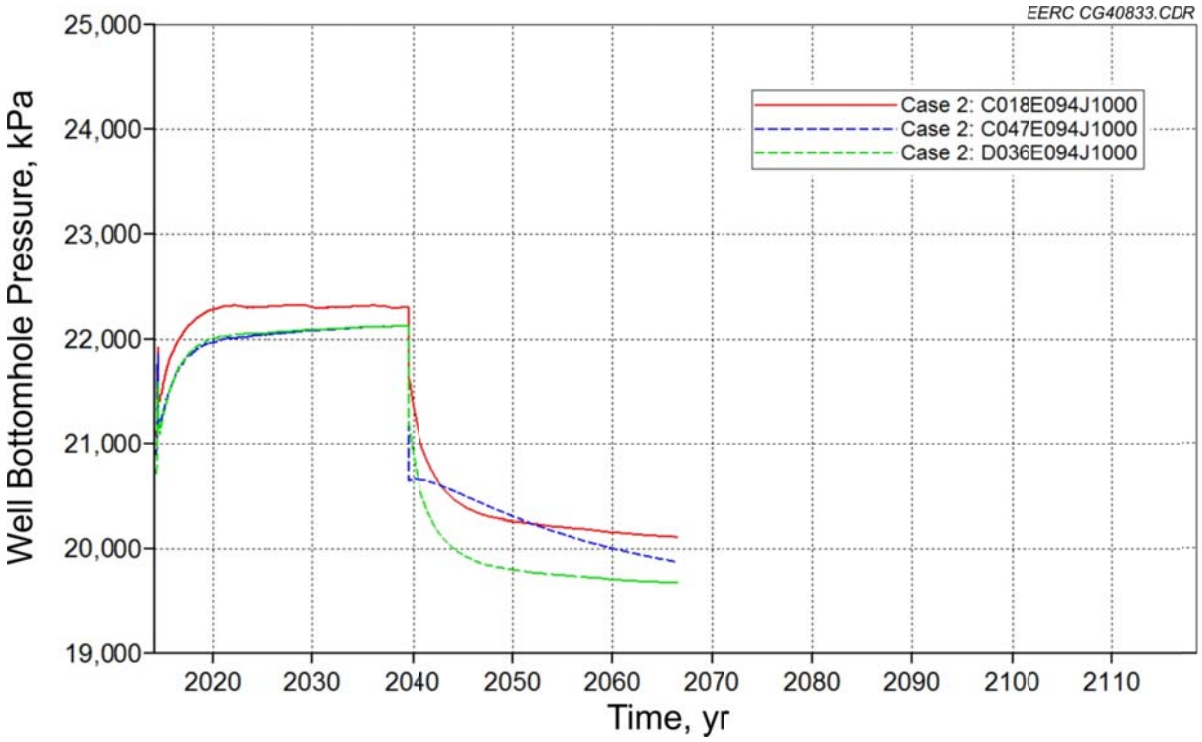

Figure E-22. BHPs of injection wells in Case 2 of History-Matching No. 1.

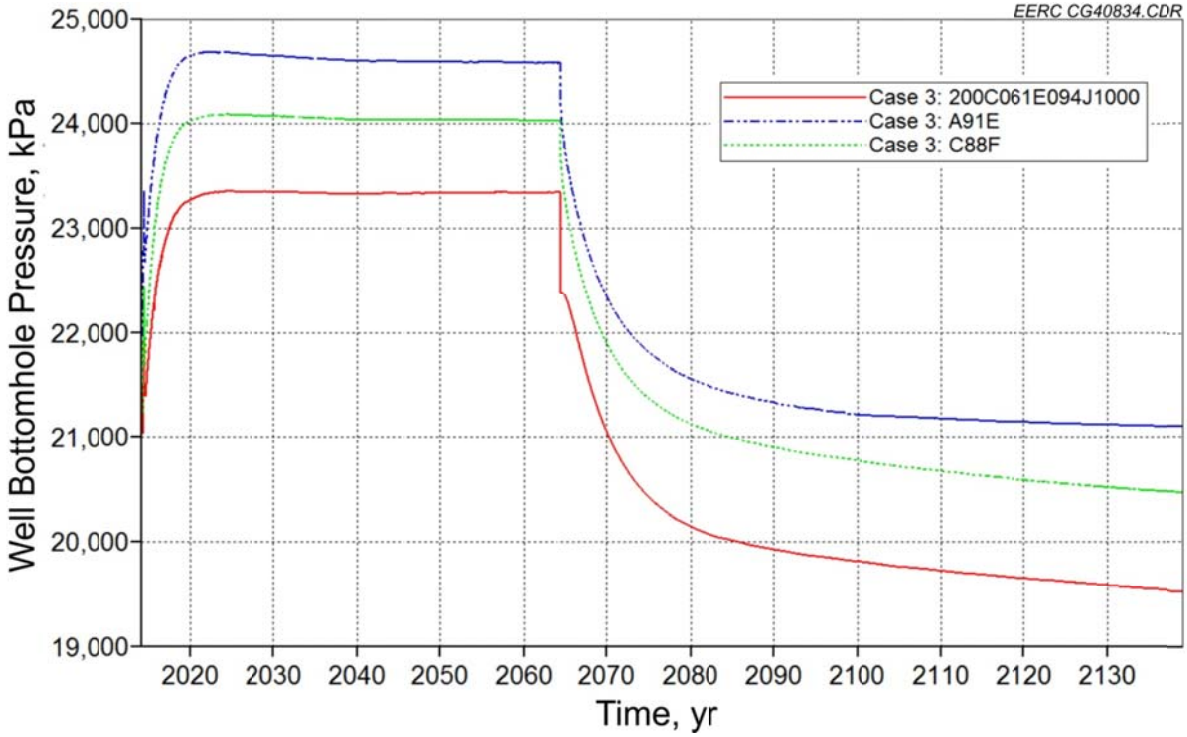

Figure E-23. BHPs of injection wells in Case 3 of History-Matching No. 1.

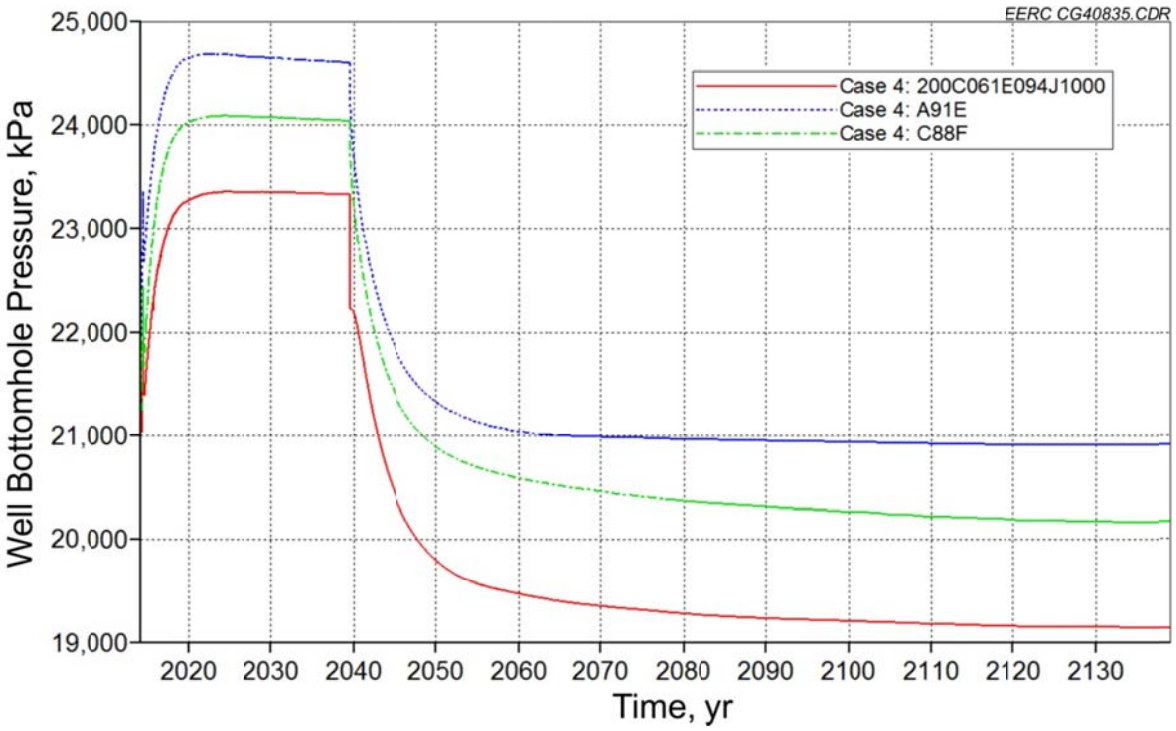

Figure E-24. BHPs of injection wells in Case 4 of History-Matching No. 1.

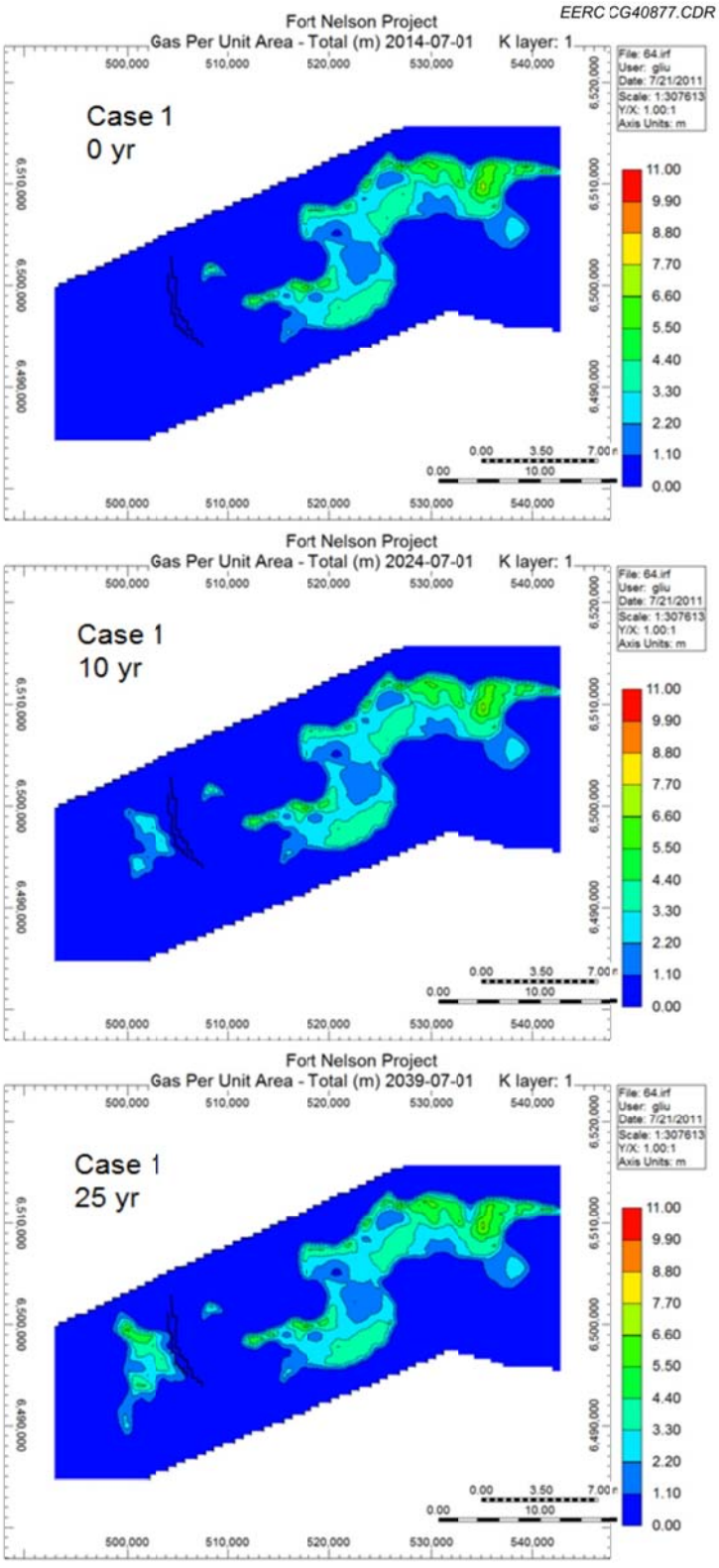

Figure E-25. Areal view of Case 1: 50 years of injection plus 50 years postinjection in and around c-47-E of History-Matching No. 1.

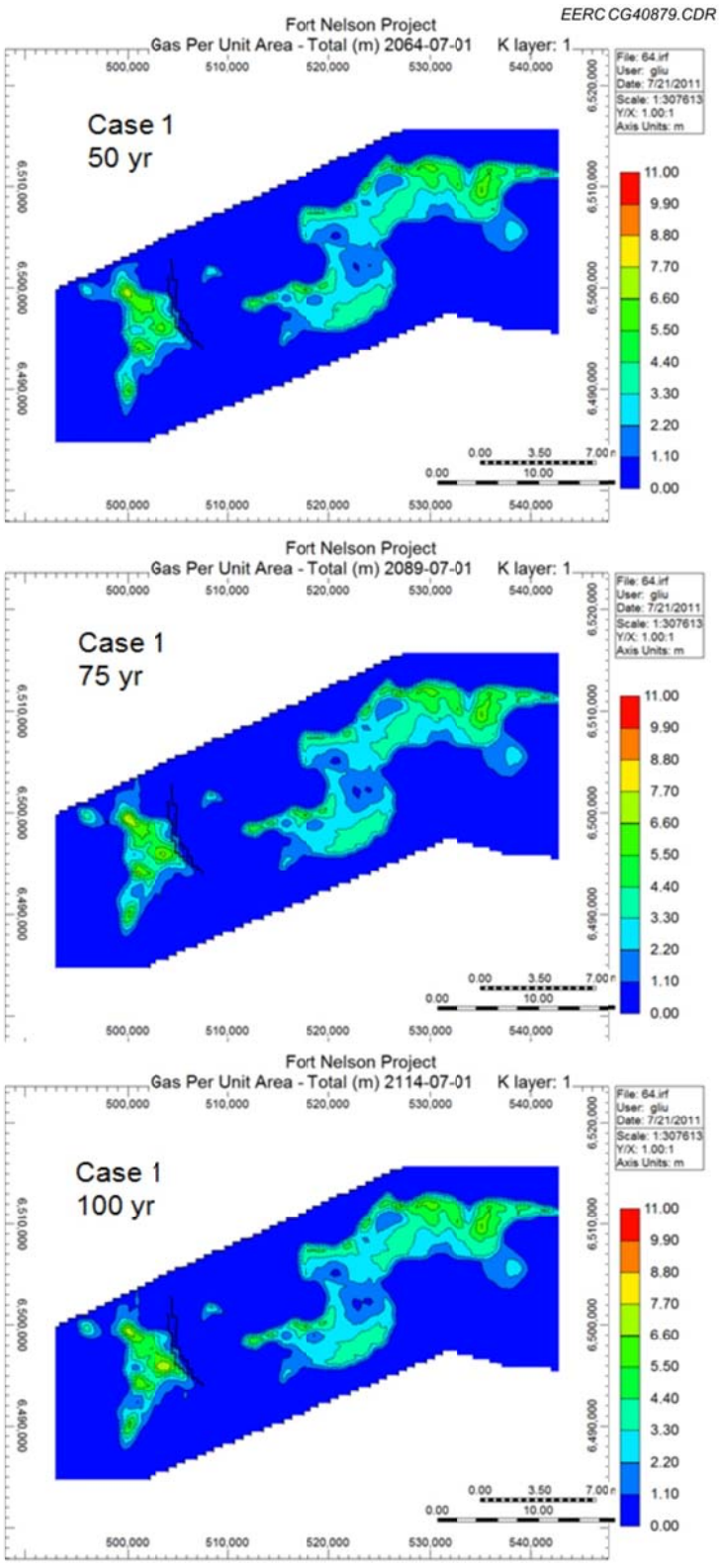

Figure E-26. Areal view of Case 1: 50 years of injection plus 50 years postinjection in and around c-47-E of History-Matching No. 1.

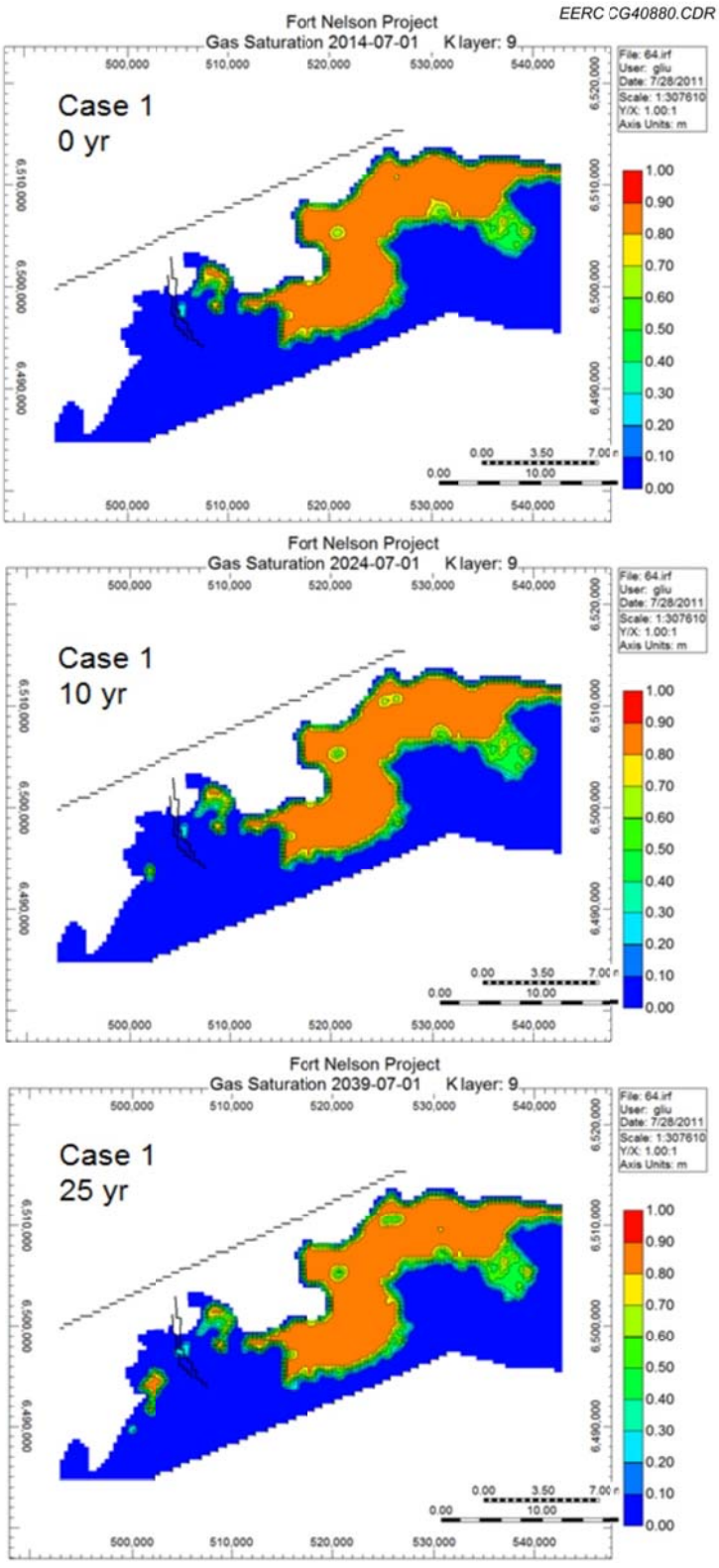

Figure E-27. Areal view of Case 1: saturation at the top of Upper Slave Point over time; 50 years of injection plus 50 years postinjection in and around c-47-E of History-Matching No. 1.

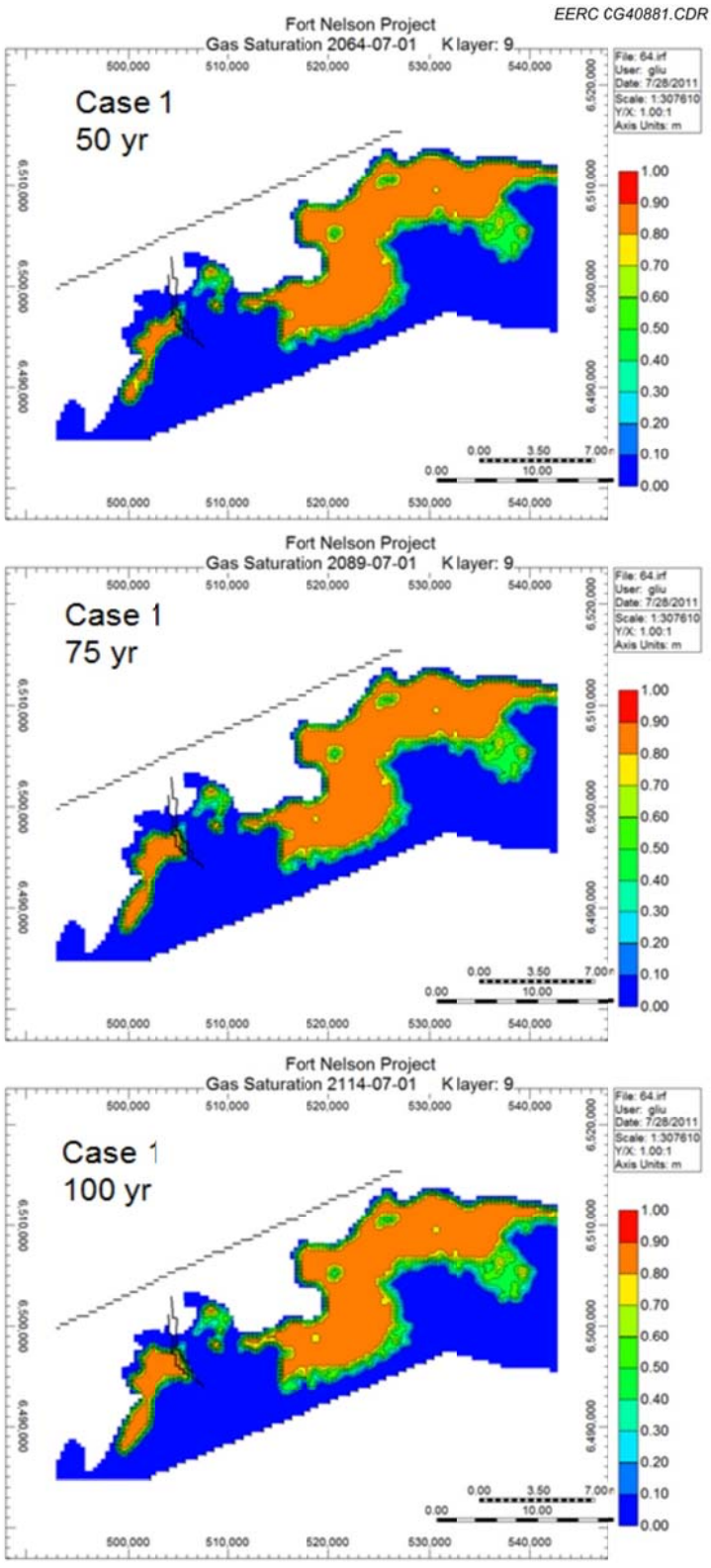

Figure E-28. Areal view of Case 1: saturation at the top of Upper Slave Point over time; 50 years of injection plus 50 years postinjection in and around c-47-E of History-Matching No. 1.

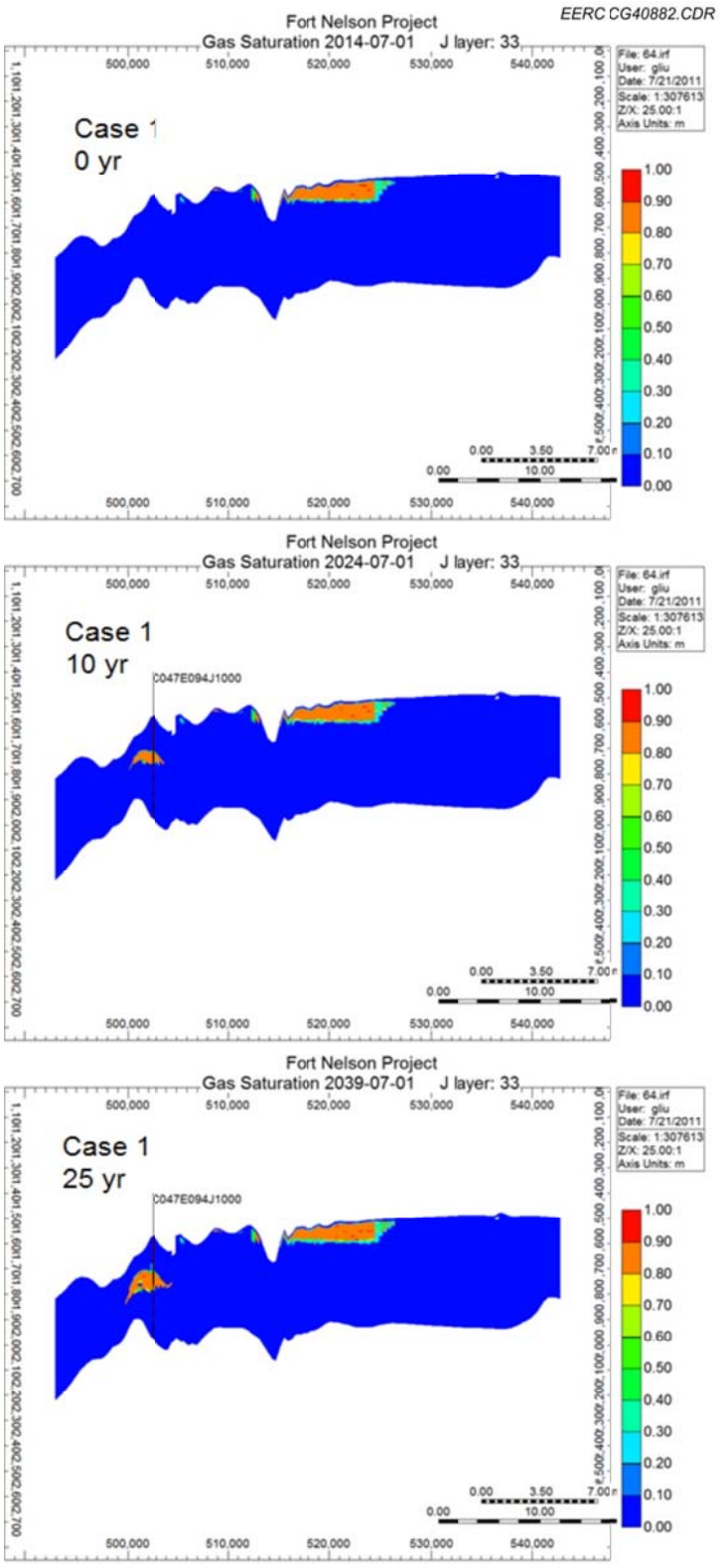

Figure E-29. Cross-sectional view of Case 1: 50 years of injection plus 50 years postinjection in and around c-47-E of History-Matching No. 1.

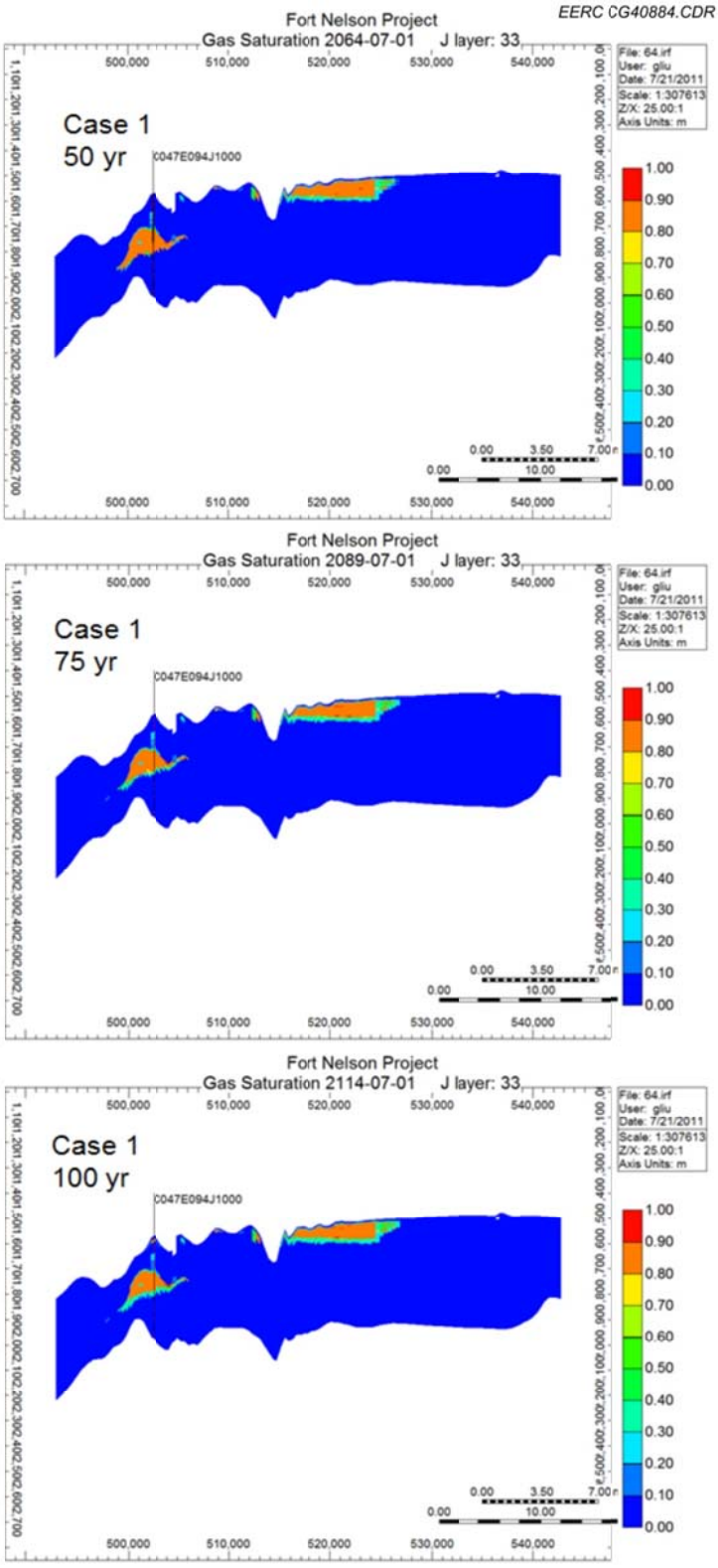

Figure E-30. Cross-sectional view of Case 1: 50 years of injection plus 50 years postinjection in and around c-47-E of History-Matching No. 1.

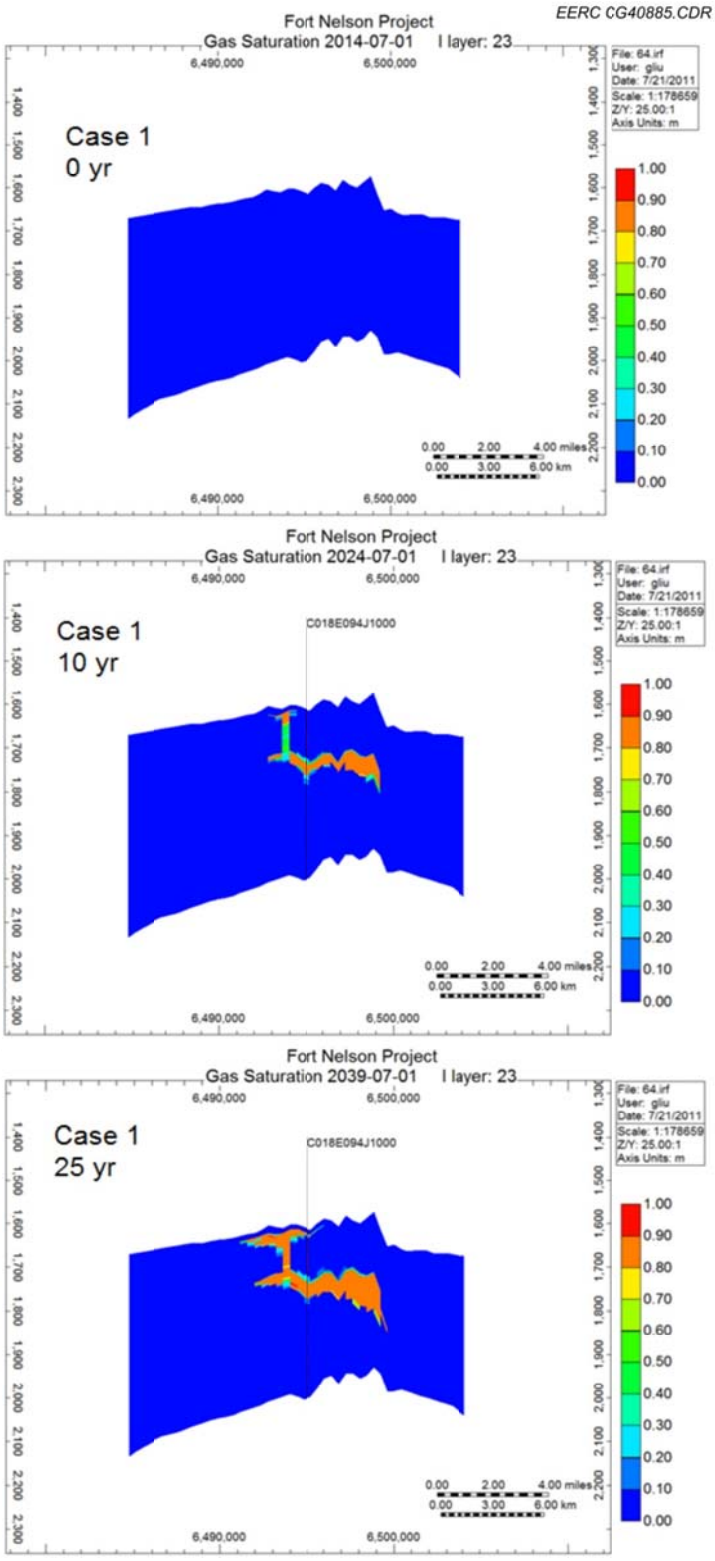

Figure E-31. Cross-sectional view of Case 1: CO_2 moved upward from Sulphur Point through sag. 50 years of injection plus 50 years postinjection in and around c-47-E of History-Matching No. 1.

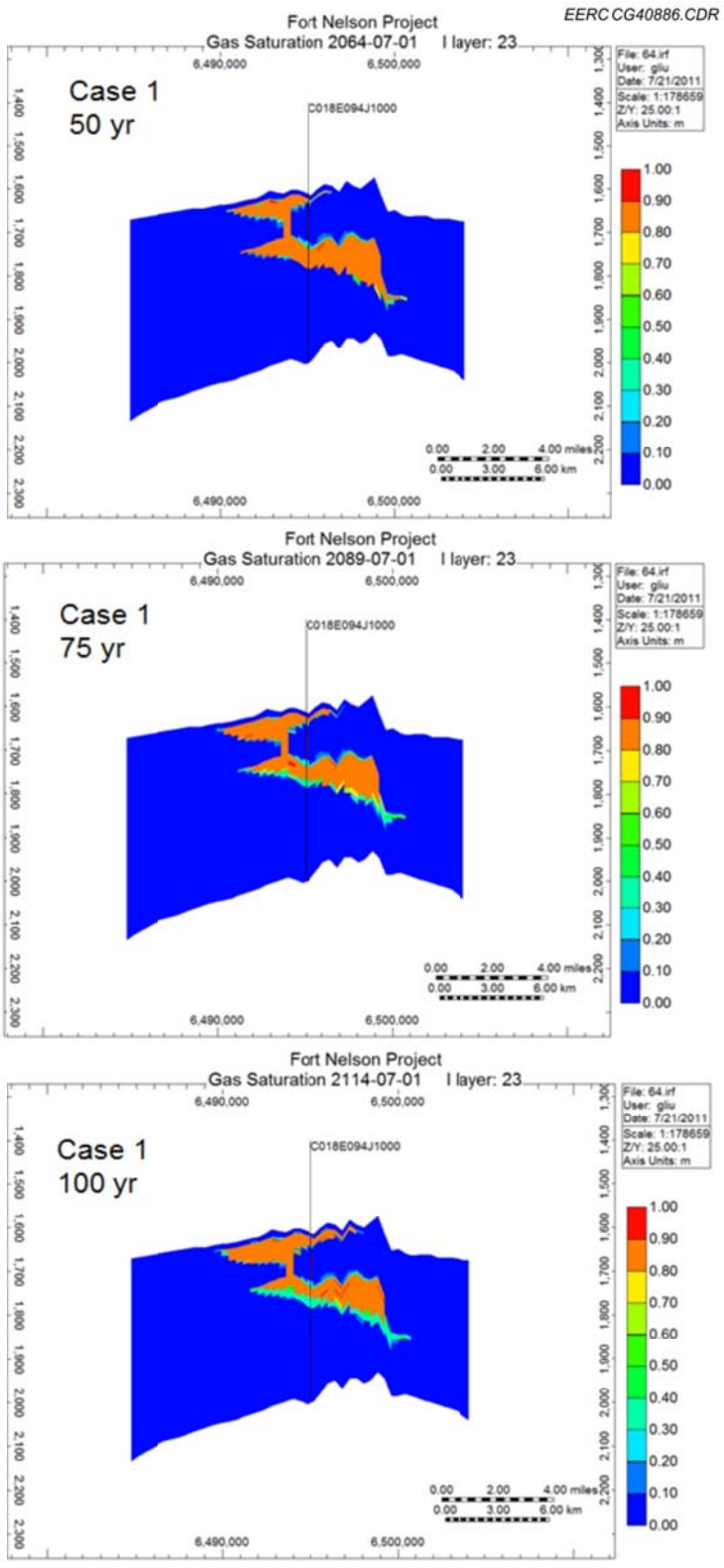

Figure E-32. Cross-sectional view of Case 1: CO_2 moved upward from Sulphur Point through sag; 50 years of injection plus 50 years postinjection in and around c-47-E of History-Matching No. 1.

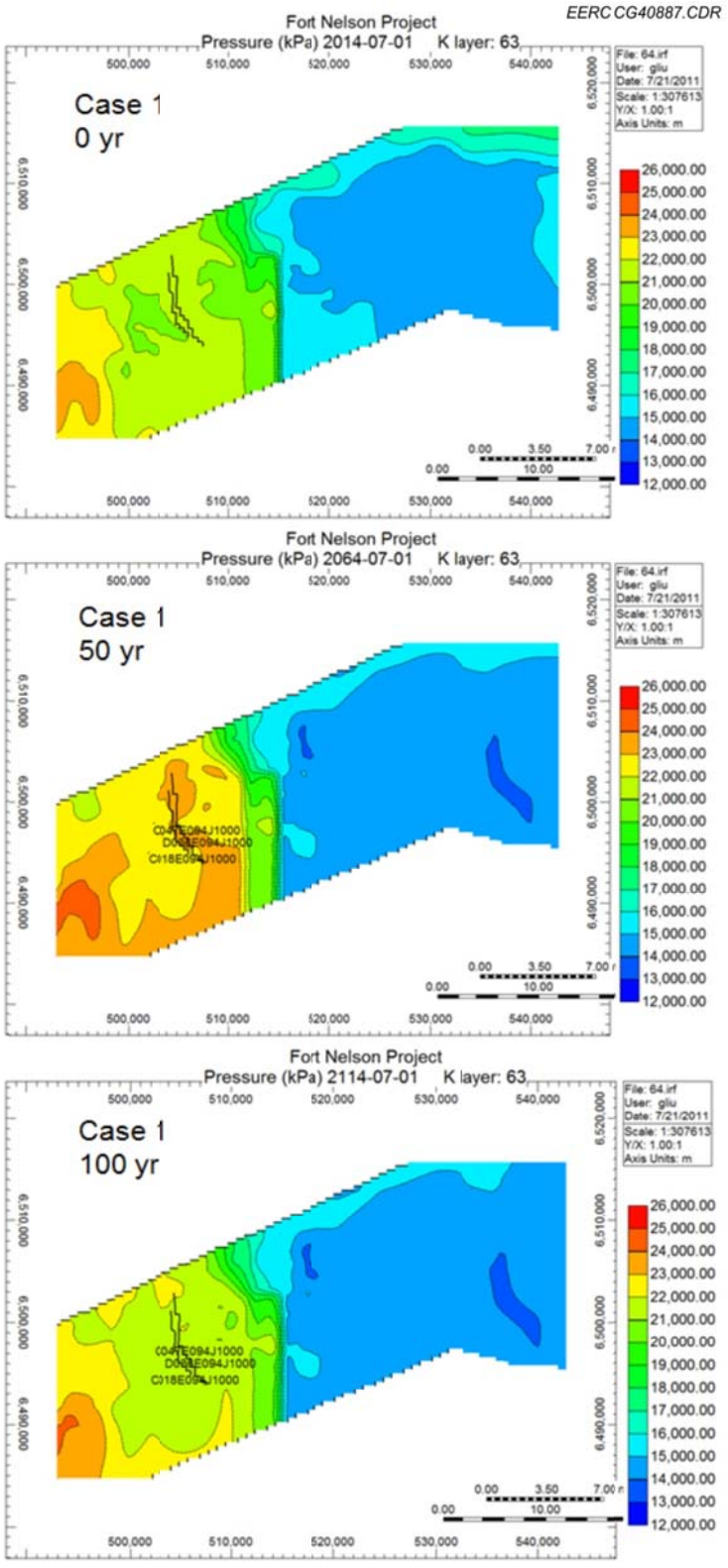

Figure E-33. Areal view of Case 1: pressure distributions; 50 years of injection plus 50 years postinjection in and around c-47-E of History-Matching No. 1.

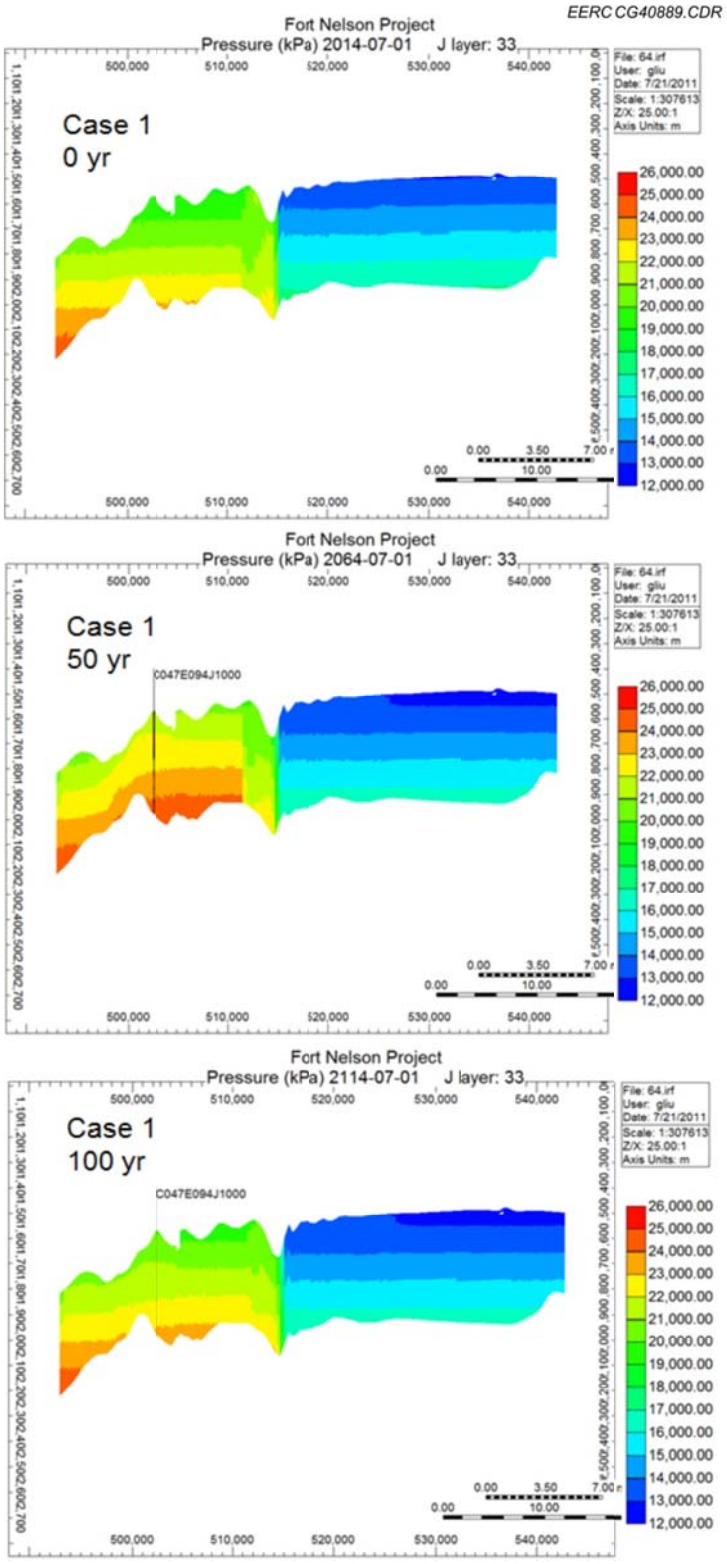

Figure E-34. Cross-sectional view of Case 1: pressure distributions; 50 years of injection plus 50 years postinjection in and around c-47-E of History-Matching No. 1.

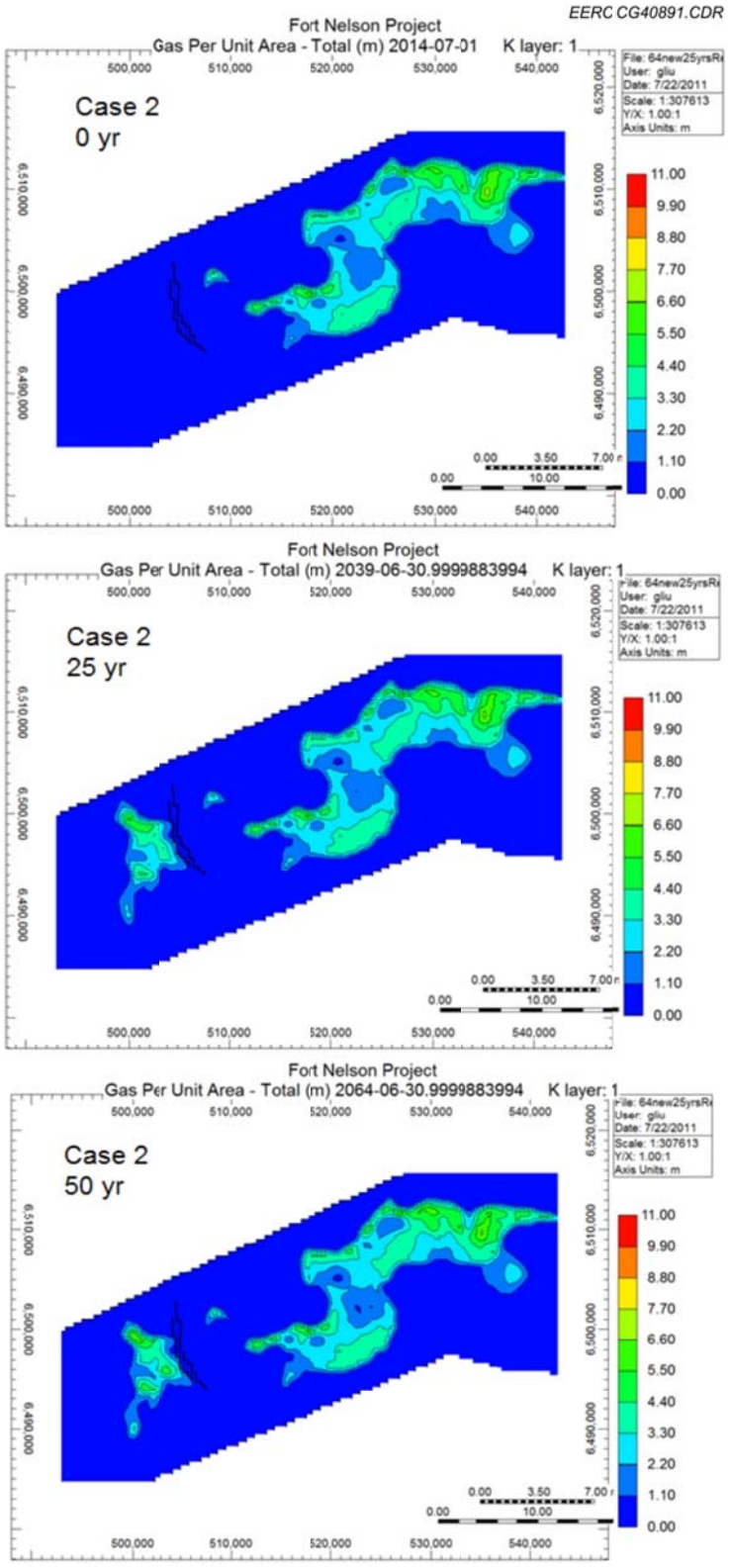

Figure E-35. Areal view of Case 2: 25 years of injection plus 25 years postinjection in and around c-47-E of History-Matching No. 1.

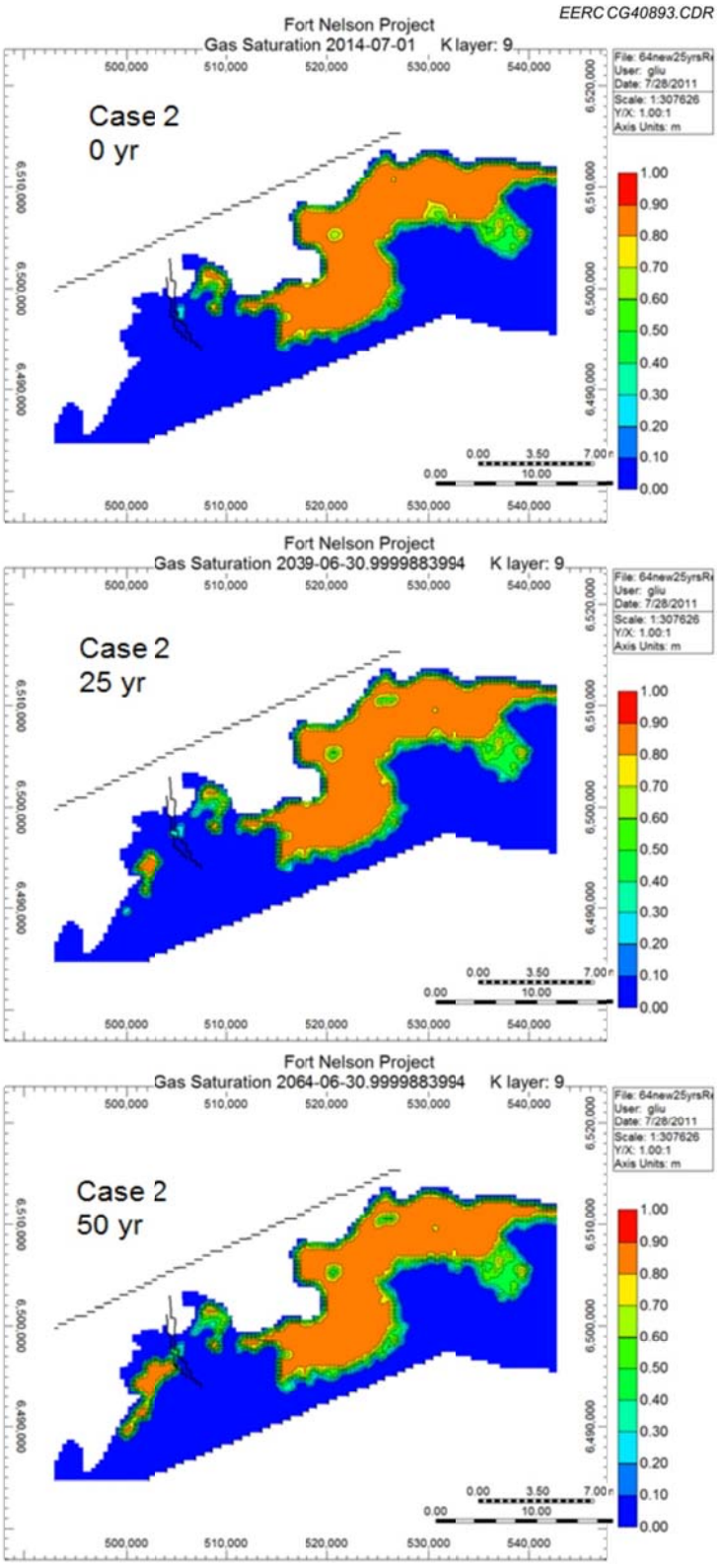

Figure E-36. Areal view of Case 2: saturation at the top of Upper Slave Point over time; 25 years of injection plus 25 years postinjection in and around c-47-E of History-Matching No. 1.

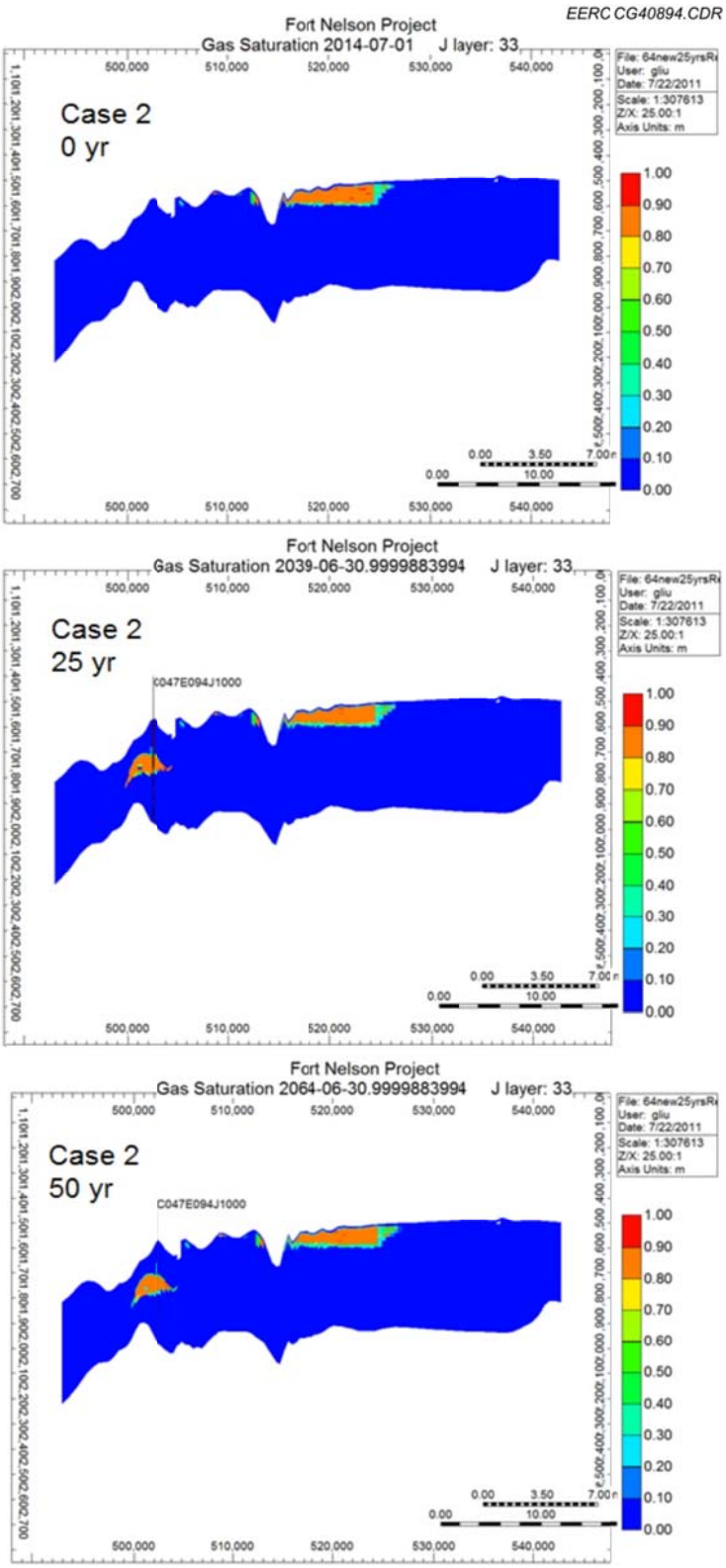

Figure E-37. Cross-sectional view of Case 2: 25 years of injection plus 25 years postinjection in and around c-47-E of History-Matching No. 1.

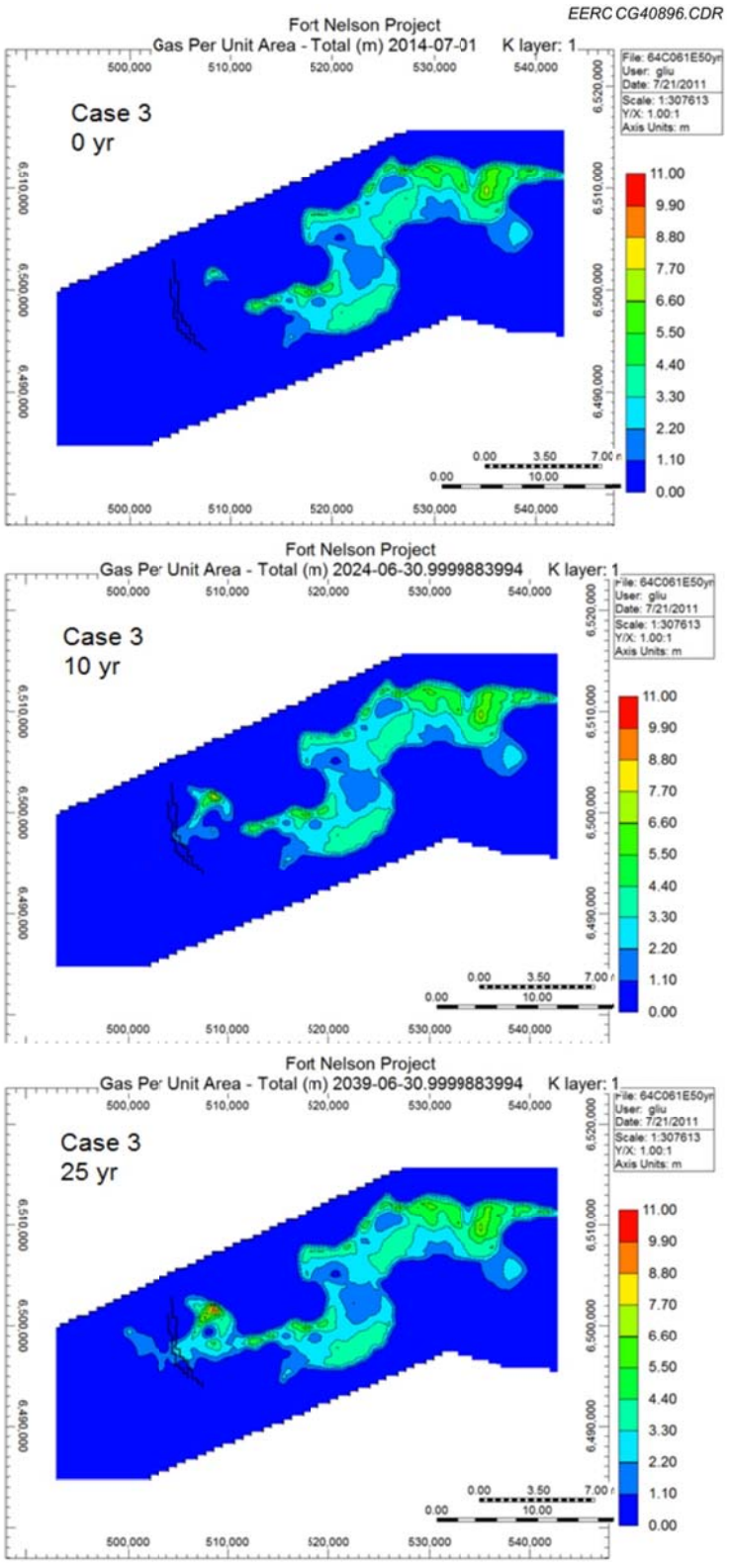

Figure E-38. Areal view of Case 3: 50 years of injection plus 50 years postinjection in and around c-61-E of History-Matching No. 1.

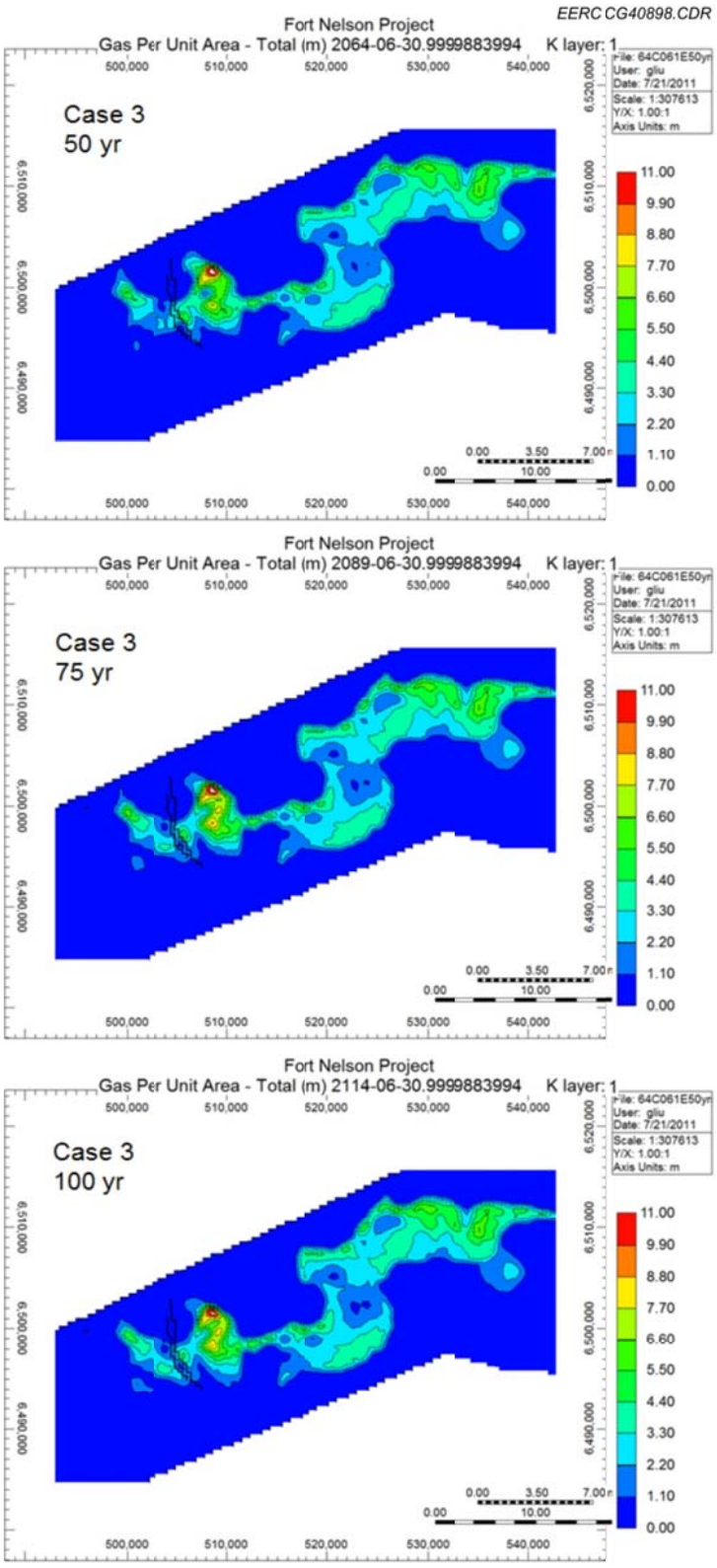

Figure E-39. Areal view of Case 3: 50 years of injection plus 50 years postinjection in and around c-61-E of History-Matching No. 1.

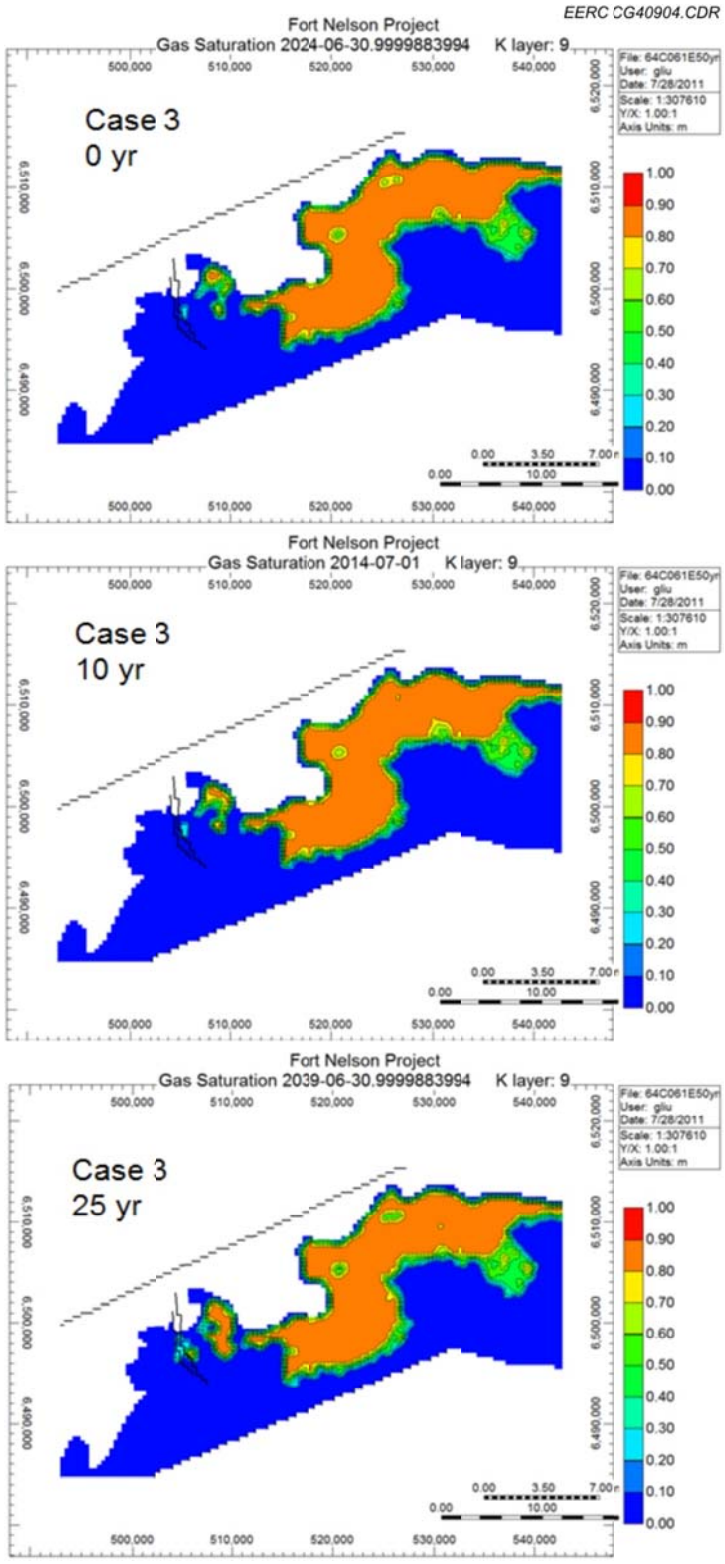

Figure E-40. Areal view of Case 3: saturation at the top of Upper Slave Point over time; 50 years of injection plus 50 years postinjection in and around c-61-E of History-Matching No. 1.

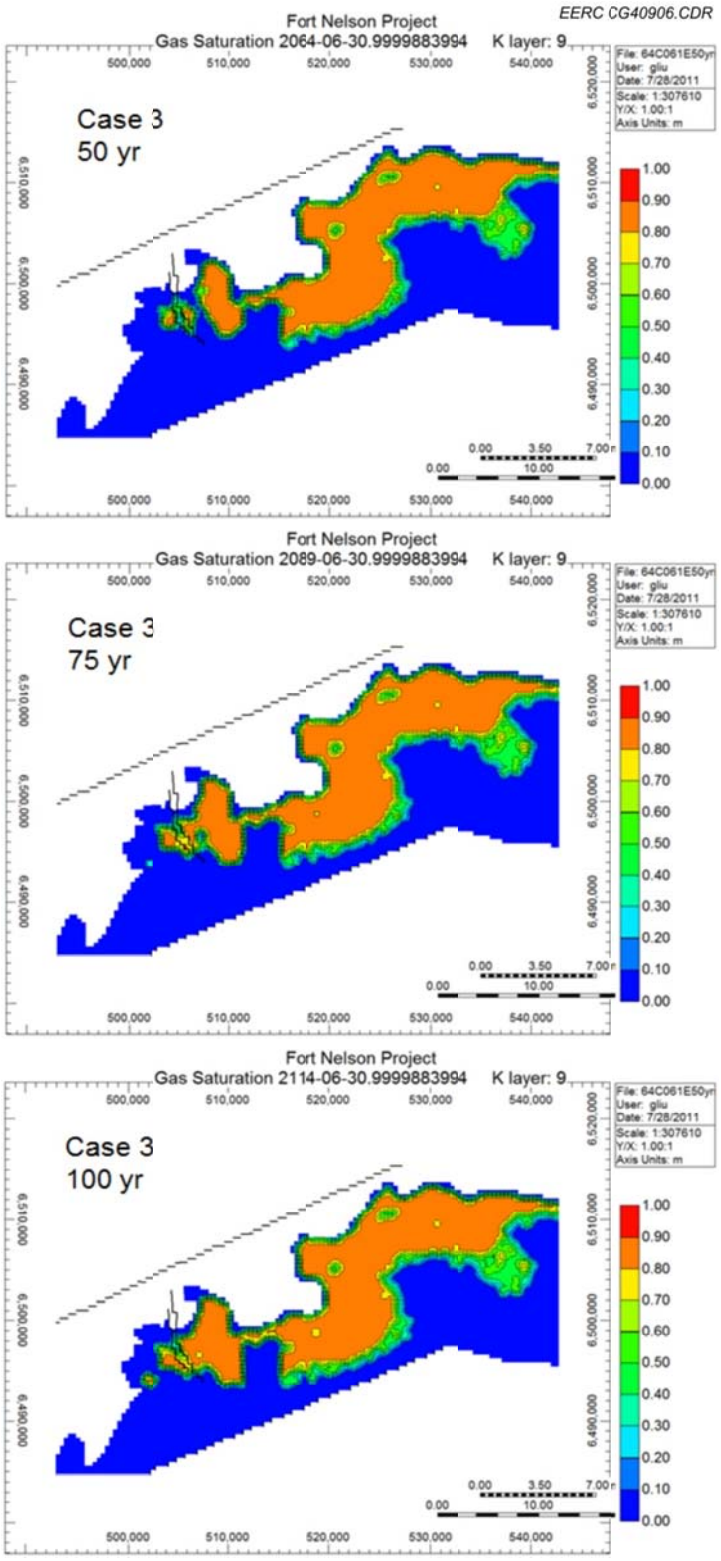

Figure E-41. Areal view of Case 3: saturation at the top of Upper Slave Point over time; 50 years of injection plus 50 years postinjection in and around c-61-E of History-Matching No. 1.

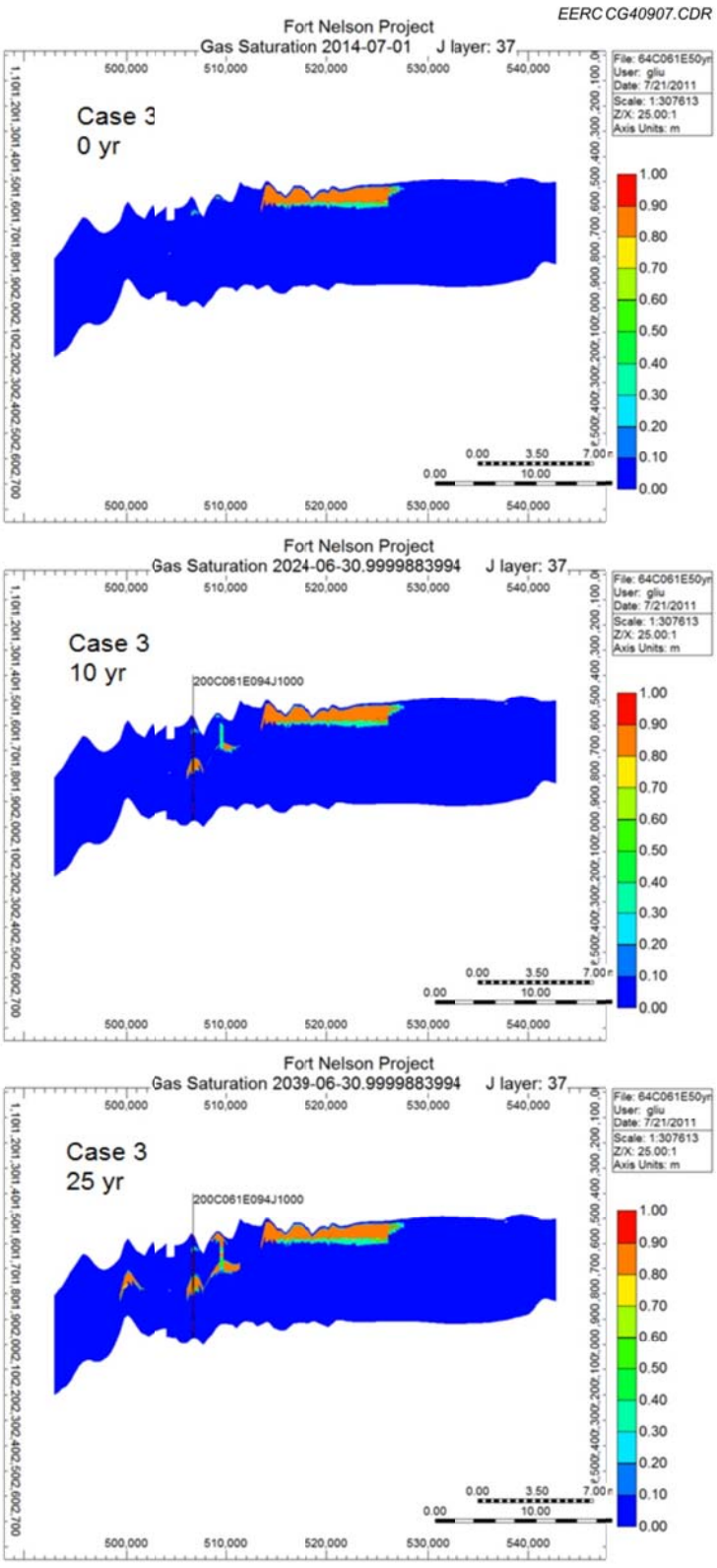

Figure E-42. Cross-sectional view of Case 3: 50 years of injection plus 50 years postinjection in and around c-61-E of History-Matching No. 1.

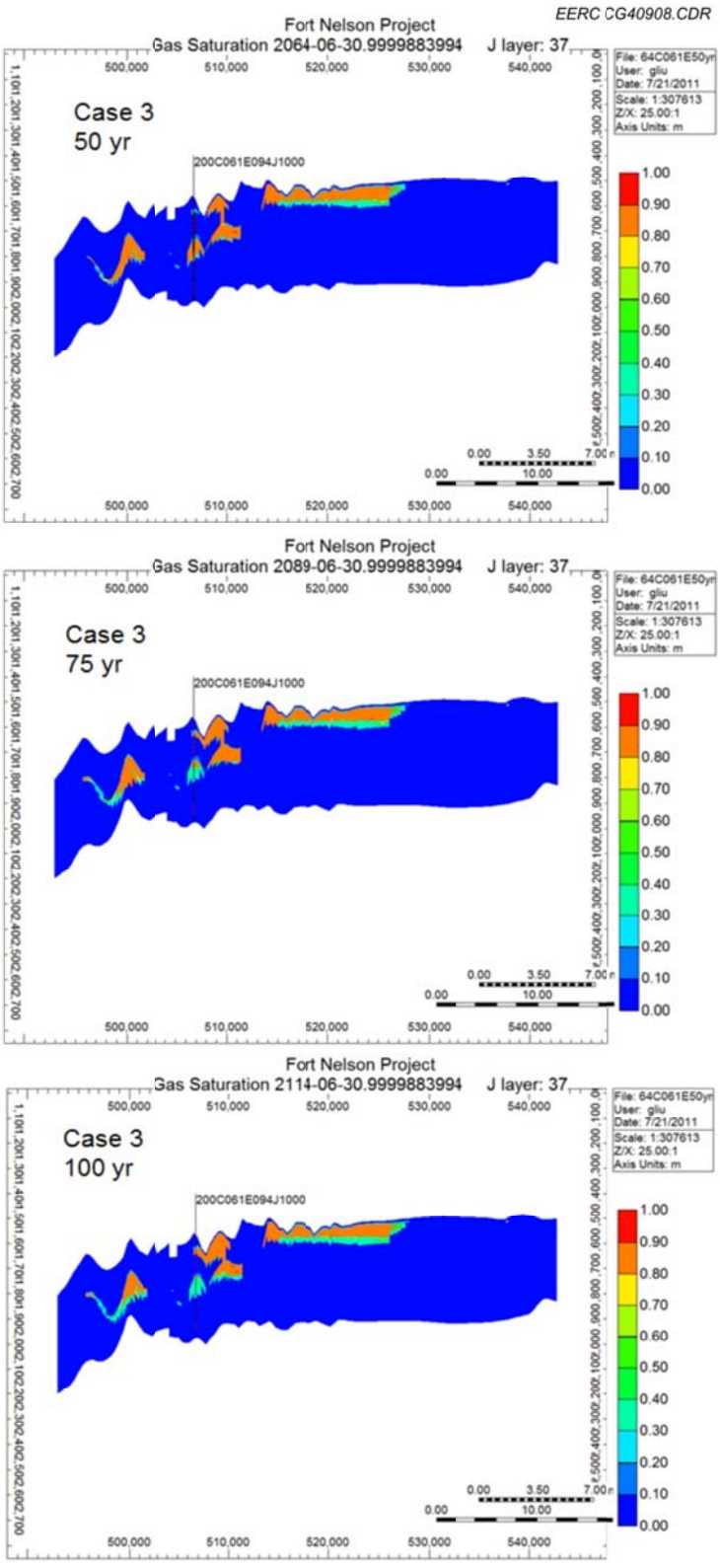

Figure E-43. Cross-sectional view of Case 3: 50 years of injection plus 50 years postinjection in and around C-61-E of History-Matching No. 1.

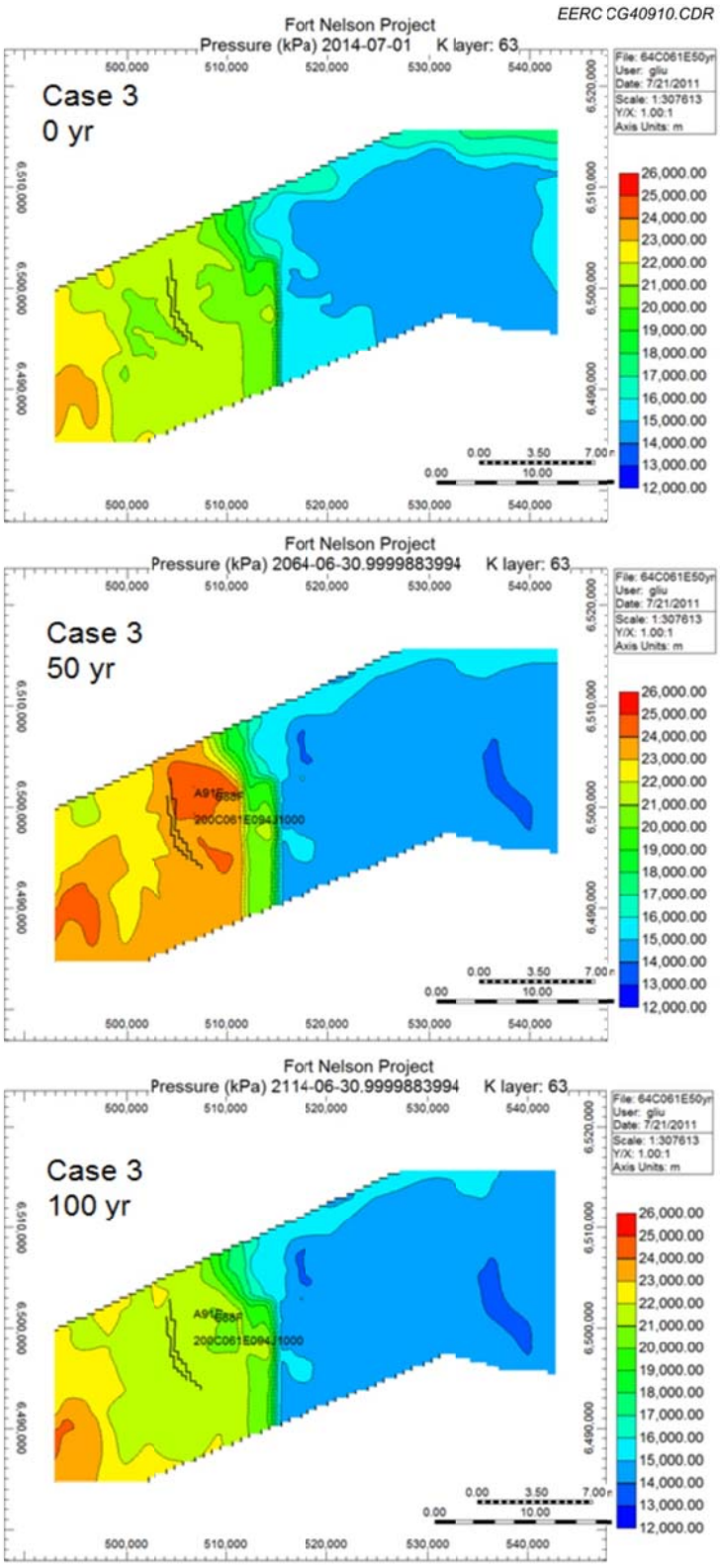

Figure E-44. Areal view of Case 3: pressure distributions; 50 years of injection plus 50 years postinjection in and around c-61-E of History-Matching No. 1.

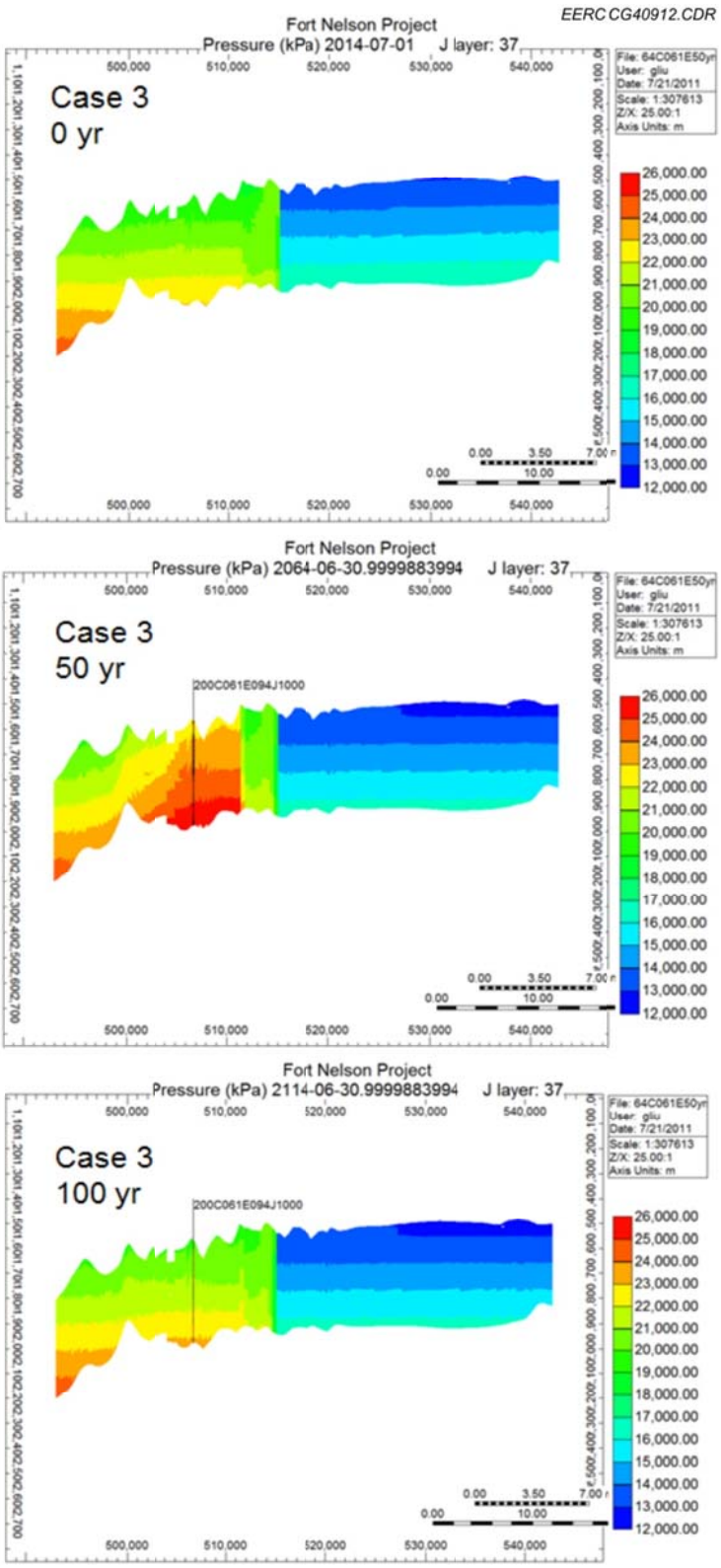

Figure E-45. Cross-sectional view of Case 3: pressure distributions; 50 years of injection plus 50 years postinjection in and around c-61-E of History-Matching No. 1.

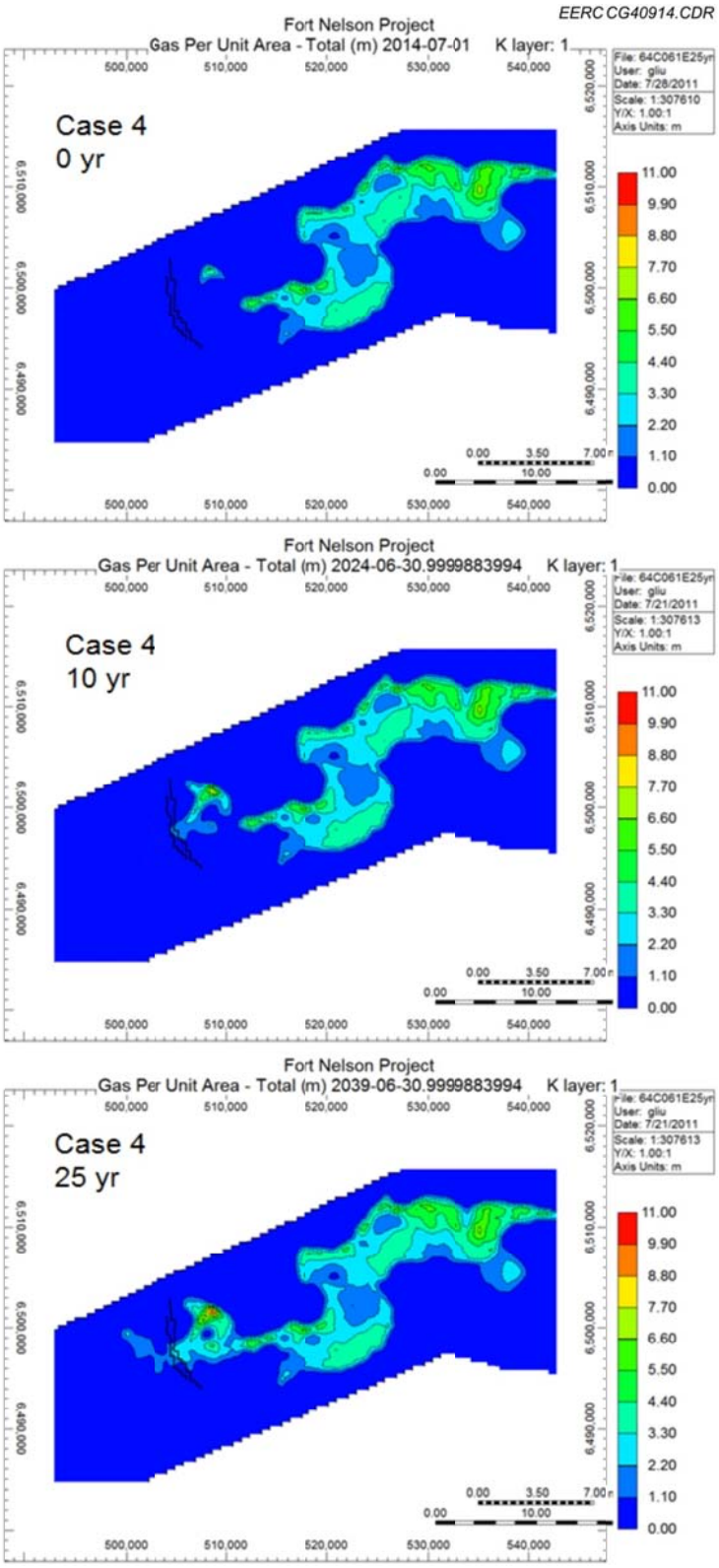

Figure E-46. Areal view of Case 4: 25 years of injection plus 75 years postinjection in and around c-61-E of History-Matching No. 1.

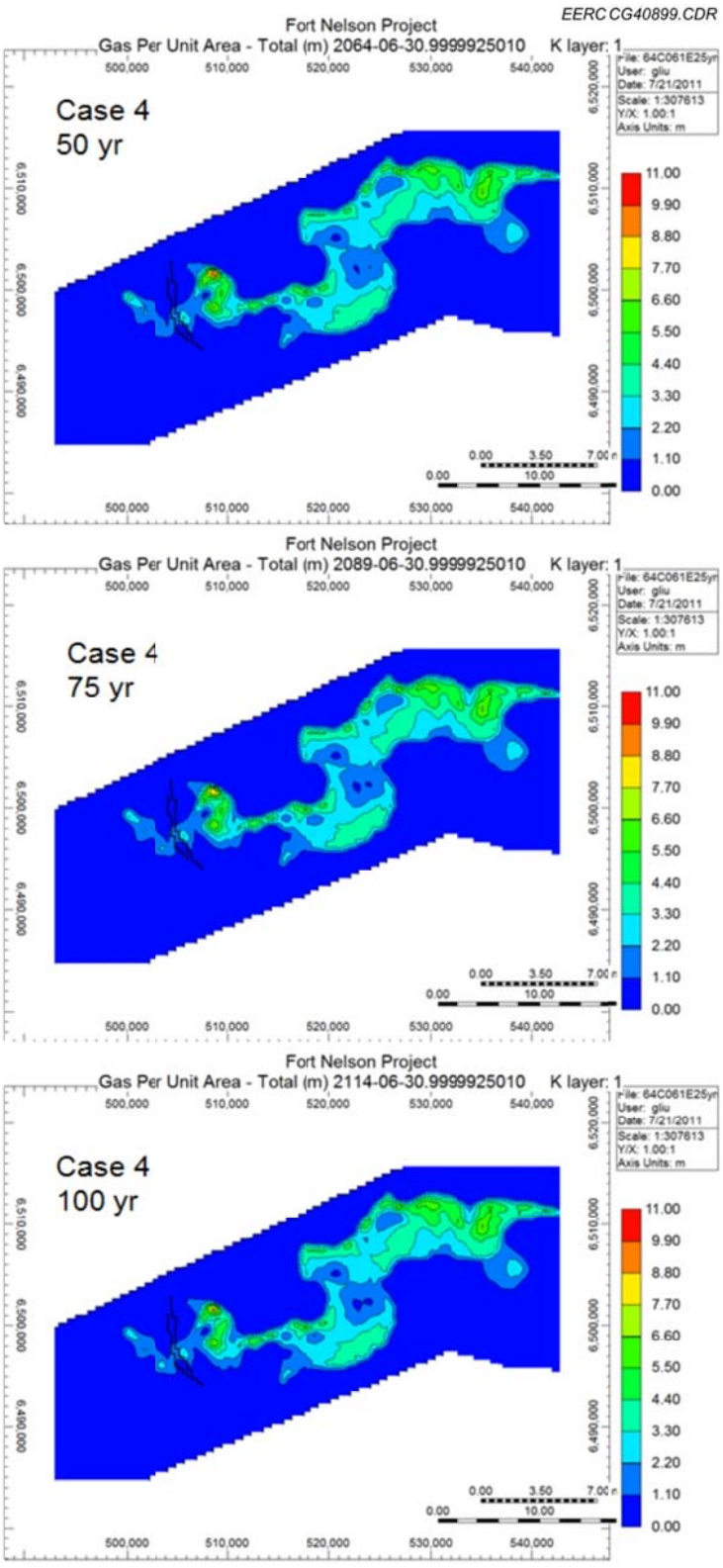

Figure E-47. Areal view of Case 4: 25 years of injection plus 75 years postinjection in and around c-61-E of History-Matching No. 1.

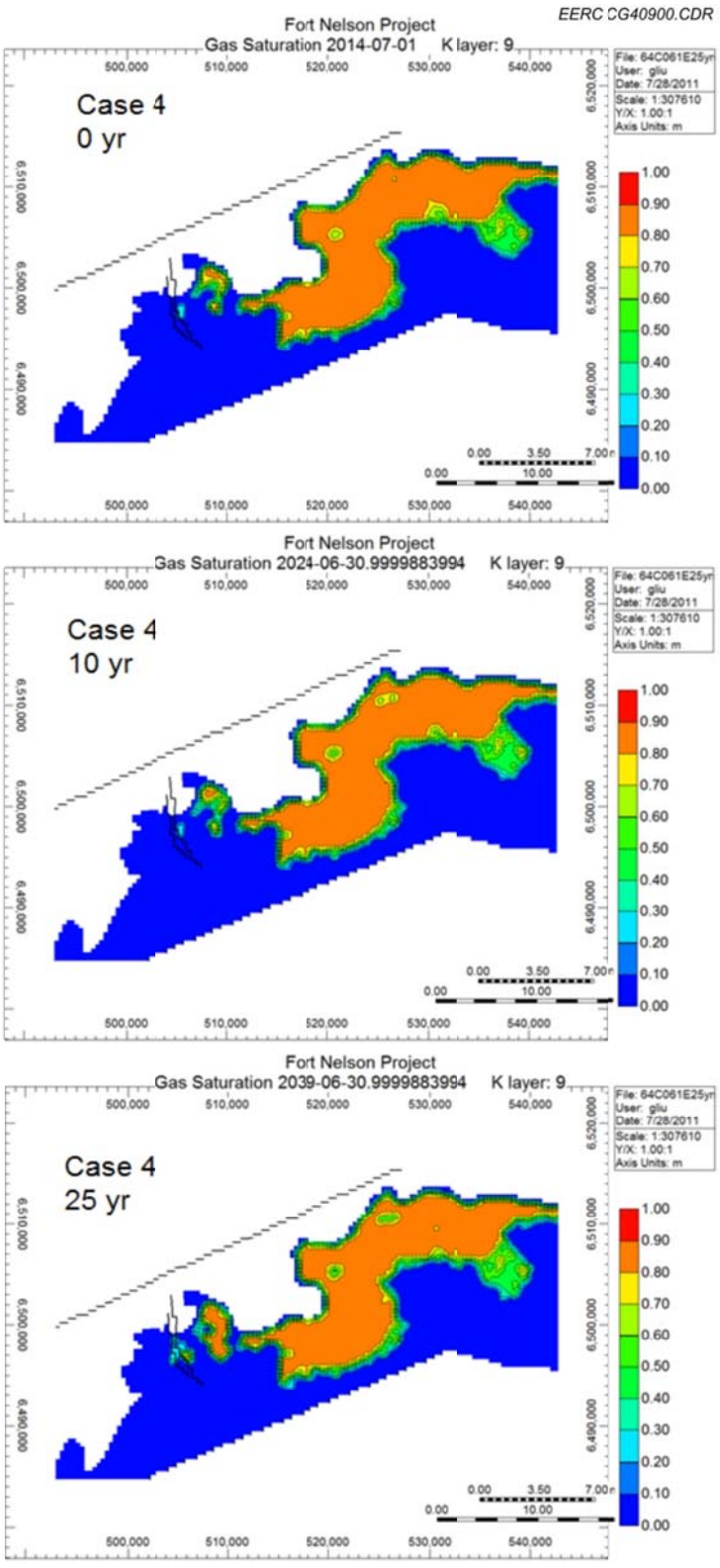

Figure E-48. Areal view of Case 4: saturation at the top of Upper Slave Point over time; 25 years of injection plus 75 years postinjection in and around c-61-E of History-Matching No. 1.

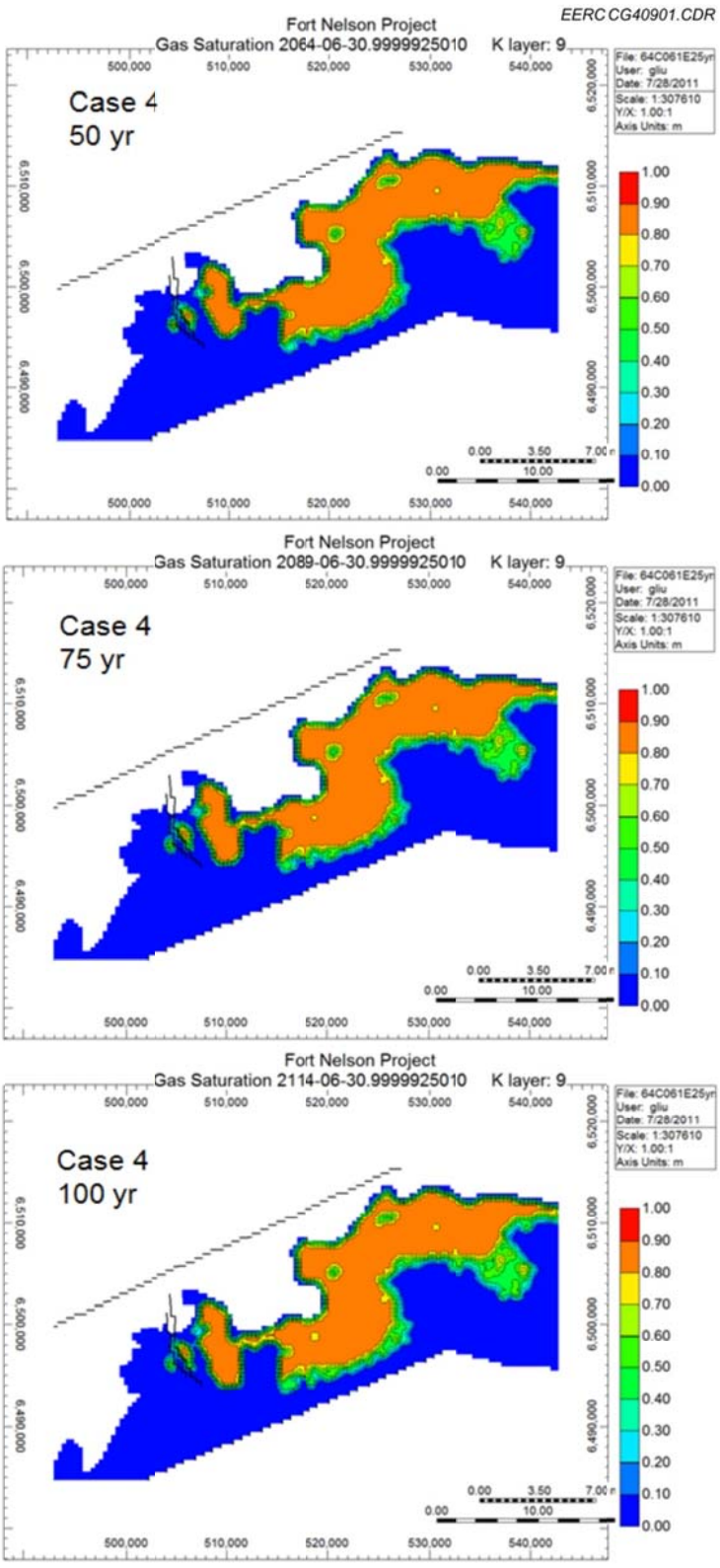

Figure E-49. Areal view of Case 4: saturation at the top of Upper Slave Point over time; 25 years of injection plus 75 years postinjection in and around c-61-E of History-Matching No. 1.

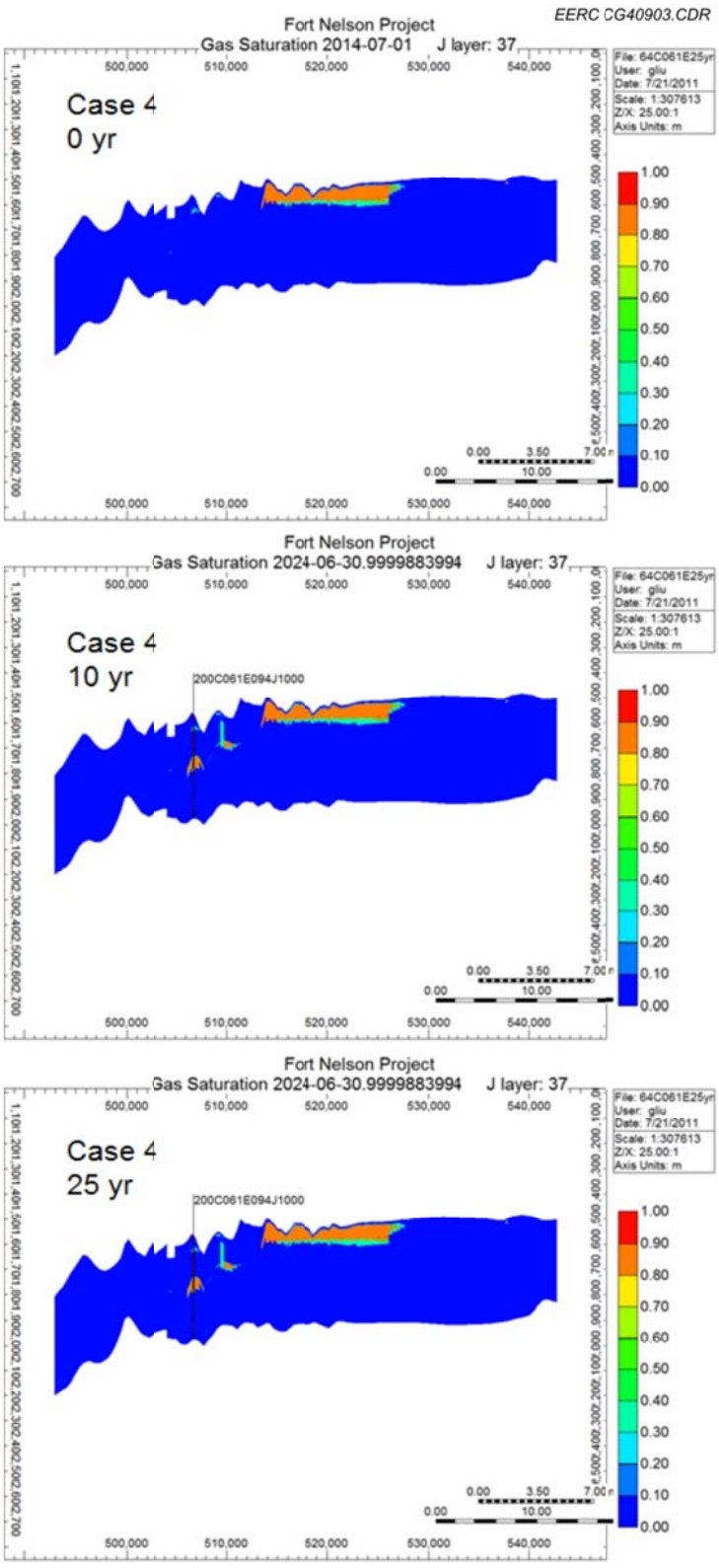

Figure E-50. Cross-sectional view of Case 4: 25 years of injection plus 75 years postinjection in and around c-61-E of History-Matching No. 1.

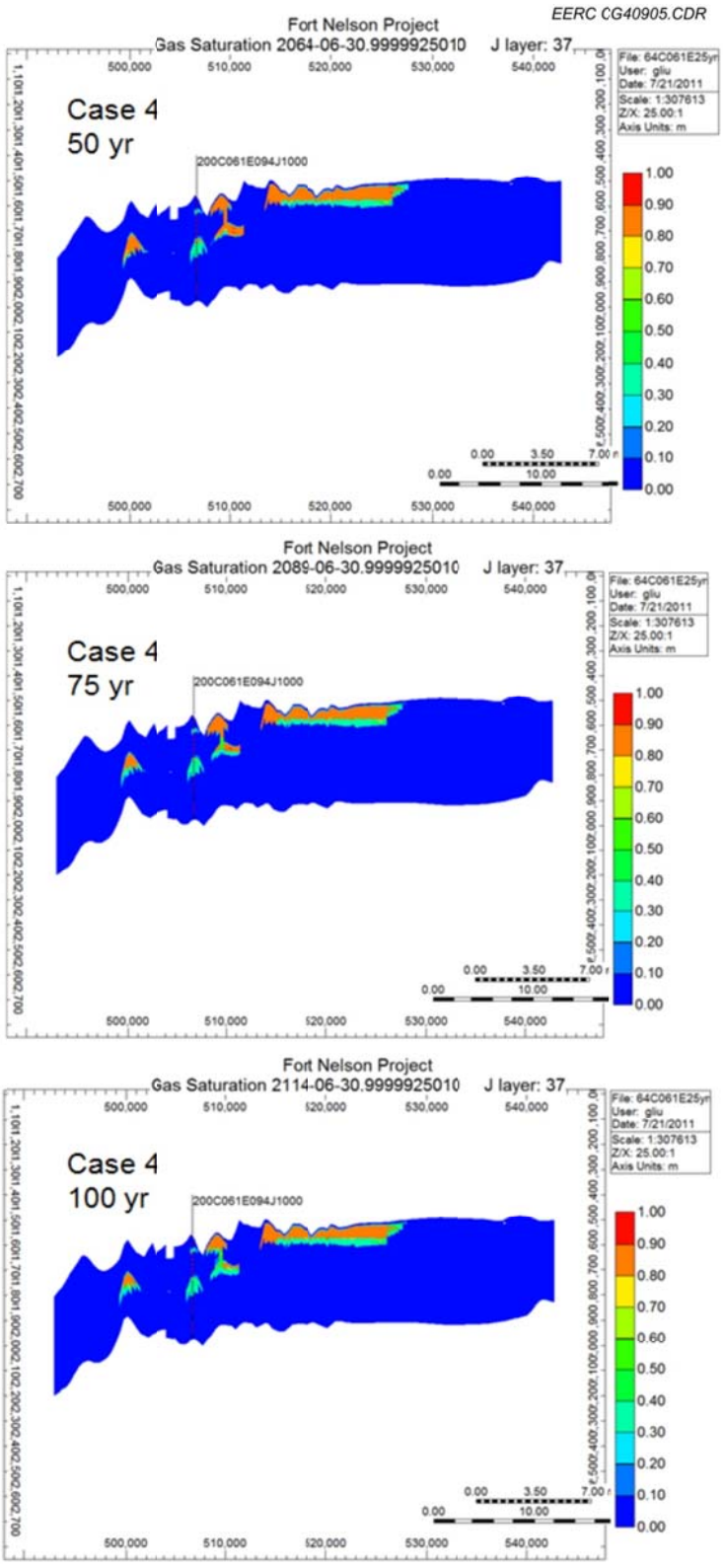

Figure E-51. Cross-sectional view of Case 4: 25 years of injection plus 75 years postinjection in and around c-61-E of History-Matching No. 1.

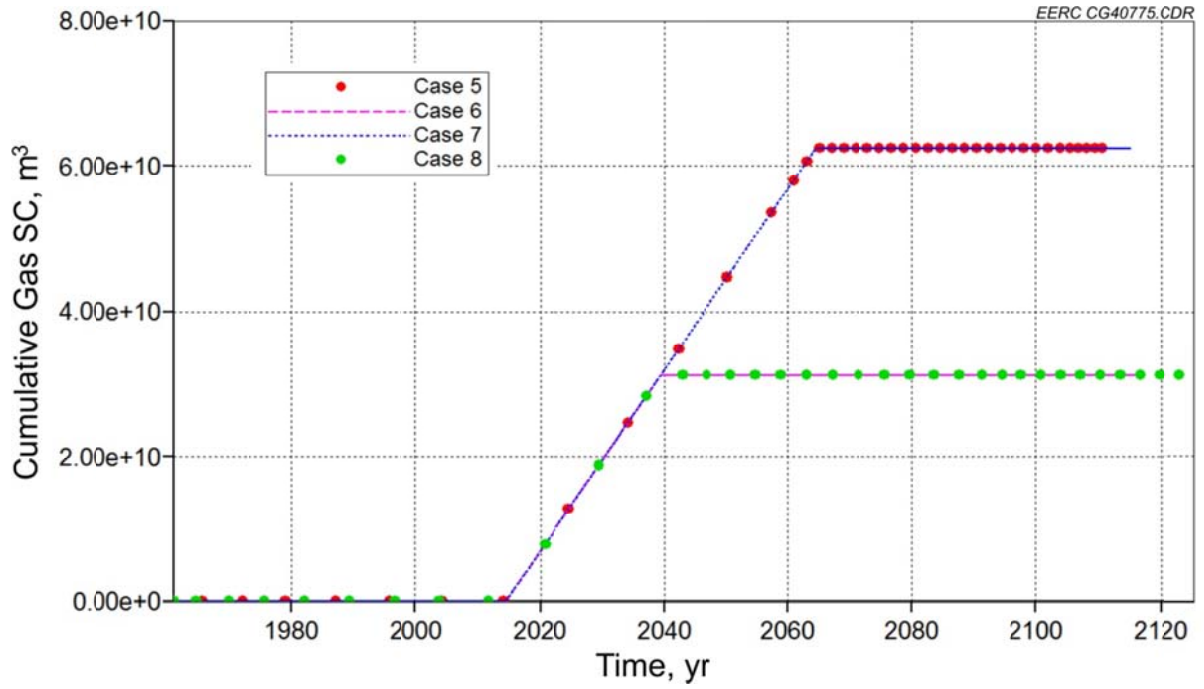

Figure E-52. Cumulative gas injection for four test cases of History-Matching No. 2.

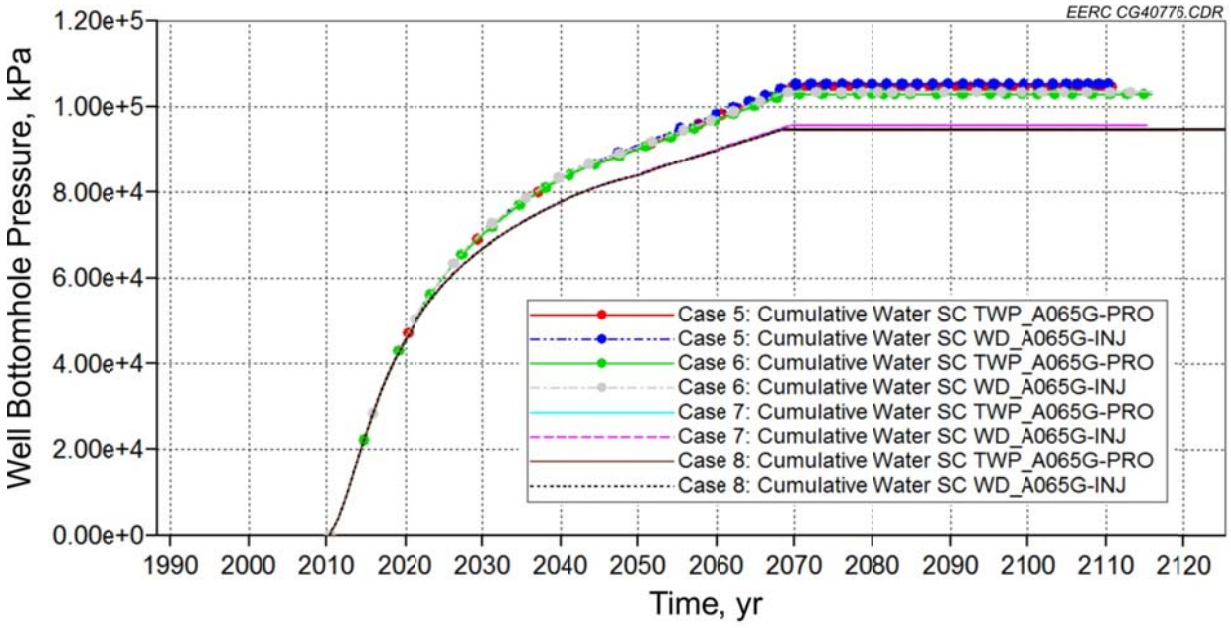

Figure E-53. Production and injection from the Water Recycle Group A065G of History-Matching No. 2.

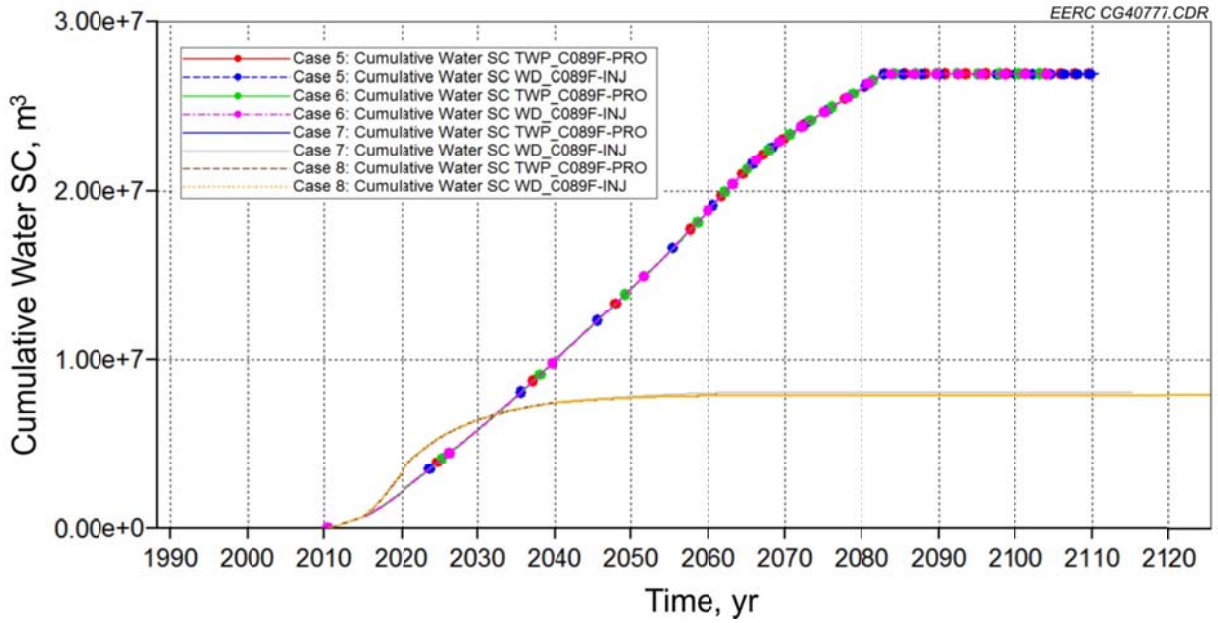

Figure E-54. Production and injection from the Water Recycle Group C089F of History-Matching No. 2.

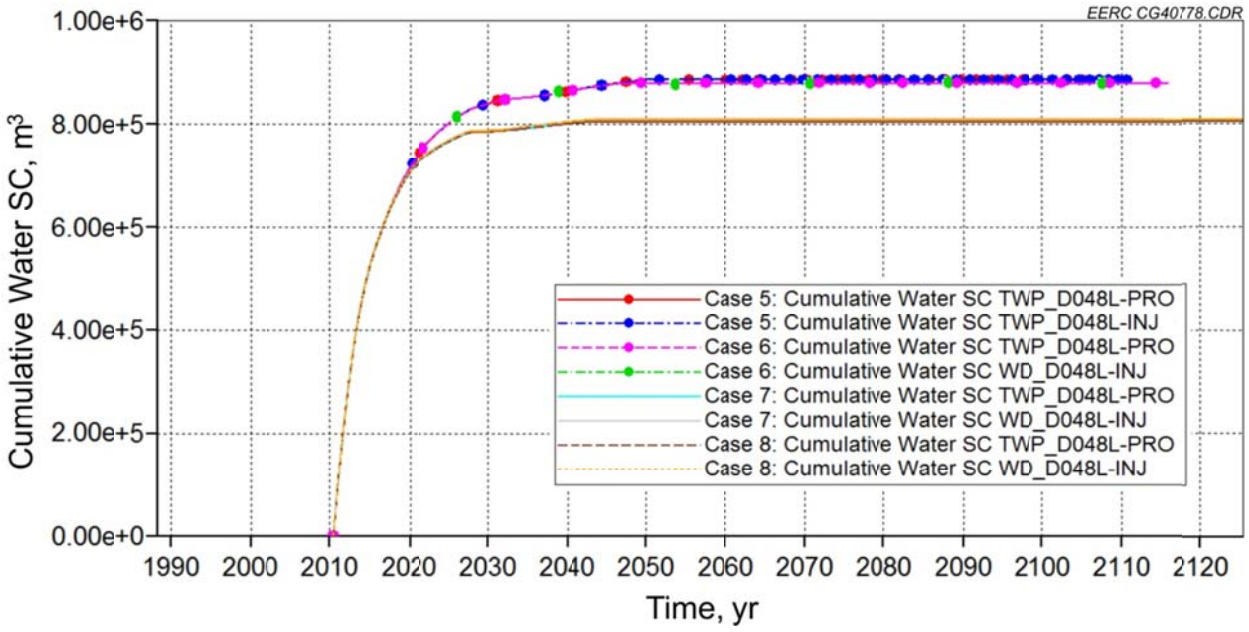

Figure E-55. Production and injection from the Water Recycle Group D048L of History-Matching No. 2.

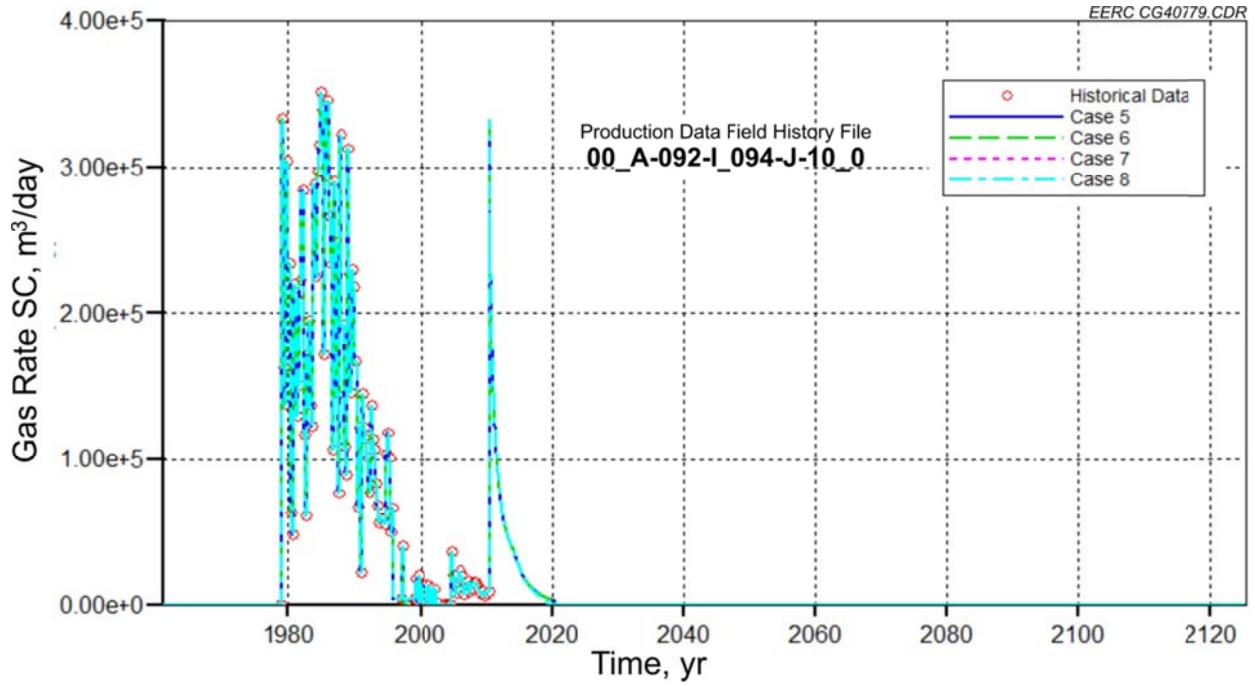

Figure E-56. Example of a well gas production rate for four test cases of History-Matching No. 2.

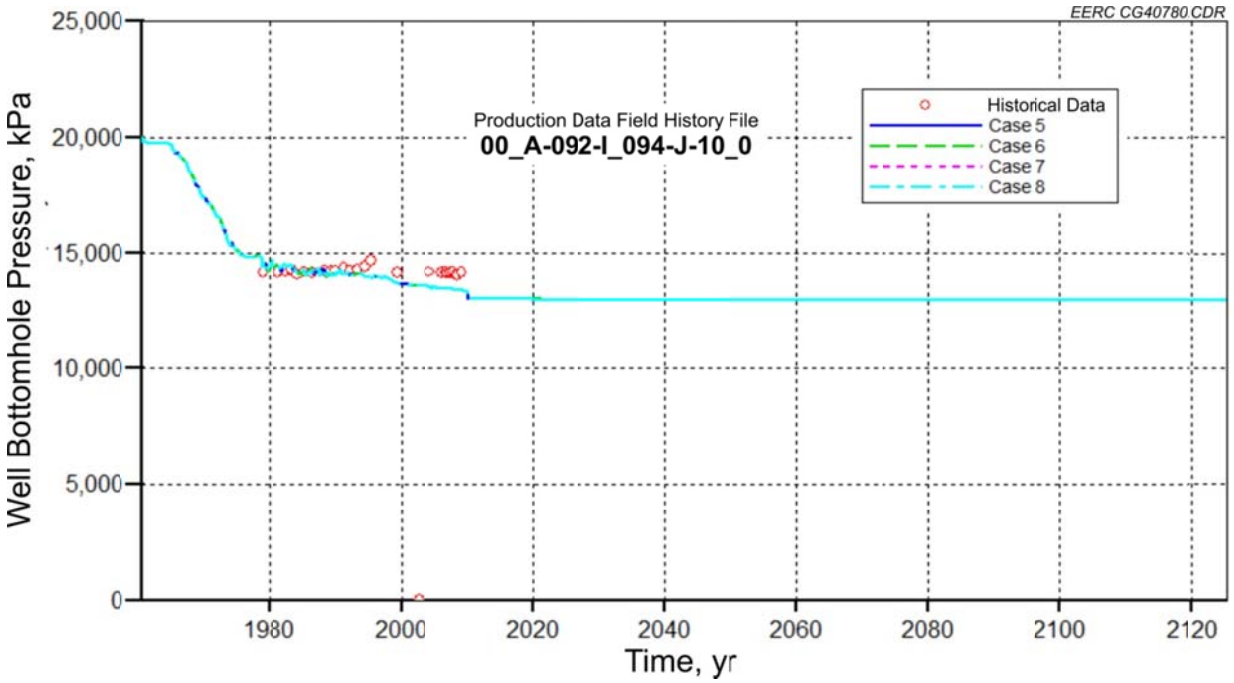

Figure E-57. BHPs of a sample well in Figure E-56.

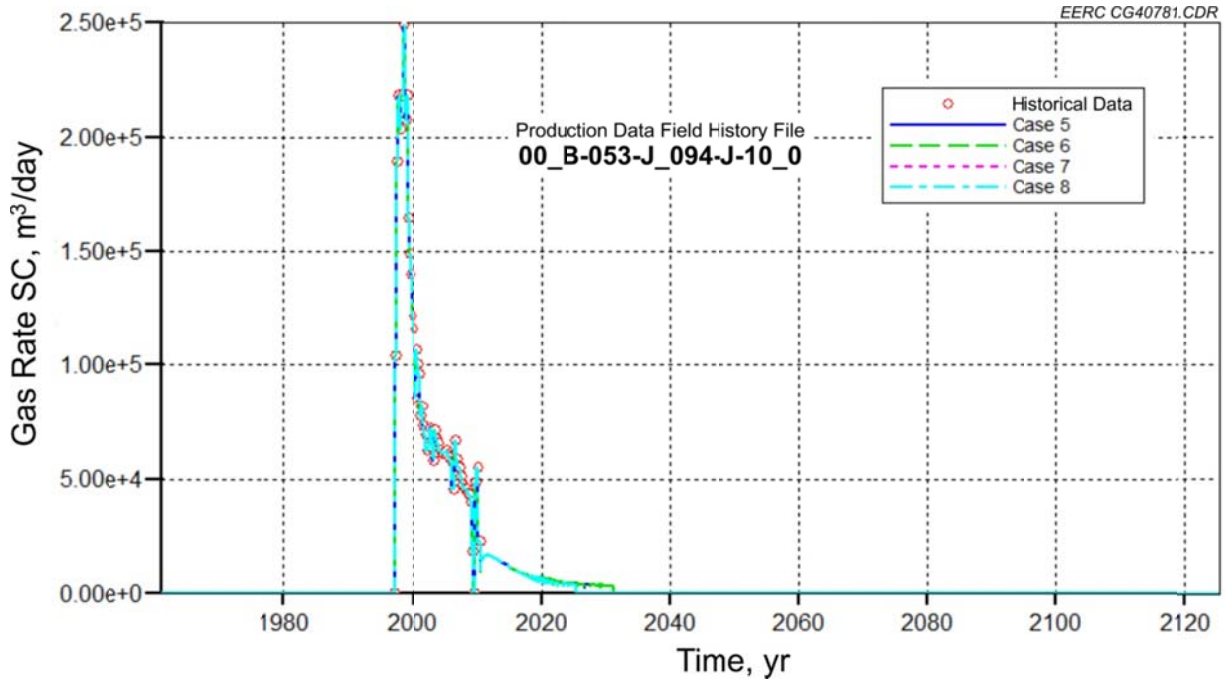

Figure E-58. Example of a well gas production rate for four test cases of History-Matching No. 2.

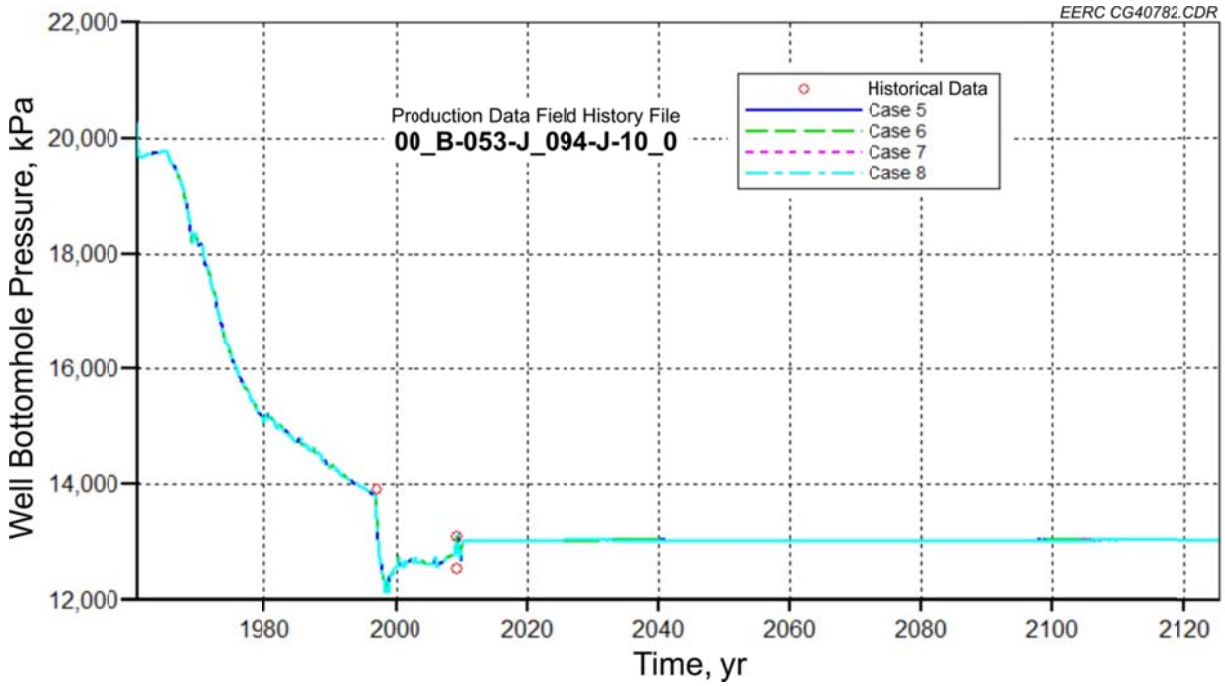

Figure E-59. BHPs of a sample well in Figure E-58.

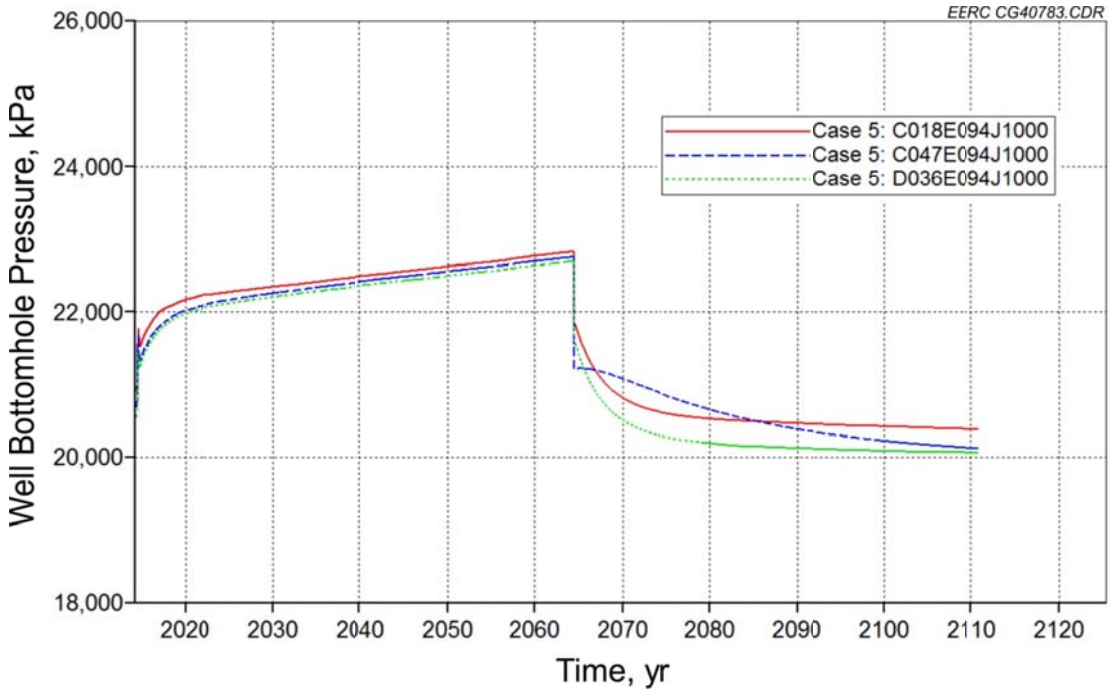

Figure E-60. BHPs of injection wells in Case 5 of History-Matching No. 2.

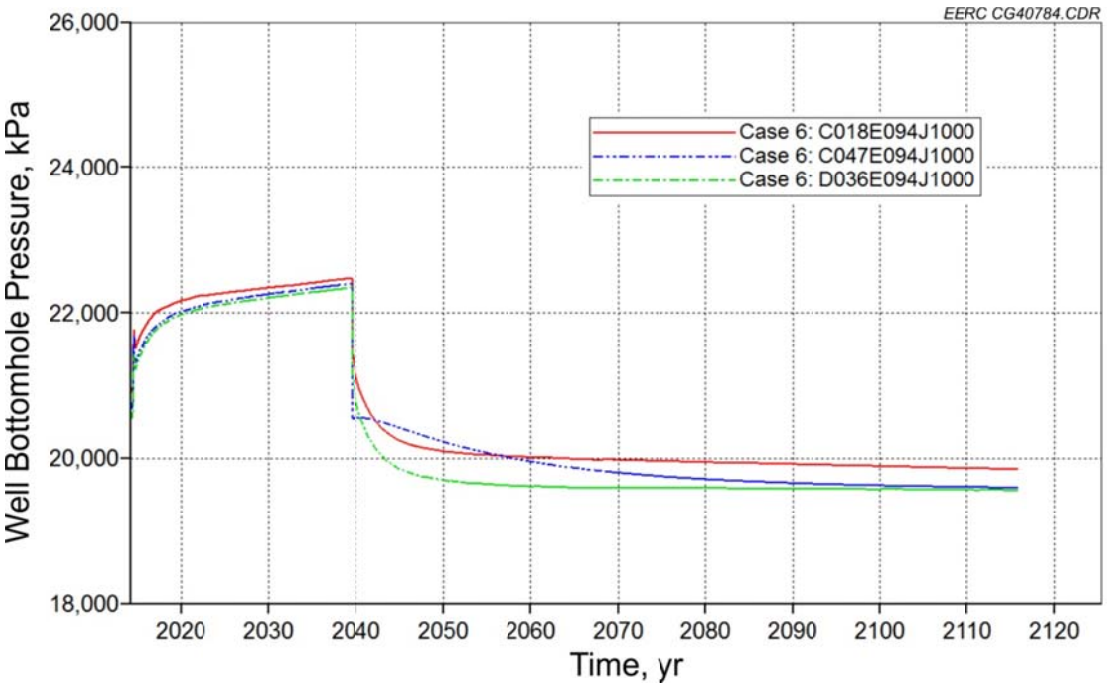

Figure E-61. BHPs of injection wells in Case 6 of History-Matching No. 2.

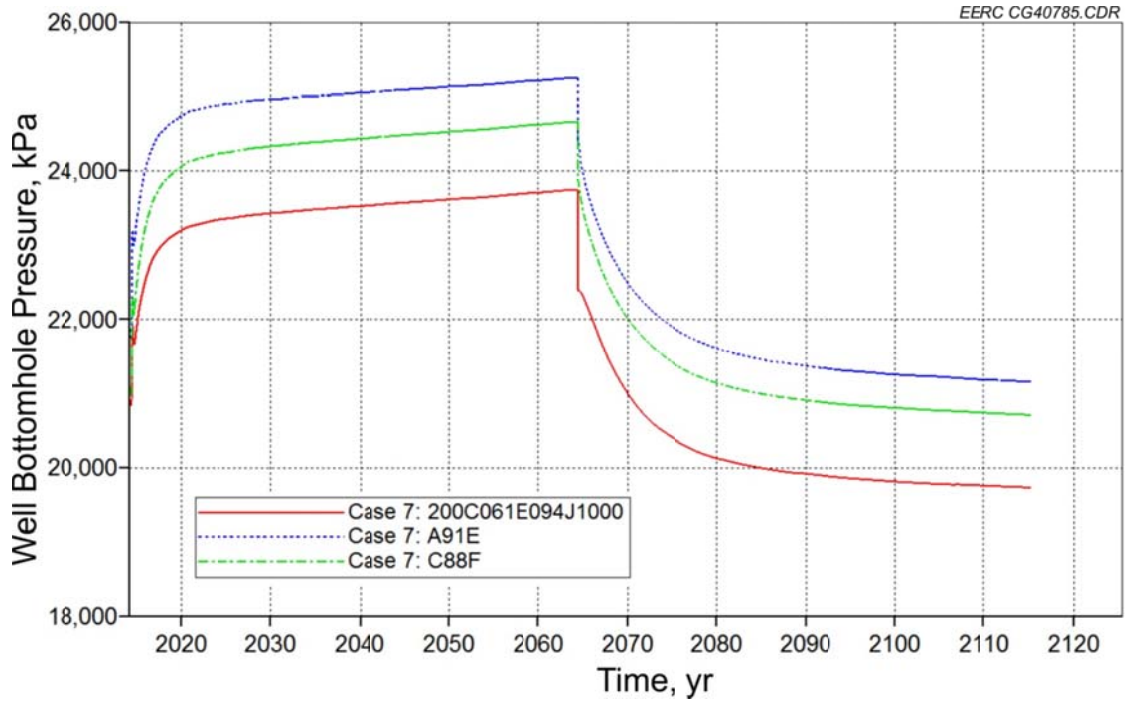

Figure E-62. BHPs of injection wells in Case 7 of History-Matching No. 2.

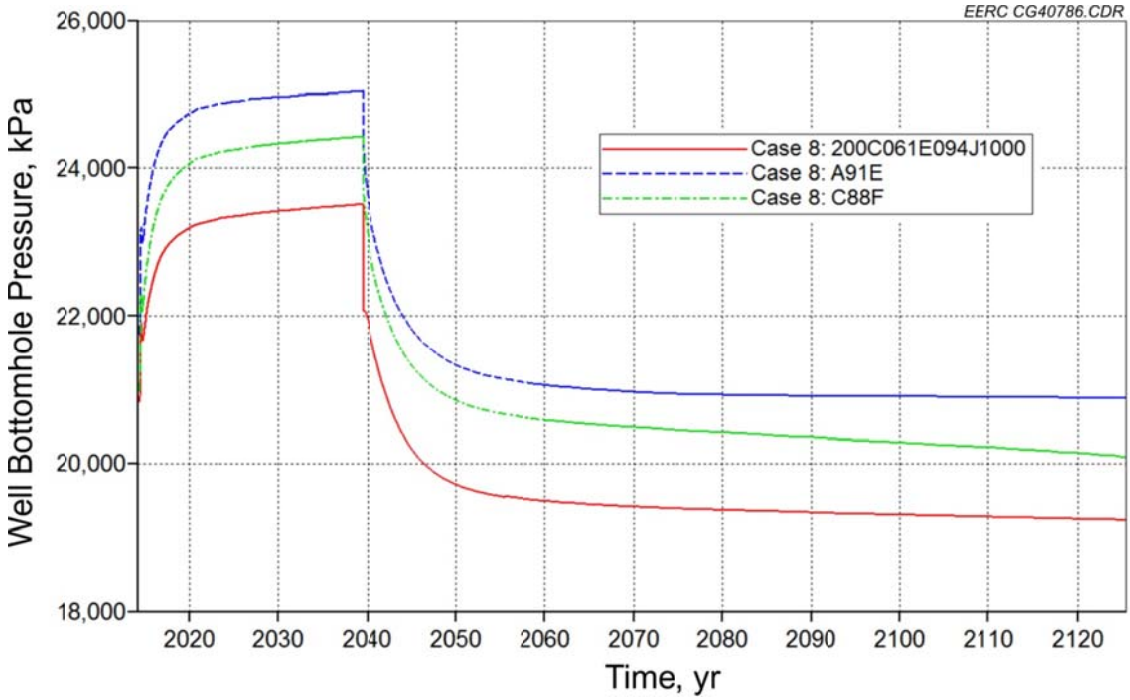

Figure E-63. BHPs of injection wells in Case 8 of History-Matching No. 2.

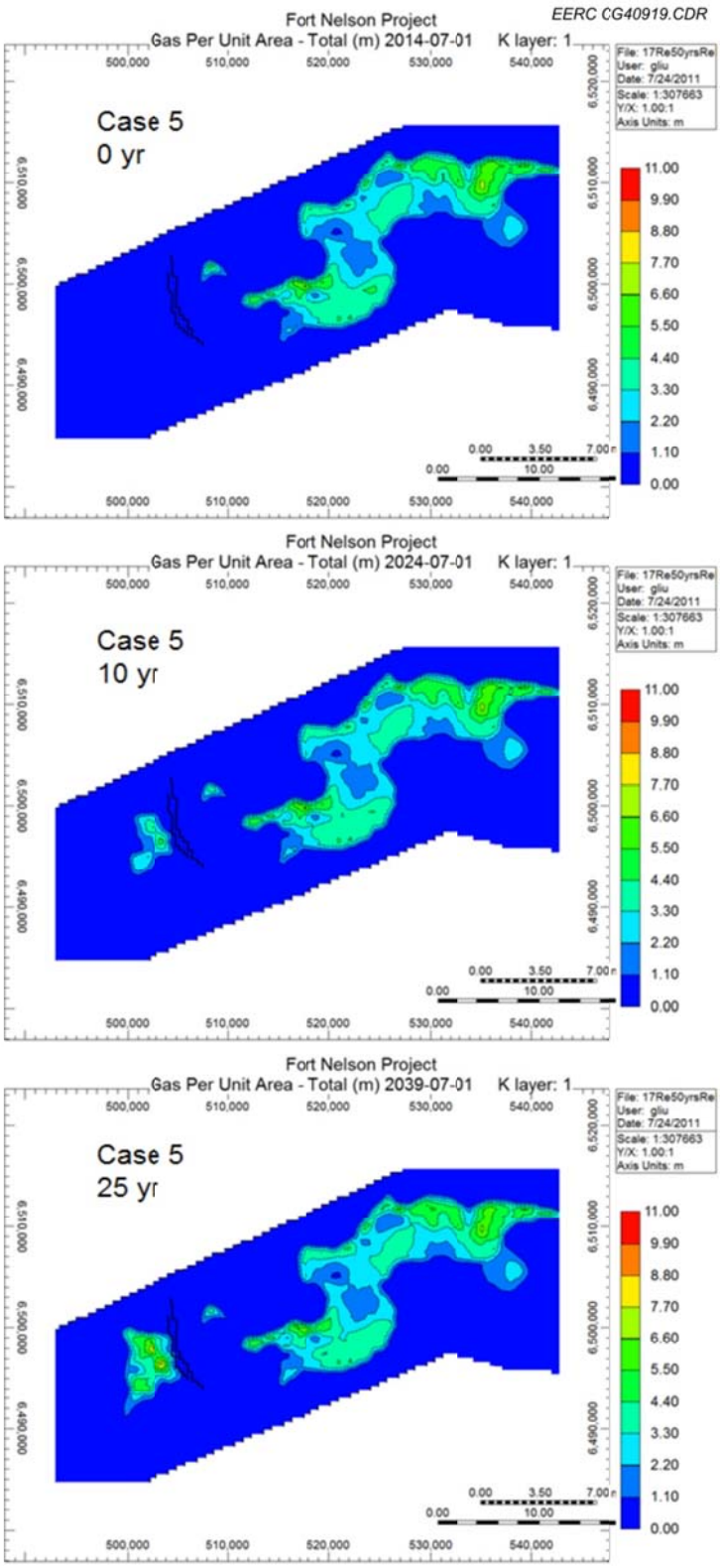

Figure E-64. Areal view of Case 5: 50 years of injection plus 46 years postinjection in and around c-47-E of History-Matching No. 2.

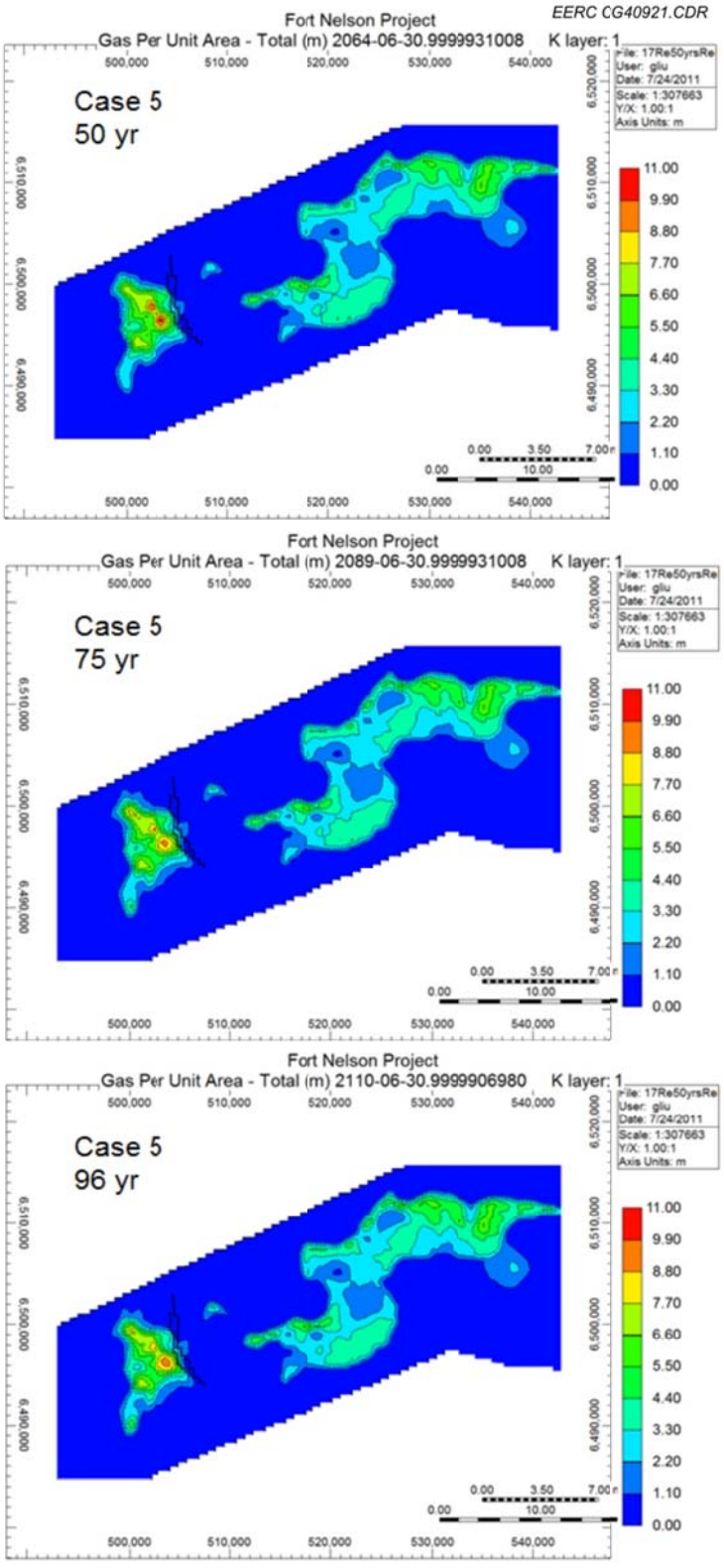

Figure E-65. Areal view of Case 5: 50 years of injection plus 46 years postinjection in and around c-47-E of History-Matching No. 1.

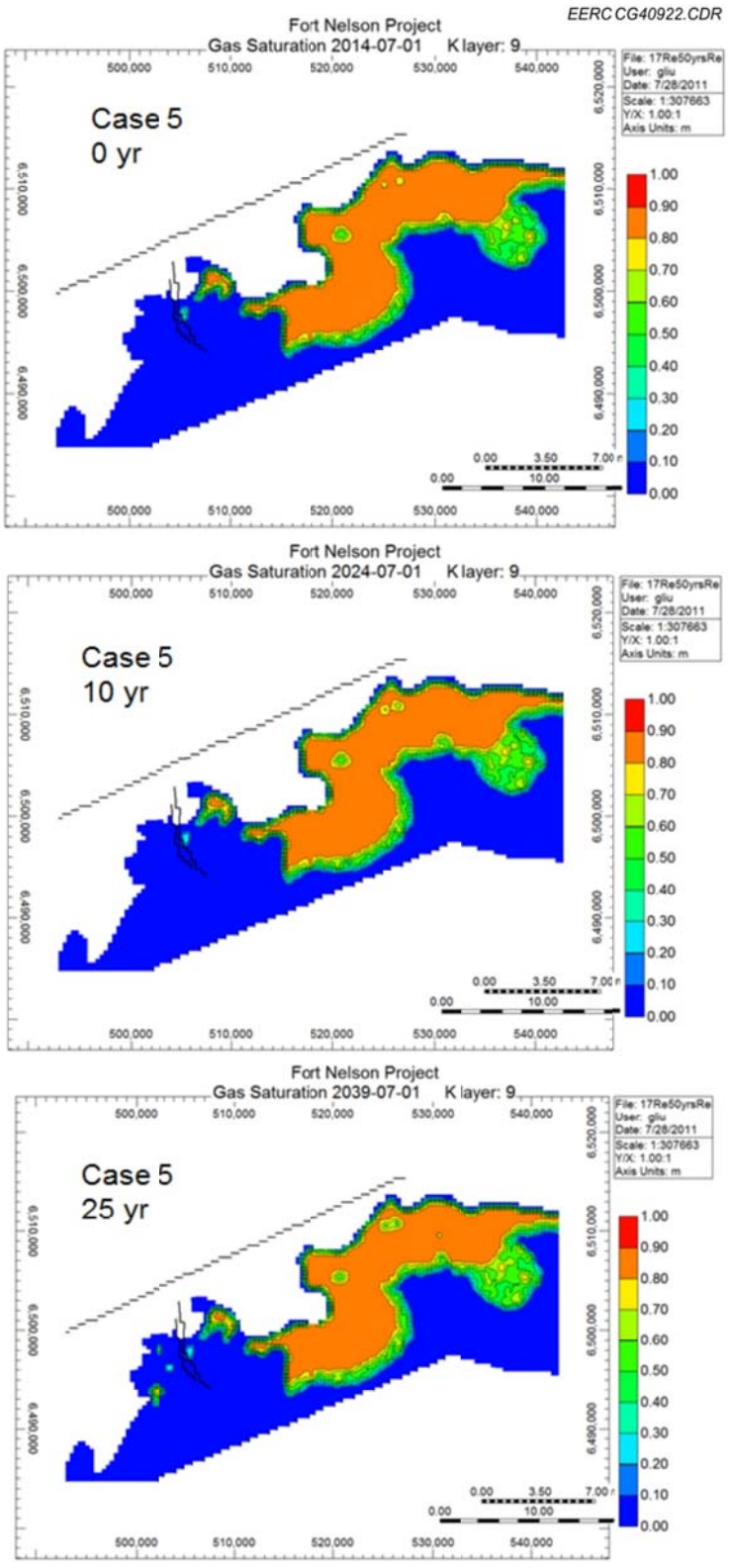

Figure E-66. Areal view of Case 5: saturation at the top of Upper Slave Point over time; 50 years of injection plus 46 years postinjection in and around c-47-E of History-Matching No. 2.

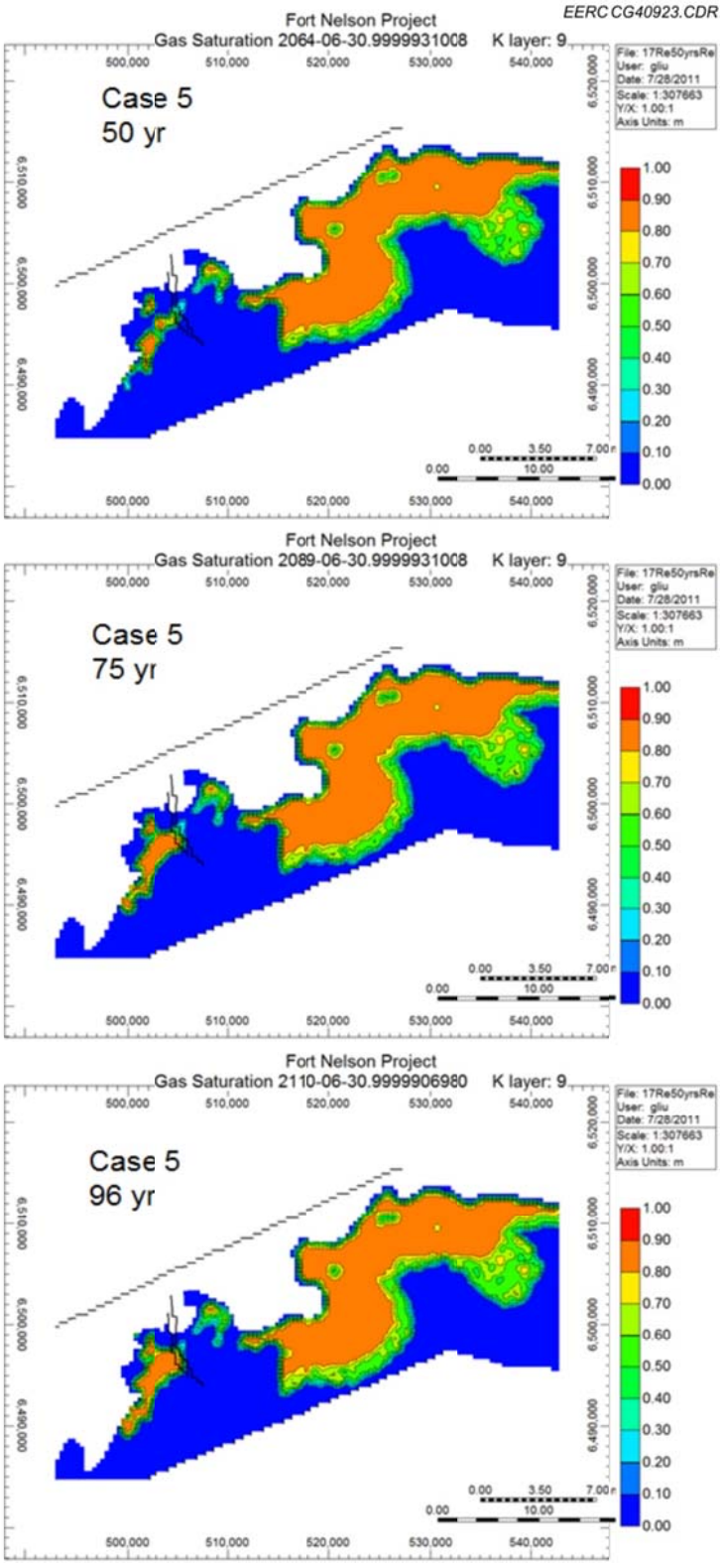

Figure E-67. Areal view of Case 5: saturation at the top of Upper Slave Point over time; 50 years of injection plus 46 years postinjection in and around c-47-E of History-Matching No. 2.

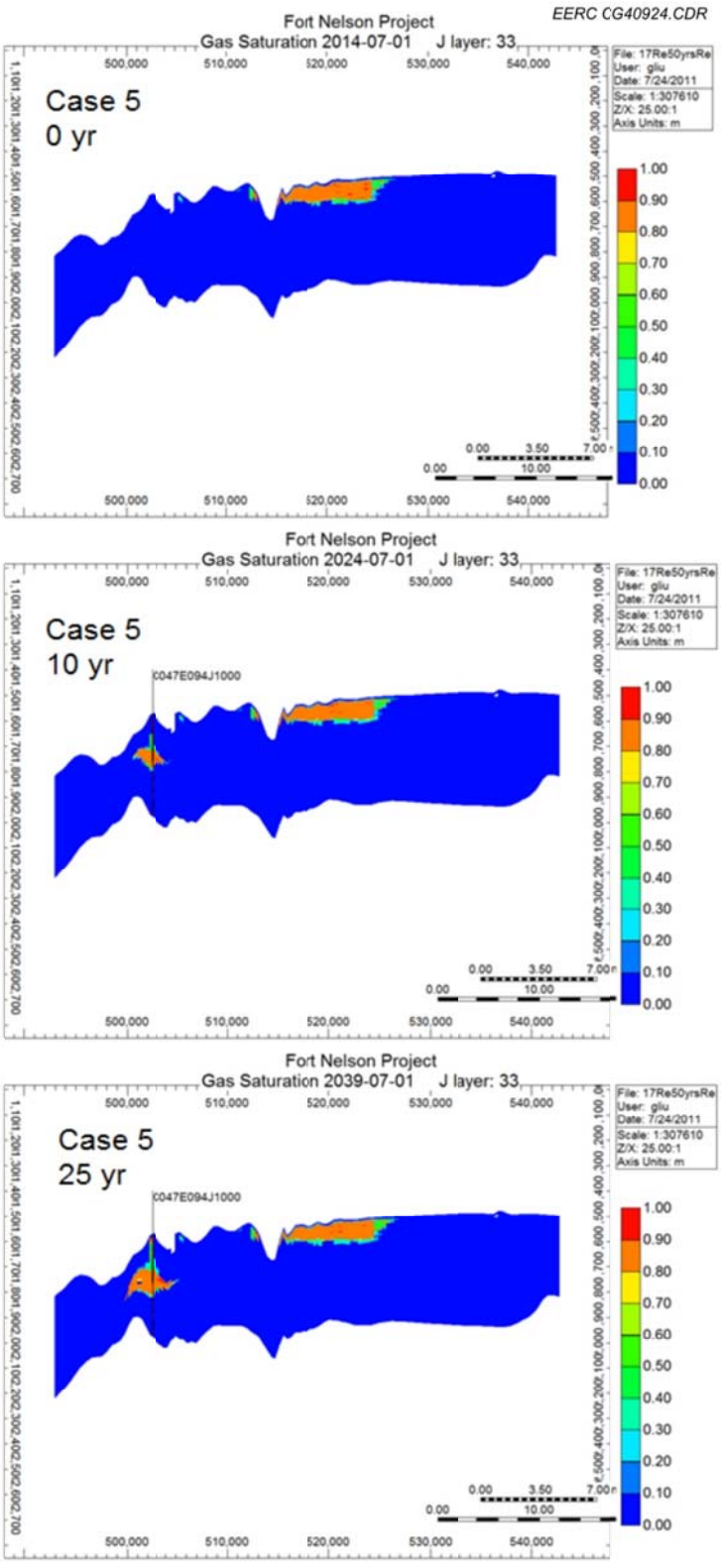

Figure E-68. Cross-sectional view of Case 5: 50 years of injection plus 46 years postinjection in and around c-47-E of History-Matching No. 2.

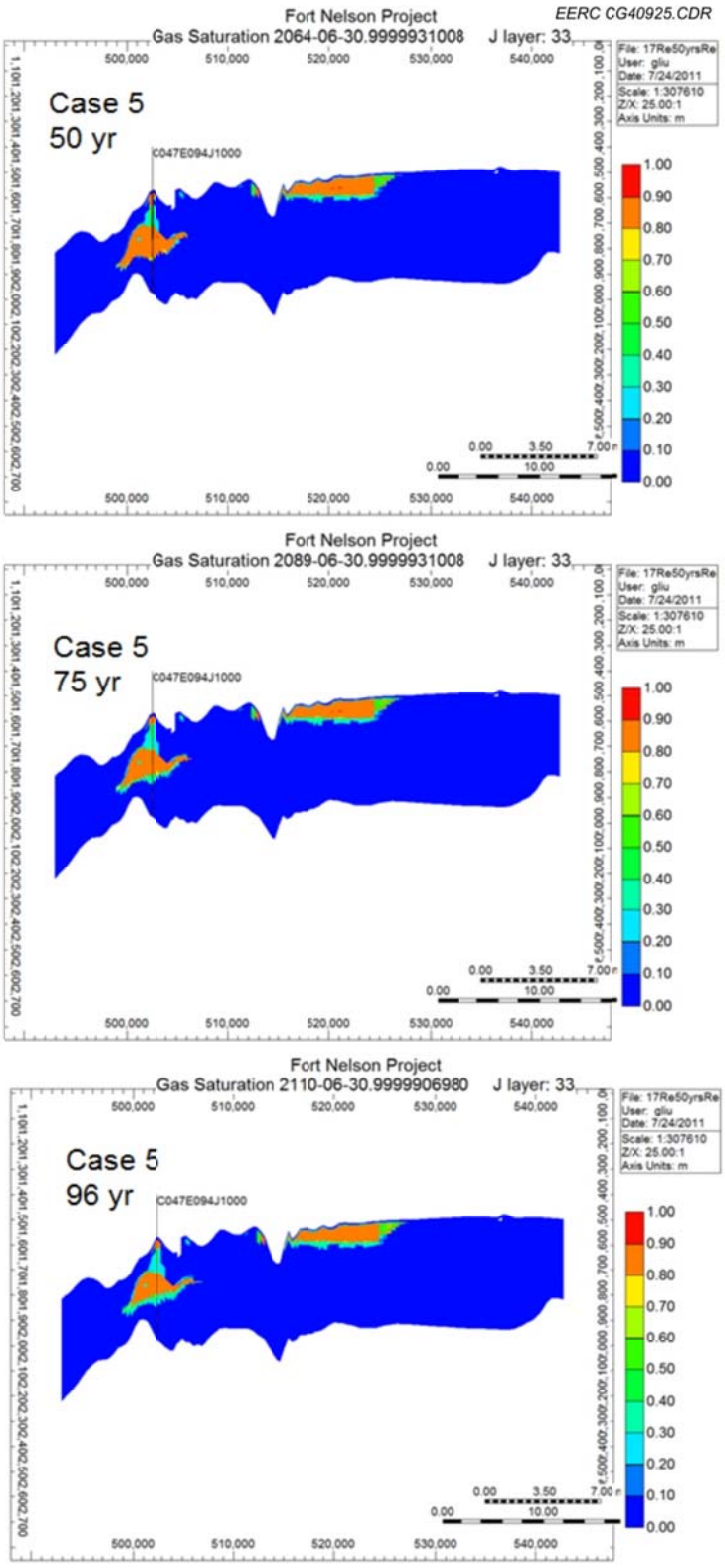

Figure E-69. Cross-sectional view of Case 5: 50 years of injection plus 46 years postinjection in and around c-47-E of History-Matching No. 2.

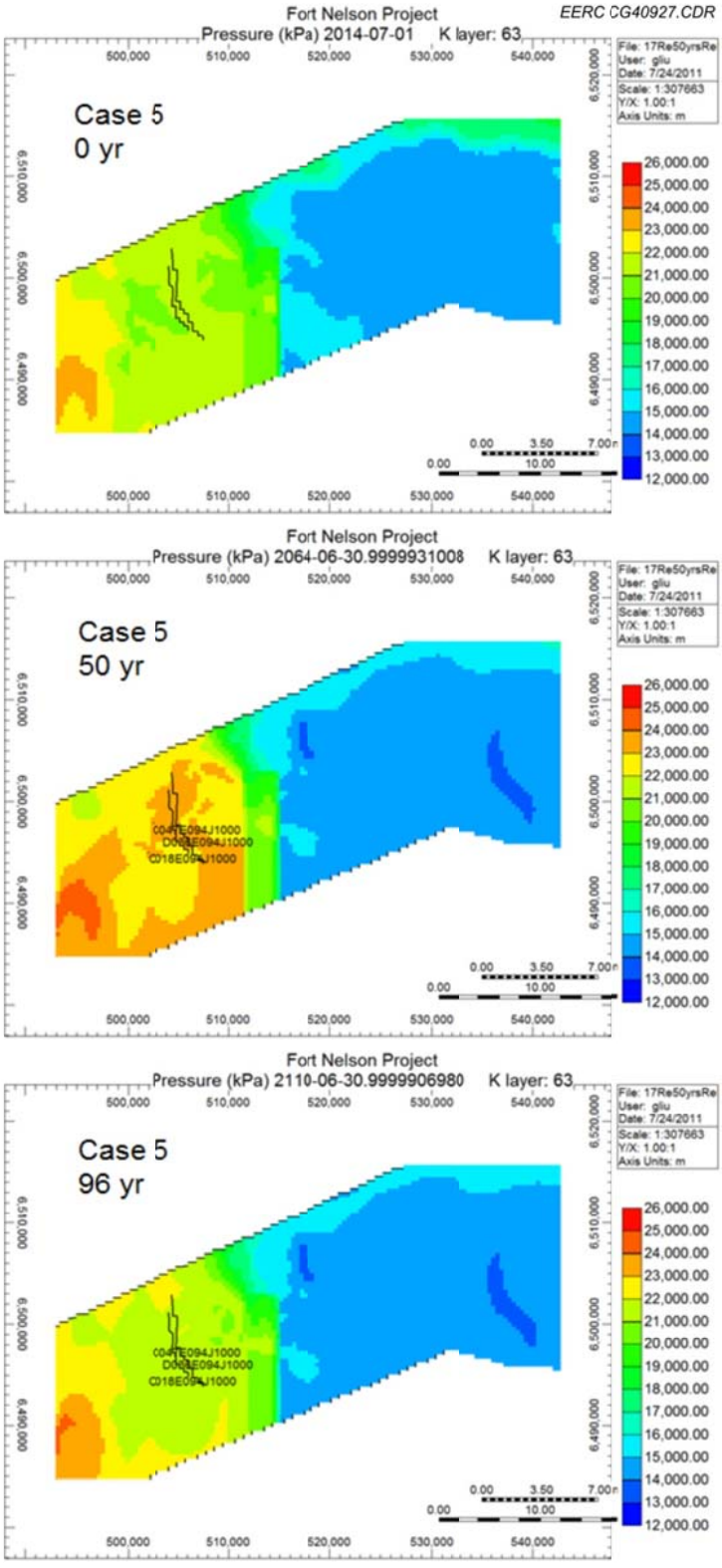

Figure E-70. Areal view of Case 5: pressure distributions; 50 years of injection plus 46 years postinjection in and around c-47-E of History-Matching No. 2.

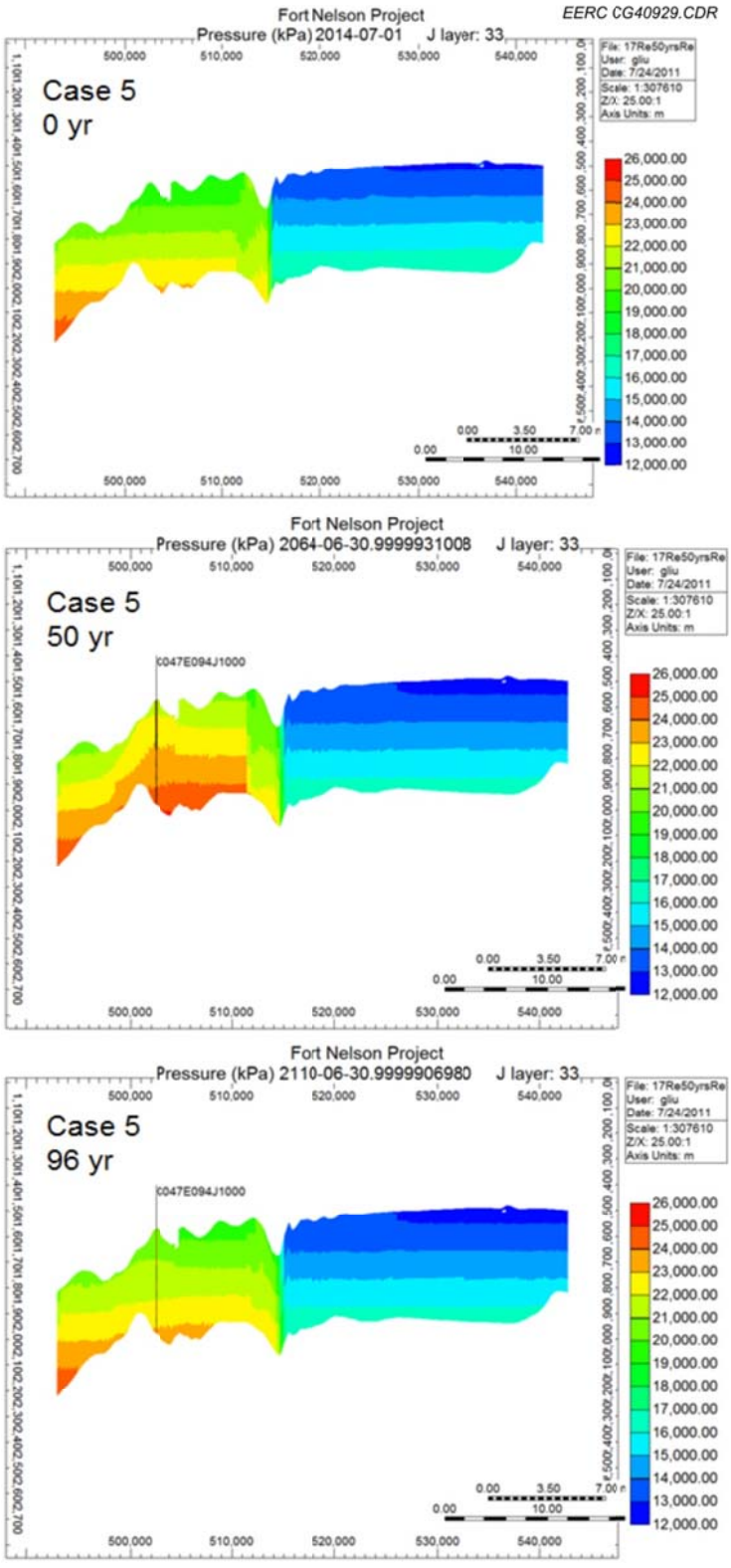

Figure E-71. Cross-sectional view of Case 5: pressure distributions; 50 years of injection plus 46 years postinjection in and around c-47-E of History-Matching No. 2.

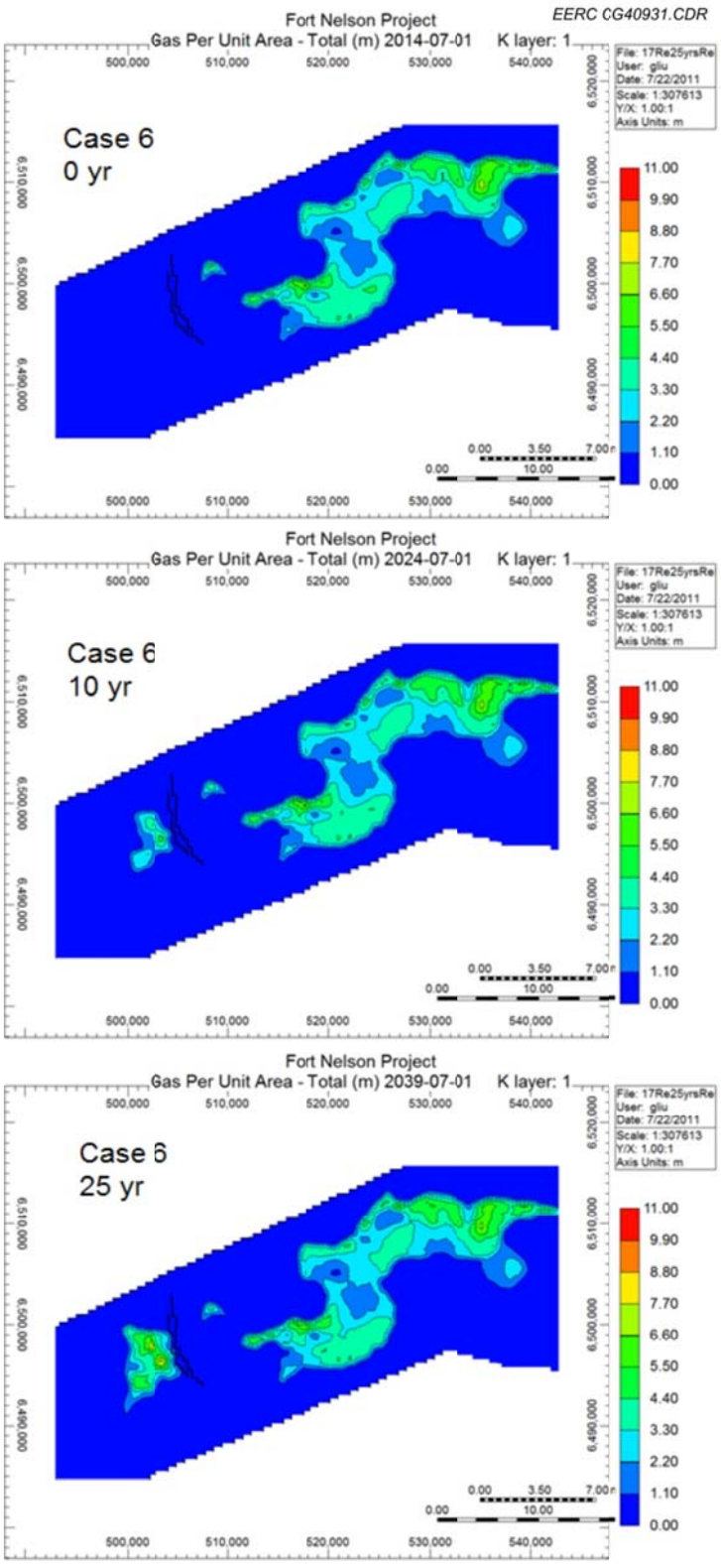

Figure E-72. Areal view of Case 6: 25 years of injection plus 75 years postinjection in and around c-47-E of History-Matching No. 2.

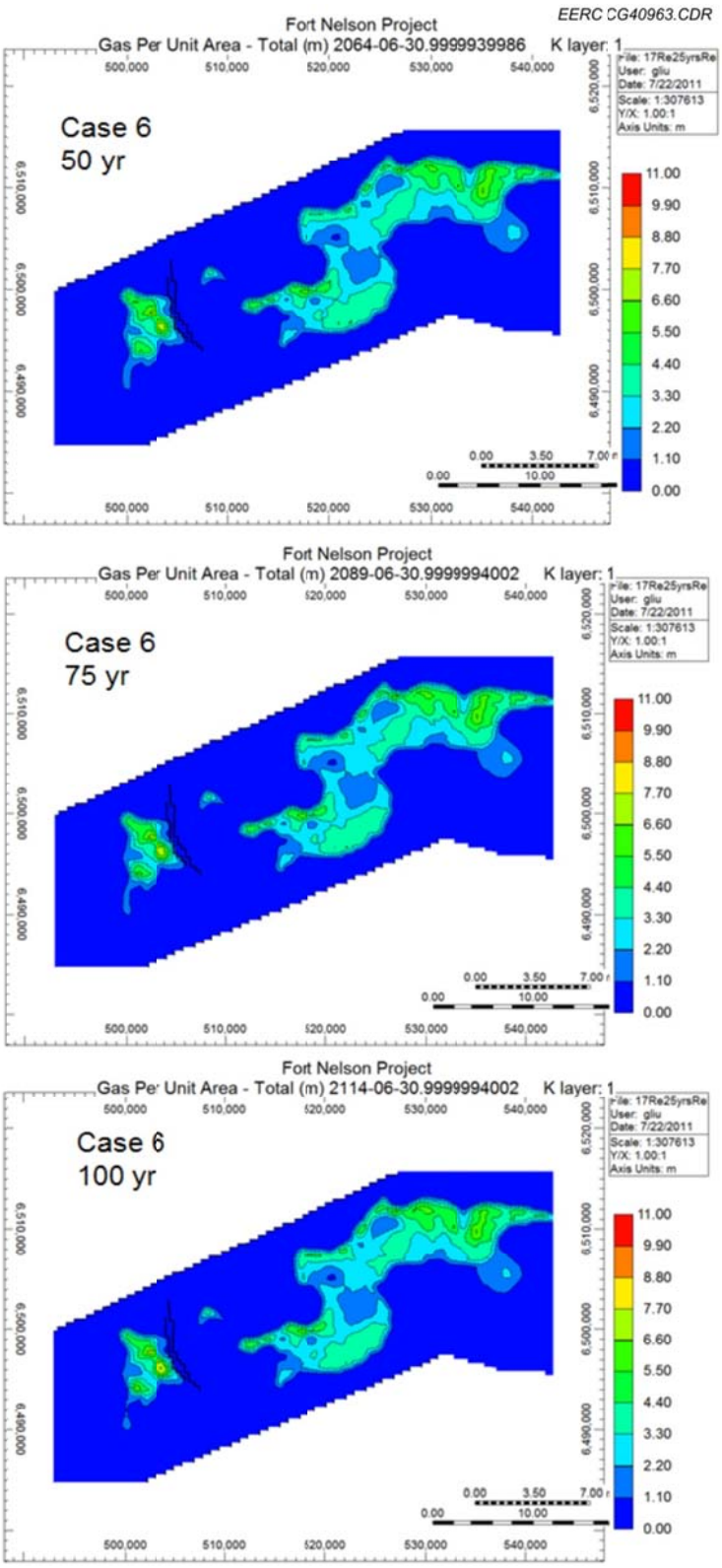

Figure E-73. Areal view of Case 6: 25 years of injection plus 75 years postinjection in and around c-47-E of History-Matching No. 2.

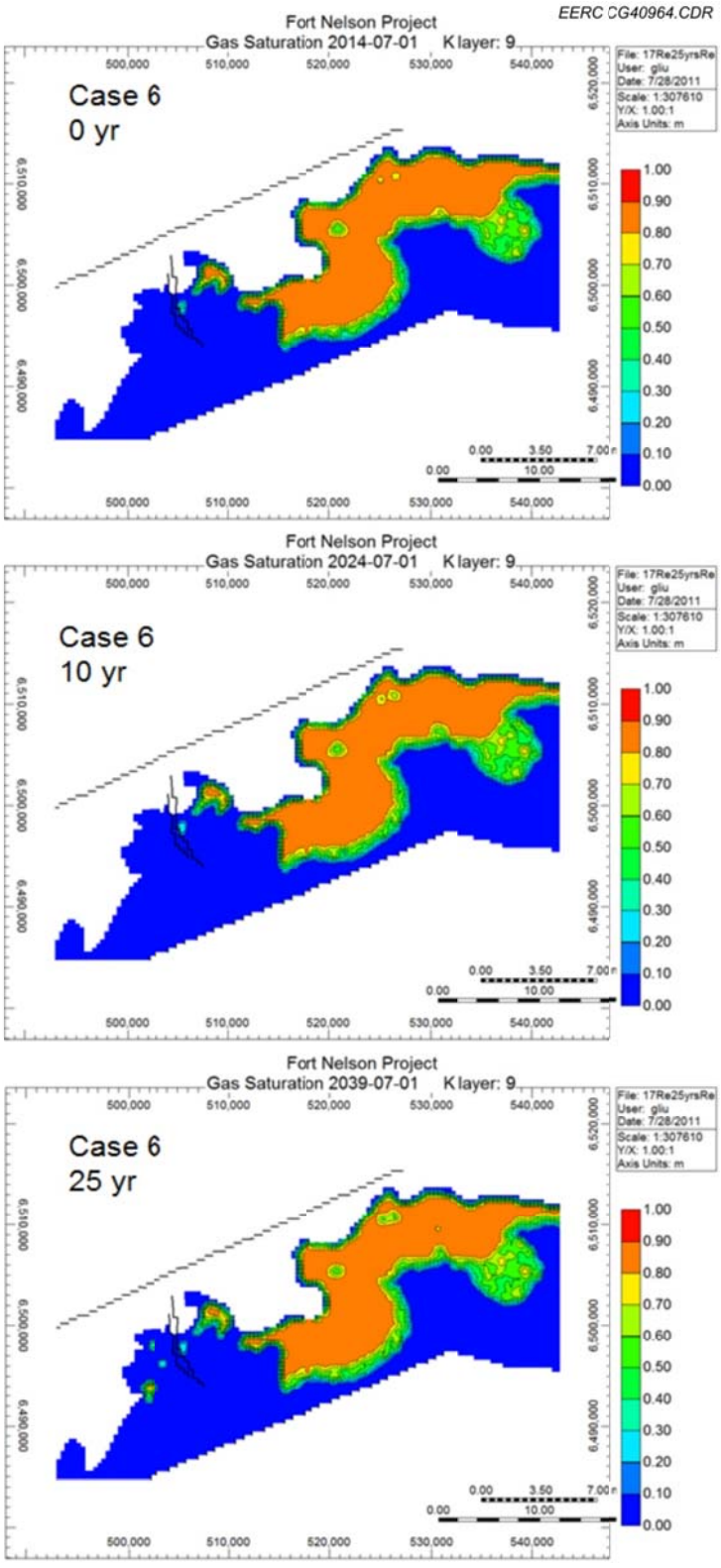

Figure E-74. Areal view of Case 6: saturation at the top of Upper Slave Point over time; 25 years of injection plus 75 years postinjection in and around c-47-E of History-Matching No. 2.

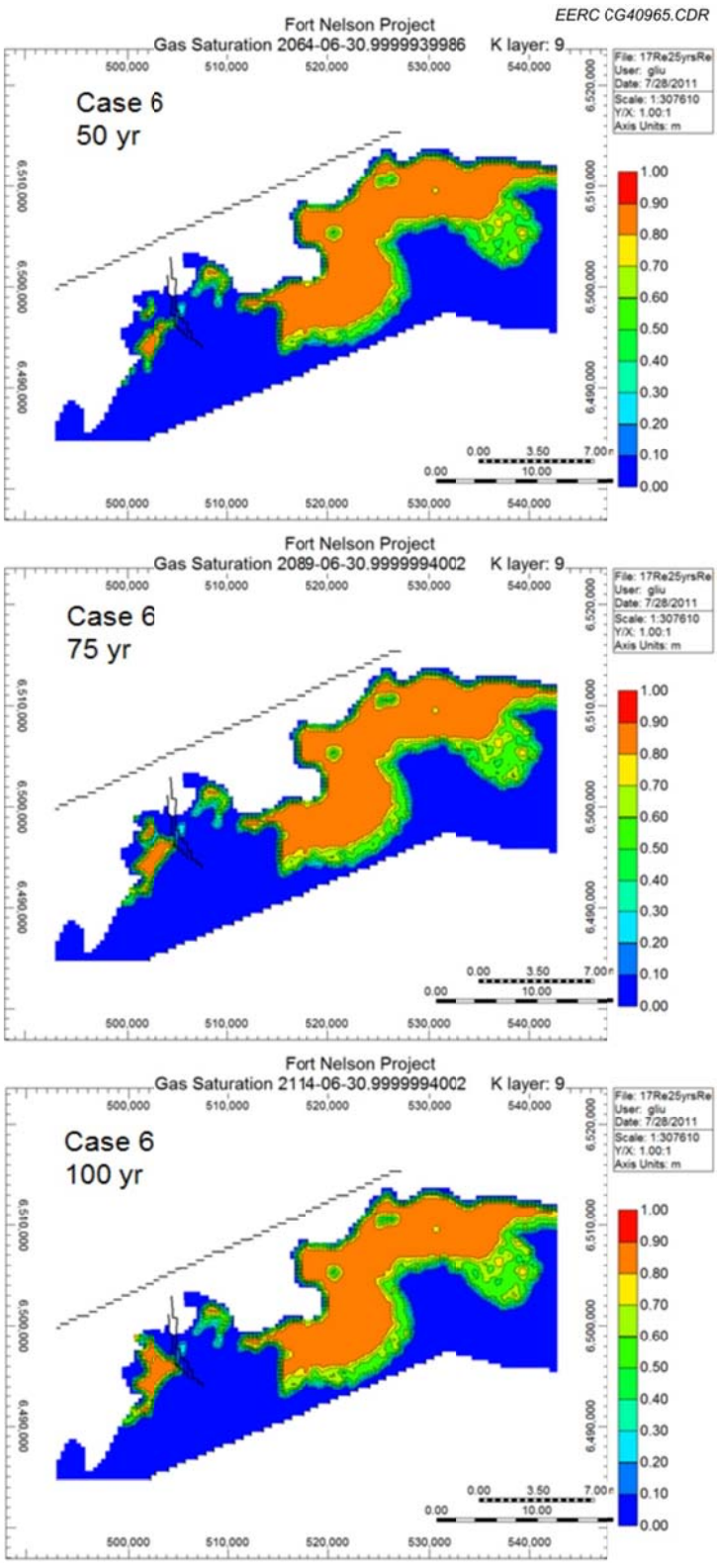

Figure E-75. Areal view of Case 6: saturation at the top of Upper Slave Point over time; 25 years of injection plus 75 years postinjection in and around c-47-E of History-Matching No. 2.

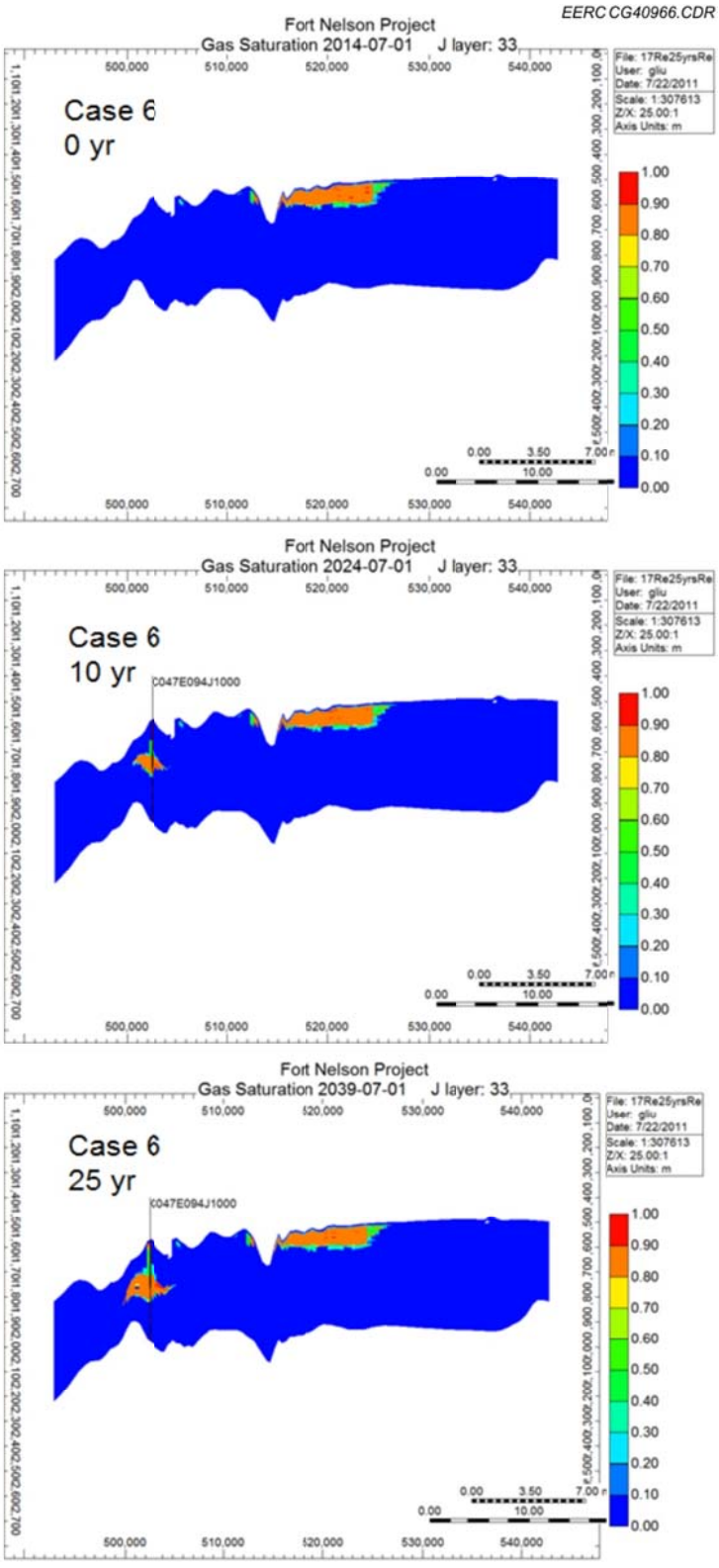

Figure E-76. Cross-sectional view of Case 6: 25 years of injection plus 75 years postinjection in and around c-47-E of History-Matching No. 2.

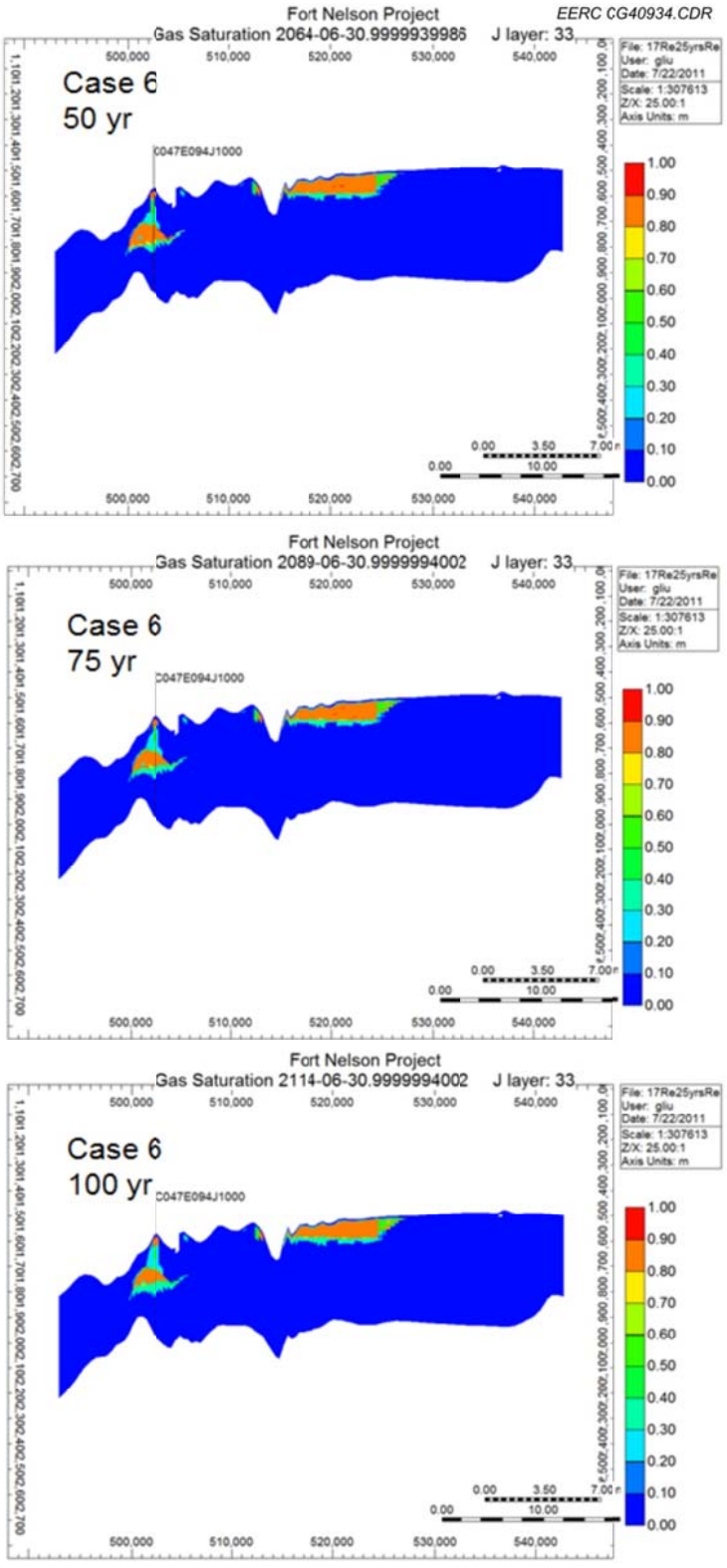

Figure E-77. Cross-sectional view of Case 6: 25 years of injection plus 75 years postinjection in and around c-47-E of History-Matching No. 2.

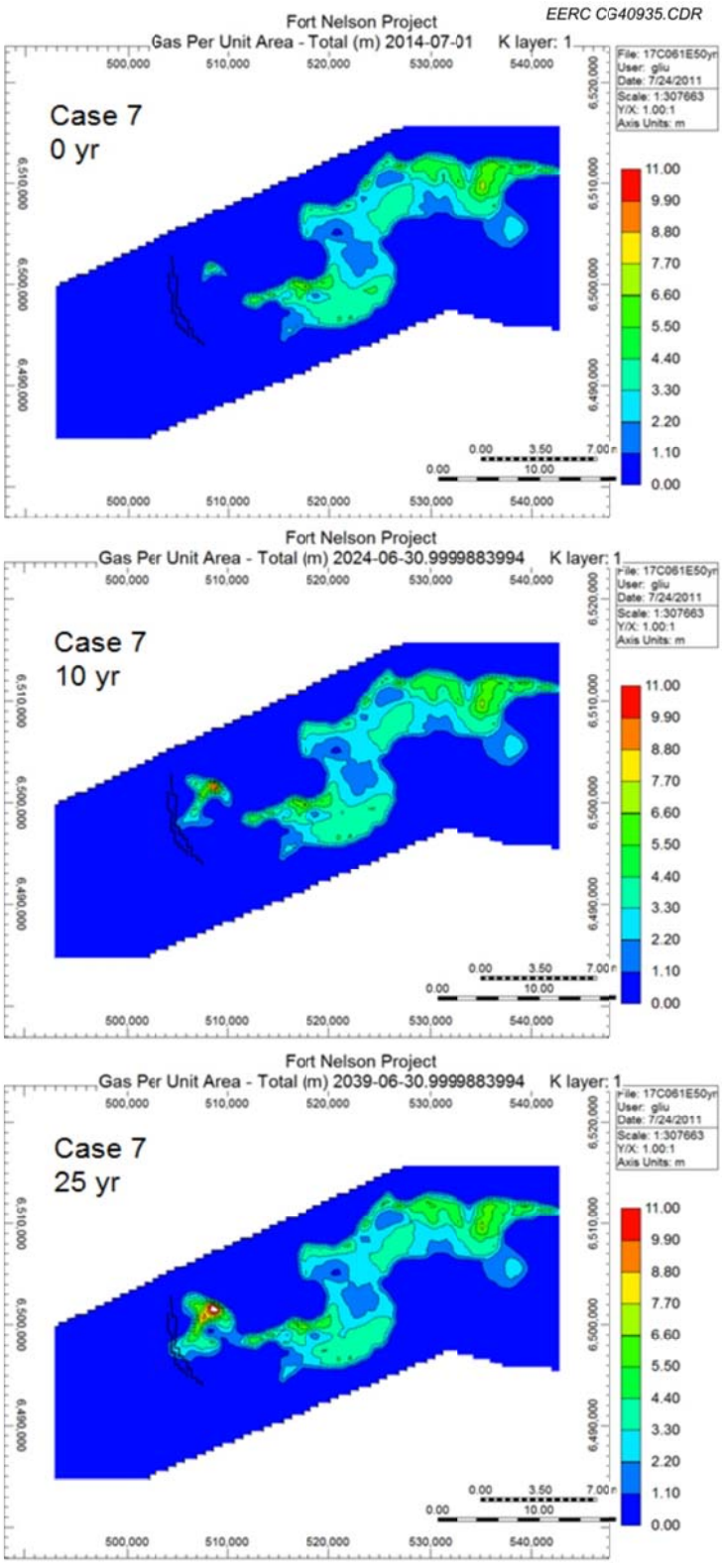

Figure E-78. Areal view of Case 7: 50 years of injection plus 50 years postinjection in and around c-61-E of History-Matching No. 2.

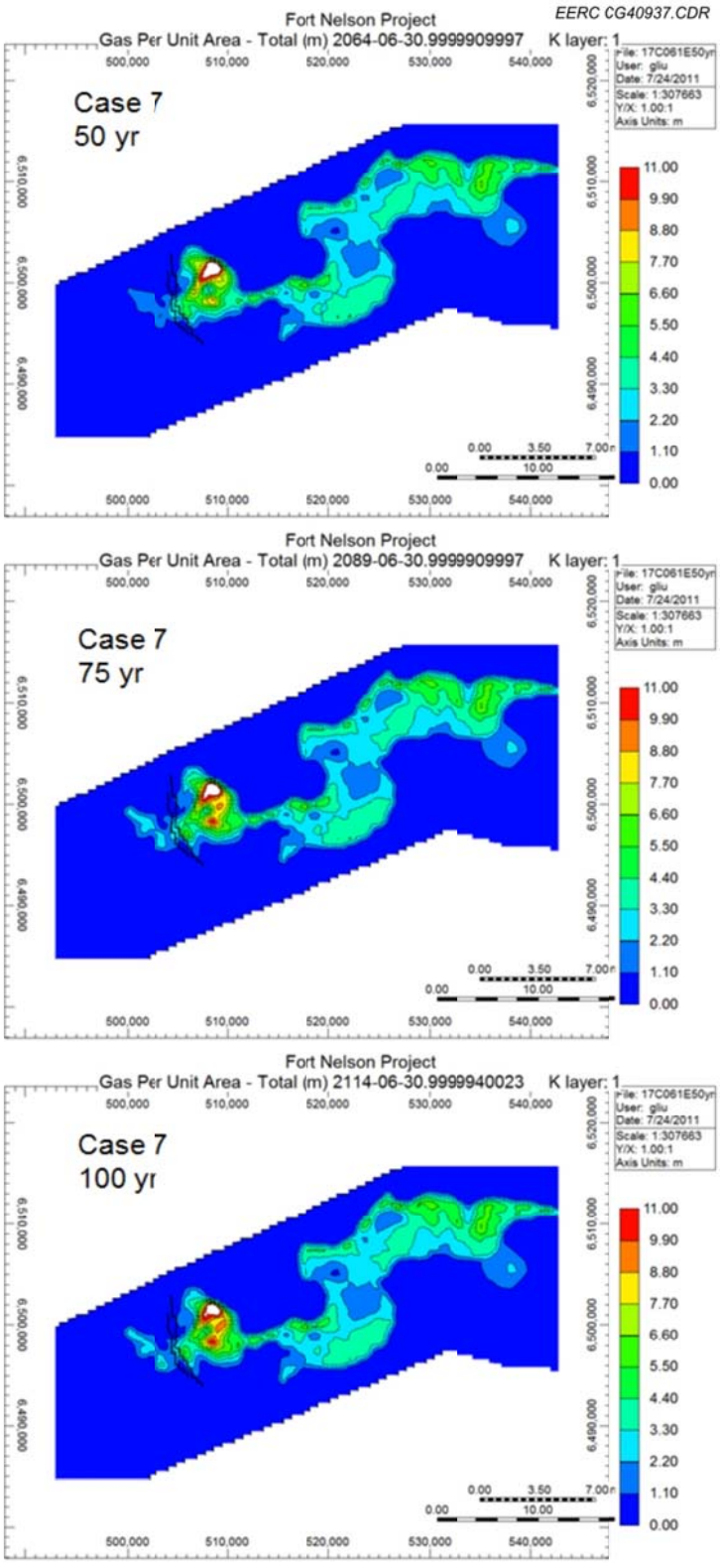

Figure E-79. Areal view of Case 7: 50 years of injection plus 50 years postinjection in and around c-61-E of History-Matching No. 2.

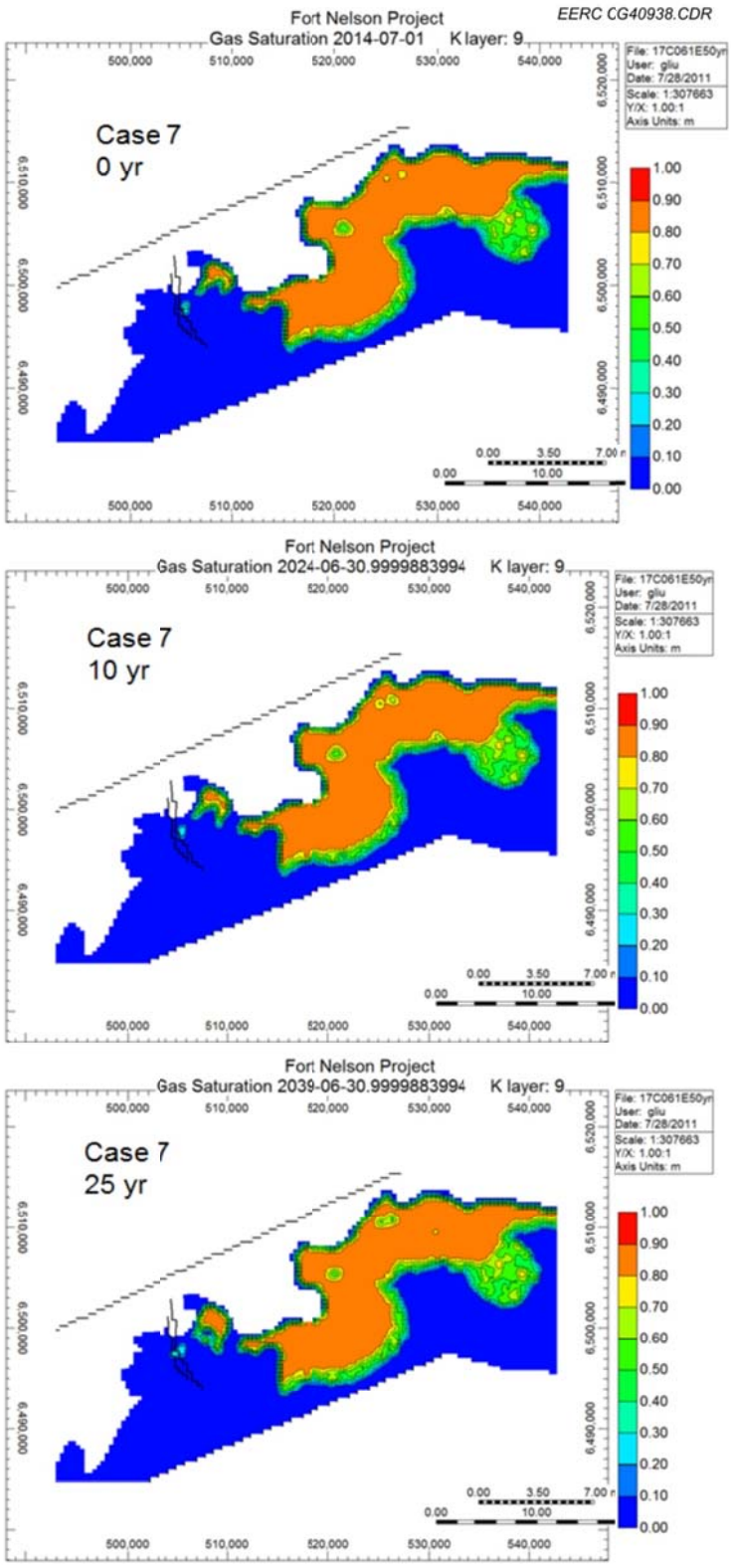

Figure E-80. Areal view of Case 7: saturation at the top of Upper Slave Point over time; 50 years of injection plus 50 years postinjection in and around c-61-E of History-Matching No. 2.

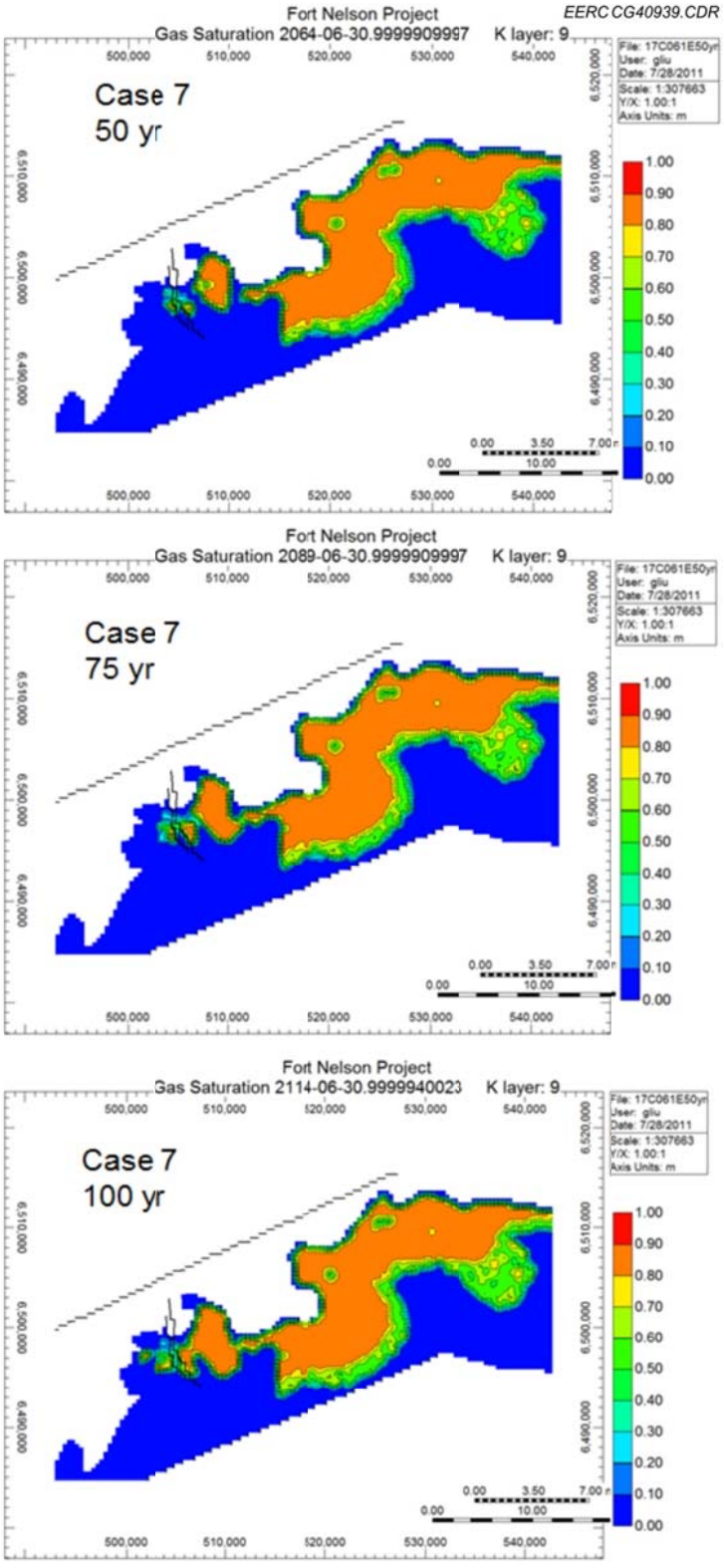

Figure E-81. Areal view of Case 7: saturation at the top of Upper Slave Point over time; 50 years of injection plus 50 years postinjection in and around c-61-E of History-Matching No. 2.

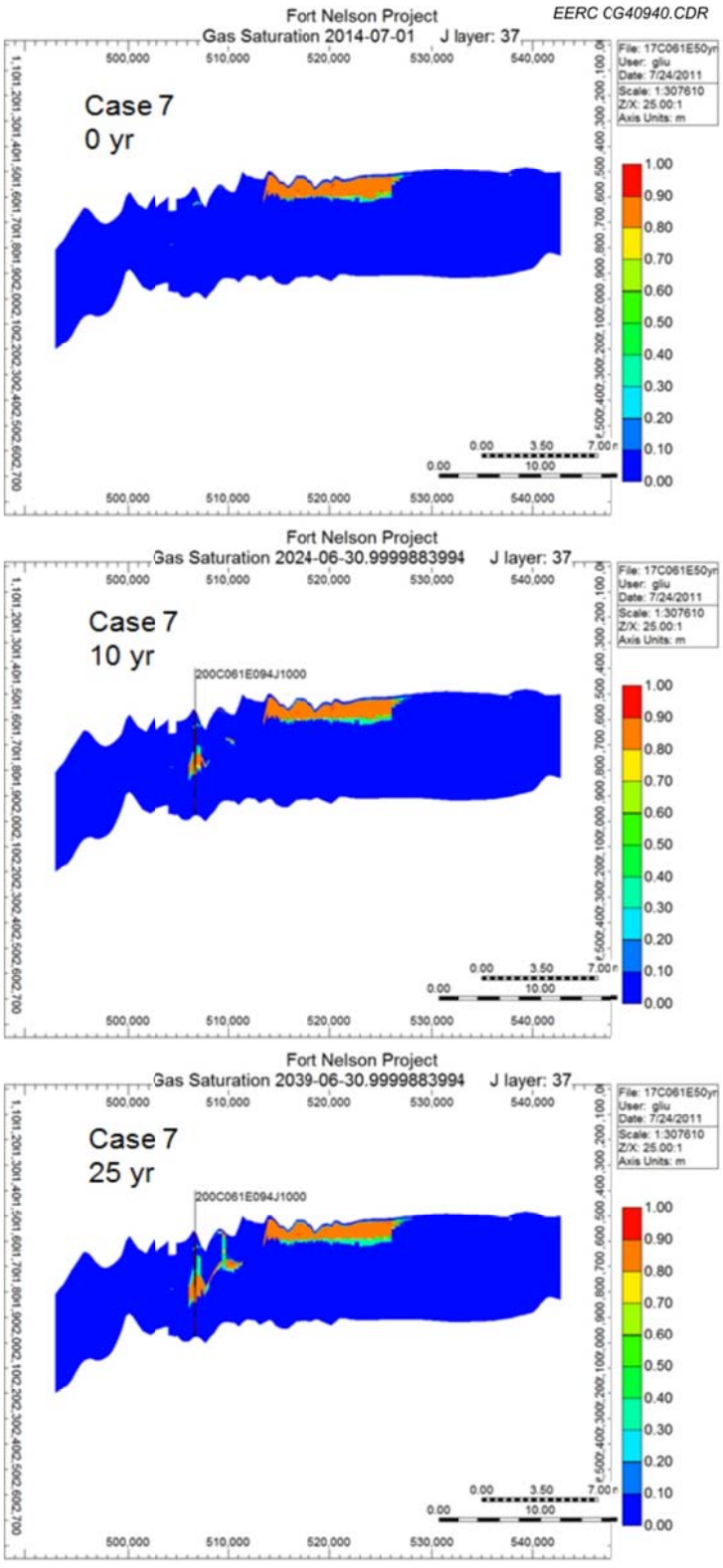

Figure E-82. Cross-sectional view of Case 7: 50 years of injection plus 50 years postinjection in and around c-61-E of History-Matching No. 2.

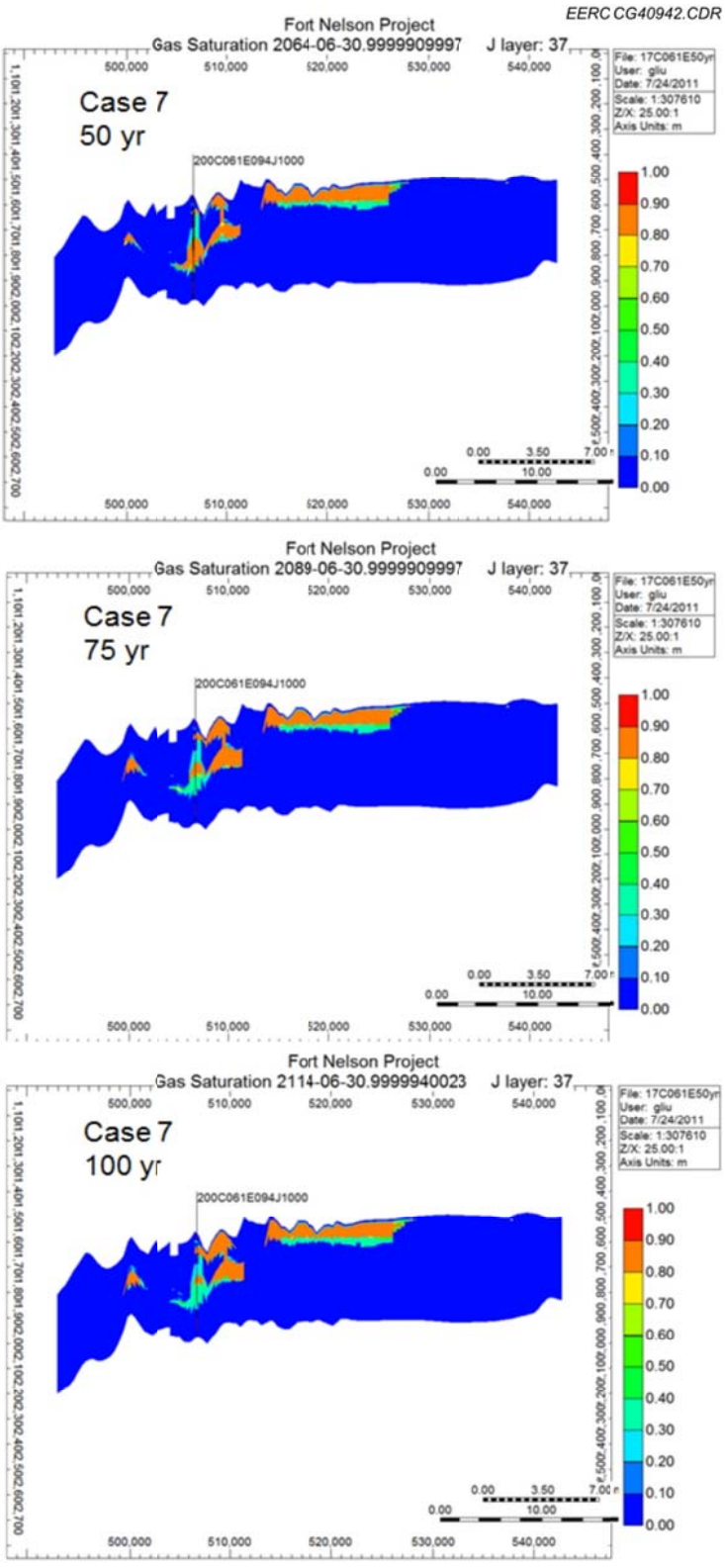

Figure E-83. Cross-sectional view of Case 7: 50 years of injection plus 50 years postinjection in and around c-61-E of History-Matching No. 2.

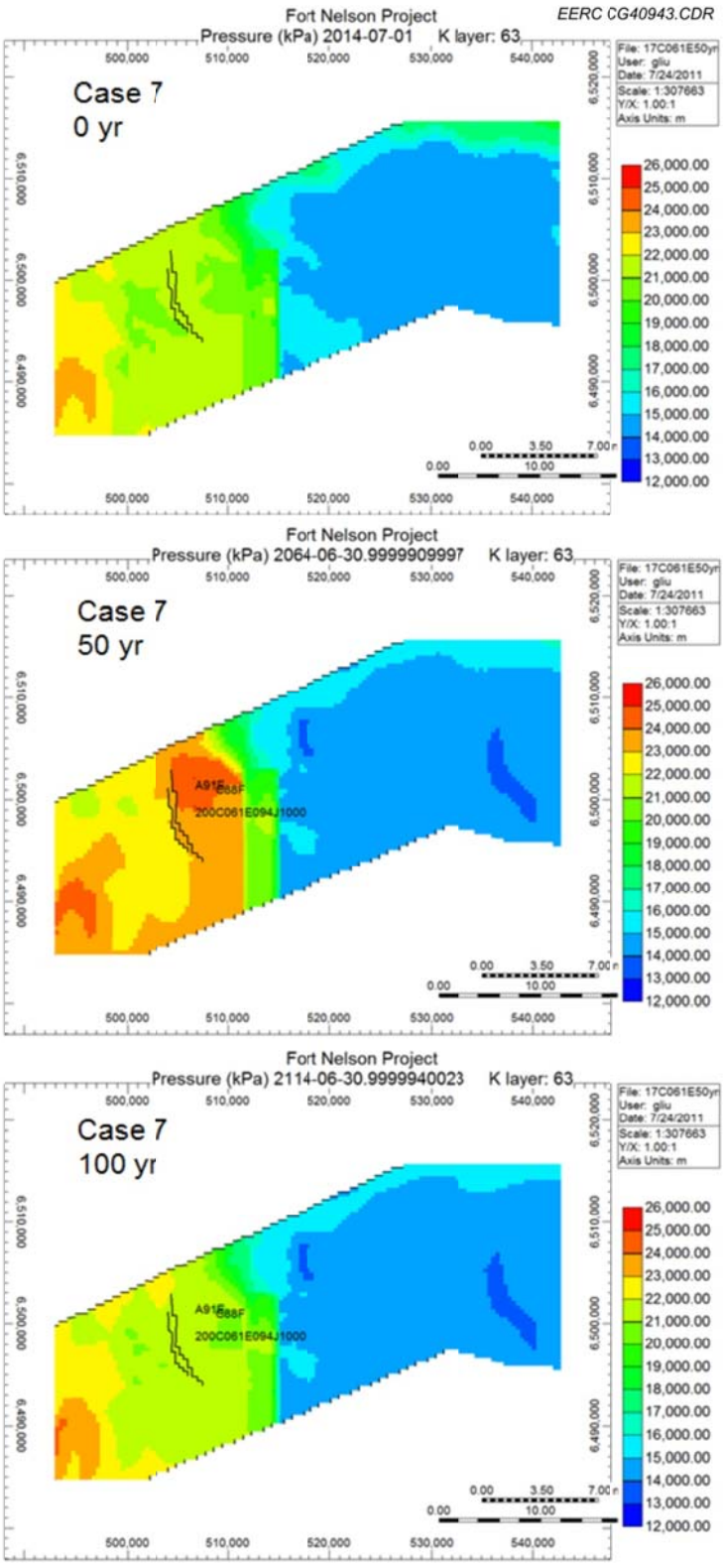

Figure E-84. Areal view of Case 7: pressure distributions; 50 years of injection plus 50 years postinjection in and around c-61-E of History-Matching No. 2.

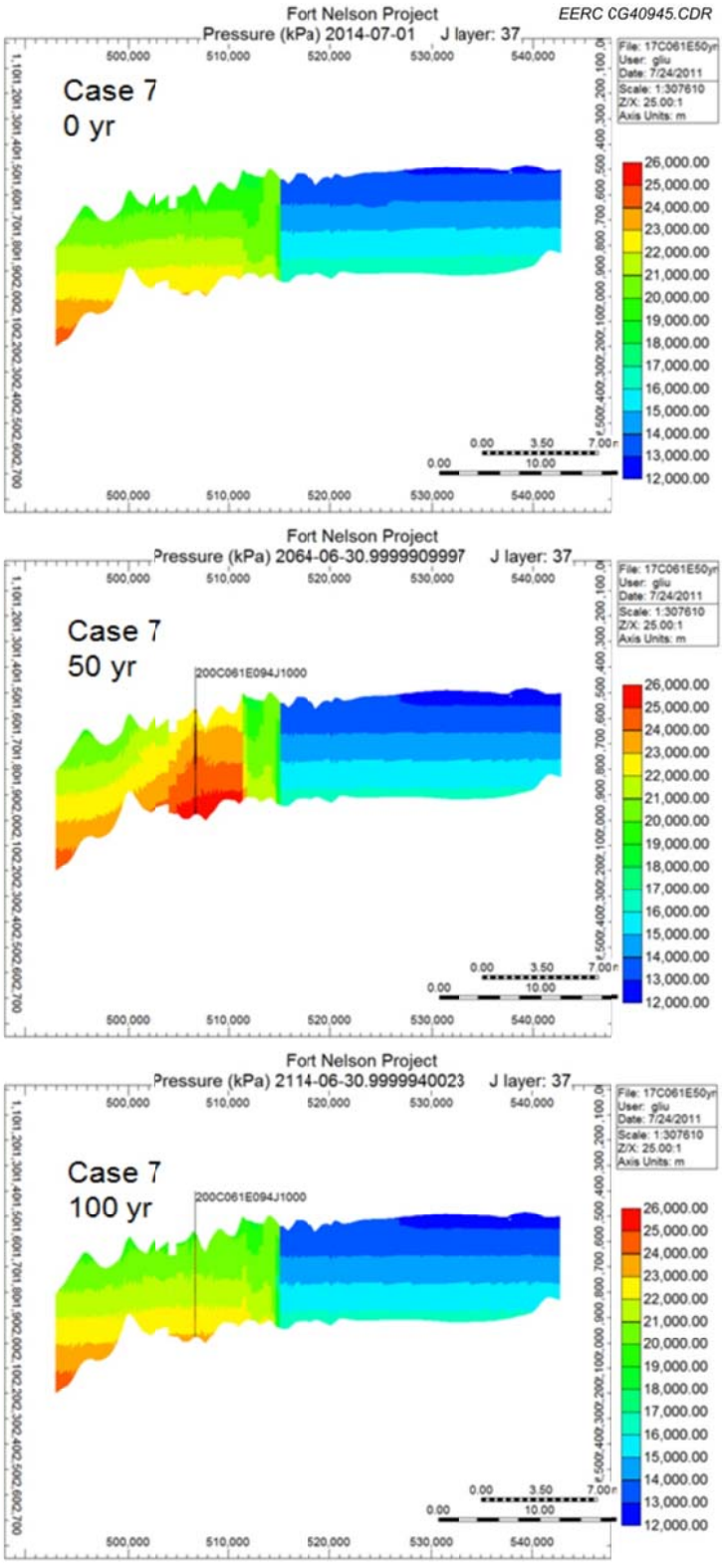

Figure E-85. Cross-sectional view of Case 7: pressure distributions; 50 years of injection plus 50 years postinjection in and around c-61-E of History-Matching No. 2.

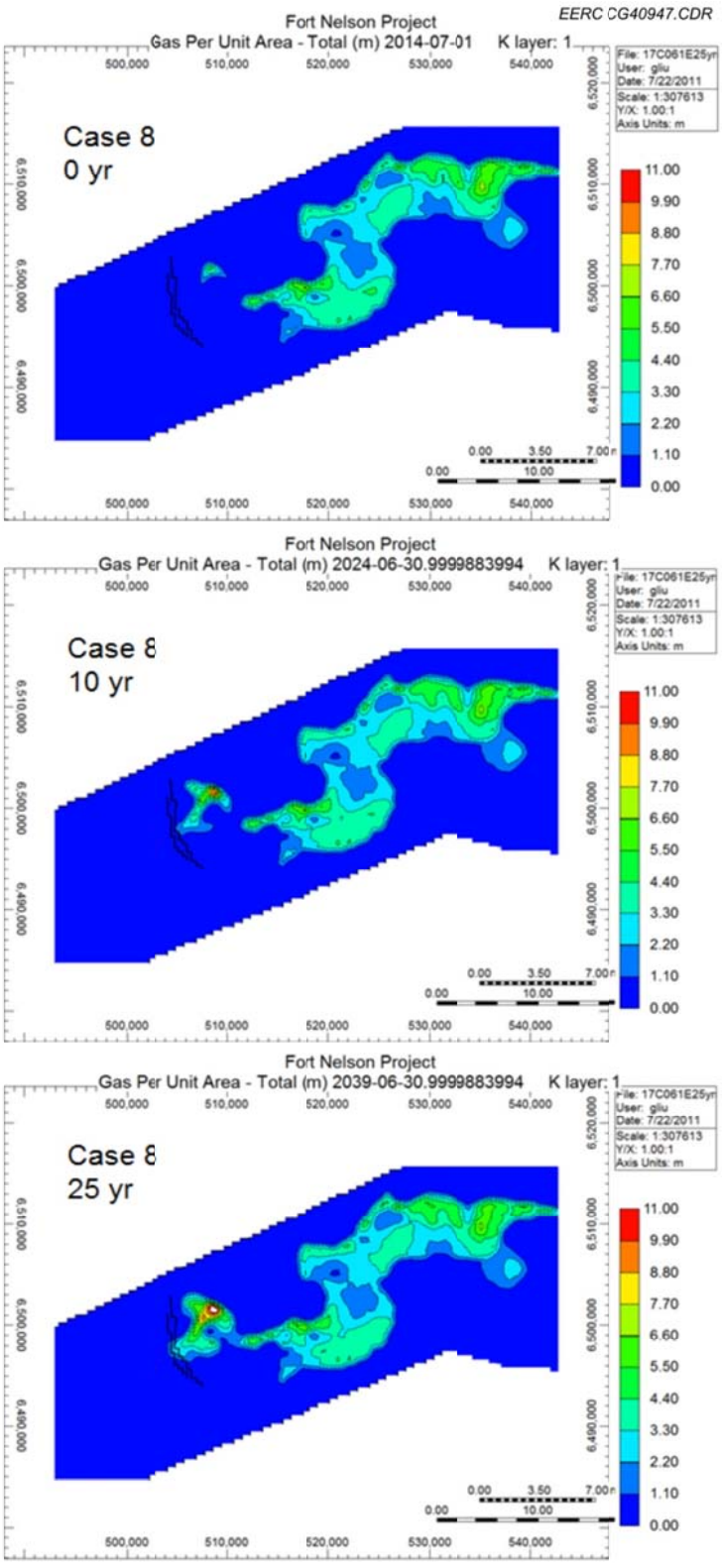

Figure E-86. Areal view of Case 8: 25 years of injection plus 75 years postinjection in and around c-61-E of History-Matching No. 2.

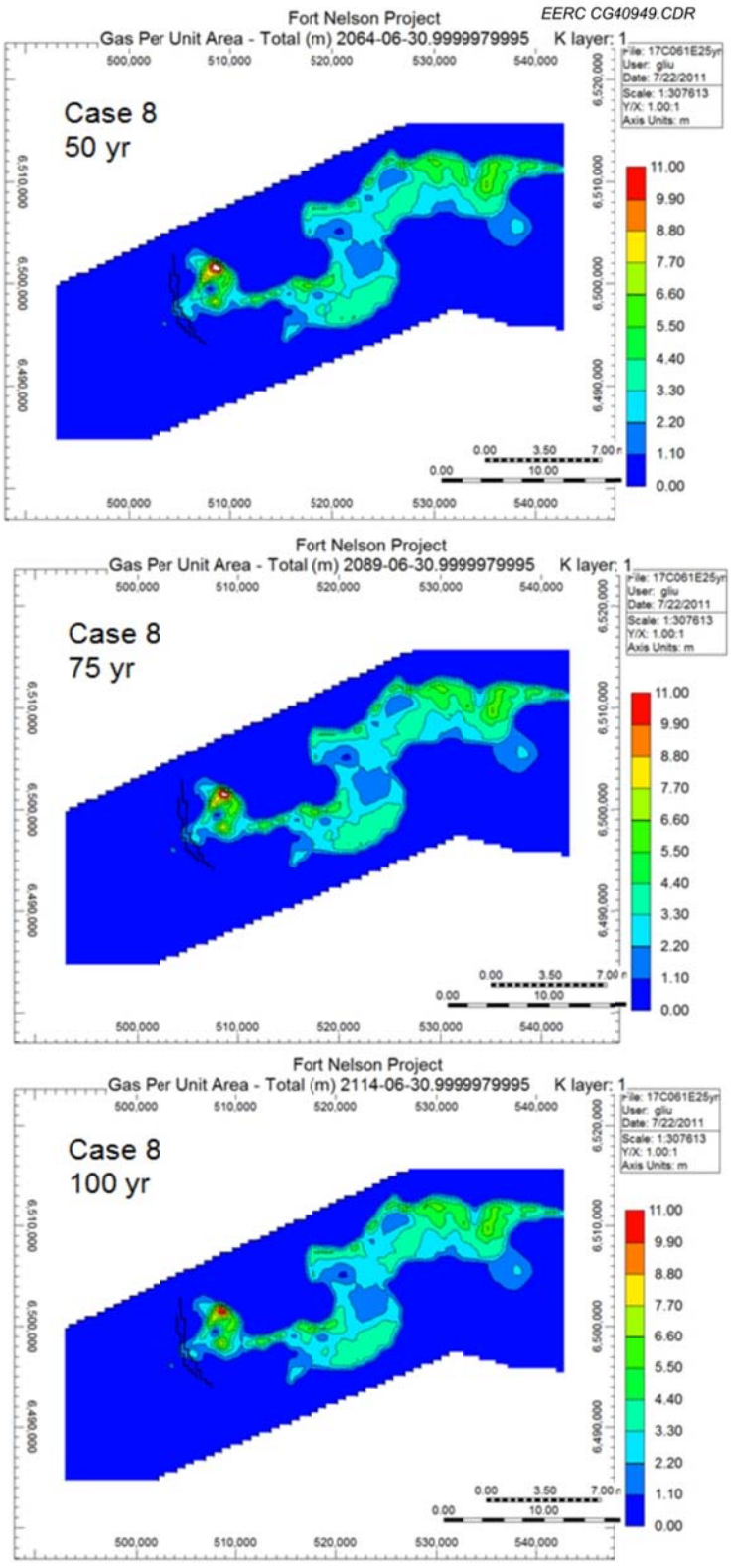

Figure E-87. Areal view of Case 8: 25 years of injection plus 75 years postinjection in and around c-61-E of History-Matching No. 2.

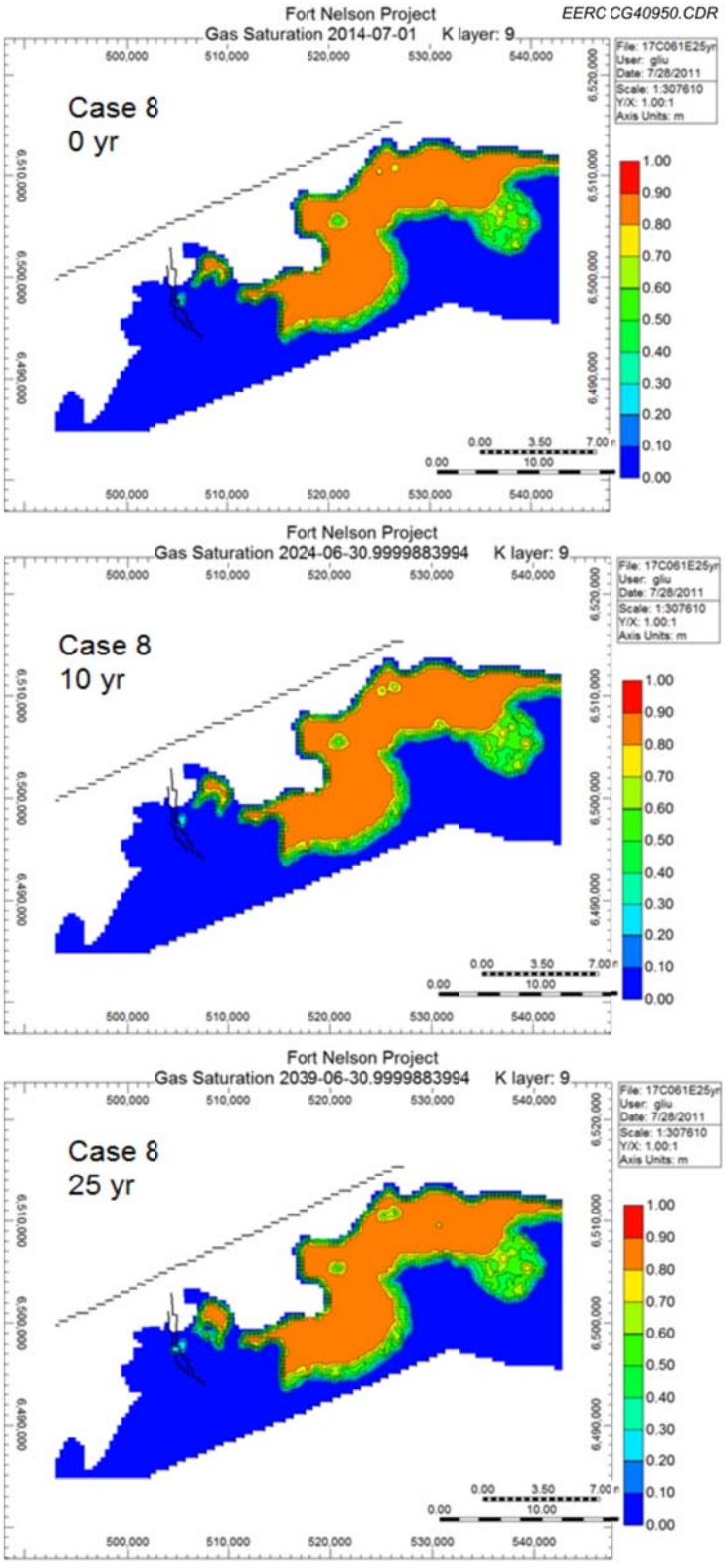

Figure E-88. Areal view of Case 8: saturation at the top of Upper Slave Point over time; 25 years of injection plus 75 years postinjection in and around c-47-E of History-Matching No. 2.

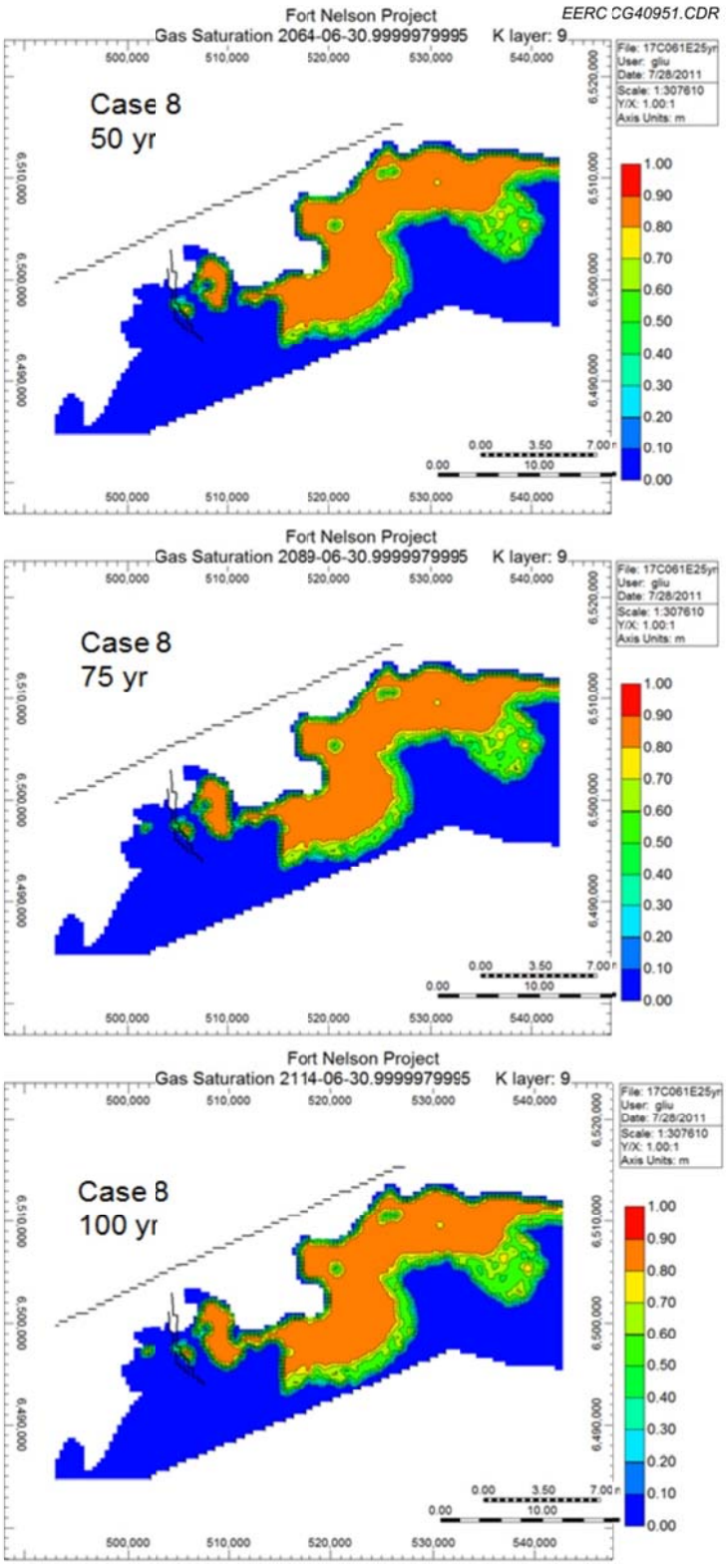

Figure E-89. Areal view of Case 8: saturation at the top of Upper Slave Point over time; 25 years of injection plus 75 years postinjection in and around c-61-E of History-Matching No. 2.

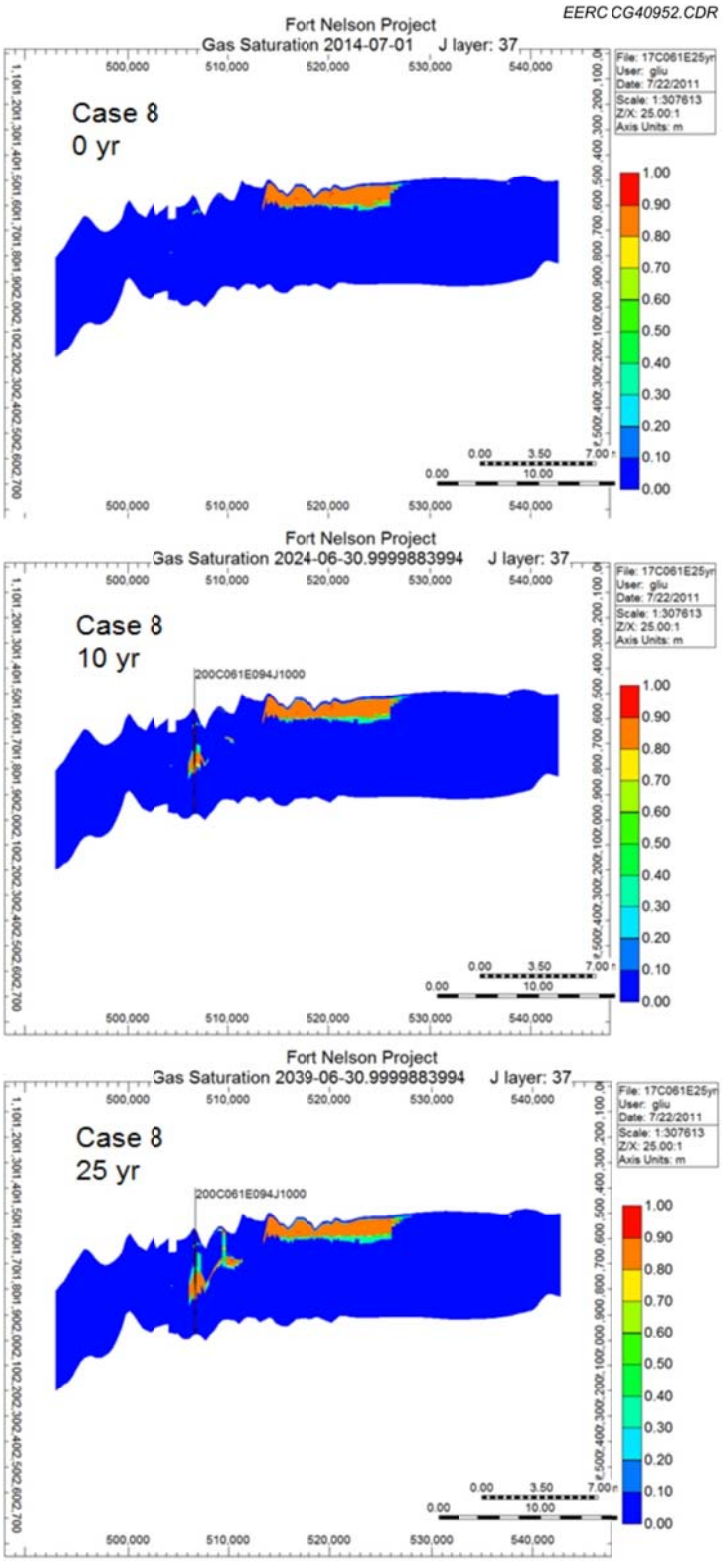

Figure E-90. Cross-sectional view of Case 8: 25 years of injection plus 75 years postinjection in and around c-61-E of History-Matching No. 2.

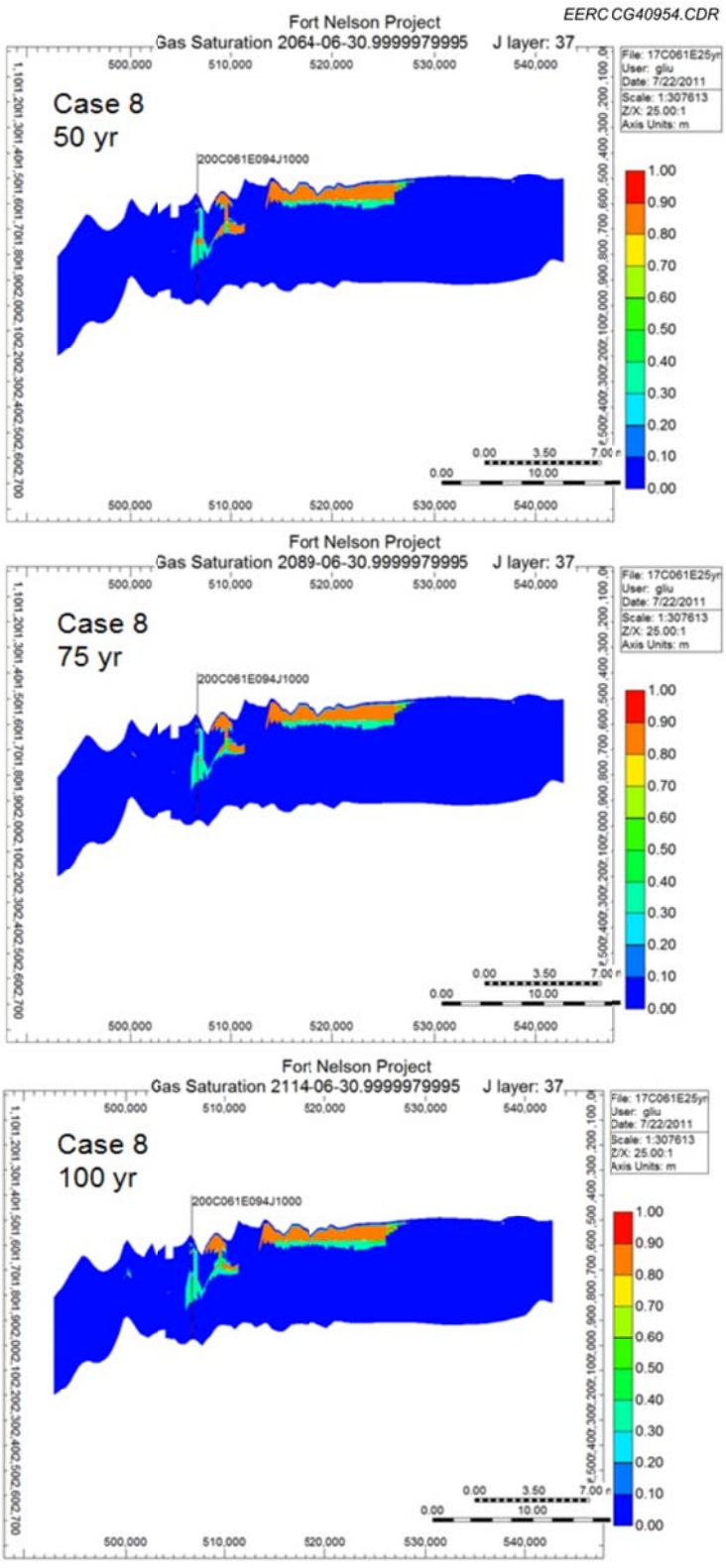

Figure E-91. Cross-sectional view of Case 8: 25 years of injection plus 75 years postinjection in and around c-61-E of History-Matching No. 2.

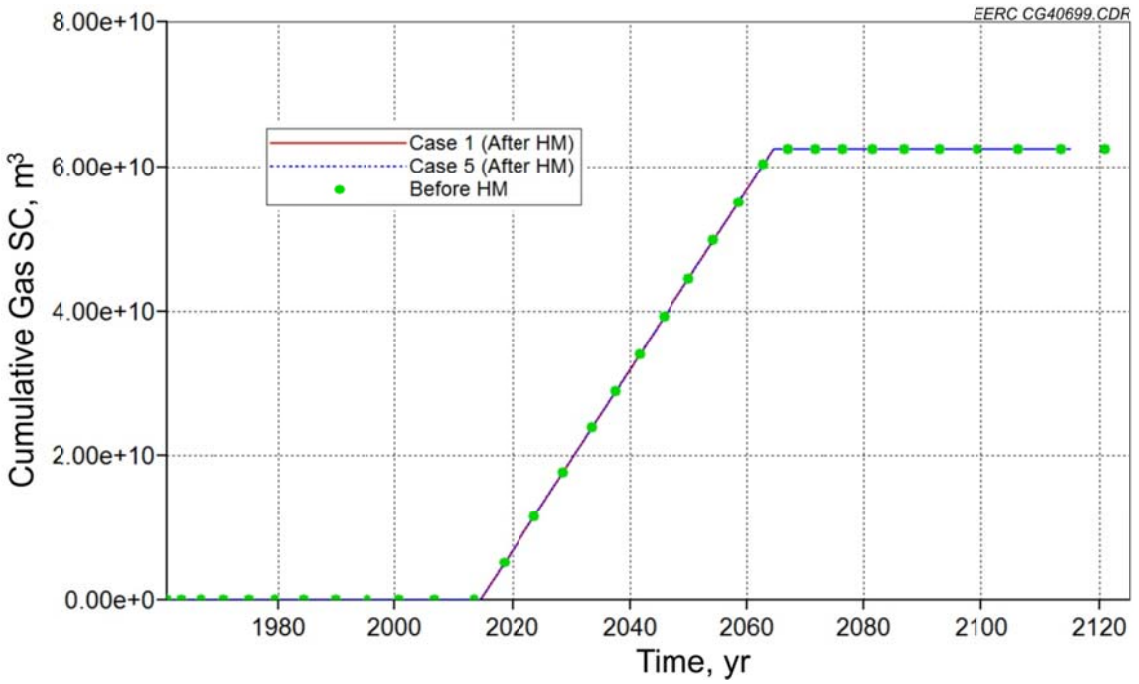

Figure E-92. Cumulative gas injection for test cases before and after history matching in and around c-47-E.

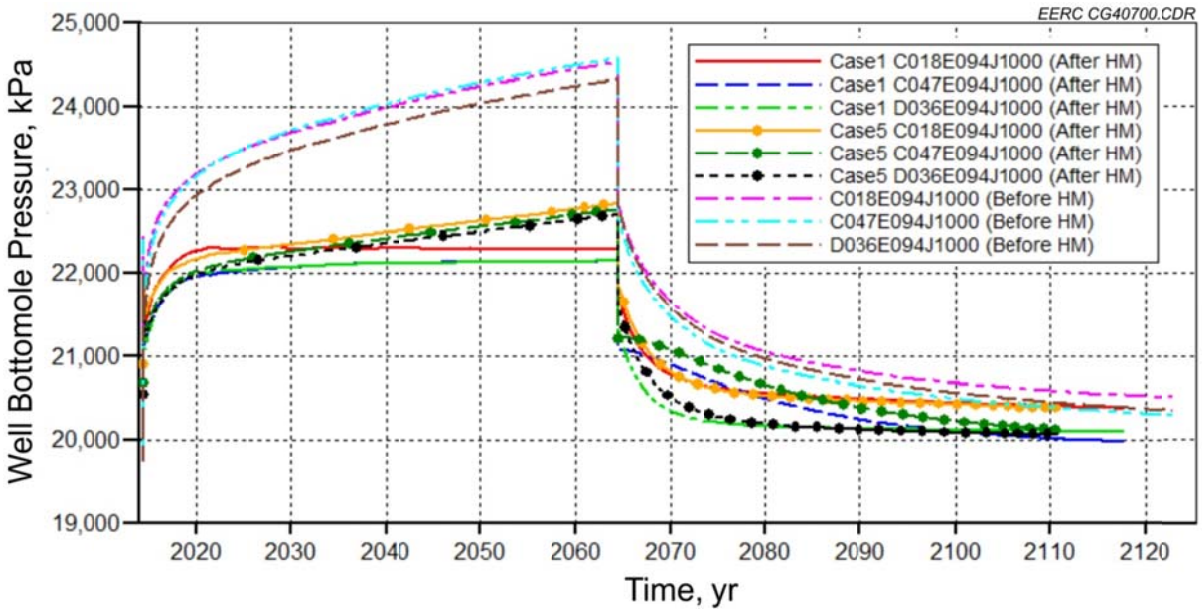

Figure E-93. BHPs for test cases before and after history matching in and around c-47-E.

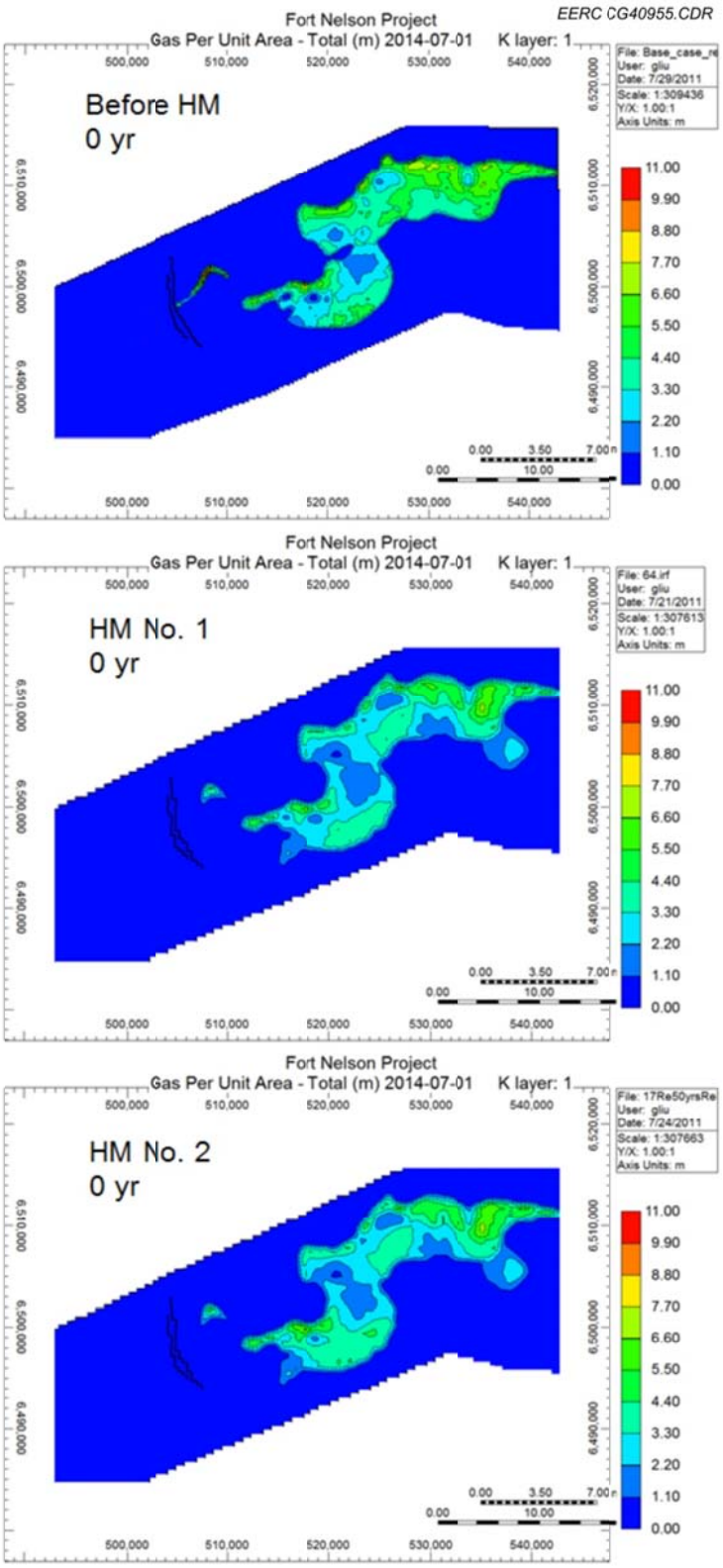

Figure E-94. Areal view of the test case before and after history matching: zero year of injection in and around c-47-E.

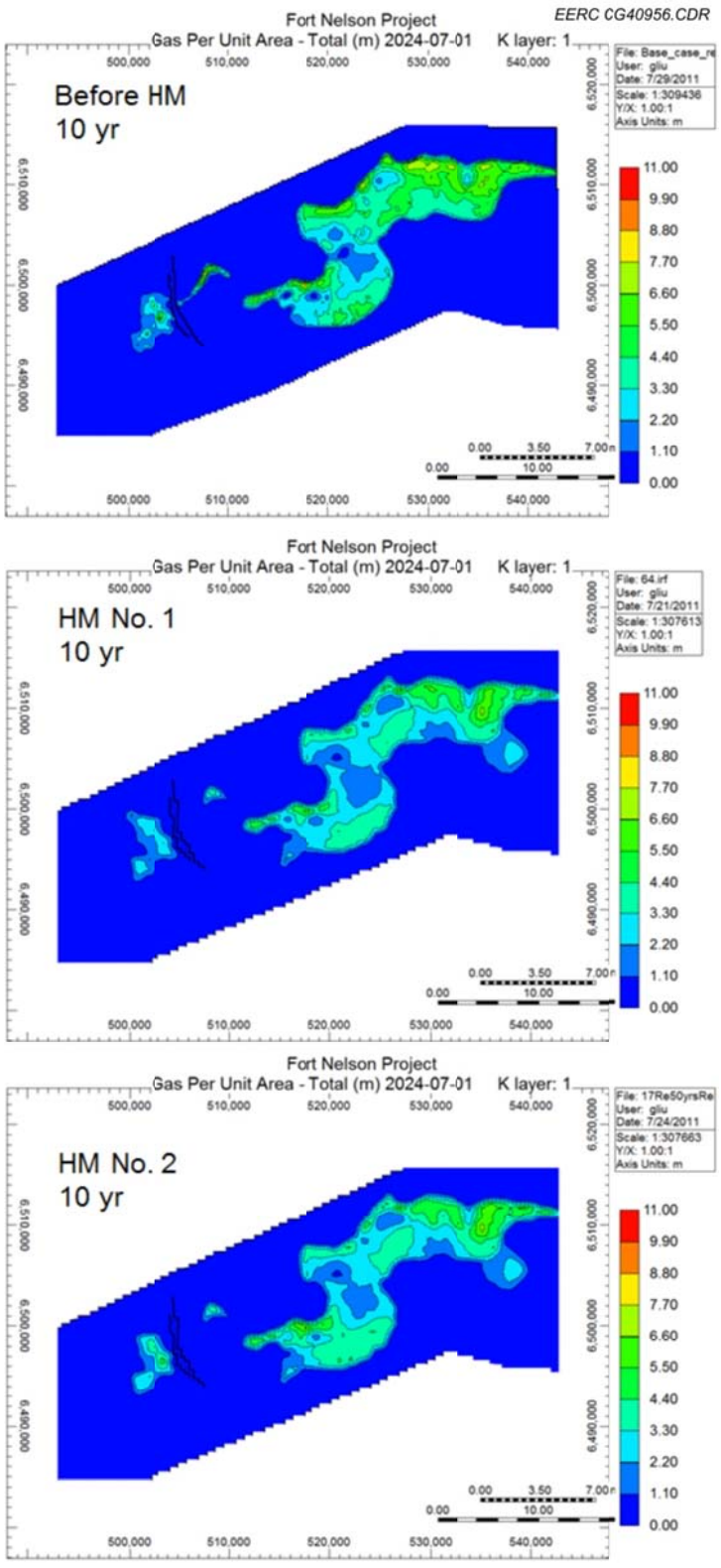

Figure E-95. Areal view of the test case before and after history matching: 10 years of injection in and around c-47-E.

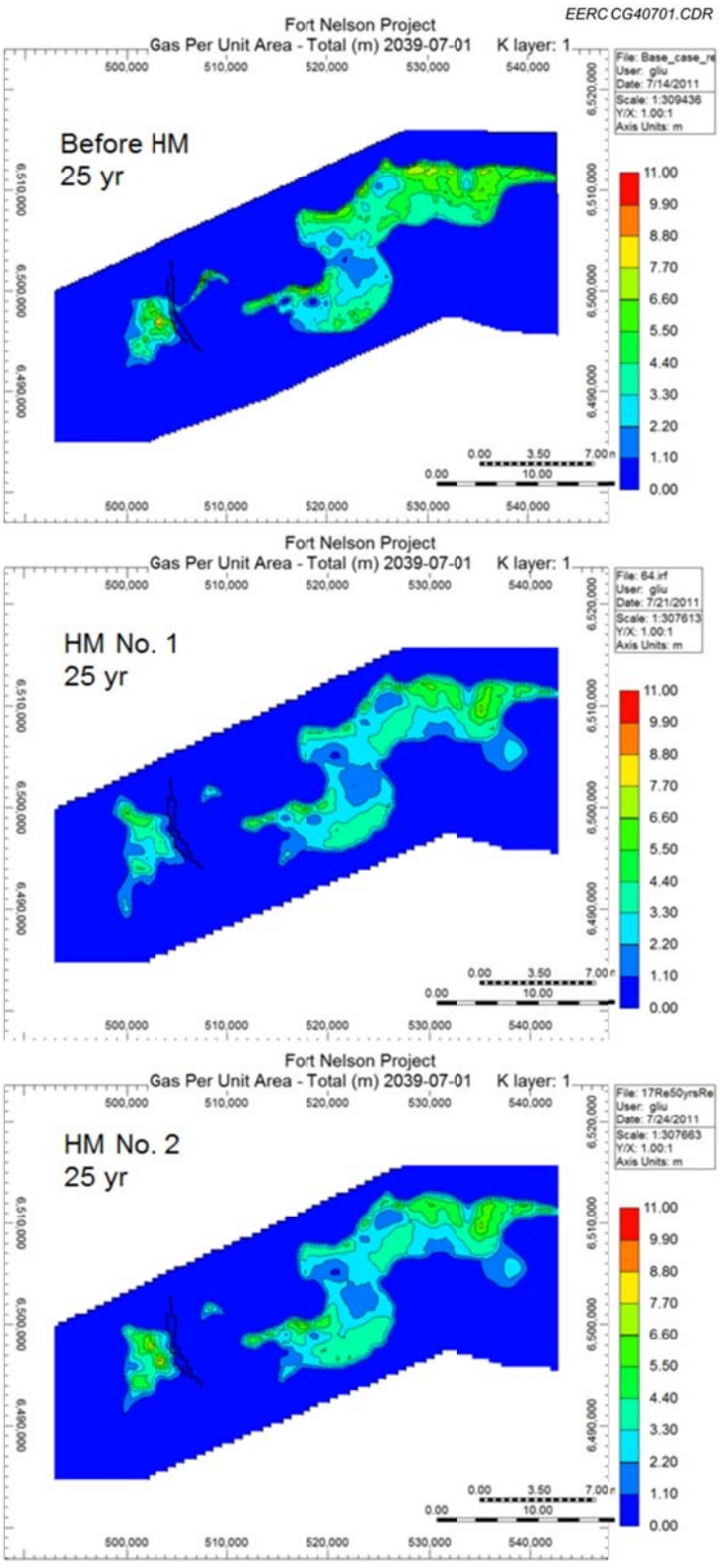

Figure E-96. Areal view of the test case before and after history matching: 25 years of injection in and around c-47-E.

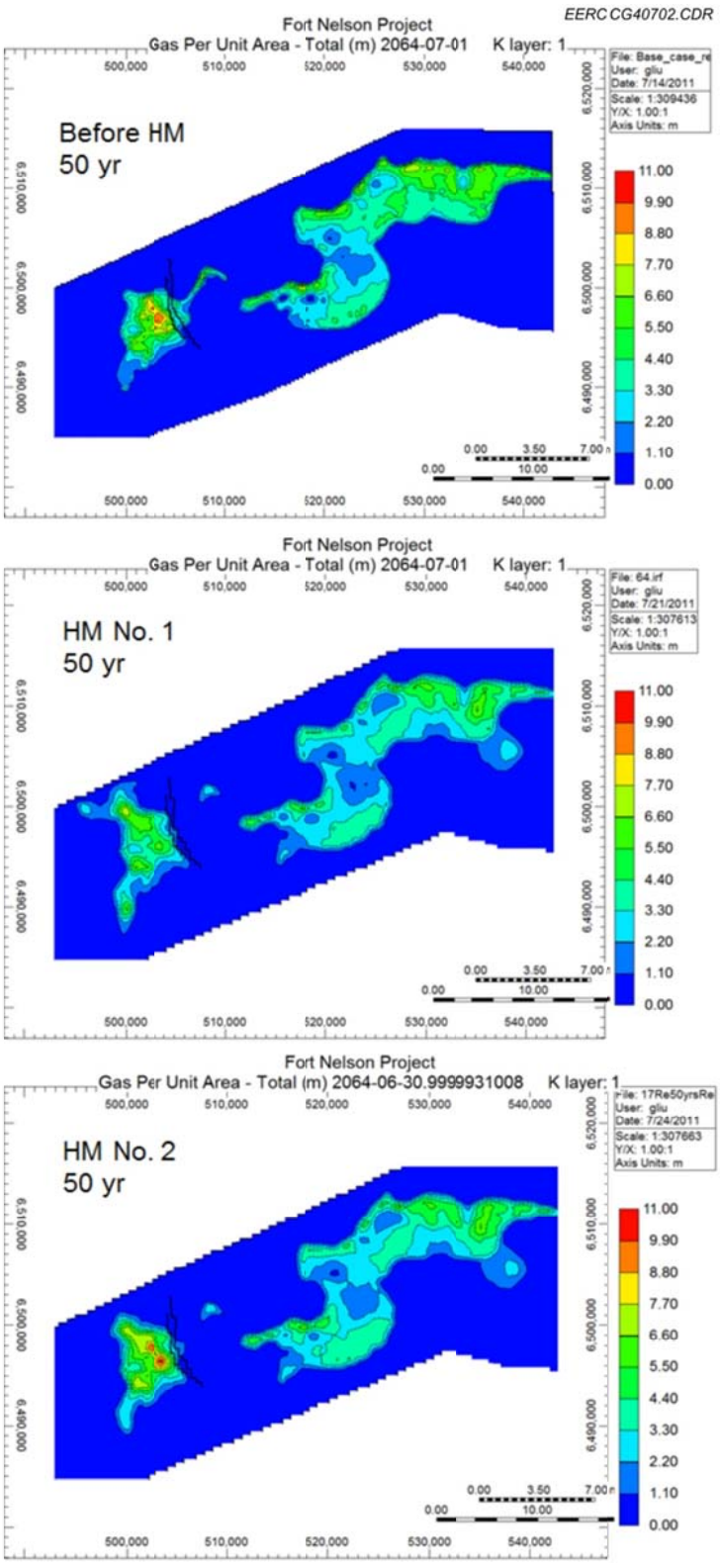

Figure E-97. Areal view of the test case before and after history matching: 50 years of injection in and around c-47-E.

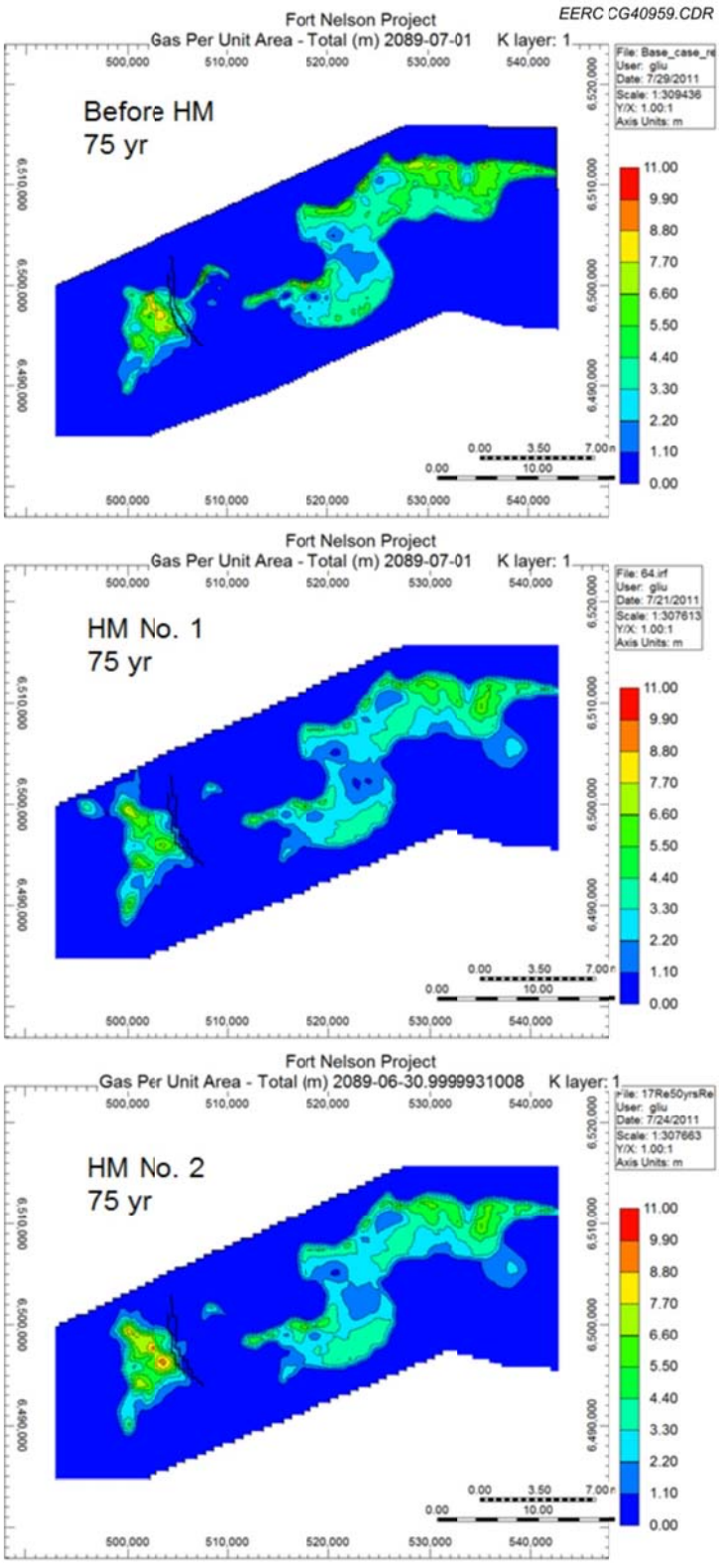

Figure E-98. Areal view of the test case before and after history matching: 50 years of injection plus 25 years postinjection in and around c-47-E.

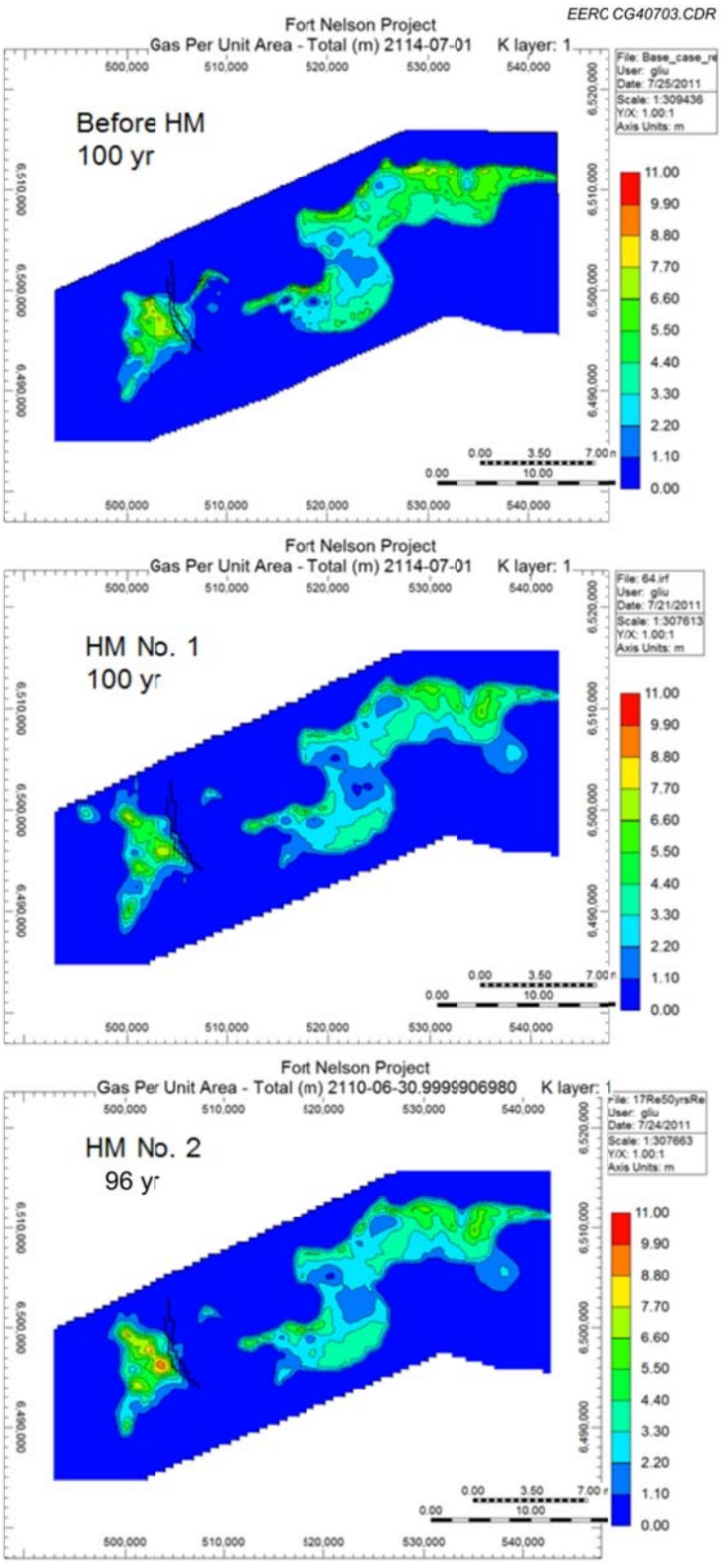

Figure E-99. Areal view of the test case before and after history matching: 50 years of injection plus 50 (46 for History-Matching No. 2) years postinjection in and around c-47-E.

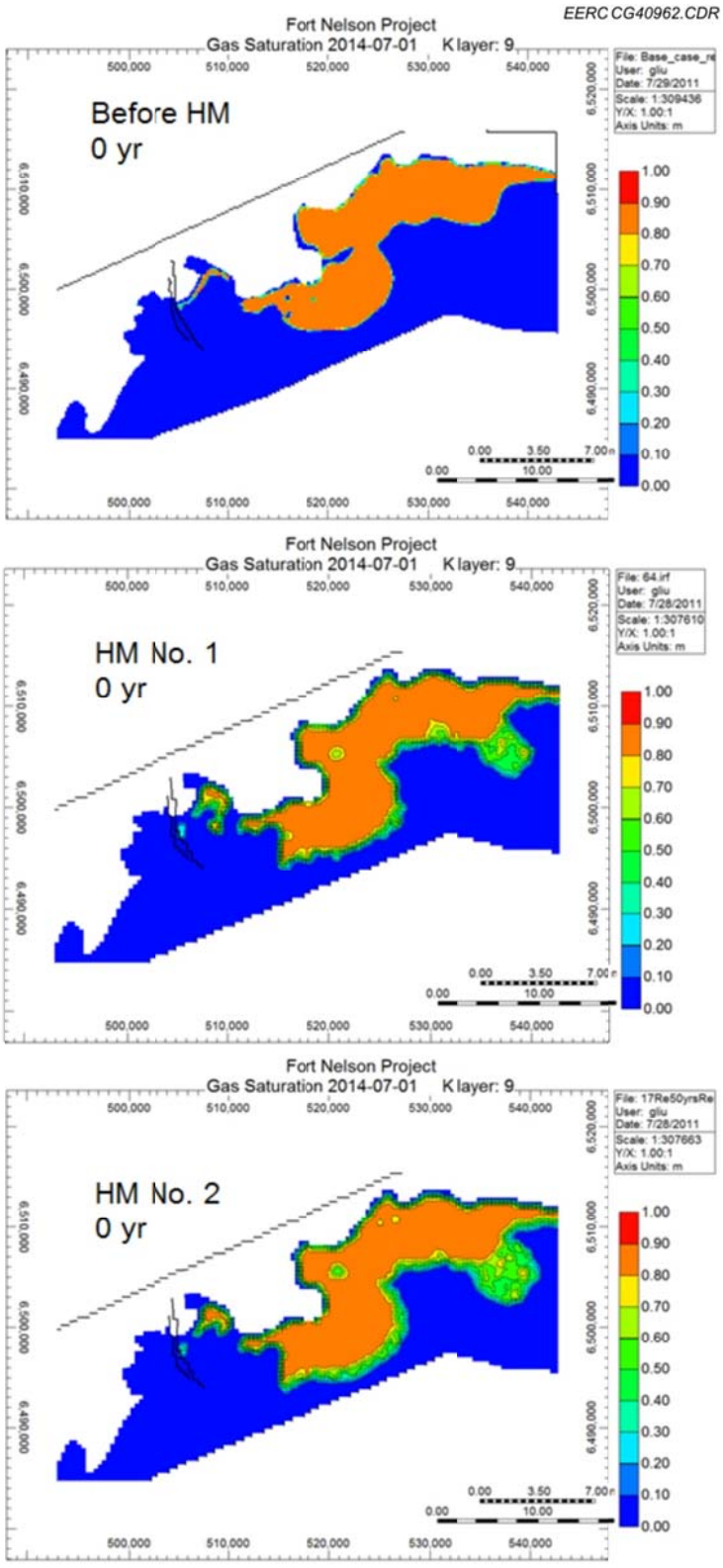

Figure E-100. Areal view of the test case before and after history matching: saturation at the top of Upper Slave Point over time; zero year of injection in and around c-47-E.

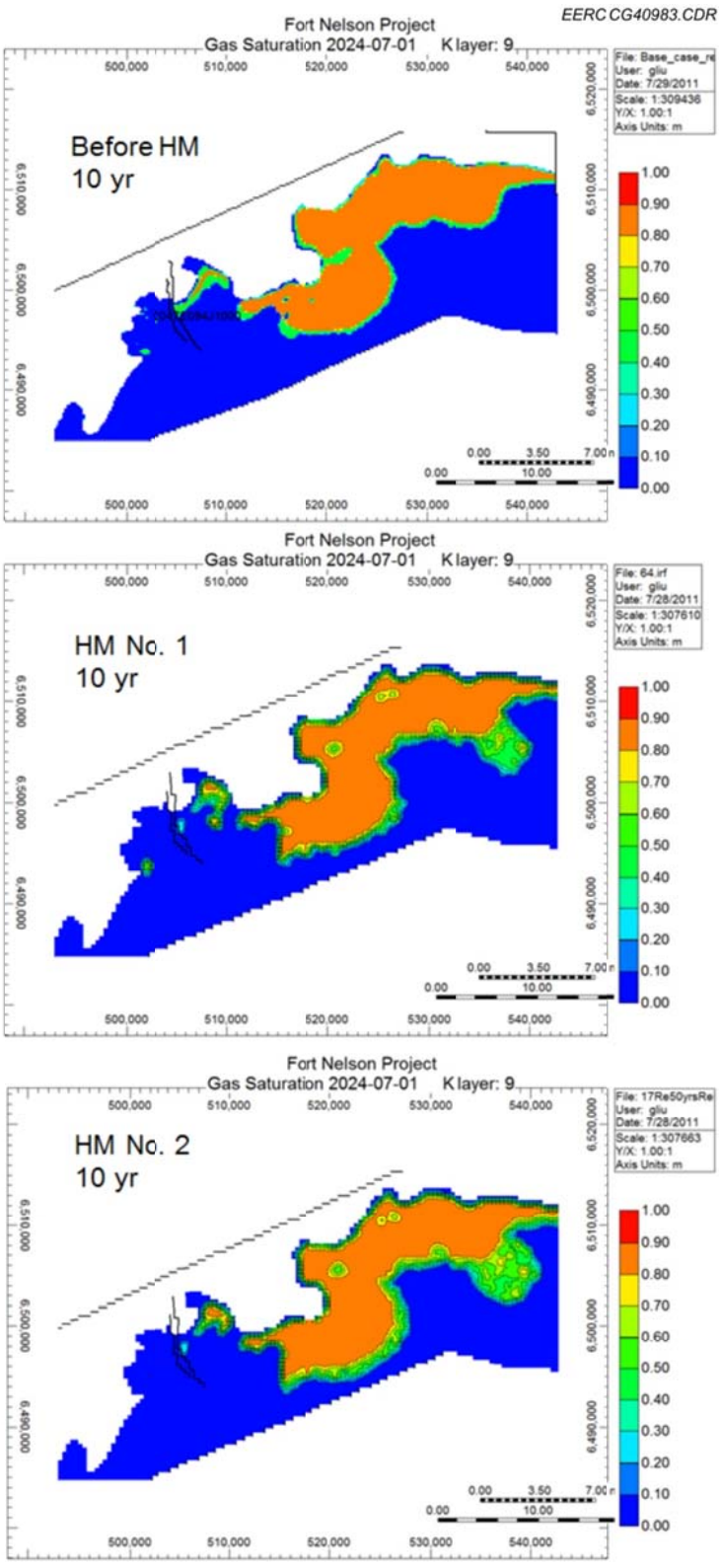

Figure E-101. Areal view of the test case before and after history matching: saturation at the top of Upper Slave Point over time; 10 years of injection in and around c-47-E.

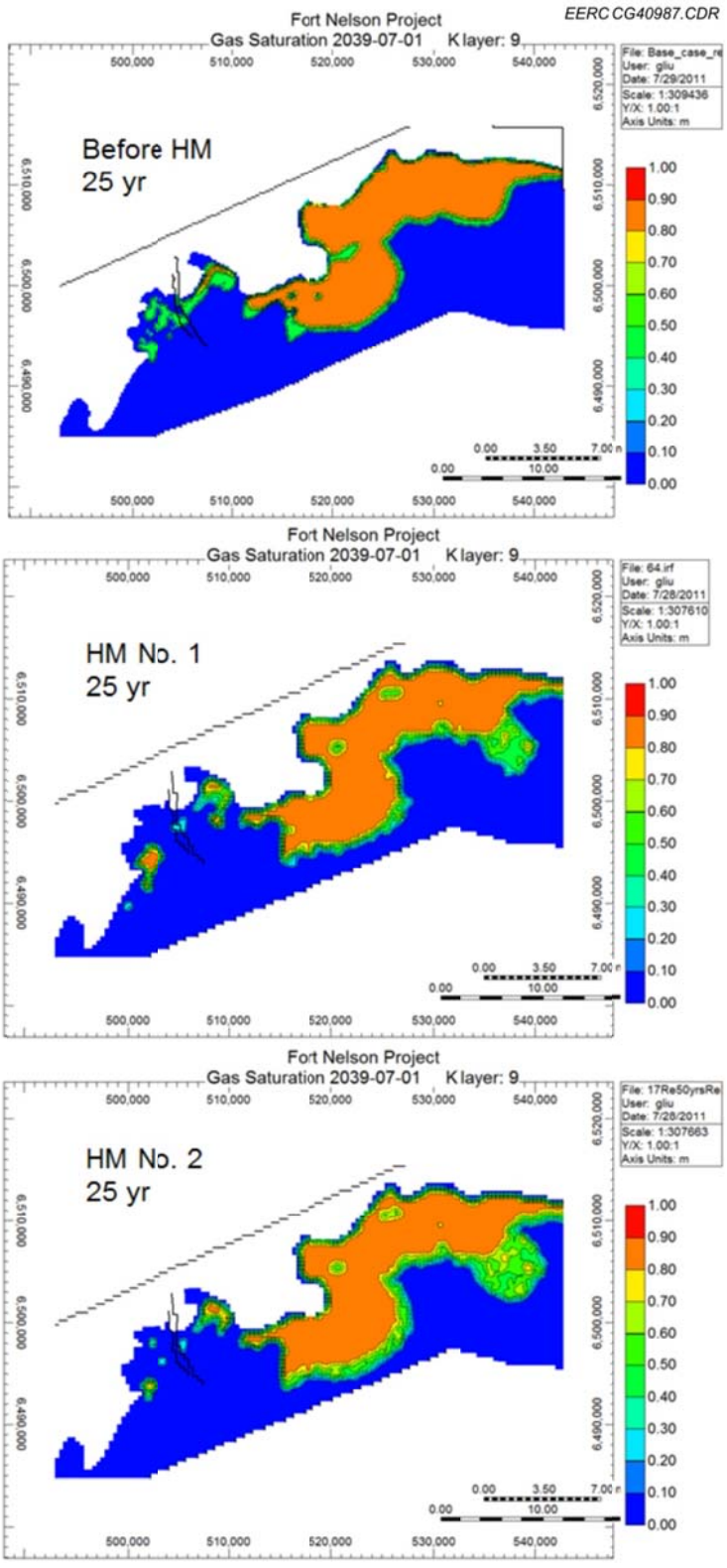

Figure E-102. Areal view of the test case before and after history matching: saturation at the top of Upper Slave Point over time; 25 years of injection in and around c-47-E.

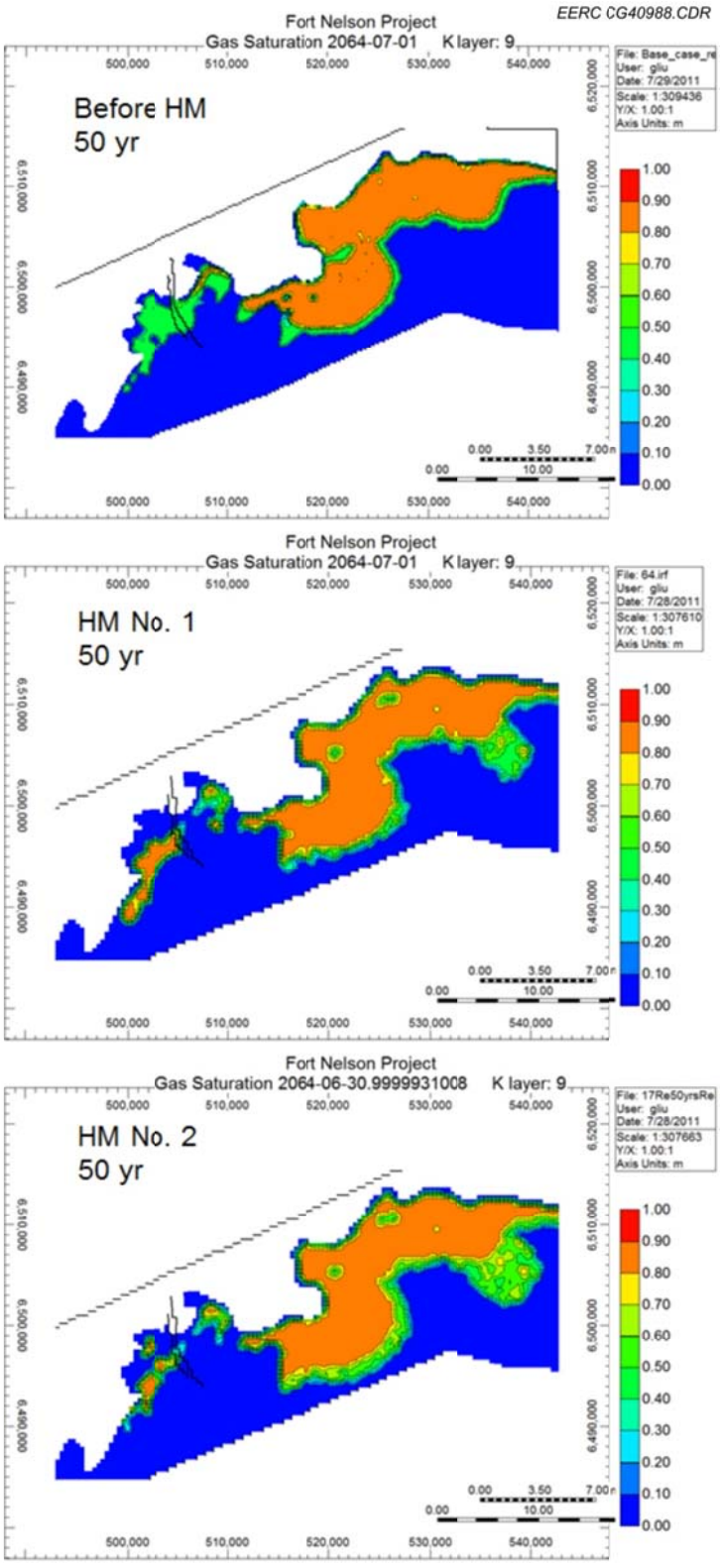

Figure E-103. Areal view of the test case before and after history matching: saturation at the top of Upper Slave Point over time; 50 years of injection in and around c-47-E.

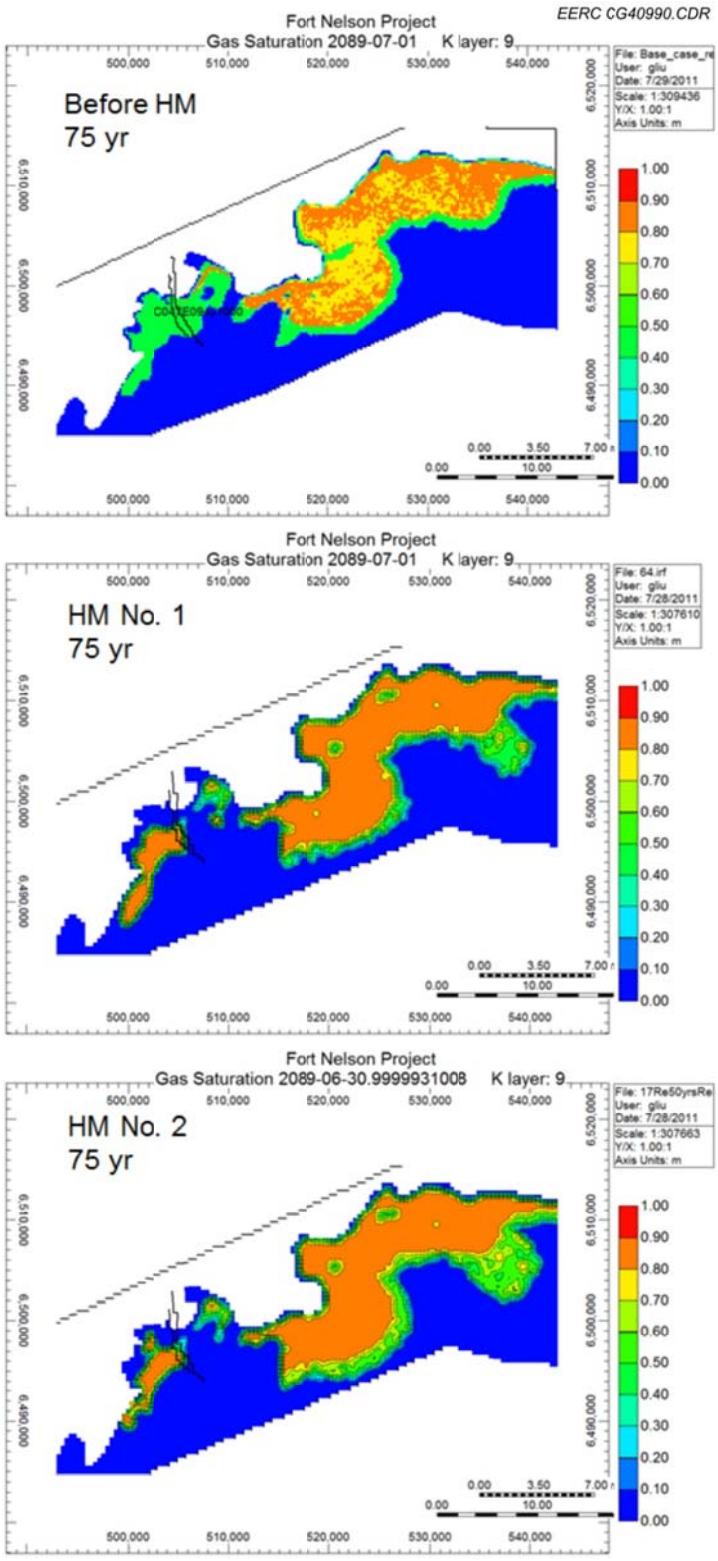

Figure E-104. Areal view of the test case before and after history matching: saturation at the top of Upper Slave Point over time; 50 years of injection plus 25 years postinjection in and around c-47-E.

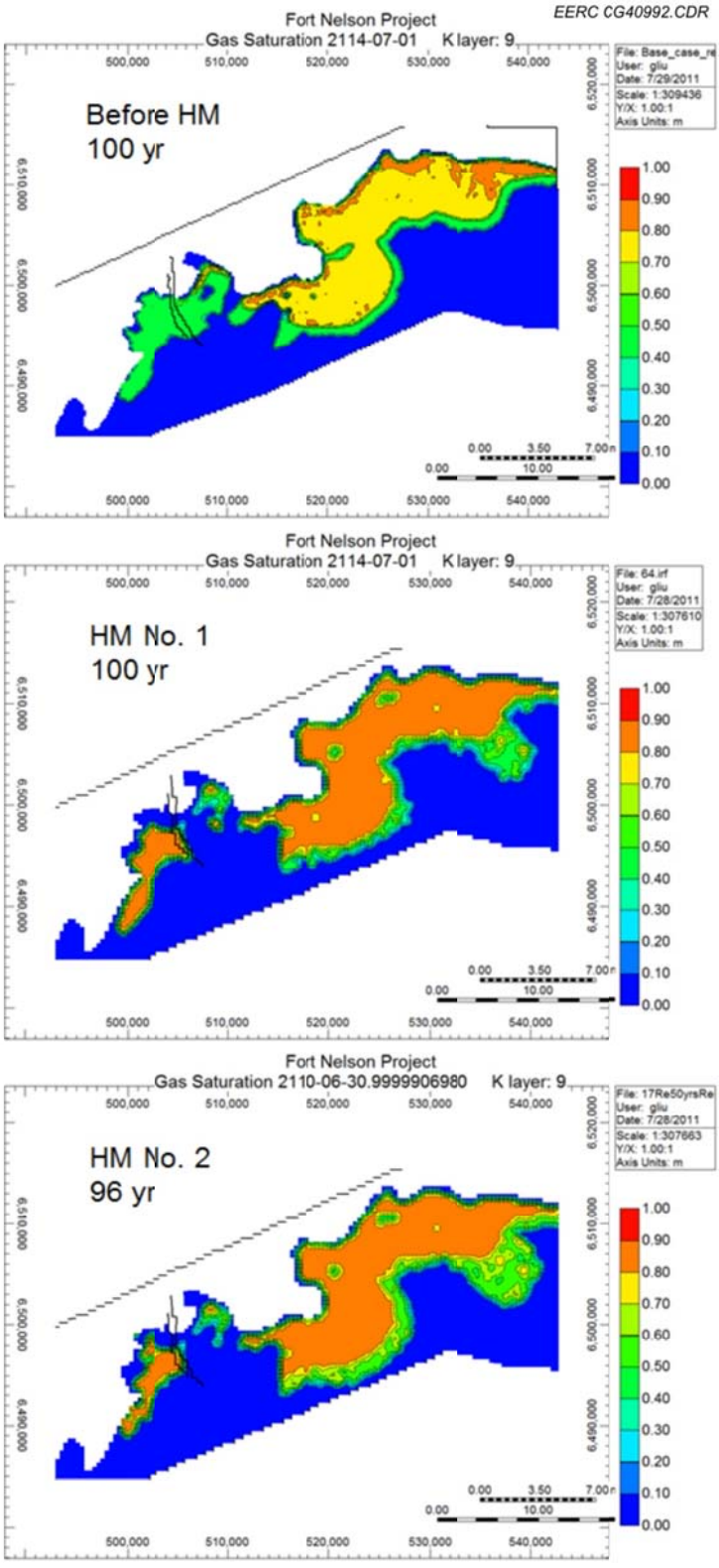

Figure E-105. Areal view of the test case before and after history matching: saturation at the top of Upper Slave Point over time; 50 years of injection plus 50 (46 for History-Matching No. 2) years postinjection in and around c-47-E.

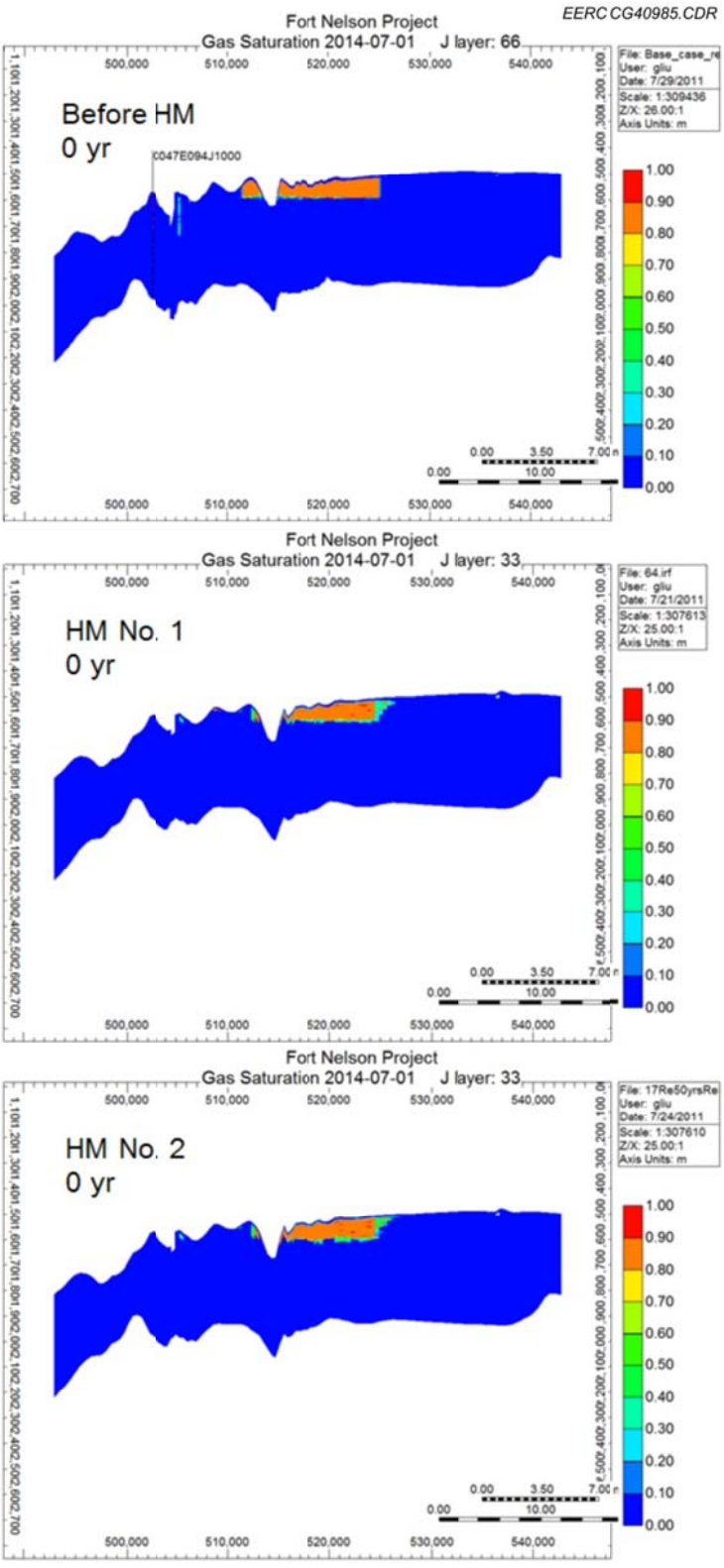

Figure E-106. Cross-sectional view of the test case before and after history matching: zero year of injection in and around c-47-E.

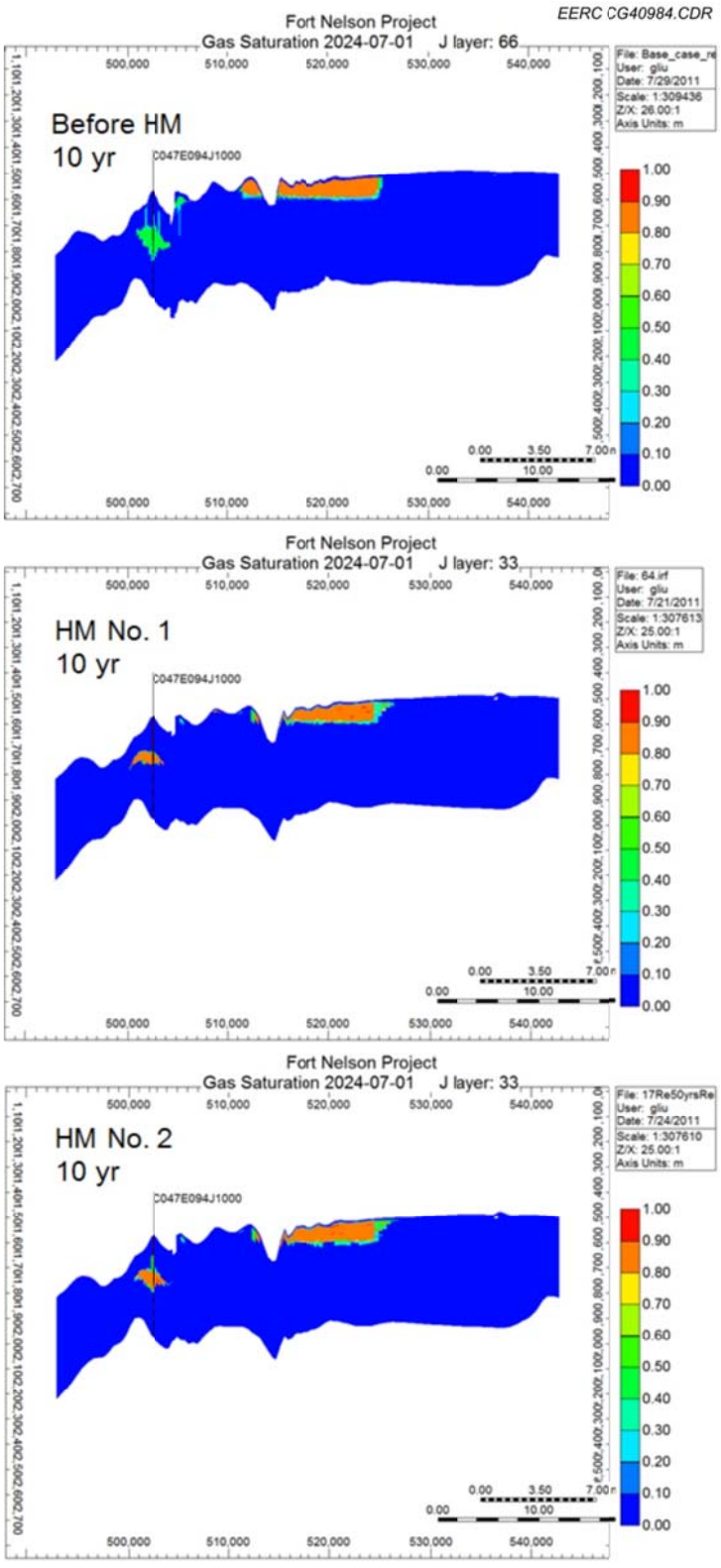

Figure E-107. Cross-sectional view of the test case before and after history matching: 10 years of injection in and around c-47-E.

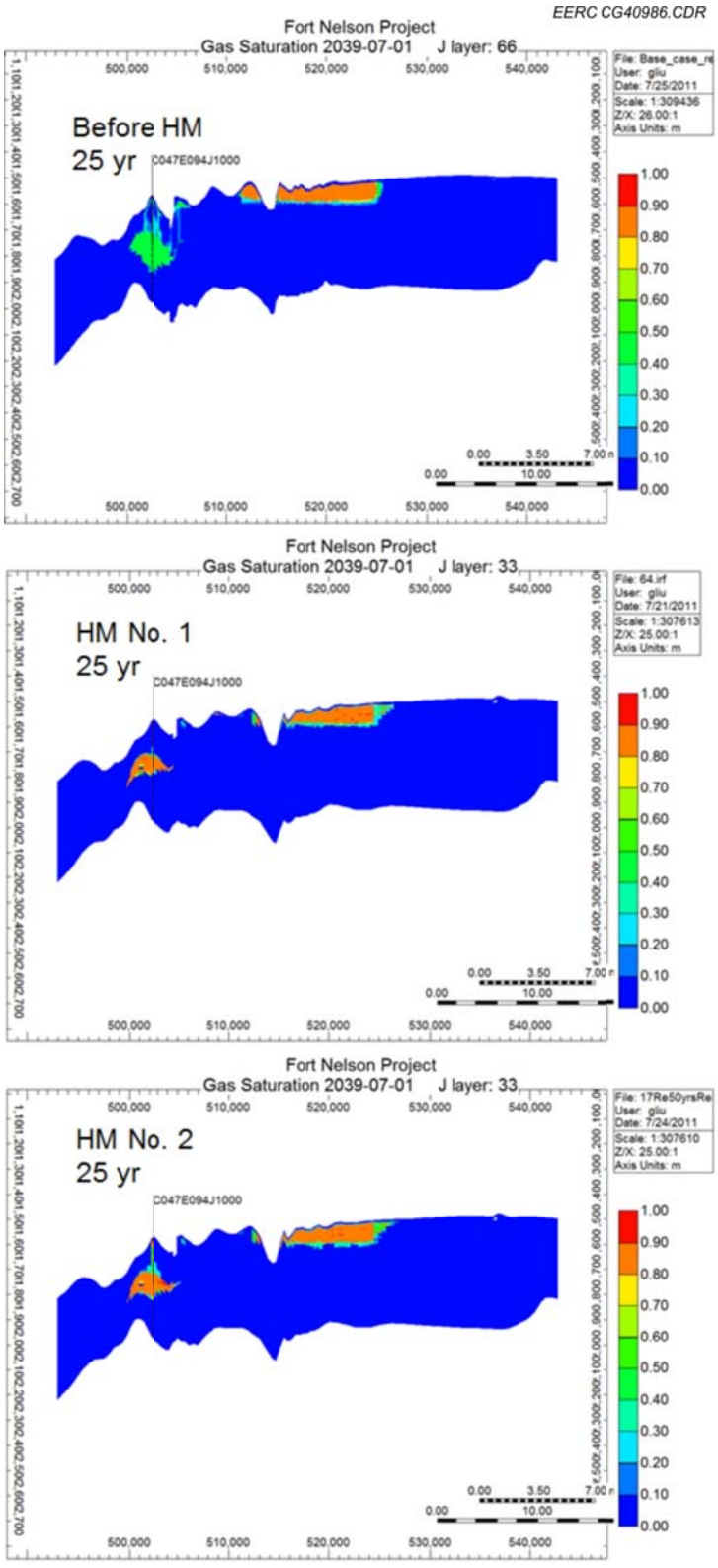

Figure E-108. Cross-sectional view of the test case before and after history matching: 25 years of injection in and around c-47-E.

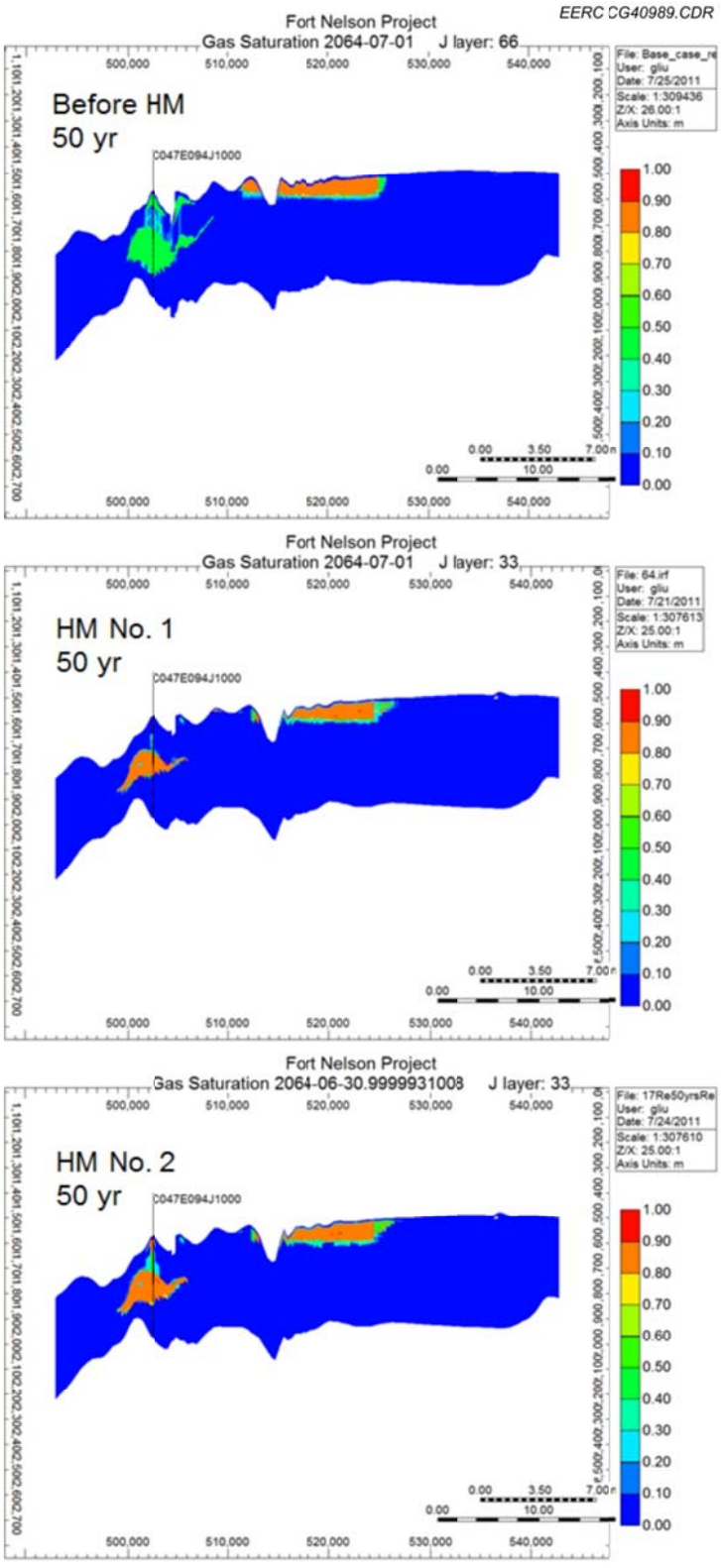

Figure E-109. Cross-sectional view of the test case before and after history matching: 50 years of injection in and around c-47-E.

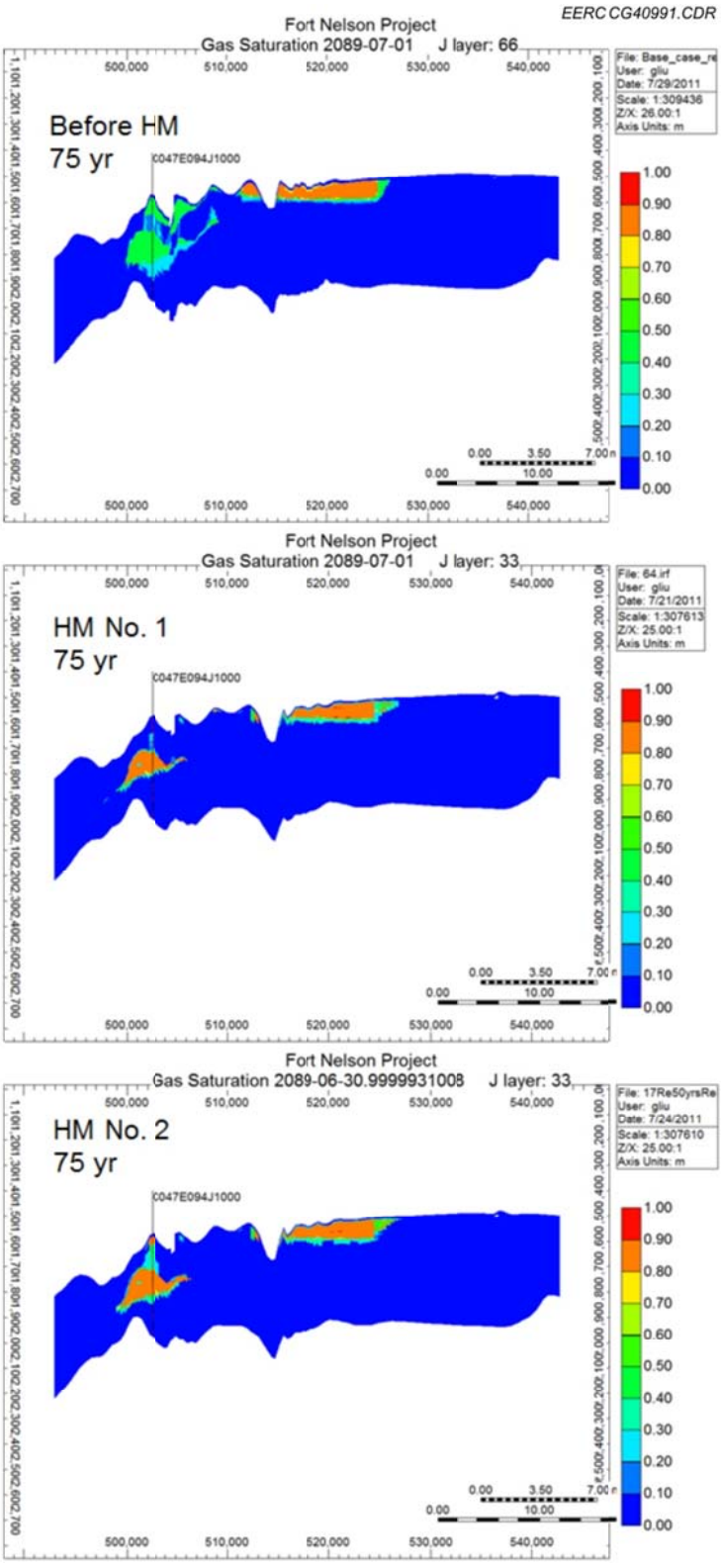

Figure E-110. Cross-sectional view of the test case before and after history matching: 50 years of injection plus 25 years postinjection in and around c-47-E.

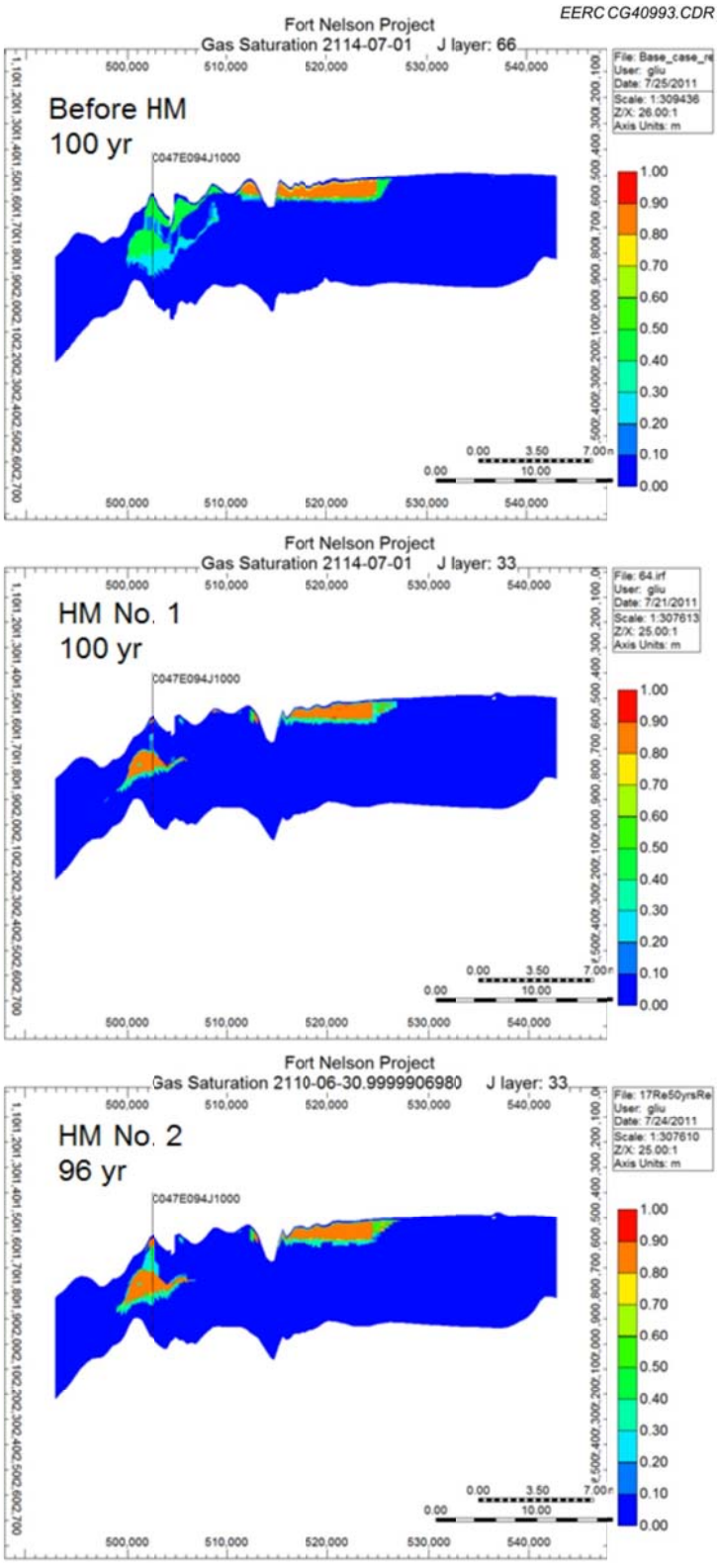

Figure E-111. Cross-sectional view of the test case before and after history matching: 50 years of injection plus 50 (46 for HM No. 2) years postinjection in and around c-47-E.

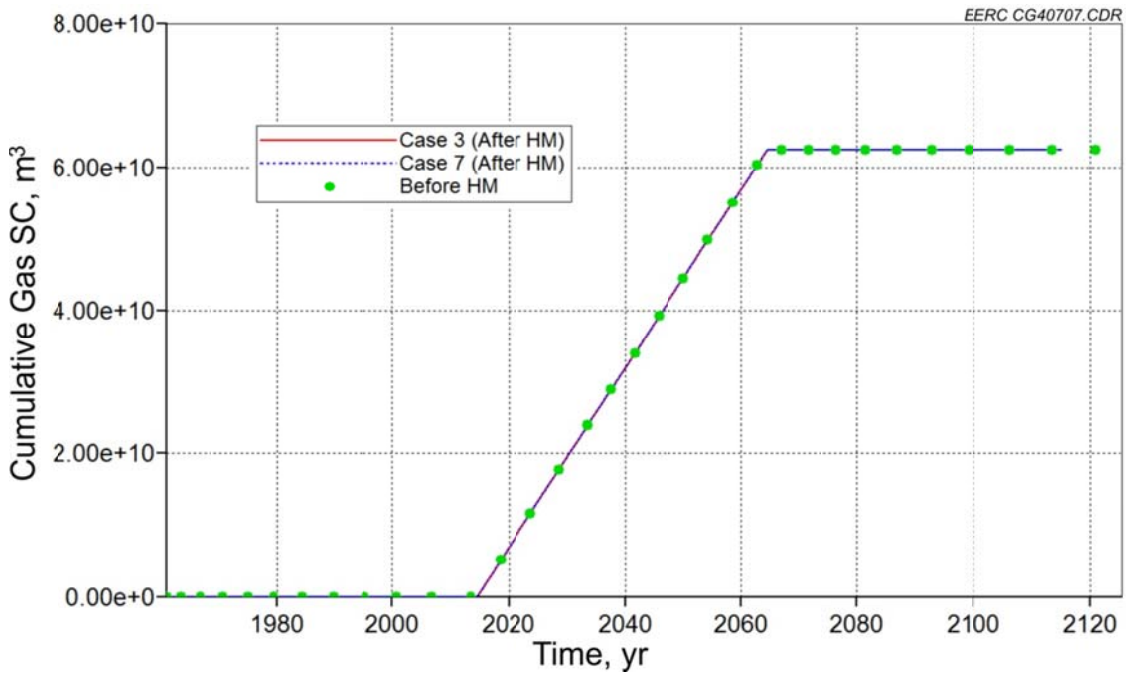

Figure E-112. Cumulative gas injection of test cases before and after history matching in and around c-61-E.

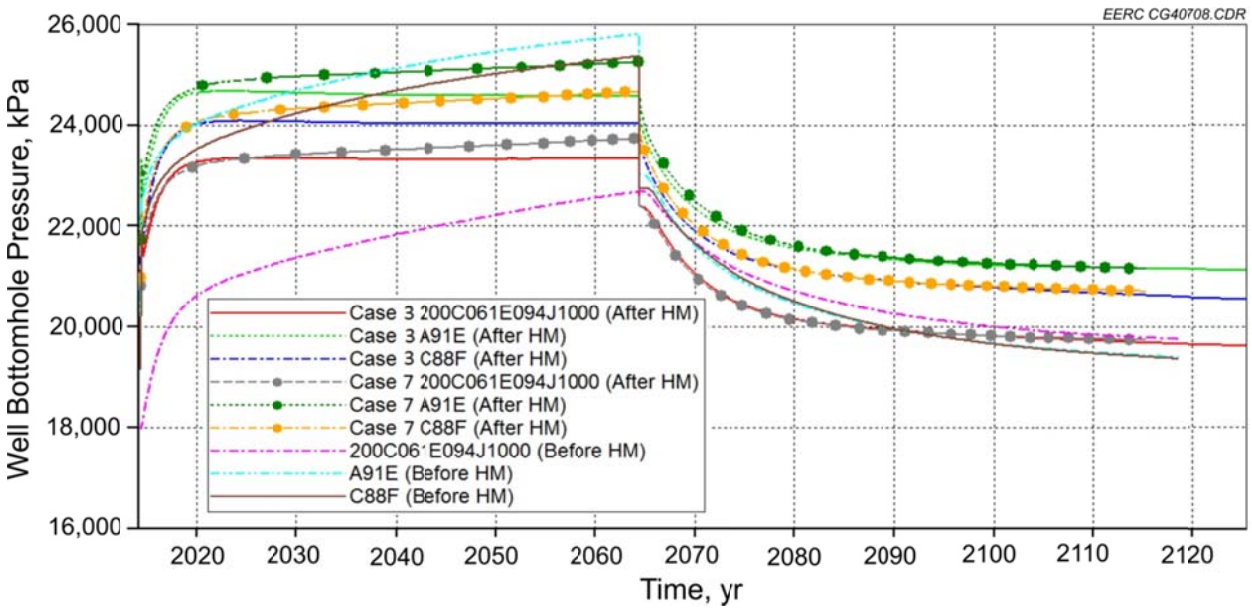

Figure E-113. BHPs of test cases before and after history matching in and around c-61-E.

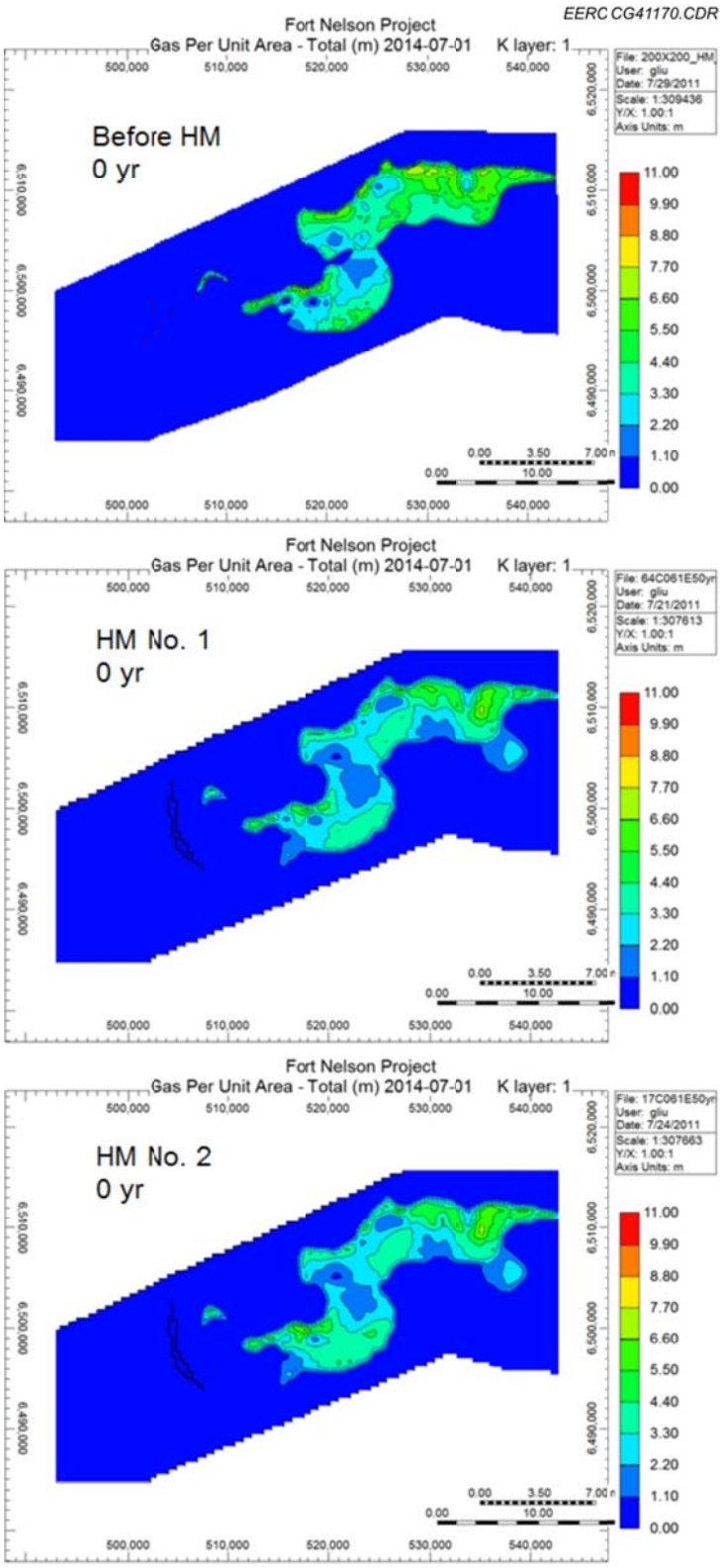

Figure E-114. Areal view of the test case before and after history matching: zero year of injection in and around c-61-E.

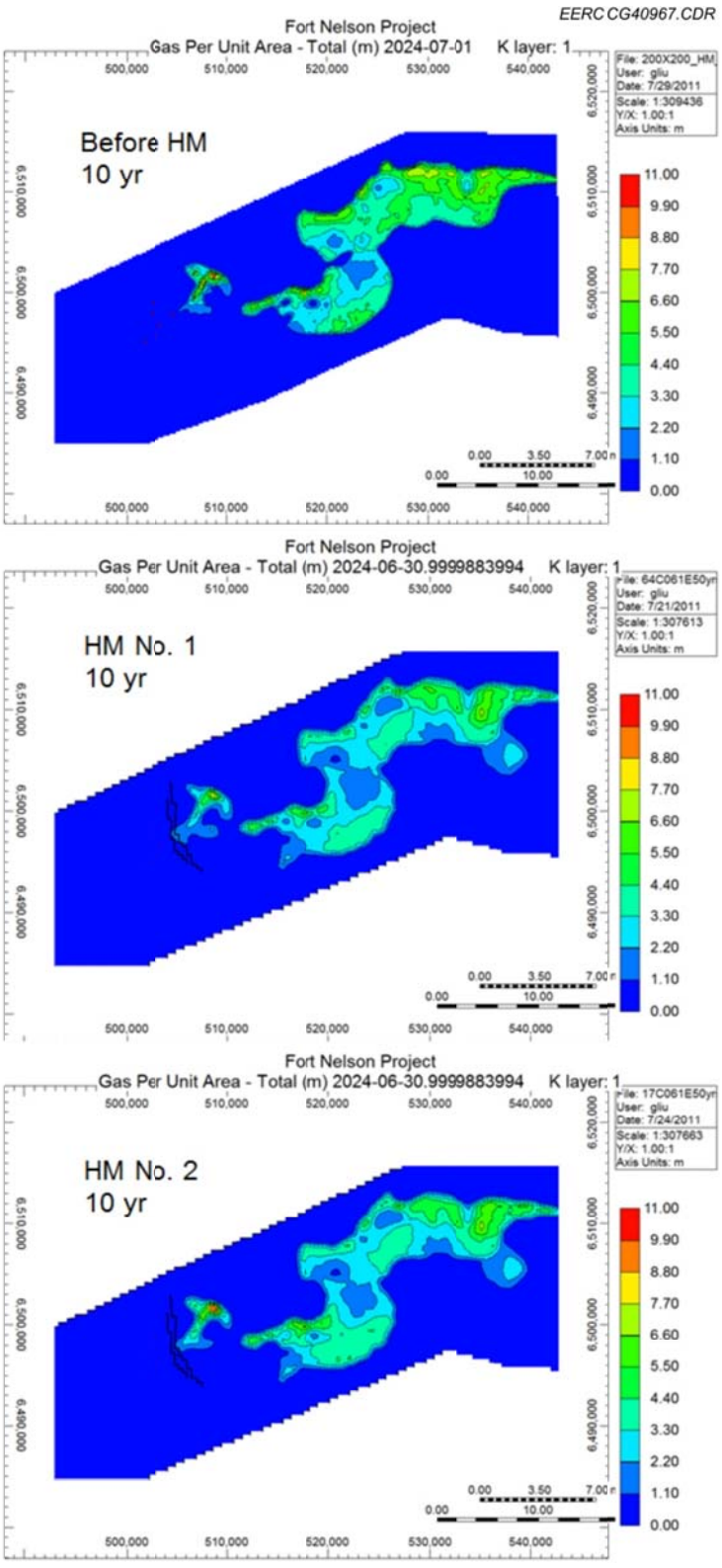

Figure E-115. Areal view of the test case before and after history matching: 10 years of injection in and around c-61-E.

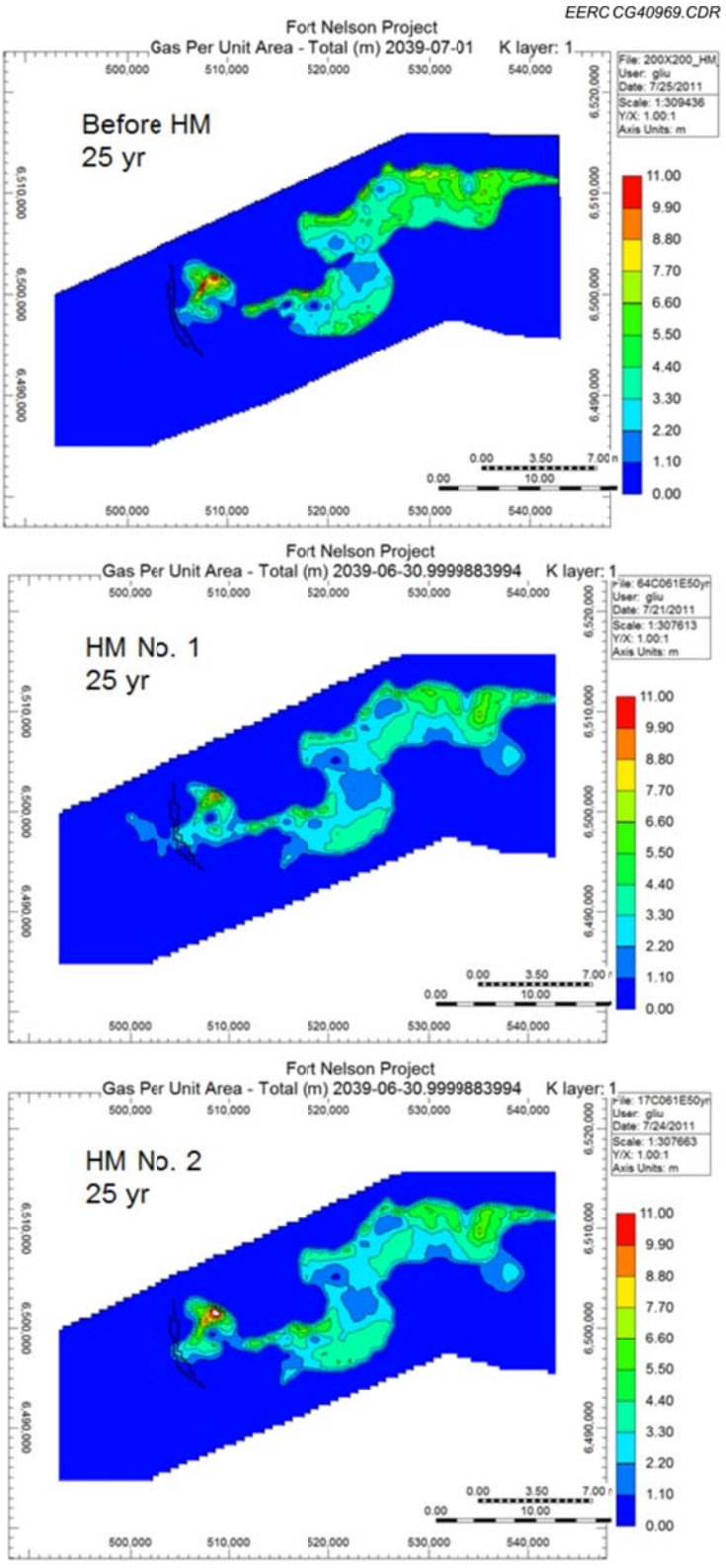

Figure E-116. Areal view of the test case before and after history matching: 25 years of injection in and around c-61-E.

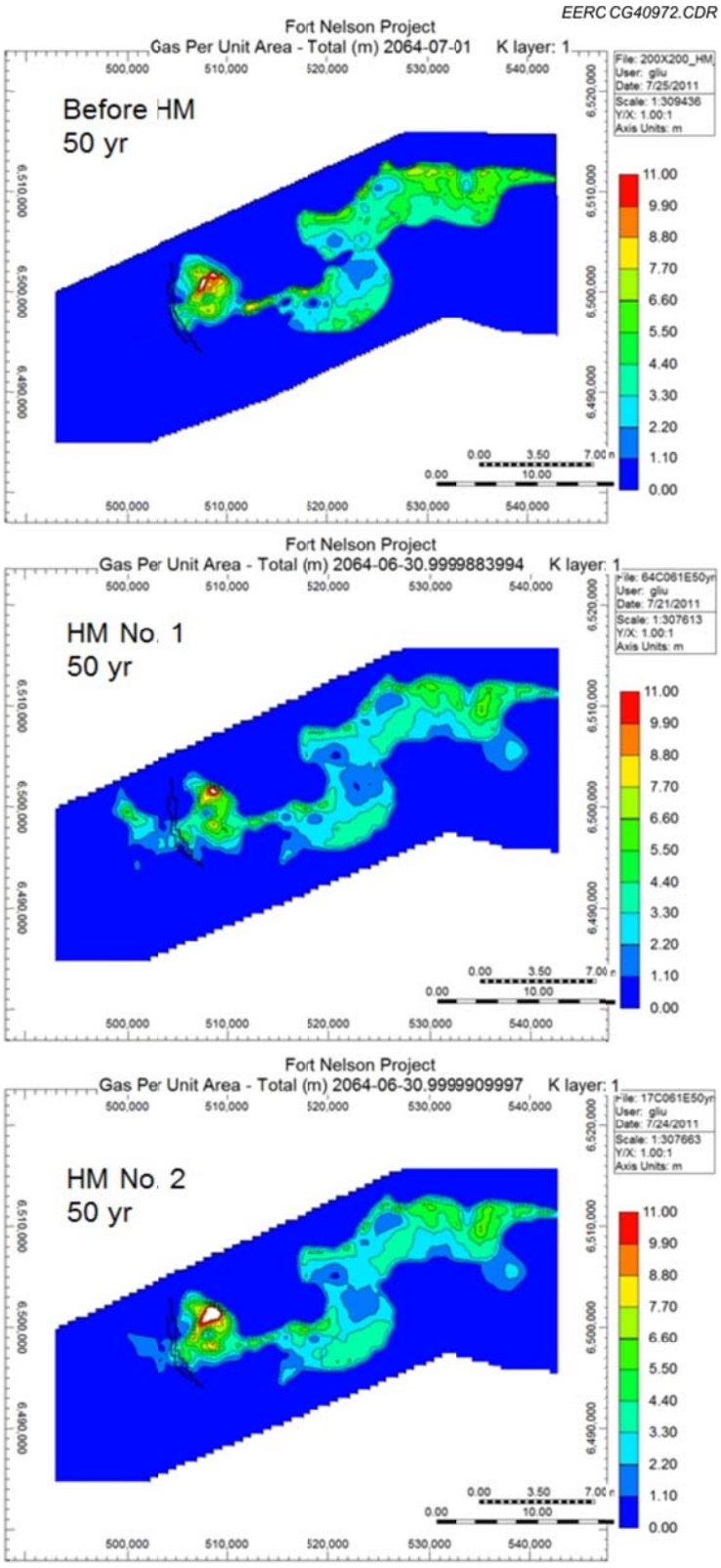

Figure E-117. Areal view of the test case before and after history matching: 50 years of injection in and around c-61-E.

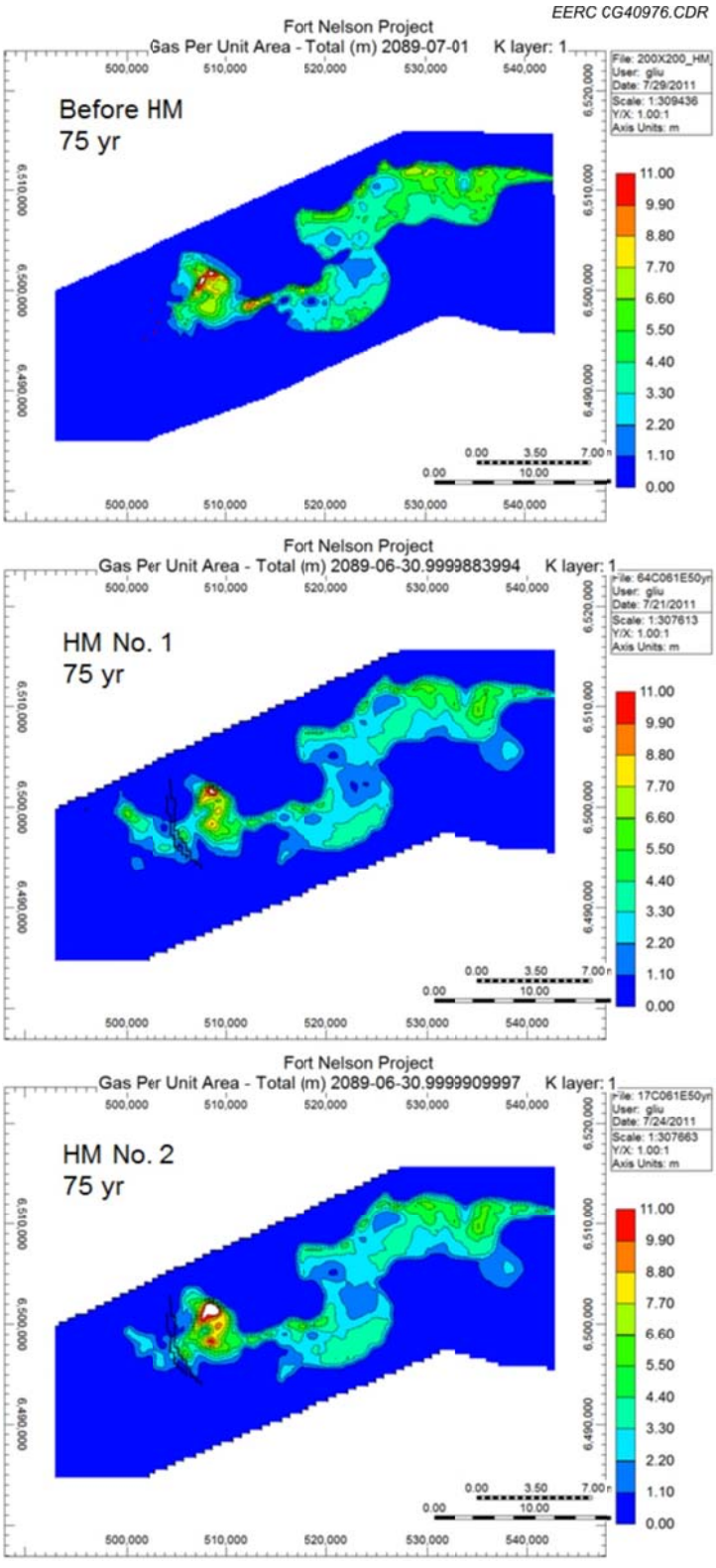

Figure E-118. Areal view of the test case before and after history matching: 50 years of injection plus 25 years postinjection in and around c-61-E.

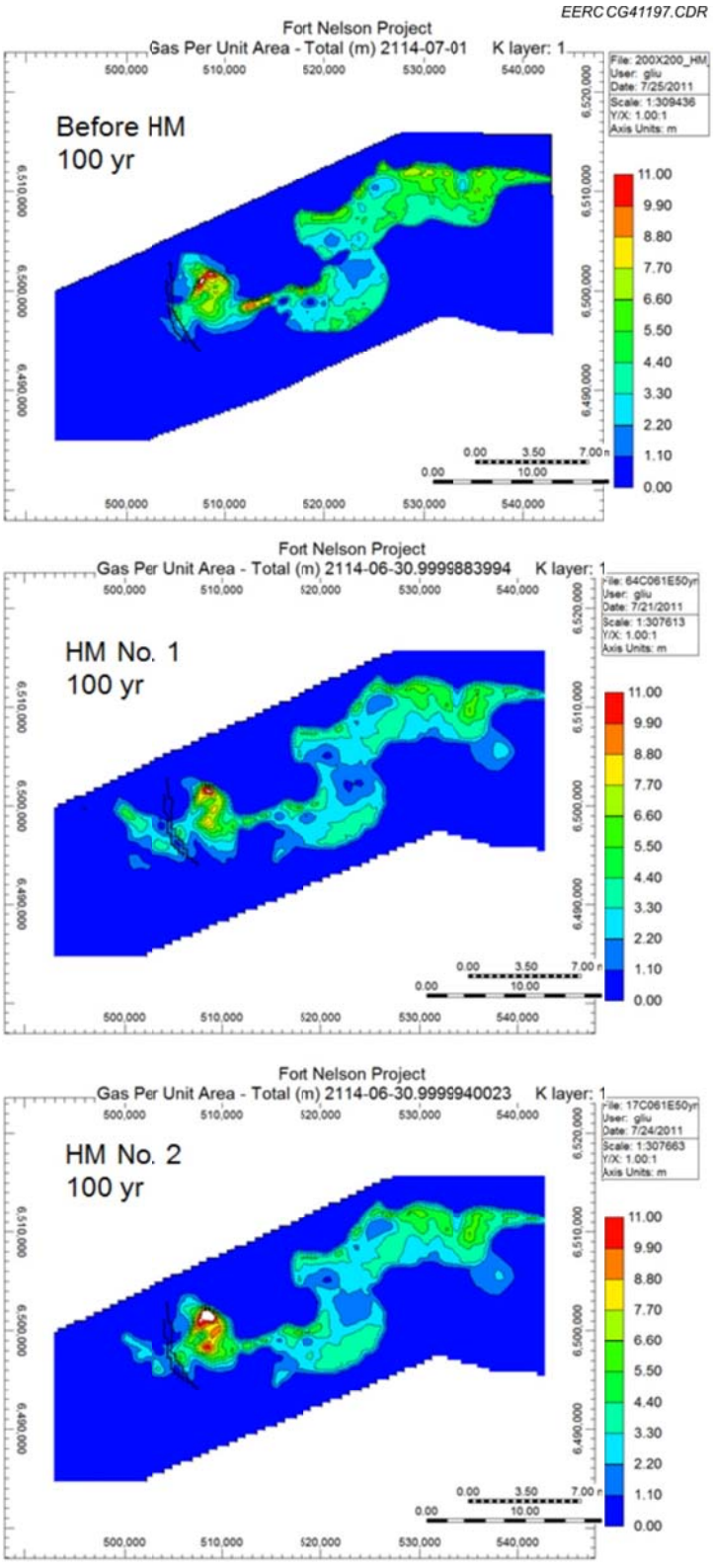

Figure E-119. Areal view of the test case before and after history matching: 50 years of injection plus 50 years postinjection in and around c-61-E.

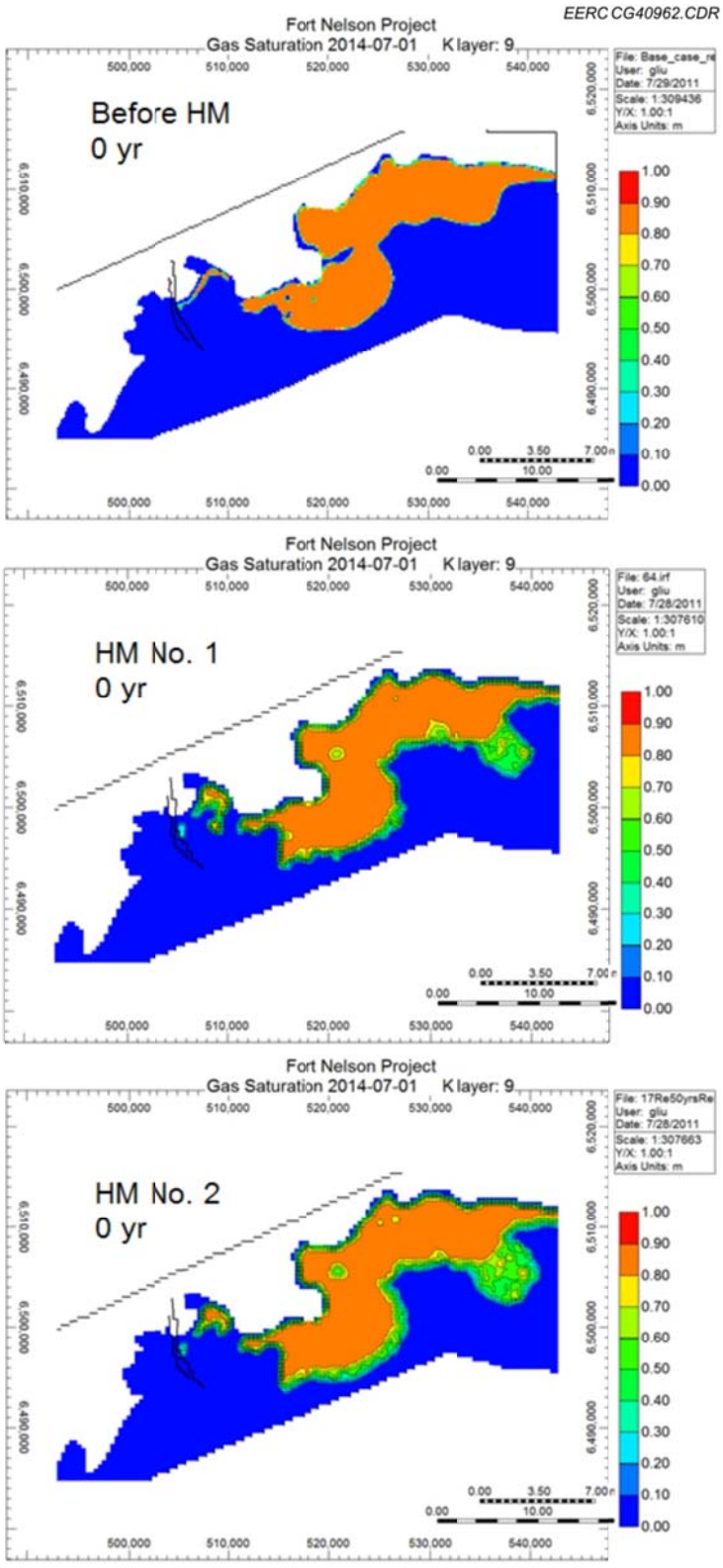

Figure E-120. Areal view of the test case before and after history matching: saturation at the top of Upper Slave Point over time; zero year of injection in and around c-61-E.

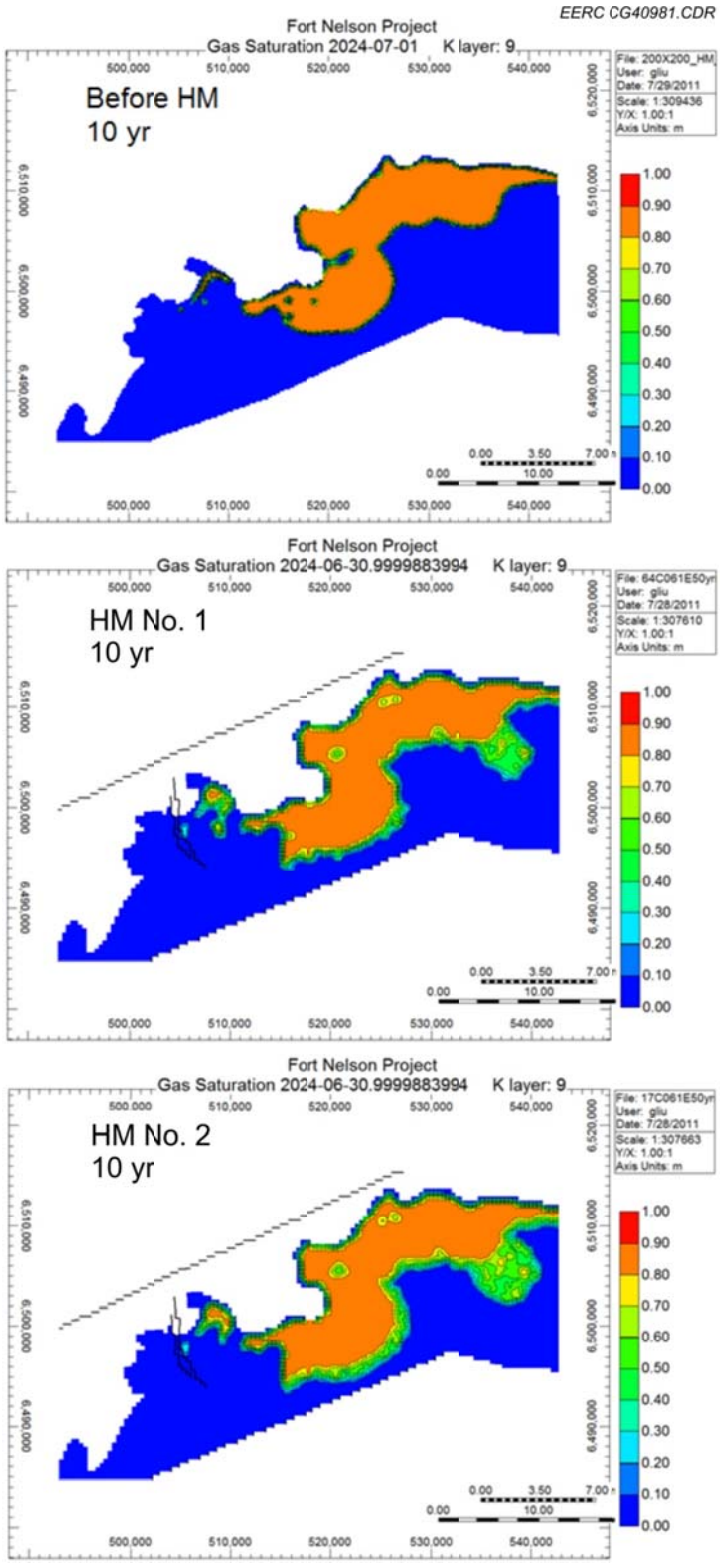

Figure E-121. Areal view of the test case before and after history matching: saturation at the top of Upper Slave Point over time; 10 years of injection in and around c-61-E.

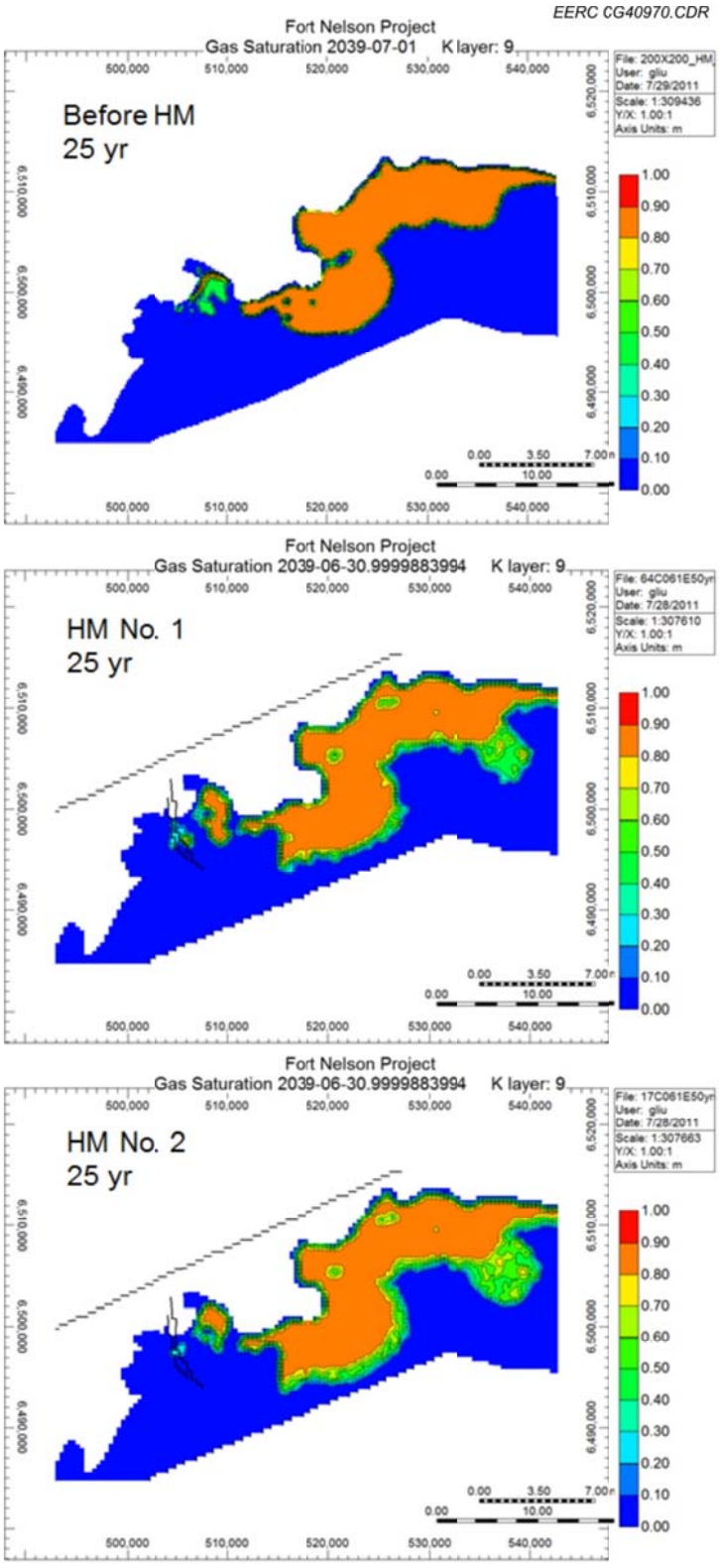

Figure E-122. Areal view of the test case before and after history matching: saturation at the top of Upper Slave Point over time; 25 years of injection in and around c-61-E.

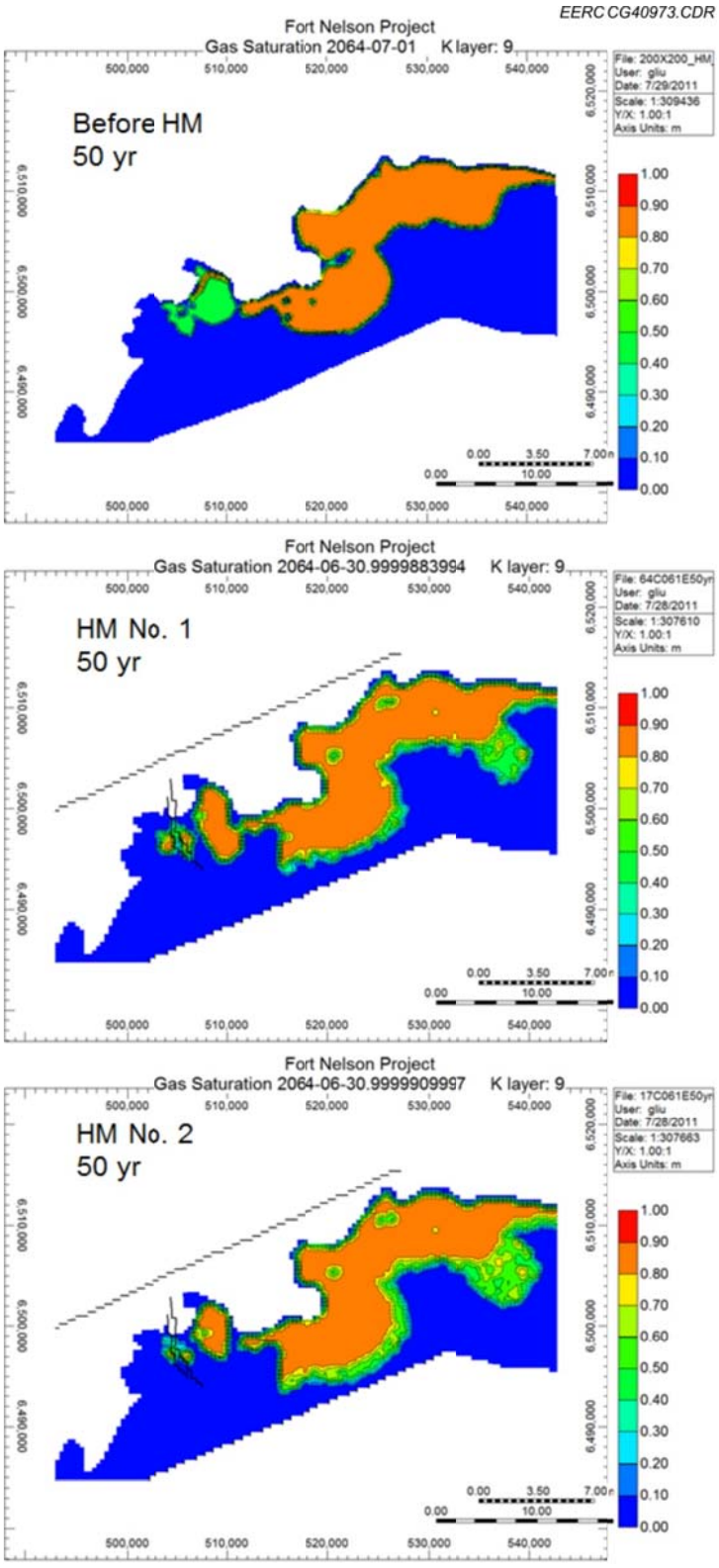

Figure E-123. Areal view of the test case before and after history matching: saturation at the top of Upper Slave Point over time; 50 years of injection in and around c-61-E.

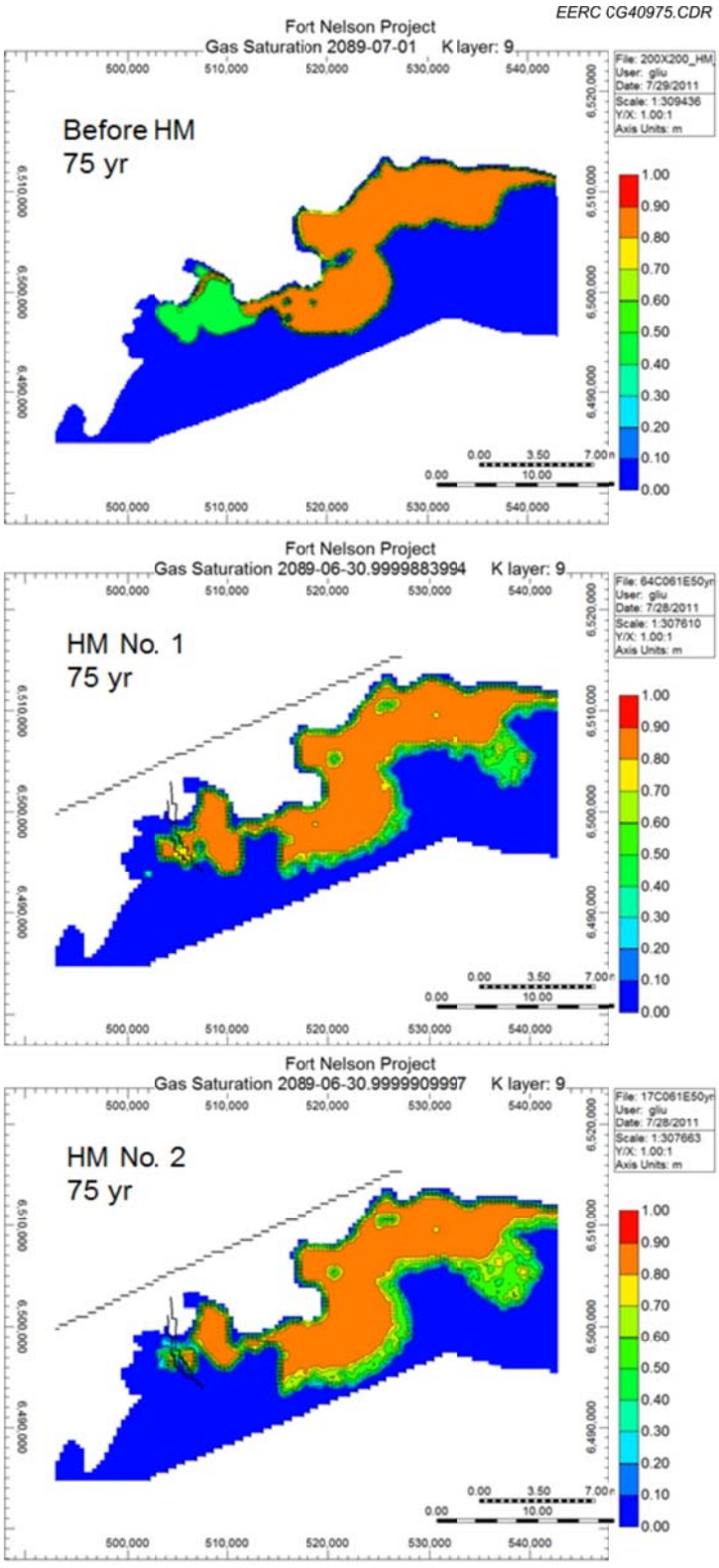

Figure E-124. Areal view of the test case before and after history matching: saturation at the top of Upper Slave Point over time; 50 years of injection plus 25 years postinjection in and around c-61-E.

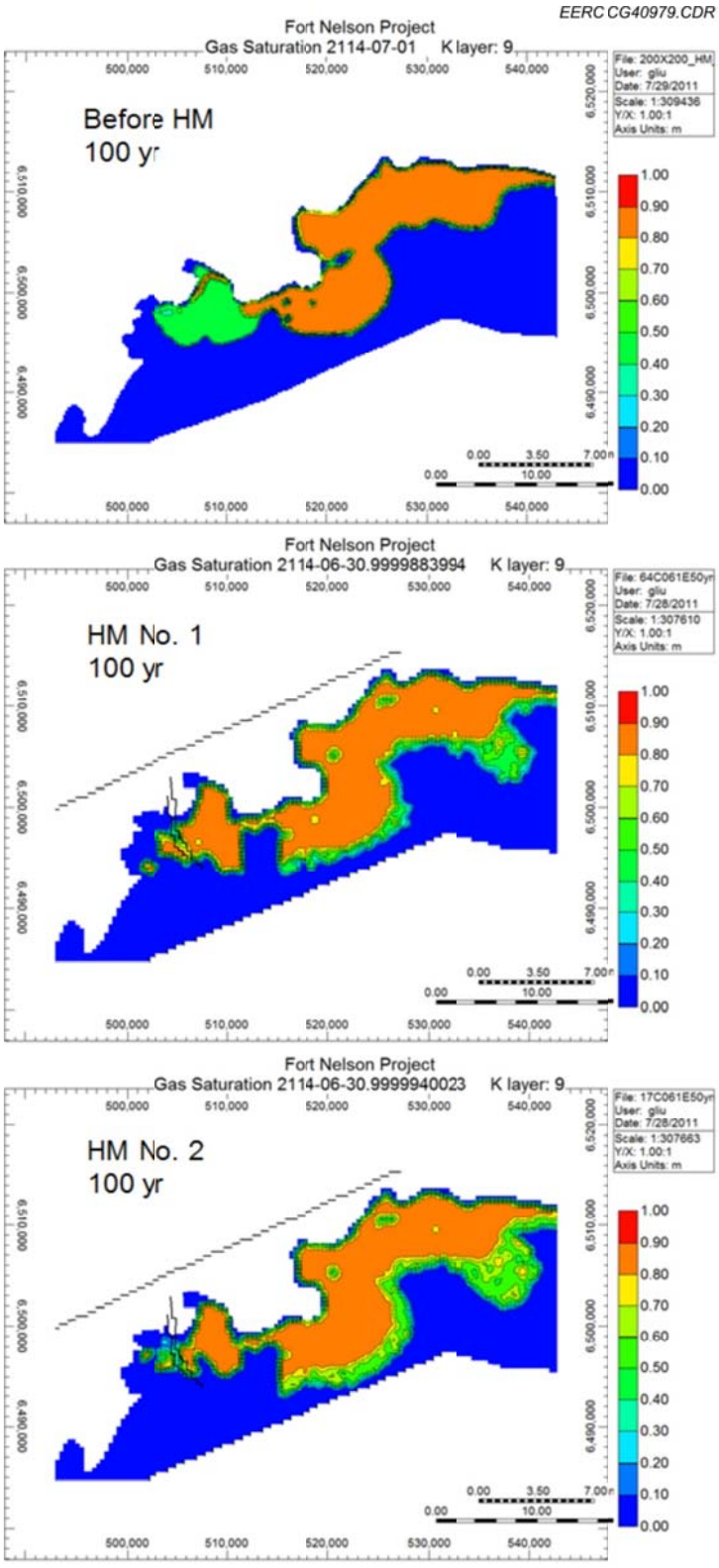

Figure E-125. Areal view of the test case before and after history matching: saturation at the top of Upper Slave Point over time; 50 years of injection plus 50 years postinjection in and around c-61-E.

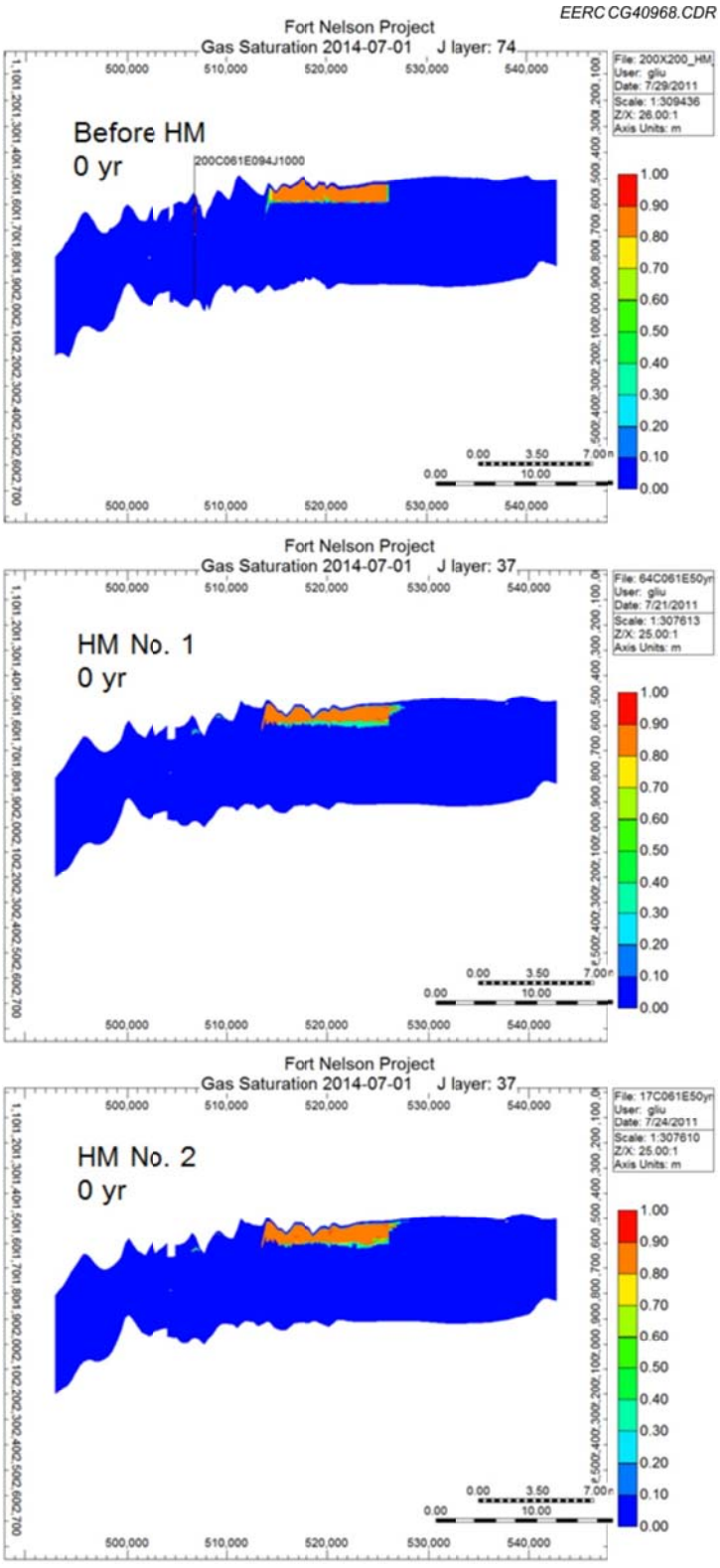

Figure E-126. Cross-sectional view of the test case before and after history matching: zero year of injection in and around c-61-E.

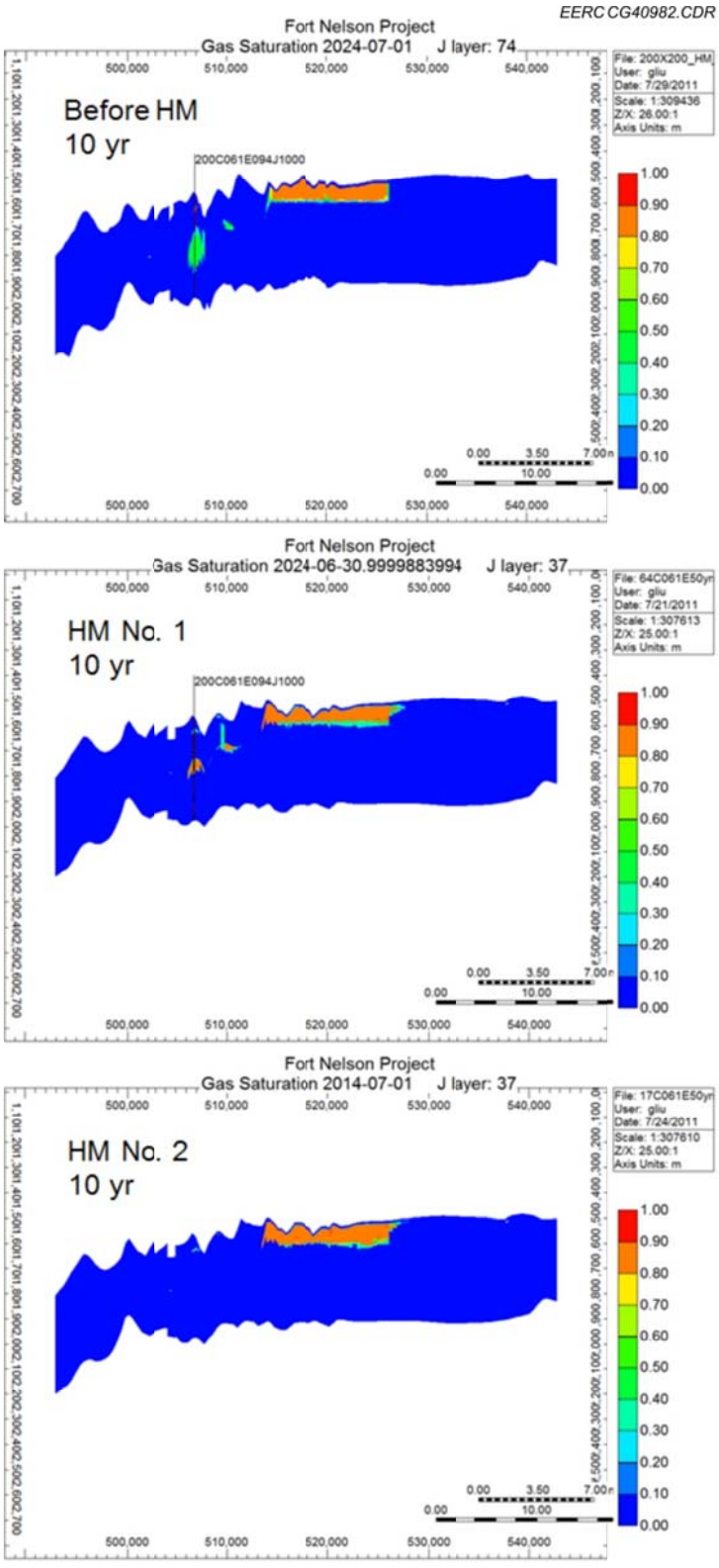

Figure E-127. Cross-sectional view of the test case before and after history matching: 10 years of injection in and around c-61-E.

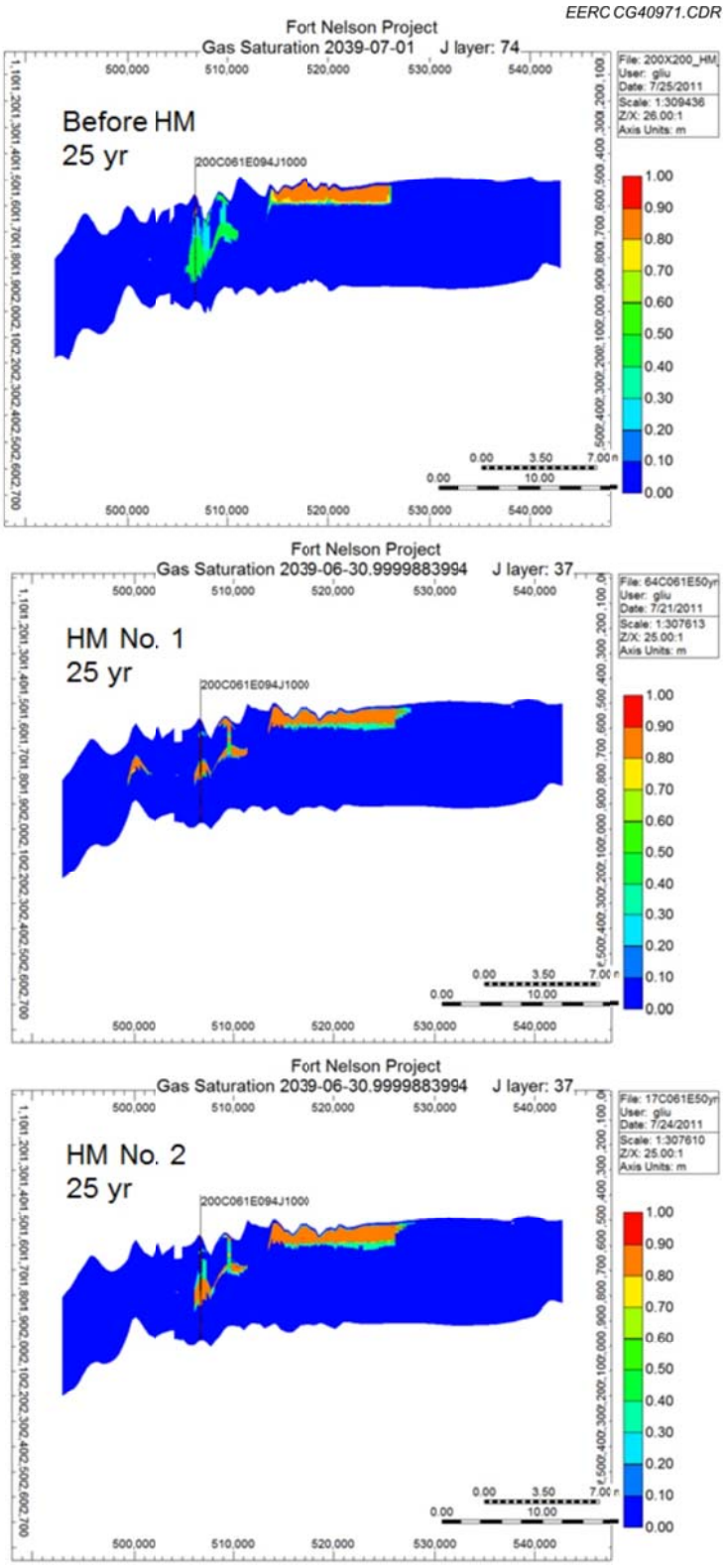

Figure E-128. Cross-sectional view of the test case before and after history matching: 25 years of injection in and around c-61-E.

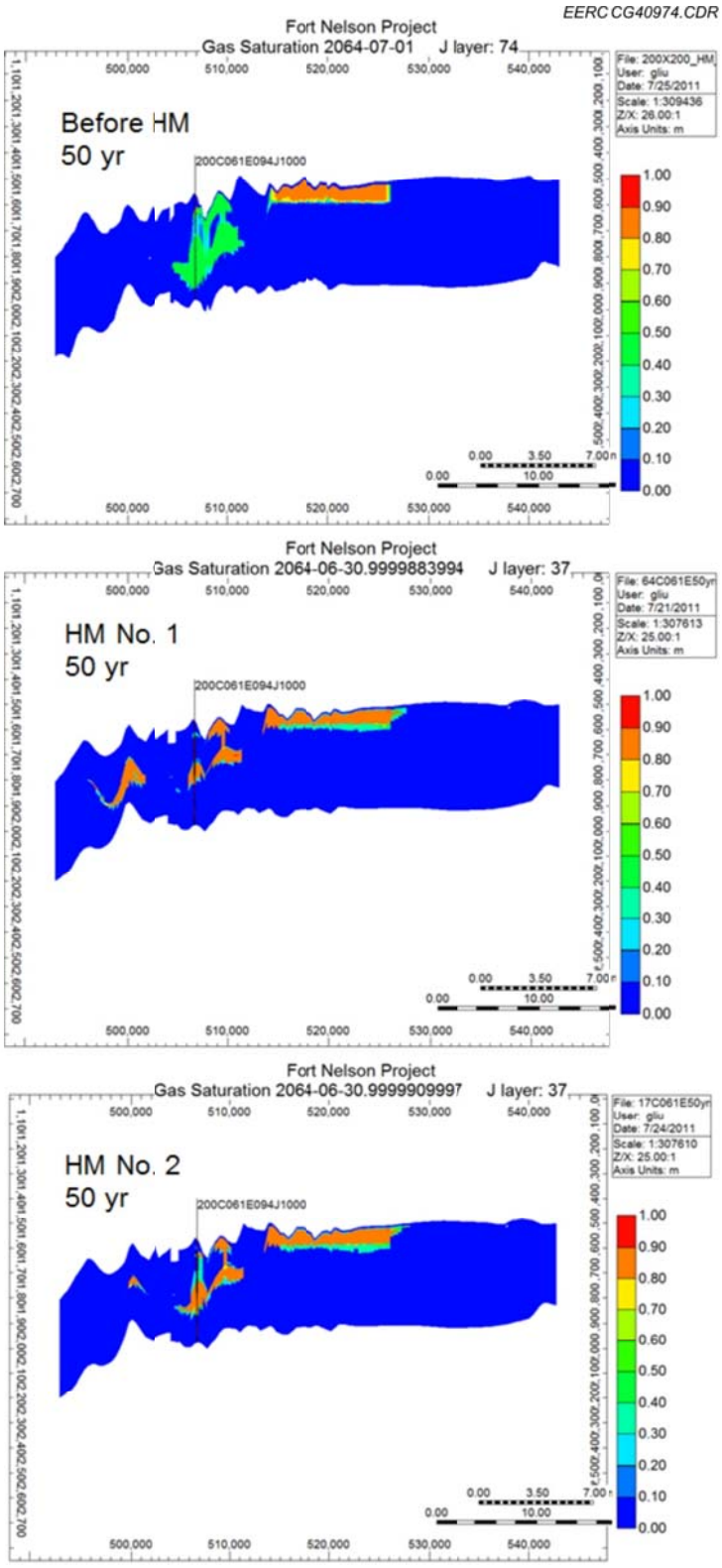

Figure E-129. Cross-sectional view of the test case before and after history matching: 50 years of injection in and around c-61-E.

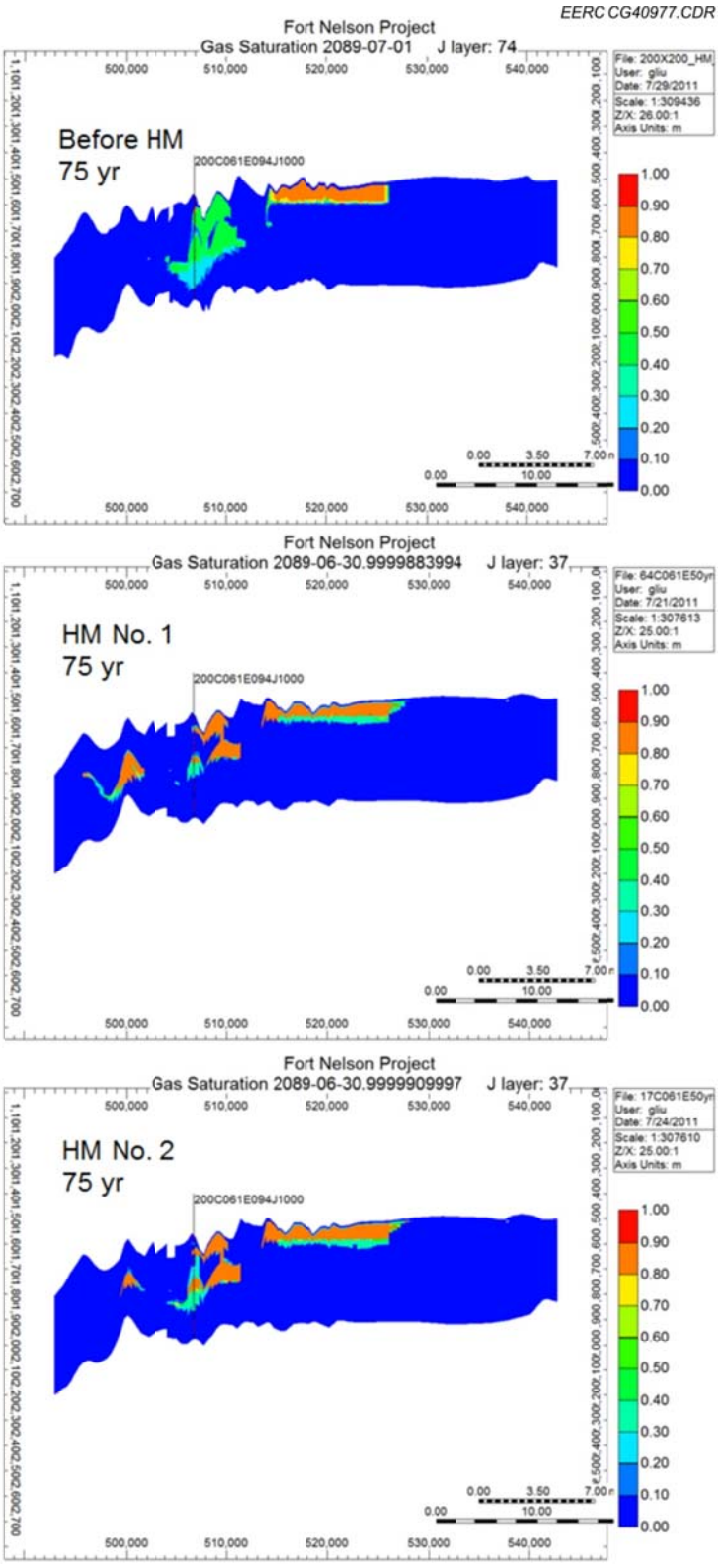

Figure E-130. Cross-sectional view of the test case before and after history matching: 50 years of injection plus 25 years postinjection in and around c-61-E.

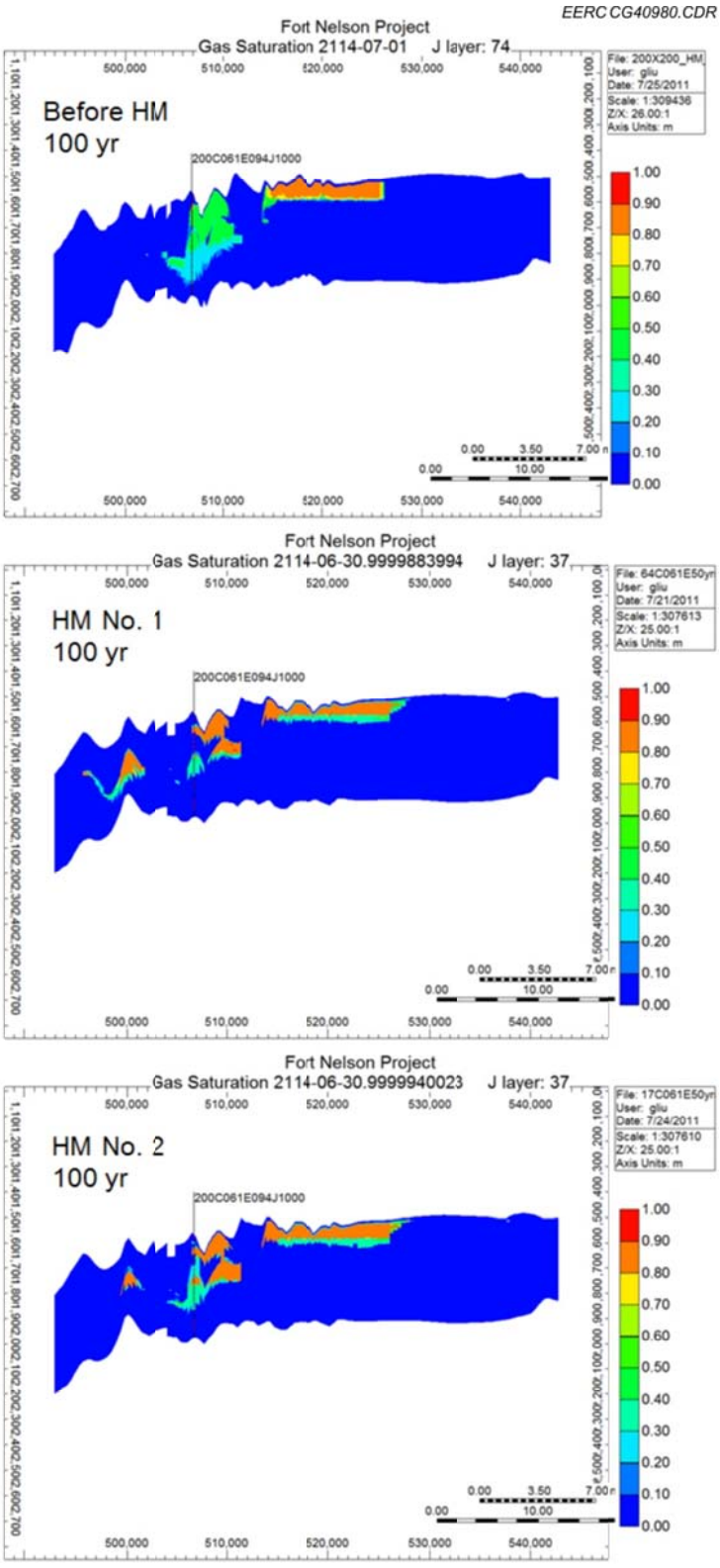

Figure E-131. Cross-sectional view of the test case before and after history matching: 50 years of injection plus 50 years postinjection in and around c-61-E.